University of Aston
in Birmingham

GAS HOLD-UP AND MIXING IN THE LIQUID-PHASE OF BUBBLE COLUMNS USED FOR CONTINUOUS FERMENTATION

by

JOHN McCALLUM DOWNIE

being a thesis submitted in support of an
application for the degree of Doctor of Philosophy.

October 1972

SUMMARY

The bubble column has recently received a great deal of attention since its applications are increasing. Recent work has shown that there is a viable possibility of utilising bubble columns in aerobic systems such as fermentation.

At present there is a considerable amount of knowledge available on the various parameters affecting the operation of systems. Unfortunately the majority of the research work carried out has been with simple two-phase systems such as air/water. Consequently there is virtually no working design-data for complex two-phase and three-phase systems.

The object of this research programme was to attempt to apply present two-phase knowledge to three-phase systems and to endeavour to determine the effects of various parameters, if they act differently.

The initial experimental work was concerned with obtaining a reliable and reproducible means of determining bubble diameters and a preliminary study of the factors affecting the size of bubbles generated from single orifices in yeast suspensions. The work then progressed to some small-scale studies of two-phase systems in an effort to relate the initial single bubble data to bubble swarm systems.

The physical size of the apparatus was then increased to simulate industrial type equipment. Extensive studies were carried out with this equipment to measure the effects of gas and liquid flow-rates and column diameter on gas hold-up in yeast suspensions of varying concentrations, in comparison to air/water systems. Finally, a study of the liquid-phase mixing was made, using the same parameters.

The overall object of this thesis is to put forward preliminary data on two and three-phase systems which, it is hoped, will enable more extensive studies to be carried out on various aspects of the work.

CONTENTS

CONTENTS

CONTENTS

LIST OF FIGURES

LIST OF FIGURES Continued

LIST OF FIGURES Continued

LIST OF FIGURES Continued

LIST OF FIGURES Continued

LIST OF TABLES

LIST OF TABLES Continued

LIST OF TABLES Continued

LIST OF TABLES Continued

LIST OF TABLES Continued

LIST OF TABLES Continued

ACKNOWLEDGEMENTS

I would like to acknowledge the following for their assistance.

The University of Aston for financial assistance in the form of a Studentship;

the academic, clerical and laboratory staff of the Chemical Engineering Department;

Prof. Z. Sterbacek of Microbiological Institute of the Czechoslovak Academy of Sciences, Prague, who initiated the research programme;

Dr. Archer-Hall of the Physics Department, University of Aston, for his valuable advice in the work with single bubble size measurements;

Dr. E. L. Smith of the Chemical Engineering Department, University of Aston, for his continuous encouragement and guidance;

and my wife Julia for her patience in typing this thesis.

1. INTRODUCTION

1.1. THE PROBLEM

The bubble-column is a simple and relatively inexpensive device for achieving intimate gas-liquid contact. In such systems gas is bubbled into a deep pool of liquid, which may be stagnant or flowing, and is dispersed as a swarm of bubbles of high interfacial area.

Bubble-columns have been most widely used as chemical reactors, and such applications have been summarised by Ostergaard[41] and Mashelkar[40]. There is also the possibility of the bubble-column being used in certain fermentation processes, and it was this that prompted the research described in this thesis.

The objective of the research was to explore the effects of column design and operating conditions on 1) the behaviour of the gas-phase and 2) mixing in the liquid-phase. Because of the applications, research[*] is also being carried out in the Biological Sciences Department at the University of Aston in Birmingham; it was also decided that special consideration should be given to the aeration of suspensions of yeast in water.

1.2. WORK PROGRAMME

The initial literature survey showed that there was a lack of physical data in general and especially about bubble formation and movement in microbial suspensions. There is also a need for physical and mechanical data for the operation of two and three-phase systems in large diameter columns.

---

[*] Greenshields and Smith

This led to a programme of work being formulated to study the effect of various parameters on, firstly, single bubbles and their formation, secondly, bubble swarms and, thirdly, mixing in air/water and air/microbiological suspensions.

1.3. LITERATURE SURVEY

1.3.1 SINGLE BUBBLE STUDIES

It is not usual in industrial practice to operate a gas/liquid contacting system with a single orifice: but, in order to carry out research into the formation and behaviour of bubbles, it is convenient to use a single-holed orifice. It is not surprising, therefore, to find that an extensive amount of work has been carried out with such systems.[1 - 8, 14 - 17, 22, 24, 36 - 39] However, the production of bubbles at a single orifice is not such a simple process as one might think, and this is confirmed by the variety of results and conclusions reported by different workers operating with essentially the same systems.

It has been suggested by Valentin[1] that the principle factors affecting the size of gas bubbles formed at a single orifice are:-

1. Orifice diameter, d_o.
2. Volumetric flow-rate of gas through the orifice, G_v.
3. Gas density, ρ_g.
4. Gas viscosity, μ_g.
5. Liquid density, ρ_l.
6. Liquid viscosity, μ_l.
7. Surface tension of liquid, τ.
8. Pressure drop across the orifice, ΔP_o.
9. Volume of the gas-chamber below the orifice, V_c.

Other factors which seem to have less effect on bubble size are:-

10. Submergence of the orifice.
11. Shape of the orifice.
12. Angle of inclination of the orifice.
13. Liquid flow-rate past the orifice and liquid turbulence around the orifice.
14. Velocity of sound in the gas.
15. Dynamic surface-tension of the liquid.
16. Surface-elasticity of the liquid.
17. Surface-viscosity of the liquid.
18. Triple angle at the gas/liquid/solid interface.

It would appear that the gas flow-rate, orifice diameter and the volume of the gas-chamber beneath the orifice are of fundamental importance, whatever the liquid-phase used.

Regimes of Bubbling.

Most workers [1 - 7, 15 - 17, 36, 39] are agreed that there are four regimes of bubbling. These can be described as 1) the constant volume regime, 2) slowly increasing volume regime, 3) the constant frequency regime and 4) high gas flow regime.

1. Constant Volume Regime.

In this regime bubble diameter is a function of orifice diameter and surface tension. As the gas flow-rate increases, bubble-size remains constant, whilst the frequency of bubble generation increases. The bubbles are formed individually and are regular in shape.

2. Slowly Increasing Volume Regime.

Bubble diameter is now a stronger function of gas flow-rate but is much less dependent on orifice diameter. The viscosity and inertia of the liquid appear to have some effect in this regime. The bubbles are again generated singly, although bubble pairs may be formed due to the influence of the gas chamber beneath the orifice.

It should be noted that Hughes et al[2] and Valentin[1] classify these two regimes together.

3. Constant Frequency Regime.

In this regime the bubble-generation frequency remains virtually constant for a given orifice diameter, whilst the bubble diameter increases with increasing gas flow-rate. Surface tension becomes less important and liquid inertia appears as the main factor in determining bubble rate. Bubbles are formed either individually or in groups and coalescence becomes evident.

4. High Gas Flow Regime.

The orifice diameter and gas flow-rate have a weak and decreasing effect on the bubble diameter, and the ultimate size depends on the turbulence in the liquid-phase. Coalescence and breaking-up occur close to the orifice and there is a considerable spread of bubble sizes and frequencies. Kupferberg[3] suggests that the bubbles formed in this region are predominantly spherical cap or toroidal.

The transition from one regime to another is difficult to define. Nevertheless, the Orifice Reynolds Number, Re_o, provides a generally accepted criterion:

regime 1 to 2, $100 \leq Re_o \leq 300$;

regime 2 to 3, $Re_o \simeq 2100$;

and regime 3 to 4, $Re_o \geqslant 10,000$;

where $$Re_o = \frac{\rho_g d_o v^*}{\mu_g} \qquad 1.1$$

where ρ_g and μ_g are the gas density and viscosity, d_o is the orifice diameter and v^* is the gas velocity through the orifice, all in c.g.s. units, as are all the following equations unless otherwise stated.

A simple expression can be derived for predicting bubble diameters in regime 1. It is obtained by equating the buoyancy and surface tension forces acting on a spherical bubble at the point of detachment. The equation simplifies to:

$$d_b = \left(\frac{6\, d_o\, \tau}{(\rho_l - \rho_g)\, g} \right)^{\frac{1}{3}} \qquad 1.2$$

A considerable amount of data has been collected by Datta et al[4] which can be correlated in terms of equation 1.2. Davidson and Amick[5] have also made use of this relationship.

Several workers have obtained results which indicate that bubble diameter in regime 1 is dependent on gas flow-rate. Wraith[6] derived the following equation from first principles, assuming a two-stage growth period (see Fig. 1.1) :

$$d_b = 1.275 \left(\frac{G_v^{\,2}}{g} \right)^{0.2} \qquad 1.3$$

Similar results have been obtained by Davidson and Schuler[7], Davidson and Harrison[8] and by Walters and Davidson[9], although differences in the value of the numerical constant are given. In all cases, a hypothetical orifice of zero diameter (i.e. a point gas source) was considered. However, Davidson and Schuler[7] suggested that for an orifice of finite size there would be a delay in bubble detachment until the bubble had risen a distance $d_o/2$ above the orifice. In their view this would result in somewhat larger bubbles than those predicted by equation 1.3. The same authors predicted that in the slowly increasing volume regime (i.e. the upper limit of regimes 1 and 2)

$$d_b = K \left(\frac{d_o \tau}{(\rho_l - \rho_g)\, g} \right)^{\frac{1}{3}} (v^* \mu_l)^{\frac{1}{4}} \qquad 1.4$$

which is similar to equation 1.2 but gives slightly larger values of d_b if $K > 1$.

Davidson and Amick[5] predicted bubble sizes in the constant frequency range (regime 3) by the following equation:

$$d_b = K \left(G_v \, d_o^{0.5} \right)^{w} \qquad 1.4\,b$$

Using their own data and that of Maier[10], Sprague[11], Hagarty[12] and Eversole[13], they found that equation 1.4 b could be written in the form

$$d_b = 0.634 \left(G_v \, d_o^{0.5} \right)^{0.318} \qquad 1.5$$

This shows that both gas flow and orifice diameter have an effect on the bubble size. It must be assumed that the physical properties of the system are accounted for by the constant.

Van Krevelen[14] has suggested that at gas flow-rates encountered within the constant frequency regime, bubble sizes can be estimated using

$$d_b = 0.432 \left(\frac{G_v \, \mu_l}{\rho_l - \rho_g} \right)^{0.25} \qquad 1.6$$

It will be noted that d_o, the orifice diameter, does not appear in the equation. In contrast to this, Leibson et al[15] have put forward the equation:

$$d_b = 4.22 \; d_o^{1/6} \left(\frac{G_v \, \rho_l}{\mu_l} \right)^{1/3} \qquad 1.7$$

This shows d_o as having a slight effect on d_b: the reversal of liquid viscosity and density in the last term should also be observed.

At higher flow-rates Van Krevelen[14] applied dimensional analysis to correlate existing data for both slowly and rapidly forming bubbles. For the turbulent regime, i.e. $Re_o > 2000$, he found that:

$$d_b = 0.0279\ G_v^{0.4} \left(\frac{\rho_l}{\rho_l - \rho_g} \right)^{0.2} \qquad 1.8$$

Neither viscosity nor surface tension appeared to have an effect on d_b. Equation 1.8 also indicates that the orifice diameter has no effect, although only small diameter orifices were used. If $\rho_l \gg \rho_g$, which is frequently the case, equation 1.8 simplifies to:

$$d_b = 0.0279\ G_v^{0.4} \qquad 1.9$$

A more complex relationship has emerged from the research of Quigley et al[16]. At higher gas flow-rates, they found that 1) the orifice diameter had a relatively strong effect and 2) of the liquid phase properties, viscosity had only a weak influence, whilst surface tension had none at all. They suggested that:

$$d_b = 0.222\ d_o^{0.33}\ G_v^{0.125}\ \mu_l^{0.02} + 3.02 \times 10^{-4}\ G_v^{1.09} \qquad 1.10$$

At very high gas flow-rates Calderbank[17] and Leibson et al[15] observed that bubble diameters were almost constant and could be estimated from the equation:

$$d_b = 0.71\ Re_o^{-0.05} \qquad 1.11$$

This shows that d_b is only slightly dependent on orifice diameter, gas flow-rate and gas physical properties.

Bubble Formation and Shape

Kupferberg and Jameson[3] define three stages during the growth of a bubble, viz. 1) the growing stage, 2) the elongating stage and 3) the waiting stage.

1. Growing Stage.

During this stage, the bubble grows while remaining at the orifice. This stage terminates when the upward buoyancy forces on the bubble equal the downward force and the bubble begins to rise, although still attached to the orifice.

2. Elongating Stage.

The bubble continues to grow whilst still attached to the orifice by a small tail. This stage ends when the tail breaks and the bubble starts to move away from the orifice.

3. Waiting Stage.

During this stage there is no outflow of gas from the orifice chamber and the pressure builds up again and another bubble begins to form.

These three stages are very similar to those proposed by Wraith[6] (see Fig. 1.1) where (b) and (c) are the growing stage, (d) is the elongating stage and (e) and (a) are the waiting stage. Four major assumptions were made to enable these stages to be defined:

(1) The bubble is spherical throughout its formation;

(2) The effect of viscosity is ignored because the magnitude of the viscous stress is very much less than the inertial pressure stress due to the liquid motion around the bubble;

(3) The liquid is very deep compared to the diameter of the bubble;

and (4) The momentum of the gas is ignored.

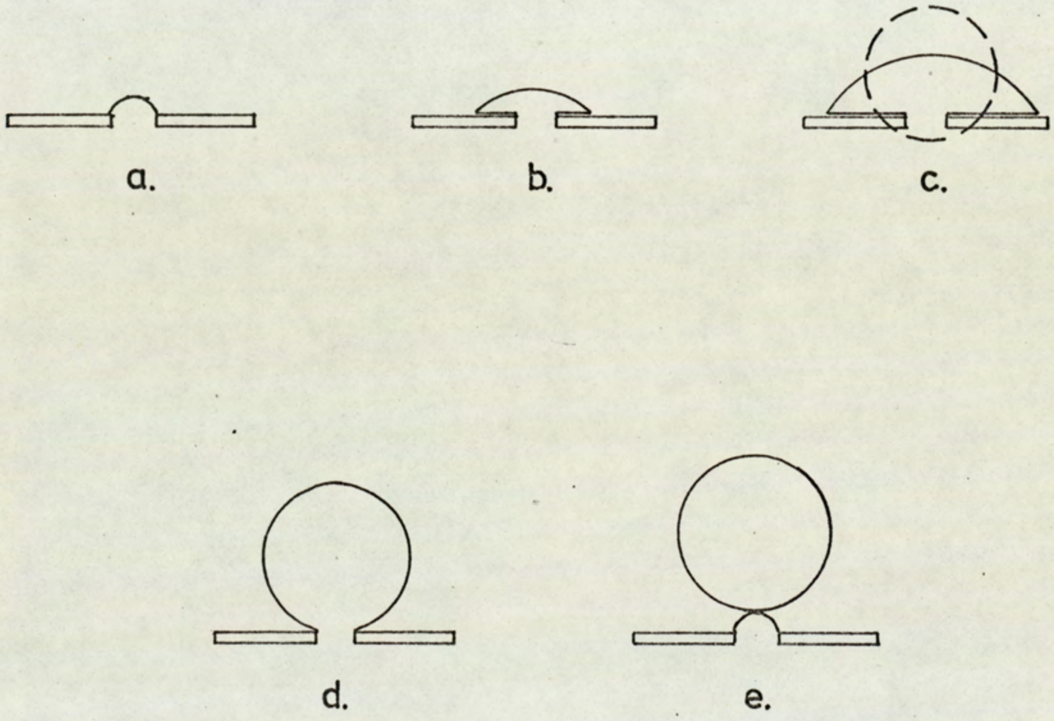

FIG 1.1 Two-stage bubble growth, showing transition from hemispherical, stage1, to spherical, stage 2, at (c).

Kupferberg and Jameson go on to propose a criterion for multiple bubble formation: when the bubble detaches it leaves a dome of gas which either a) detaches immediately as a small bubble and coalesces or b) it is depressed by ΔP_H, the hydrostatic pressure head, resulting in some weeping through the orifice. If the pressure in the dome is greater than the hydrostatic pressure, then a second bubble starts growing immediately the first one detaches.

The earliest work on bubble shape was that of Bashforth and Adams[18]. They considered the internal and external forces acting on a bubble and derived equations based on a force balance. Their results, expressed in tabular form, can be used to predict bubble shape. These workers also derived an expression for the volume of a bubble formed above a stationary, horizontal surface. This work was extended considerably by Poultanen and Johnson[19] who defined the shape of a slowly growing bubble above a stationary, horizontal orifice as

$$r^n \theta = 1 \qquad 1.12$$

where r and θ are polar co-ordinates and n is time-dependent during the formation of the bubble.

Houghton et al[20] have characterised bubbles in the form of oblate spheroids. On plotting the "major" against the "minor" axis on log/log paper, a line of 45° could be drawn through the data for bubbles of diameter 0.1 to 0.6 cm. in a wide range of liquids. This plot leads to the following expression:

$$b = 1.2a \qquad 1.13$$

where b and a are the major and minor axes respectively. Valentin[1] takes this a stage further and divides bubbles into four groups according to diameter. These are represented in Table 1.1 and apply to stable bubbling conditions only.

Table 1.1 Classification of Bubble Shape.

d_b cm.	Bubble Shape Description
<0.1	Spherical
0.1 - 0.6	Oblate spheroids
0.6 - 1.7	Irregular ellipsoids
>1.7	Spherical caps

Toroidal bubbles, when formed at high gas flow-rates, tend to disintegrate immediately, under their own turbulence. However, Walters and Davidson[9] have managed to produce some stable toroidal bubbles under carefully controlled conditions.

Davis and Taylor[21], using the eccentricity E (i.e. major axis/minor axis), found that bubbles could be divided into the following groups:

Spherical Cap Bubbles:

$$E = 3.5 \qquad 1.14$$

Ellipsoidal Bubbles:

$$E = 0.675\,(Re_o\,M^{0.23})^{0.528} \qquad 1.14a$$

for $2 < Re_o\,M^{0.23} < 6$;

and $$E = 0.4\,(Re_o\,M^{0.23})^{0.84} \qquad 1.15$$

for $6 < Re_o\,M^{0.23} < 16.5$;

where $$M = \frac{g\,\mu_l^4}{\rho\,\tau^3} \qquad 1.16$$

Effect of Liquid Physical Properties

Most workers seem to have operated mainly with air/water systems, and there is little information concerning gas physical properties: but one would expect very little effect. Some researchers have varied the liquid physical properties considerably, but the conclusions reached are often contradictory.

Surface Tension

Datta et al[4] found that a decrease in surface tension decreased the bubble diameter, whilst Quigley et al[16] found that it had no effect. Valentin[1] suggests that at low gas-flows the effect is fairly complex and in fact a decrease in surface tension decreases the bubble diameter. A clue to this discrepancy is in a paper by Davidson and Schüler[22], who found that the effect of surface tension was negligible in regime 1 when using a high pressure-drop, but considerable under constant pressure conditions. This suggests that surface tension is only important when inertial forces are negligible.

This problem is discussed at length by Pattle[23]. He found that equation 1.2 holds approximately at low gas flow-rates, but if the liquid-phase contains a substance that hinders coalescence then the growing bubble is pushed aside and broken off prematurely. This phenomenon is especially marked at low and medium gas flow-rates.

Hayes et al[24] report that at low gas rates the surface tension forces are greater than the rate of change of momentum of the gas entering the bubble, whilst the reverse is true at higher flow-rates. The critical gas flow-rate is given by

$$G_v = \frac{\pi}{2}\left[\frac{d_o^{3}\,\tau\,(1 - {}^{d_o}/_{d_b})}{\rho_g}\right]^{\frac{1}{2}} \qquad 1.17$$

Liquid Viscosity

Datta et al[4] found a slow increase in bubble diameter as the viscosity was increased, whilst Quigley et al[16] found a slight decrease in bubble diameter. Davidson and Schüler[7], however, found a marked decrease in bubble size with increasing viscosity.

Houghton et al[20] found a slight difference in bubble size when operating with glycerol, but this tended to disappear as the gas flow-rate was increased. Other results[5, 14, 15] have already been discussed (equations 1.4, 1.6, 1.7).

Liquid Density

Relatively, there seems to be little effect on bubble size of varying the density of the liquid-phase. Davidson and Schüler[7] found a slight increase in bubble diameter as the liquid density increased. On the other hand, Quigley et al[16] found that there was no effect when the density was changed, although they report that the combined effect of increasing viscosity and decreasing density slightly increased bubble size.

Orifice Chamber Volume

The effect of the upstream gas-chamber volume has been studied by several workers[2, 3, 5, 7, 25, 26]. Hughes et al[2] found that the volume of the gas chamber, V_c, has quite a strong effect on bubble size. This is especially marked when:

$$V_c \doteqdot \frac{A_o \rho_g c^2}{g(\rho_l - \rho_g)} \qquad 1.18$$

where A_o is the orifice cross-sectional area and c is the velocity of sound in the gas. When V_c is smaller than the expression shown on the right-hand side of equation 1.18 steady bubble growth occurs, but when V_c is larger, constant pressure conditions are set up, thus affecting bubble growth; which led to the definition of the so-called Capacitance Number, N_c, where

$$N_c = \frac{g(\rho_l - \rho_g) V_c}{A_o \rho_g c^2} \qquad 1.19$$

N_c was then used as a parameter in predicting the growth rate and ultimate size of the bubbles. Davidson and Amick[5] also used this method of approach, whereas Davidson and Schüler[7] attempted to model the system from first principles. All these workers were mainly concerned with the extreme cases of constant gas-flow (no effect of gas chamber-volume) and constant pressure (infinite chamber-volume)

Hughes and co-workers[2] found that when N_c was approximately 0.85 V_c had no effect on bubble-size, but when N_c was less than 0.85 bubble release was delayed until the bubble was dragged away by buoyancy forces. When operating in the frequency range of 5 to 30 bubbles/s, a fifteen-fold increase in N_c caused d_b to double. At lower frequencies a change in bubble chamber-volume had very little effect on the bubble diameter, a fact confirmed by Lockhart and Martinelli[26].

Kupferberg and Jameson[3] found that for an orifice diameter of 0.6 cm. and low gas flow-rates ($Re_o < 300$), the results agree well with their[2] theory (see page 13). However, it seems that the volume of the gas-chamber has a more complex effect than simply increasing the bubble diameter. For example they[3] noted that at moderate flow-rates ($325 \leq Re_o \leq 990$), and with $V_c = 1500$ cm^3 there were two modes of bubbling: either small bubbles were formed at high frequencies or large bubbles at low frequencies. For larger values of V_c this effect virtually disappeared. They also obtained similar results, using an orifice 0.3 cm. in diameter and a gas-chamber volume less than 2250 cm^3. This sort of behaviour is confirmed by the results of Davidson and Amick[5].

Other Factors affecting Bubble Size

In general, smaller bubbles are formed whenever a bubble is detached prematurely from the orifice. This may be caused by turbulence in the liquid-phase, by the inclination of the orifice, or by use of an orifice shape other than circular.

Grease or impurities on or at the orifice as well as the wettability of the orifice will also have an effect on bubble formation under certain conditions.

Bubble Rise Velocities

The rise of single air-bubbles through different fluids has been studied by many workers[4, 19, 20, 27-30] operating in the range $10^{-5} \leqslant Re_o \leqslant 3000$, but the results are mainly empirical.

In general, for $Re_o \leqslant 2$, there is good agreement with Stokes Law[30] (equation 1.20). However, Garner and Hammerton[32] found that when operating with an oil (viscosity 198 centistokes) and at a bubble frequency $\geqslant 3$ bubbles/s, the rise-velocity was approximately 2.5 times that predicted by Stokes' Law, whilst Coppock and Meiklejohn[31] observed a 30% increase in v_∞ for air/water systems operating at 1 bubble/s with $d_b \simeq 0.2$ cm. These workers[31] also observed that as the bubble diameter increased, the discrepancy with Stokes' Law became less until at $d_b = 0.6$ cm. there was no difference, due to the fact that the bubble shape altered as d_b increased, thus altering the drag coefficient.

Haberman and Morton[27], who studied the rise of single air-bubbles in various liquids, also observed differences in v_∞ dependent on the circulation inside the bubbles, but they obtained no correlations. They[27] also detected a critical bubble diameter of 0.15 cm. at which the rise velocity in water attains a maximum value of 34 cm/s. Bubbles greater in size no longer behave as rigid spheres (see Table 1.1).

From Stokes Law

$$v_\infty = \frac{d_b^{\,2}}{18} \left(\frac{\rho_l - \rho_g}{\mu_l}\right) g \qquad 1.20$$

which if $\rho_l \gg \rho_g$ becomes

$$v_\infty = \frac{1}{18} \frac{g\, d_b^{\,2}}{\nu} \qquad 1.21$$

where ν is the kinematic viscosity. Hadamard[33] and Lamb[34] derived an expression for bubble rise-velocity where internal circulation was present by showing that the resistance to motion, F, is given by

$$F = 3\pi\mu d_b v_\infty k, \qquad 1.22$$

where

$$k = \frac{2\mu_1 + 3\mu_g}{3\mu_1 + 3\mu_g} \qquad 1.23$$

If $\mu_1 \gg \mu_g$, equation 1.22 reduces to

$$F = 2\pi\mu d_b v_\infty \qquad 1.24$$

and

$$v_\infty = {}^1/_{12} \frac{g d_b^2}{\nu} \qquad 1.25$$

Equation 1.25 predicts a 50% increase in v_∞ compared with that calculated from Stokes Law.

Angelino[29] measured the rise velocities of single bubbles in various liquids and proposed an equation of the form:

$$v_\infty = K V_b^n \qquad 1.26$$

where V_b is the bubble volume. Two assumptions were made in analysing the data, viz. that there were no wall effects and that the bubble volume remained constant throughout the system. He[29] found that for low viscosity systems:

$$v_\infty = 32.67 \; d_b^{\frac{1}{2}}, \qquad 1.27$$

where V_b has been replaced by d_b, the equivalent spherical diameter. Angelino[29] extended this correlation and found that a decrease in viscosity increased K and decreased n.

Houghton et al[20] have proposed that the rise velocity of single bubbles should be related to the superficial gas velocity, v_{gs}, by the equation:

$$v_\infty = v_{gs} \frac{\rho_l - \rho_b}{\rho_b} , \qquad 1.28$$

where ρ_b is the bed density. This suggests that v_∞ is dependent to a great extent on gas hold-up, that is the proximity of other bubbles hinders the rise. They also found that

$$v_\infty \text{ (gas swarms)} < v_\infty \text{ (single gas bubbles)} :$$

this subject is taken up again in Section 1.3.2.

Haberman and Morton[27] correlated the rise velocities of spherical cap bubbles ($d_b > 1.8$ cm.) with Re_o. This approach led to the following equation:

$$v_\infty = 1.02 \left(\frac{g\, d_b}{2} \right)^{\frac{1}{2}} \qquad 1.29$$

This is similar to the equation of Angelino, although the flow regimes in the two cases were very different.

Uno and Kintner[35] carried out work using columns of different diameters and found that if the column diameter to bubble diameter ratio was greater than 10 then there was no wall effect on the bubble rise velocity.

1.3.2 BUBBLE SWARM SYSTEMS

INTRODUCTION

As mentioned in the previous section, the reason why so many workers have looked at the factors affecting the formation of single bubbles is the relative simplicity of the system. However, in most practical gas/liquid contacting systems the gas bubbles are formed at a large number of orifices in order to achieve the maximum interfacial area per unit volume of the system. Consequently, it is necessary to consider the differences between bubble formation from multiple orifices and from single orifices and the effects that operating parameters have in the more complex situation.

Regimes of Bubbling in Two-Phase Systems.

The outstanding feature of two-phase flow is the variety of possible flow-patterns that are encountered. At one extreme a small volume of gas can be dispersed as bubbles in a continuous liquid medium, and at the other extreme a small volume of liquid can be dispersed as droplets in a continuous gas stream.

The various regimes commonly used for classifying air/water systems are shown diagrammatically in Fig. 1.2, for the case of low liquid flow and increasing gas flow. These regimes have been described by Scott[42] as follows:

1. Bubble Flow.

Gas is dispersed in the upward flowing liquid in the form of discrete bubbles of various sizes. As the gas flow-rate increases the bubbles increase both in size and number.

2. Slug Flow.

The gas bubbles coalesce to form bullet-shaped slugs having a parabolic leading edge. These slugs increase in length and diameter (eventually reaching the diameter of the column) as the gas flow-rate is increased. The slugs are separated by short stretches of liquid containing quite large numbers of small bubbles.

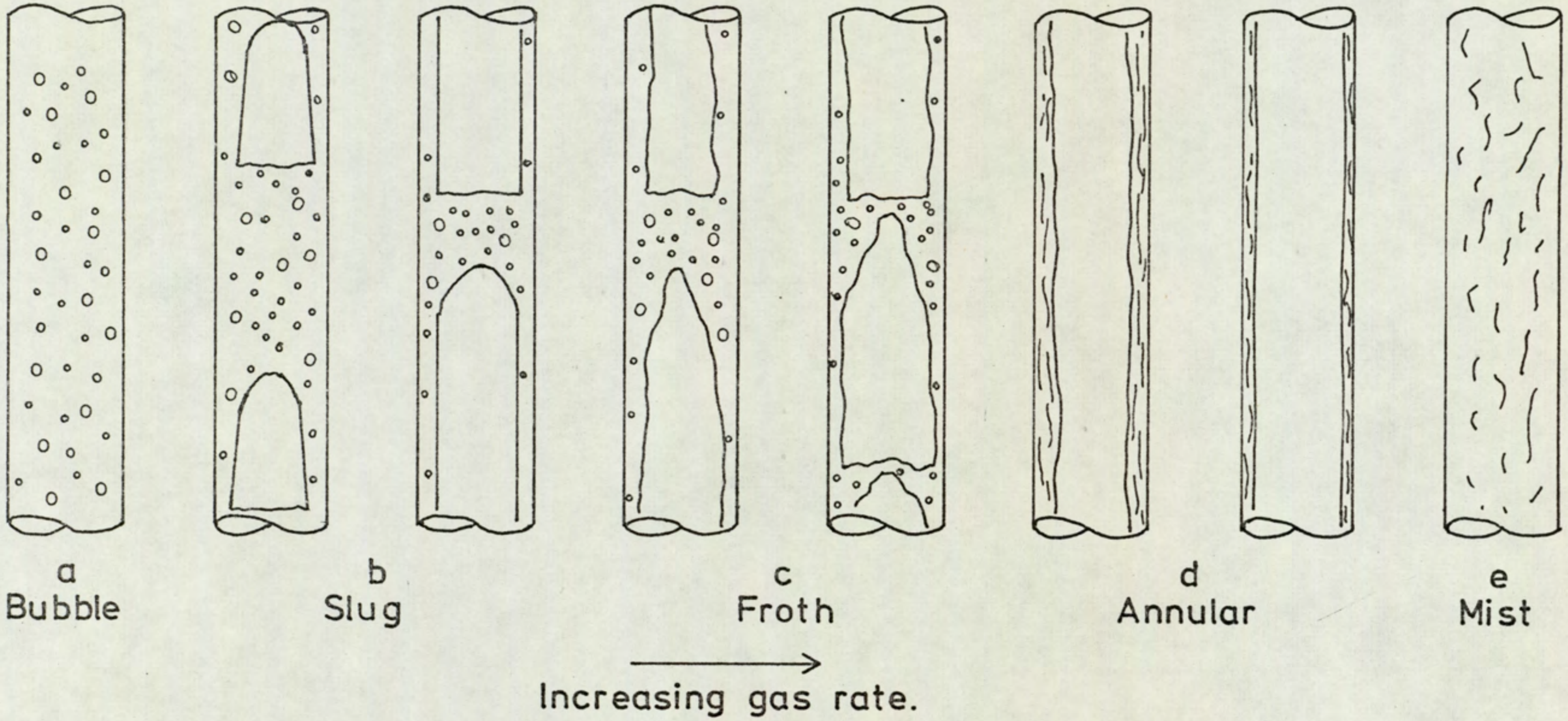

FIG 1.2 Development of flow régimes in two-phase flow.

3. Froth Flow.

When the liquid back-flow around the gas slugs nearly stops, the slugs become unstable and seem to merge with the liquid into a patternless, turbulent mixture, having the general appearance of a coarse emulsion. The main feature of this regime is a continuous process of collapse and reformation.

4. Annular Flow.

In this regime gas travels up the core of the tube at a high velocity and the liquid-phase forms an annular film around the tube walls. Initially, the film may be quite thick but as the gas flow-rate increases the film becomes thinner and the amount of liquid entrained as droplets in the central core increases.

5. Mist Flow

At very high gas velocities the amount of liquid entrainment increases until apparently all the liquid is carried up the tube as a mist. Although a thin liquid film may exist on the wall, its presence is not obvious in this regime.

Griffith and Wallis[43] have presented a phase diagram (see Fig. 1.3) defining bubble, slug and froth regimes in terms of the system parameters. They state that the transition point between bubble and slug flow is difficult to determine and is highly dependent on the method of introducing the gas and liquid phases.

Govier et al[44] and Brown et al[45] attempted to characterise the various flow patterns following studies of the effects of gas/liquid ratios (R_v), gas volumetric flow (G_v), liquid volumetric flow (L_v) and column diameter (d_c) on the gas hold-up (ϵ). They presented a correlation of the form:

$$\epsilon = f\,(R_v\,\rho_g^{\frac{1}{3}}\,d_c^{\;n}) \qquad 1.30$$

where n depends on the flow regime. This approach can be used to predict flow-patterns varying from bubble to annular.

Recently, Nicklin[46], Griffith[43] and Wallis[47] have put forward a more detailed analysis of vertical slug-flow, and given a clearer picture of the microscopic behaviour in this region.

Probably the simplest classification of the flow regimes is by means of Superficial Reynolds Numbers. Such a number is based on the column diameter, gas or liquid superficial velocity and the liquid viscosity. At least four types of flow can then be defined, depending on whether the gas or liquid-phase is in apparent laminar or turbulent flow. There seems to be uncertainty about the Reynolds Number for transition from laminar to turbulent flow. Lockhart and Martinelli[26] have suggested that a value of about 2000 can be used, but Nicklin[46] reports that a superficial liquid Reynolds Number of 8000 is required to give turbulent behaviour.

Fair[48] describes two subregimes of the bubble-flow region of Scott, viz. the quiescent regime and the turbulent regime.

1. Quiescent Regime.

This regime is characterised by particulate bubbles and little liquid agitation. The gas superficial velocity (v_{gs}) for this region in the case of air-liquid systems extends upto about 5.0 cm/s.

2. Turbulent Regime.

This regime is characterised by violent contacting and poor bubble definition and the bulk mixing appears to be quite high. For this regime $v_{gs} > 7.5$ cm/s.

It is the bubble-flow region which is of greatest interest in the design of bubble-column reactors, and so the following sections will only cover work in this regime.

BUBBLE SIZES AND BUBBLE SWARM BEHAVIOUR.

Bubble Size

The large amount of research, part of which has been described in Section 1.3.1, and the many correlations of empirical data show the complexity of this subject.

A number of workers have made attempts to measure the diameter of individual bubbles in swarms, sometimes by unspecified methods and often under ill-defined operating conditions. It is probably for these reasons that differences occur in the reported data. Most of the work has been carried out with air-water and the following survey is concerned with this system unless otherwise stated.

Pasveer[49] estimated the size of bubbles generated from an "incrusted glass" distributor (pore sizes 3 to 150 μ) and found that (1) pore-size had a large effect on bubble diameter (0.05 to 0.2 cm.) and (2) bubble diameter increased with superficial gas velocity in the range 0.05 to 0.2 cm/s.

Eckenfelder[50] also assessed the dependency of bubble diameter on gas superficial velocity, using an "Aloxite" diffuser stone. He expressed his results in the following way:

$$d_b \propto v_{gs}^{\ n} \qquad 1.31$$

with n ranging from 0.05 to 0.37 and for

$$1.8 \leqslant v_{gs} \leqslant 9.0 \text{ cm/s}$$

He also quotes an exponent of 0.15 (Equation 1.31) for a 20-hole (35 μ diameter) perforated plate for the same range of gas flows: this suggests that bubble diameter is not always strongly dependent on orifice diameter.

Shulman and Molstad[51] found that, except for low gas flow-rates, there was no dependence of bubble diameter on pore diameter when operating with both coarse metal and fine carbon distributors. They found that d_b increased from 0.3 to 0.5 cm. as the gas superficial velocity (v_{gs}) increased to 9 cm/s, at which point some slugging was noted. As v_{gs} was further increased to 15 cm/s considerable slugging was observed at the bottom of the column. They found that at a gas velocity of 4.5 cm/s "hindered" bubble flow occurred, the bubble velocity reaching a maximum. This latter observation is consistent with Fair's[52] comments that bubbles lose their individual identity at a gas superficial velocity greater than 6 cm/s. This transition was not noted by Yoshida[53]; probably because his system produced larger bubbles, which would lead to greater turbulence throughout the range.

Braulick et al[54], when working with large orifices (0.5 cm. diameter), reported an increase in bubble diameter as the gas flow-rate was increased. In their equipment the transition to slug flow occurred at a superficial gas velocity of about 2.5 cm/s: this is probably due to the relatively large orifice diameters that were used.

Koide et al[55] found no effect of porosity or plate material on bubble diameter and suggested the following correlations:

$$d_b \left(\frac{g\rho}{d_o\tau}\right)^{\frac{1}{3}} = 0.64 \left(\frac{Fr}{We^{0.5}}\right)^{0.100} \qquad 1.32$$

for bubbling without coalescence, and

$$d_b \left(\frac{g\rho}{d_o\tau}\right) = 1.65 \left(\frac{Fr}{We^{0.5}}\right)^{0.160} \qquad 1.33$$

under conditions of coalescence. In these equations Fr and We are the Froude and Weber Numbers respectively:

$$Fr = \frac{v_{gs}^2}{\epsilon^2 g d_o} \qquad 1.34$$

and
$$We = \frac{v_{gs}^2\, d_o \rho}{\epsilon^2 \tau} \qquad 1.35$$

They observed that their results with various liquids lay within the limits predicted by these two equations. Koide[55] also analysed the results of Houghton et al[20] and found that, apart from those obtained with liquids of low density, equations 1.32 and 1.33 represented the data very well.

Petrick[56], on the other hand, found the average bubble diameter to be a function of liquid velocity and reported that:

$$d_b = \frac{0.52}{v_{lt}^{0.66}} \qquad 1.36$$

for $15 \leqslant v_{lt} \leqslant 150$ cm/s. Where v_{lt} is the true liquid velocity.

The effect of gas hold-up on bubble size has been investigated by several workers[51, 57-59]. Vermeulen[58], who carried out experiments in a closed, stirred tank, found a practically linear relationship between gas hold-up and bubble diameter, viz.

$$\frac{d_b}{d_{b\,0.1}} \doteqdot 2.5\epsilon + 0.75 \qquad 1.37$$

where $d_{b\,0.1}$ is the mean bubble diameter at a fractional gas hold-up of 0.1.

Calderbank[59], when operating with an agitated tank, also observed that bubble diameters were dependent on gas hold-up. However, in a later paper[60] he reported that in a sieve-plate column, bubble size was independent of hold-up when the bubble diameter was approximately 0.3 cm., but dependent on gas hold-up when greater than 0.4 cm.

Shulman and Molstad[51] also noted that at high gas hold-ups (> 0.35) and gas velocities (> 7.5 cm/s.) the bubble diameter was dependent on gas hold-up. By contrast, Bridge et al[57], working with air/water and air/glycerine systems, found that the bubble diameter was virtually independent of gas hold-up in the former case and completely independent in the latter case (for $0 < v_{gs} \leq 2.3$ cm/s and $0.02 \leq \epsilon \leq 0.12$).

Column Pressure Drop

Shulman and Molstad[51] found that the static pressure-drop for a two-phase system was made up of the pressure-drop across the wet gas distributor and the pressure-drop due to the hydrostatic head. They found that the pressure-drop across a dry, porous plate was directly proportional to the gas superficial velocity and that there was a factor of 10 between the figures for coarse and fine distributors.

Houghton et al[20] and Koide[55] showed that the pressure-drop across a porous distributor was inversely proportional to the porosity, viz.

$$d_o = \frac{4\tau}{\Delta P} \qquad 1.38$$

where τ is the surface tension of the liquid-phase, P is the wet pressure-drop and d_o is the mean pore-size. The values of d_o calculated from equation 1.38 were within ± 15% of the values given by the manufacturer.

Bubble Rise Velocity

The rise velocity of bubbles through a liquid, individually and in swarms, has been reported by several workers (see also Section 1.3.1).

Sideman et al[36] suggest that the gas hold-up is directly related to the rise velocity of bubbles in swarms, v_{bs}, in the following way:

$$\epsilon = \frac{v_{gs}}{v_{bs}} \qquad 1.39$$

However, for spherical bubbles at low bubble Reynolds Numbers Harmarthy[61] suggests that

$$v_{bs} = 1.74 \left(\frac{g \Delta\rho \, d_b}{\rho_l} \right)^{0.5} \qquad 1.40$$

and for moderately ellipsoidal bubbles at a bubble Reynolds Number greater than 500

$$v_{bs} = 1.53 \left(\frac{g \; \Delta\rho \; \tau}{\rho_1} \right)^{0.25} \qquad 1.41$$

On the other hand Van Krevelen[14] proposed that

$$v_{bs} = \left(\frac{g \; d_b}{2} \right)^{0.5} \qquad 1.42$$

without specifying any limits on flow-rate and bubble diameter. Both of these workers [14 and 61] indicate that the rise velocity is strongly dependent on bubble size. Quigley, Johnson and Harris[16] obtained similar results, although they expressed the rise velocity in terms of orifice diameter, d_o, viz.

$$v_{bs} = 32.8 \left(v^* \; d_o^{\,2} \right)^{0.16} \qquad 1.43$$

Equation 1.43 was obtained when operating with a small but undefined liquid velocity. Also, all the equations from 1.40 to 1.43 inclusive only hold at low gas hold-ups where there is no inter-bubble hinderance. At high gas flows when hindered flow conditions exist, both visual and experimental results obtained by Shulman[51], West et al[62] and Yoshida[53] indicate that there is an increase in bubble rise velocity.

Calderbank[59], using a sieve-plate (100 orifices of unspecified diameter), found that the rise velocity of bubbles was constant (26.5 cm/s) for gas hold-ups less than 0.7, gas superficial velocities less than 1.5 cm/s and bubble diameters ranging from 0.2 cm. to 0.4 cm.

According to Nicklin[63], the rise velocity of bubbles in swarms is dependent on the gas velocity, gas hold-up and the liquid velocity according to the equation:

$$v_{bs} = \frac{v_{gs}}{\epsilon} - (v_{gs} - v_{ls}) \qquad 1.44$$

Since $(v_{gs} - v_{ls})$ can be expressed as the relative superficial velocity, v_{Rs},

$$\text{then} \quad v_{bs} = \frac{v_{gs}}{\epsilon} - v_{Rs} \qquad 1.45$$

Wallis[64] has attempted to correlate the bubble swarm velocity, gas superficial velocity and gas hold-up from first principles and obtained the equation:

$$v_{gs} = v_{bs}\,\epsilon(1 - \epsilon) \qquad 1.46$$

On plotting data for air/water systems obtained by Verchoor[65], Novasad[66] and Kolbel[67], Wallis[64] obtained the following relationship:

$$v_{gs} = 19.2\,\epsilon(1 - \epsilon) \qquad 1.47$$

This indicates that the swarm velocity has a constant value of 19.2 cm/s for any hold-up.

Towell et alia[68] have related the rise velocity of bubbles in swarms to the true relative velocity of the system by the equation:

$$v_{Rt} = v_{\infty} + 2\,v_{gs} \qquad 1.48$$

They have also suggested that v_{∞} is approximately 30 cm/s for bubbles with diameters from 0.1 to 0.5 cm.

Mendelson[69] put forward an empirical correlation that seems to represent the experimental data quite well for bubble diameters greater than 0.15 cm: this is

$$v_{\infty} = \sqrt{\frac{2\,\tau}{\rho_l\, d_b} + g\,\frac{d_b}{2}} \qquad 1.49$$

Later Maneri and Mendelson[70] extended this correlation for predicting the rise velocity of single large bubbles, v_∞, in large columns:

$$\frac{v_c}{v_\infty} = \sqrt{\tanh\left(0.25 \ \frac{d_c}{d_b}\right)} \qquad 1.50$$

where v_c is the rise velocity of a single bubble in a narrow tube. By using the cell model of Happel[71] and Marrucci[72], who found that

$$\epsilon = \left(\frac{d_b}{d_c}\right)^3 \qquad 1.51$$

equation 1.50 can be further modified to give

$$v_{bs} = v_\infty \sqrt{\tanh\left(0.25 \ (\epsilon)^{\frac{1}{3}}\right)} \qquad 1.52$$

If $d_c = d_b$ (i.e. slug flow in quiescent liquid) equation 1.50 represents the rise velocity of gas slugs in a quiescent liquid medium which Maneri[70] simplified to

$$v_{sl} = 0.35 \sqrt{g \ d_s} \qquad 1.53$$

where v_{sl} and d_s are the rise velocity and diameter respectively of slugs. This is the familiar Dumitrescu[73] equation, which can be modified to give equations similar to those of Nicklin[46] and Van Krevelen[74] for the rise velocity of large slugs.

Freedman and Davidson[39] have used two equations to correlate gas superficial velocity, gas hold-up and bubble swarm velocity. The first is based on Turner's[75] equation, viz.

$$v_{bs} = \frac{v_\infty}{1 - \epsilon} \qquad 1.54$$

and the second on the Marrucci[72] equation:

$$v_{bs} = \frac{v_{\infty} (1 - \epsilon)^2}{(1 - \epsilon^{1.66})} \qquad 1.55$$

which holds for $1 \leqslant Re \leqslant 300$,

where $$Re = \frac{\rho_l \, v_{\infty} \, d_b}{\mu_l} \qquad 1.56$$

By assuming that the slip velocity was equal to the true relative velocity, Freedman and Davidson[39] obtained

$$v_{gs} = v_{\infty} \cdot \epsilon \qquad 1.57$$

using equation 1.54 and

$$v_{gs} = \frac{\epsilon (1 - \epsilon)}{(1 - \epsilon^{1.66})} v_{\infty} \qquad 1.58$$

using equation 1.55

Gas Hold-up

The gas hold-up in a bubble column characterises the gas retention by the liquid-phase and is clearly an important operating parameter. A considerable number of workers have obtained information relating to gas hold-up for all regimes of bubbling. Unfortunately, the results of the various researchers are not always in very good agreement. In this subsection, some reference is also made to regimes outside the bubble-flow regime.

One of the earlier hold-up correlations is the well-known Lockhart-Martinelli[26] correlation. (See Fig. 1.4)

The laminar and turbulent flow regimes are arbitrarily defined at superficial Reynolds Numbers of less than 1000 or greater than 2000 respectively. The correlation is presented in the form of a graph in which an empirical function, ϕ, is plotted against a pressure parameter, X, where

$$\phi_g^2 = \frac{(\Delta P/\Delta Z)_{TP}}{(\Delta P/\Delta Z)_g} \quad \text{or} \quad \phi_l^2 = \frac{(\Delta P/\Delta Z)_{TP}}{(\Delta P/\Delta Z)_l} \qquad 1.59$$

and

$$X^2 = \frac{(\Delta P/\Delta Z)_l}{(\Delta P/\Delta Z)_g} \qquad 1.60$$

$(\Delta P/\Delta Z)_l$ and $(\Delta P/\Delta Z)_g$ are calculated from conventional single-phase correlations on the basis that liquid or gas is flowing in the column alone at the same mass-flow rate as in the two-phase case.

Fig. 1.4 shows the relationships between hold-up, X, ϕ_g and ϕ_l .

Hughmark and Pressburg[76] correlated data for vertical two-phase flow in terms of the slip velocity, v_s, and $(\Delta P_{TP} - \Delta P_l)/\Delta Z$. They obtained a family of curves which could be defined in terms of a parameter, Ψ . Ψ was predicted from the empirical equation:

$$\Psi = {}^1/_{\,l^{0.147}}\ \tau^{0.194}\ (G_m + L_m)^{0.07} \qquad 1.61$$

where $(G_m + L_m)$ is the total mass flow-rate.

A modification of the Lockhart-Martinelli[26] correlation is that due to Chisholm and Laird[77], who accounted for tube roughness in the turbulent/turbulent regime, using the basic equation:

$$\phi^2 = 1 + \frac{21}{X} + \frac{1}{X^2} \qquad 1.62$$

Hughmark and Pressburg statistically analysed their own and other data for vertical flow. They found that when the Lockhart-Martinelli parameter X was estimated from the empirical equation:

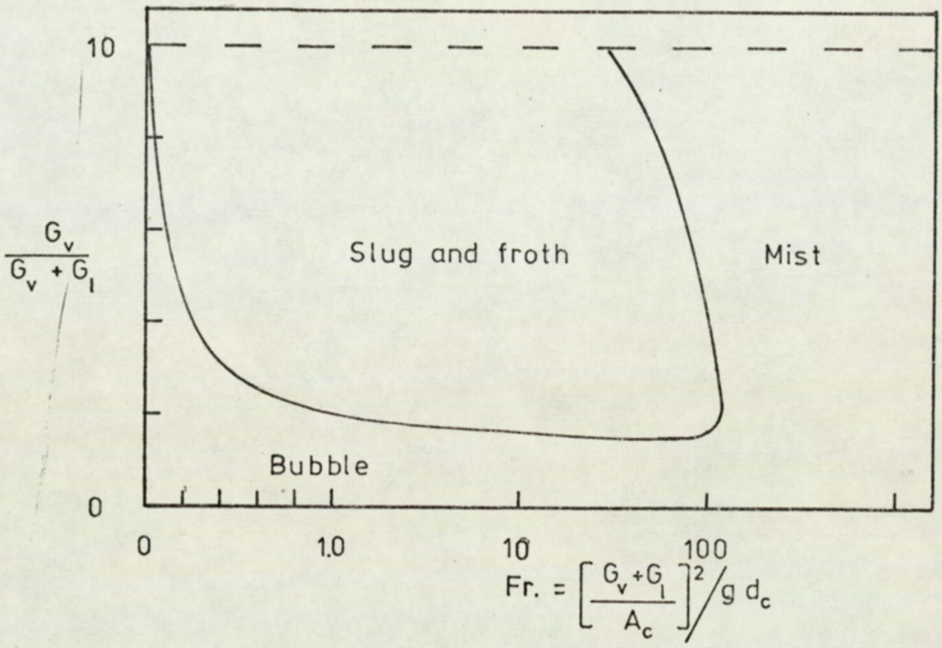

FIG 1.3 Flow régimes map.

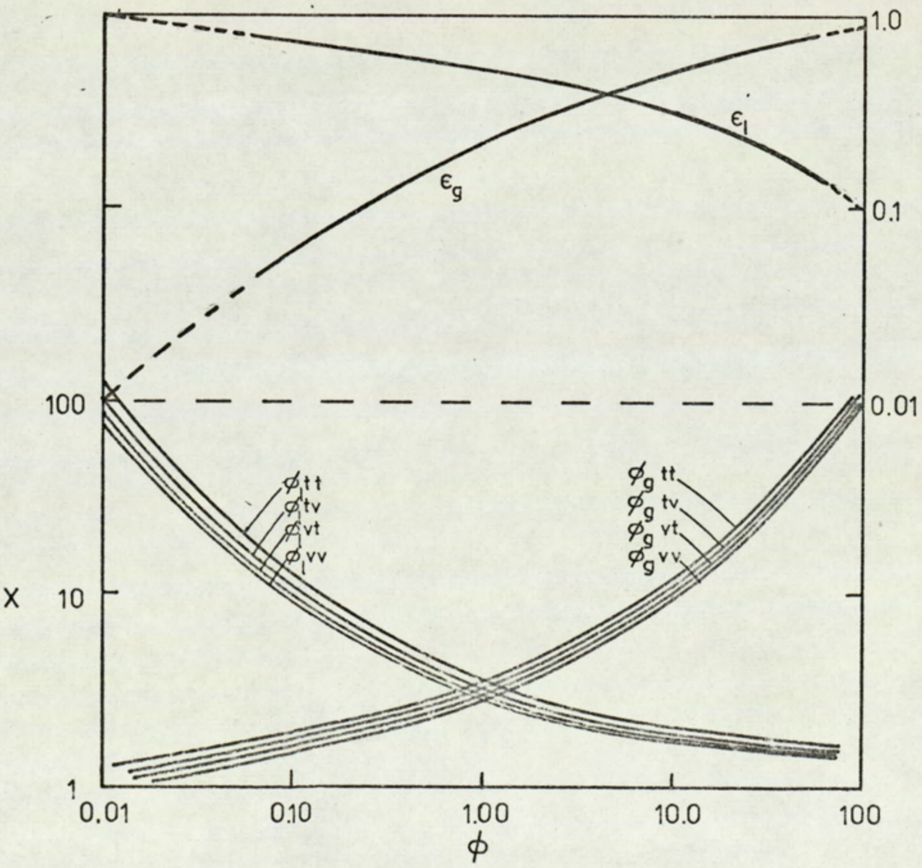

FIG 1.4 Lockhart-Martinelli corelation.

$$X = \left(\frac{G_m}{L_m}\right)^{0.9} \frac{\mu_l^{0.19}\ \tau^{0.205}\ \rho_g^{0.70}}{G_m^{0.435}\ \rho_l^{0.72}} \qquad 1.63$$

gas hold-up could be predicted with an average deviation of ± 0.038 for air and a variety of liquids in columns of diameters from 1.0 to 5.9 cm.

Another analysis of two-phase flow, proposed by Bankhoff[78], makes use of a different model. The two-phase system is treated as a single-phase fluid, having a variable radial density due to the bubble population being greatest at the centre of the column. Then by making a number of simplifying assumptions Bankhoff arrived at the following relationship:

$$\epsilon = K \left(\frac{G_v + L_v}{G_v}\right) \qquad 1.64$$

According to Bankhoff, bubble-flow occurs up to a gas hold-up of 0.8 and he shows that in this range, with $K = 0.89$, equation 1.64 fits the experimental data well.

It is interesting to compare the results obtained by Bankhoff with Nicklin's[46] analysis of slug-flow. Nicklin arrived at the following result:

$$v_{bs} = 1.2 \left(\frac{G_v + L_v}{A_c}\right) = \frac{G_v}{\epsilon A_c} \qquad 1.65$$

or

$$\epsilon = \frac{0.83\ G_v}{(G_v + L_v)} \qquad 1.66$$

Equation 1.66 is of the same form as equation 1.64.

Hughmark[79] extended this approach to the correlation of a wide range of data for air/water systems. Equation 1.64 was used with a variable value of K (from 0.15 to 0.98), where K is given by the relationship:

$$K = f \frac{(Re)^{1/6} \quad (Fr)^{1/8}}{(1 - \epsilon)^{1/4}} \qquad 1.67$$

In equation 1.67 Re and Fr are the superficial Reynolds and Froude Numbers for the mixture, and ϵ is the volumetric gas hold-up, assuming that there is no slip between the phases. When compared with experimental data, the predicted values differ by up to 30%.

Gomezplata and Nichols[80] have suggested a very simple way of estimating gas hold-up, viz.

$$\epsilon = v_{gs} \; (\phi + v_{gs} + v_{ls})^{-1} \qquad 1.68$$

where ϕ is a characteristic velocity parameter which for upward flow of gas and liquid equals 60 cm/s. If v_{ls} is put equal to zero then equation 1.68 reduces to

$$\frac{1}{\epsilon} = \frac{60}{v_{gs}} + 1 \qquad 1.69$$

Assuming that $v_{\infty} \simeq 30$, this equation reduces to:

$$\frac{1}{\epsilon} = \frac{2\, v_{\infty}}{v_{gs}} + 1 \qquad 1.70$$

which, when multiplied through by v_{gs}, leads to:

$$\frac{v_{gs}}{\epsilon} = v_{Rt} = 2\, v_{\infty} + v_{gs} \qquad 1.71$$

which is similar in form to the equation proposed by Towell et al[68] if v_{gs} and v_{∞} are of the same order (equation 1.48)

Wallis[64] has predicted gas hold-up for air/water systems using equation 1.47:

$$v_{gs} = 19.2\,\epsilon\,(1 - \epsilon) \qquad 1.47$$

This gives reasonable results for values of gas hold-up up to about 0.2. Above this value ϵ tends to break away and levels out at about 0.4. However, for non-coalescing systems, equation 1.47 is in good agreement with Wallis' experimental data for gas hold-ups up to 0.3.

Hughmark in another paper[81] summarises data for a wide range of column sizes and liquid physical properties by the equation:

$$\epsilon = v_{gs}\left(\frac{72}{\rho_l \tau}\right)^{-\frac{1}{3}} \qquad 1.72$$

Mashelkar[40] in a recent review has suggested for air/water systems that the equation:

$$\epsilon = \frac{v_{gs}}{30 + 2\,v_{gs}} \qquad 1.73$$

should be used. For systems other than air/water, he recommends the expression:

$$\epsilon = \left(\frac{v_{gs}}{30 + 2\,v_{gs}}\right)\left(\frac{1}{\rho_l}\right) / \left(\frac{72}{\tau}\right)^{\frac{1}{3}} \qquad 1.74$$

which, although taking into account variations in density and surface tension, neglects viscosity, an important variable.

Calderbank[82] found that on sieve trays gas hold-up was dependent only on gas superficial velocity and gas density, according to the relationship

$$\ln\left[\frac{1}{1-\epsilon}\right] = 1.58\,v_{gs}\sqrt{\rho_g} + 0.45 \qquad 1.75$$

This result is confirmed by the work of Leibson et al[15] for the range of gas superficial velocities from 10 to 75 cm/s. In the upper part of this range froth formation is observed. In the lower range of gas velocities the experimental data of most workers appears to follow an almost linear relationship between gas hold-up and gas superficial velocity, of the form:

$$\epsilon = \frac{v_{gs}}{K} \qquad 1.76$$

Values of K taken from the literature are listed in Table 1.2. At higher gas velocities the hold-up was found to level off at some value between 0.25 and 0.8, depending on the system being studied.

Table 1.2 Effect of Gas Flow-Rate on Gas Hold-up.

Reference	K	Operating Conditions *
Shulman and Molstad[51]	17.4	$v_{gs} \leqslant 6.0$ cm/s
Bridge et al[57]	21.5	$v_{gs} \leqslant 3.0$ cm/s $0.2 \leqslant d_b \leqslant 0.34$ cm $v_\infty = 23.5$ cm/s
Fair et al[52]	9	$v_{gs} \leqslant 5.0$ cm/s 1" and 2" column
"	16.7	" 4" column
"	33.4	" 18" and 42" column
Reith et al[83]	25.0	$v_{gs} \leqslant 50.0$ cm/s **
Argo and Cova[84]	20.0	unspecified
Braulick et al[54]	33.0	$L/D = 7$ air/sulphite solution $v_{gs} \leqslant 10$ cm/s
"	35.5	$L/D = 7$ $v_{gs} \leqslant 5$ cm/s
Houghton et al[20]	24.5	$v_{gs} \leqslant 5.0$ cm/s
"	11.1	" air/sea water
"	11.1-75.6	" air/acetic acids

* Air/Water systems unless otherwise stated.

** Slug flow occurred at $v_{gs} \geqslant 5.0$ cm/s in a 5 cm column but not observed at $v_{gs} < 45$ cm/s in larger columns.

EFFECT OF COLUMN GEOMETRY.

Column Diameter

In general most workers have found that as the column diameter is decreased, so the gas hold-up for a given gas flow-rate increases.

Fair[52] and Yoshida[53] found no effect of column diameter when this exceeded 15 cm., but a slight decrease was reported by Yoshida for the case of a 7.5 cm. column.

Shulman[51] found that changing from a column diameter of 5 cm. to one of 10 cm. has no effect on hold-up. However, a slight increase was observed when using a 2.5 cm. column at a fixed gas velocity.

Reith et al[83] have suggested that the critical column diameter is about 5 cm.; certainly there was no effect when the diameter exceeded 14 cm. Unfortunately no data was obtained for columns of intermediate diameter.

Ellis and Jones[85] indicate that wall-effects increase the value of gas hold-up in columns less than 7.5 cm. diameter, but not with diameters greater than 7.5 cm. They also found that perforated baffles increase the gas hold-up significantly. This is confirmed by Fair[52] who reported that when the baffles were vibrated even greater hold-ups could be obtained at any given superficial gas velocity.

Bischoff and Phillips[86] also looked at gas hold-up in a column containing a number of perforated plates. They observed that the gas hold-up tended to level out at about 0.35 at a gas velocity of 18 cm/s and that the plate spacing had only a slight effect on gas hold-up.

Similar results were noted by Argo and Cova[84] and some of Braulick's[54] data show similar trends.

Column Height

In general no effect of column height on gas hold-up has been reported. Bridge et al[6] found that there was a 12% increase in gas hold-up at the top of a column operated counter-currently, but Sideman et al[36] observed no difference when operating co-currently. This latter result was confirmed by Fair[52].

Effect of Bubble Diameter and Orifice Diameter

Yoshida[74] found appreciably lower gas hold-ups when operating at similar gas flow-rates to other workers, when using larger-holed orifices. Bartholomew et al[87] also found this to be the case when changing from orifice plate to porous plate distributors: however, within each group of distributors, very little effect of orifice or pore diameter was noticed. This was confirmed by Van Krevelen[14], Quigley et al[16] and Shulman and Molstad[51]. Fair et al[52], however, found somewhat larger gas hold-ups than the above workers when operating with fritted glass discs (for which no pore sizes were given).

Houghton, McLean and Ritchie[20] found that plate porosity had little effect on gas hold-up in general, although a porous bronze disc (porosity approximately ten times that of glass) showed a slight variation of gas hold-up with throughput when operating with water. With glycerol, however, the results showed that even a 15% change in porosity had an appreciable effect on gas hold-up (approximately 200% difference).

Dukler et al[88] have gathered a considerable amount of existing data and applied many of the existing correlations to it and found that Hughmark's[79] best represented the existing data. Bhatia[89] has also correlated some of the existing data and found that Mendelson's[69] correlation is very good (see Figs. 1.5 to 1.6).

Distribution of Gas Phase

Freedman and Davidson[39] report a decrease in hold-up of approximately 60% for a decrease in operational area of the base of the column of 85%, the bulk of which (40%) occurs when the operational area decreases from 100% to 62%.

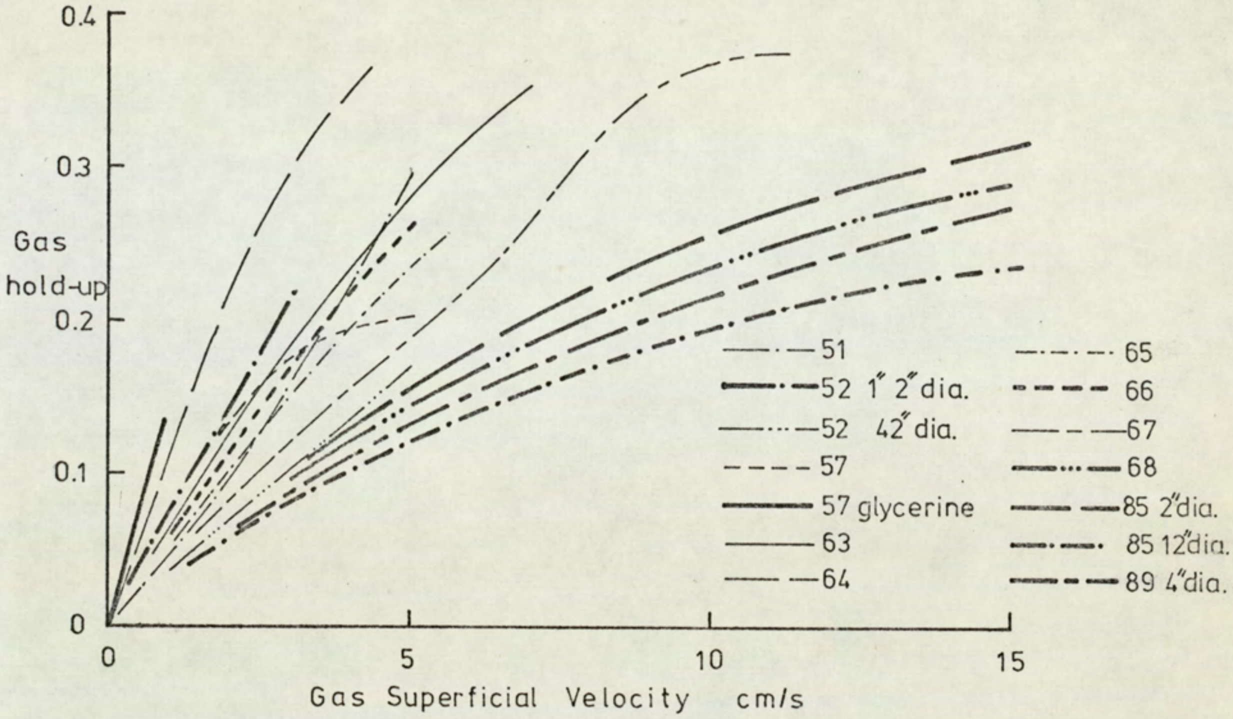

FIG 1.5 Gas hold-up as a function of gas flow.

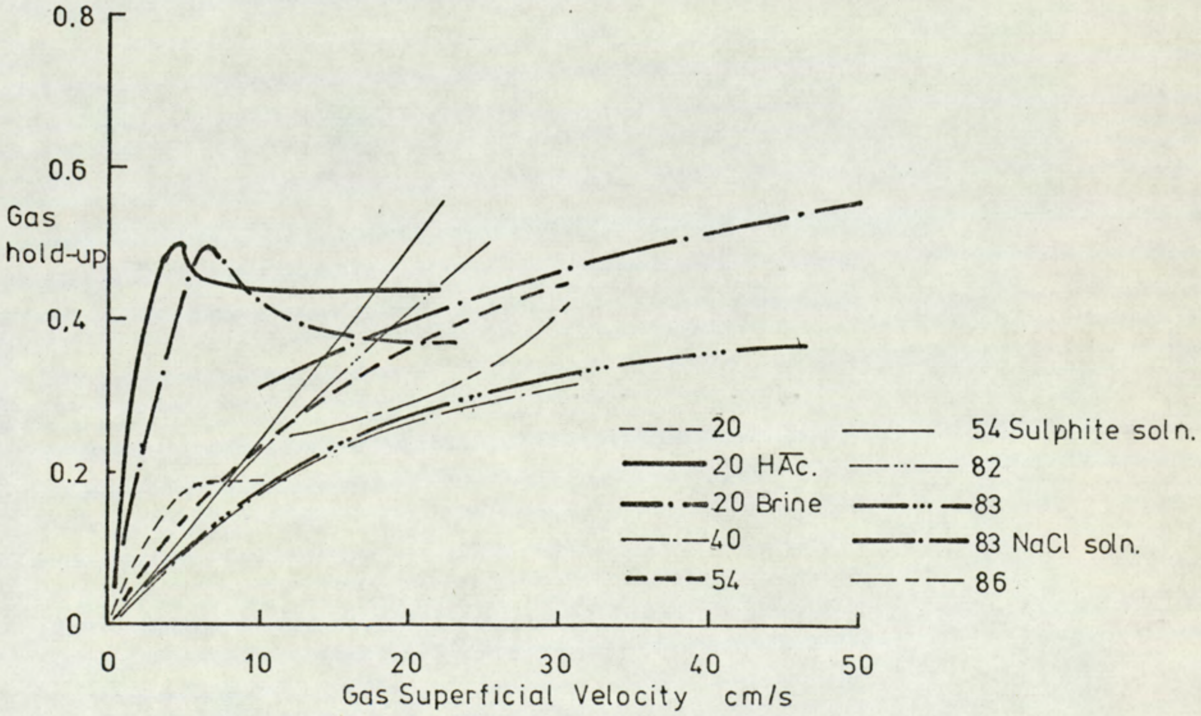

FIG 1.6 Gas hold-up as a function of gas flow.

This survey shows that gas fractional hold-up is not a simple function of gas superficial velocity, the published data showing widely differing results. These differences may be due in part to the following:

1. different gas distributors giving different bubble diameters for similar superficial gas velcoities;

2. surface active effects influencing both the formation and subsequent coalescence and/or break-up of bubbles;

3. liquid circulation, induced by bubbles, profoundly changing the gas hold-up;

4. liquid flow in the column itself;

and 5. maldistribution of the gas-phase.

1.3.3 LIQUID-PHASE MIXING IN BUBBLE COLUMNS.

Mixing Models and Axial Dispersion.

In spite of the extensive use made of bubble columns, little consistent information concerning the relationship between gas and liquid velocities, gas hold-up fraction and longitudinal mixing has been published. Longitudinal fluid mixing in bubble columns has been studied qualitatively by Othmers and Rase[90] and quantitatively by a number of other workers[68, 83, 84, 86, 90-95, 98, 102-106].

Othmers and Rase[90] studied two basic systems involving single and multiple-hole orifice plates. With the single-hole orifice they observed that the fluid flow at the walls of the column was in the opposite direction to the bulk flow of the liquid and concluded that considerable back-mixing was taking place. However, they found that with the multiple-hole orifice plate the flow patterns were significantly different; they noted that the eddies produced were much smaller and they concluded that there was very little back-mixing taking place. On the basis of these observations, they suggested that each section of the system could be divided into different zones. The three zones were designated as:

(1) turbulent, where the fluid motion was very turbulent and the gas-phase was distributed as very small discrete bubbles;

(2) dispersed, where the gas was finely divided but the liquid-phase was no longer turbulent; and

(3) coalesced, where the gas bubbles were beginning to coalesce and were no longer finely divided.

Towell et al[68] analysed high speed motion pictures taken during the operation of a 40 cm. diameter column. They observed turbulent eddies (with a scale approximately equal to the column diameter) and systematic large-scale circulation patterns superimposed on this random eddying. Their films confirmed the observation of Othmers and Rase[90] that the liquid at the wall was flowing downwards when the bulk-flow was upwards.

In contrast, Reith et al[83] found no evidence of a systematic circulation pattern. They also showed that the radial mixing was so complete that large circulation patterns could not be effective in describing axial mixing. Fig. 1.7 shows the basis of the model they used to interpret their experimental data. The tracer is injected at the plane $l = lt$ which is perpendicular to the direction of the liquid-flow. The tracer is then transported down the column by eddy diffusion, and since under steady-state conditions there is no nett transport of tracer across any cross-section, a mass balance leads to

$$D_l \frac{dC}{dl} - v_{lt} C = 0 \qquad 1.77$$

where D_l is the dispersion coefficient (cm^2/s), C is the concentration of tracer in (g/cm^3), l is the axial distance (cm) and v_{lt} is the true liquid velocity (cm/s). Using equation 1.77 and the boundary condition

$$C = C_o \quad \text{at} \quad l = l_t \, ,$$

leads to

$$\frac{C}{C_o} = \exp\left[\frac{v_{lt} \cdot (l_t - l)}{D_l}\right] \qquad 1.78$$

Having analysed their experimental data Reith et al[83] found that the axial dispersion in the fluid-phase was characterised by a nearly constant Peclet Number (Pe_d) based on column diameter. The numerical value of Pe_d was 3.0 ± 0.2 for superficial gas and liquid velocities upto 45 cm/s and 2.0 cm/s respectively. A constant value for Pe_d implies that D_l increases as column diameter is increased. This is probably due to the formation of larger eddies in the bigger columns. Frequently column length rather than diameter is used in defining the Peclet Number: the relationship between the two is

$$Pe_l = \frac{v_{lt}\, l}{D_l} = \frac{v_{lt}\, l}{v_{Rt}\, d_c} \quad Pe_d \simeq 3\, \frac{v_{lt}\, l}{v_{Rt}\, d_c} \qquad 1.79$$

where v_{lt} and v_{Rt} are the true liquid velocity and true relative velocity respectively and l and d_c are the column length and diameter respectively.

It should be noted that equation 1.79 is valid for $v_{gs} > 10$ cm/s; this is well within the so-called turbulent regime defined by Fair[48] (see page 21)

Recently Argo and Cova[84] studied backmixing in three sizes of columns (4.6, 10.2 and 44.8 cm diameter) in which there was a counter-current flow of gas and liquid. Tracer was injected continuously into the top of the column and the steady-state concentration profile over the length of the

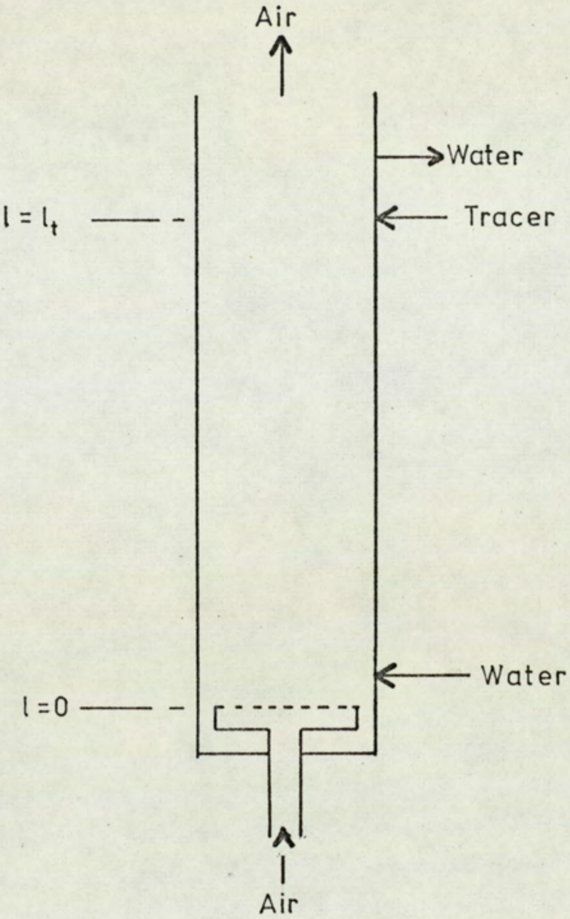

FIG 1.7 Basis for the Reith[83] mixing model.

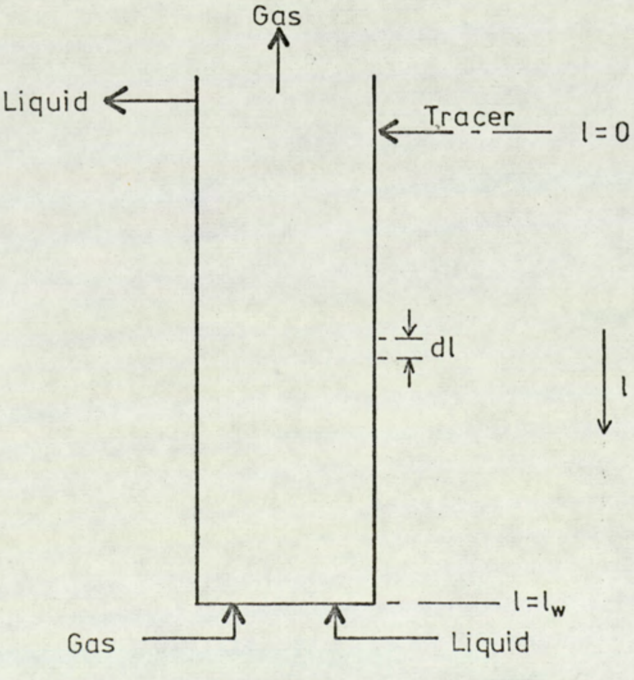

FIG 1.8 Basis for the Argo-Cova[84] mixing model.

column was measured. In such a system the longitudinal mixing of the liquid tends to carry the tracer upstream of the injection point, whilst the bulk flow of the liquid-phase tends to carry the tracer out of the column. (Gilliland and Mason[91] have used a similar approach when analysing flow in fluidised beds.) When an unsteady-state material balance on the tracer component is taken across the section dl of the column (see Fig. 1.8), the following equation is obtained:

$$\frac{A_c}{D_l}\frac{\partial C}{\partial t} = 0 = A_c \frac{\partial^2 C}{\partial l^2} - A_c \frac{v_{lt}}{D_l}\frac{\partial C}{\partial l} \qquad 1.80$$

This can be solved under steady-state conditions using the following boundary conditions:

$$C = C_l \text{ at } l = 0 \qquad 1.81$$

$$\left.\frac{dC}{dl}\right|_{l(-)} + \frac{v_{lt}}{D_l} C_{l(-)} = \frac{v_{lt}}{D_l} C_o \qquad 1.82$$

$$\text{at } l = l_w$$

where C_o is the concentration of tracer entering the column and C_l is the concentration of tracer in the outflowing liquid. The final result is

$$(C - C_o) = (C_l - C_o) \exp.\left(\frac{-v_{lt}.l}{D_l}\right) \qquad 1.83$$

This equation is of the same mathematical form as that used by Reith et al[83]. Using this model Argo and Cova found that the dispersion coefficient increased steadily with an increase in gas superficial velocity until slugging occurred: at this point there was a marked increase in D_l (as much as ten-fold) but thereafter only a slight increase with gas flow-rate was observed. They also found that the presence of baffles reduced the dispersion coefficient for a fixed gas flow-rate and by moving the baffles an even greater decrease was achieved. The dispersion coefficient was found to increase with column diameter: in fact a ten-fold increase in diameter caused the dispersion coefficient to increase by at least 20 times.

Bischoff and Phillips[86] have measured the dispersion coefficients in a 2.5 cm. column by injecting a pulse of tracer into the liquid feed and measuring the change in tracer-concentration downstream. They then estimated the axial dispersion coefficient from the variance of the residence time distribution curve (see also Section 4.2). If end-effects can be neglected, it can be shown that the variance, σ , is related to D_l by

$$\sigma^2 = 2 \frac{D_l}{v_{lt}\, l} \qquad 1.84$$

The results obtained using both single and multiple-hole orifice plates show that the mixing is relatively intense in both cases, about 2 to 3 times greater than for single-phase liquid-flow. The value of Pe_l was about 4.0 at a superficial gas velocity of approximately 12 cm/s in a column 15 cm. in diameter. Although there is quite a spread in the results reported by Bischoff and Phillips, they are similar in magnitude to those of Argo and Cova[84].

Dal'man and Zhilyaeva[92] investigated the longitudinal mixing occurring in bubble columns ranging in diameter from 4.1 to 29.6 cm. and operated counter-currently. The values of the dispersion coefficient were found under steady-state and transient conditions. The theoretical treatment was based on the work of Taylor[93], who showed that for single-phase, laminar flow with

$$\frac{l}{d_c} \gg \frac{1}{30} \, Re \, Pr$$

the effective longitudinal dispersion coefficient (D_l) can be determined from the equation:

$$Pe_d^{-1} = \frac{1}{192} \text{ Re Pr} , \qquad 1.85$$

where Pr is the Prandtl Number given by

$$Pr = \frac{\nu}{D_m} , \qquad 1.86$$

ν being the kinematic viscosity and D_m the molecular diffusivity. For the turbulent regime, Taylor[93] obtained the relationship:

$$Pe_d^{-1} = 1.79 \ (\lambda)^{\frac{1}{2}} \qquad 1.87$$

where λ is the coefficient of friction.

Ohki and Inoue[94] approached the problem in a slightly different way by using Fick's equation for one dimensional diffusion, viz.

$$\frac{\partial c}{\partial t} = D_l \frac{\partial^2 c}{\partial l^2} \qquad 1.88$$

with the following boundary conditions:

$$\frac{\partial c}{\partial l} = 0 \text{ at } l = 0 \text{ and } l = l_h$$

where l_h is the height of the bubble column, and the initial conditions:

$$C\,(l,0) = C_o \text{ for } 0 \leqslant l \leqslant l_t \qquad 1.89$$

$$\text{and} \quad C\,(l,0) = 0 \text{ for } l \geqslant l_t \qquad 1.90$$

where l_t is the height of the column filled with tracer. The solution of this set of equations leads to:

$$\frac{C}{C_E} = 1 - \frac{2\,l_h}{\pi\, l_t} \sum_{n=1}^{\infty} \left[\frac{1}{n} \sin\left(\frac{n\pi}{l_h}\, l \right) \cos\left(\frac{n\pi}{l_h} \right) \right.$$

$$\left. \cdot\, Z \;\exp. \left\{ - \left(\frac{n\pi}{l_h} \right)^2 D_l\, t \right\} \right] \qquad 1.91$$

where $C_E \; l_h = C_o \; l_t$ 1.92

If $n\, l_t \leqslant l_h$ this simplifies to

$$\frac{C}{C_E} = 1 + 2 \sum_{n=1}^{\infty} \left[\left(\cos \frac{n}{l_h}\; l \right) \exp\left(- n^2\, \frac{\pi^2}{l_h^{\,2}}\; D_l\, t \right) \right] \qquad 1.93$$

where C_E is the equilibrium tracer concentration and t is time. Plots of C/C_E and $D_l\,(\pi/l_h)^2\,t$ with l/l_h as a parameter were then used to estimate D_l from the experimental data. Having evaluated the dispersion coefficients Ohki and Inoue then correlated their results using an equation similar in form to that of Taylor[93] and the extension of Aris[95], viz.

$$D_l = \frac{d_c^{\,2}\; v_c^{\,2}}{k\, D_m} + D_m \qquad 1.94$$

where v_c is the maximum liquid velocity at the column axis and k is determined by the form of the velocity distribution. When applied to bubble-columns, Ohki and Inoue assumed that D_m could be replaced by D_B, a diffusion coefficient based on bubble motion. The characteristic velocity, v_c, has been studied previously[96] and related to v_{gs} by the equation:

$$v_c = 24\, v_{gs}^{\;0.6} \qquad 1.95$$

Consequently equation 1.94 becomes:

$$D_l = \frac{576\ d_c^{\ 2}\ v_{gs}^{\ 1.2}}{\kappa\ D_B} + D_B \qquad 1.96$$

To use equation 1.96, D_B must first be estimated at extremely low gas flow-rates. Data obtained by Kato[97] and also by Reith[61] can be used for this purpose and a value of about 10 cm^2/s is obtained. It is then possible to estimate κD_B using equation 1.96 and experimental data. Ohki and Inoue[94] did this and found that for large columns:

$$D_l = 0.30\ d_c^{\ 2}\ v_{gs}^{\ 1.2} + D_B \qquad 1.97$$

A rather more accurate value for D_B was then obtained, using iterative calculations and finally D_B was related to the pore diameter of the gas distributor, d_o, by the equation:

$$D_B = 170\ d_o \qquad 1.98$$

The complete correlation for air/water systems presented by these workers was:

$$D_l = 0.30\ d_c^{\ 2}\ v_{gs}^{\ 1.2} + 170\ d_o \qquad 1.99$$

By further manipulation of the experimental data they obtained a relationship between the dispersion coefficient, the column diameter (d_c) and the gas hold-up (ϵ):

$$D_l = \frac{14\ d_c}{(1-\epsilon)^2} \qquad 1.100$$

This is valid in the regime of bubble flow, where coalescence is starting, whereas equation 1.99 is valid in the bubble-flow regime only.

Aoyama et al[98] also used a one-dimensional diffusion model to analyse their data. Their experiments were based on the measurement of temperature profiles within bubble columns. Then, using the analogy between heat- and mass-transfer, they estimated values of D_l using an equation similar in form to equation 1.83.

Radial Dispersion

Reith et al[83] investigated the extent of radial mixing by introducing a steady stream of tracer at the axis of the column and measuring the concentration downstream of the injection point at several radial positions. They found that for a gas superficial velocity of 9.3 cm/s and liquid superficial velocity (co-current) of 1.6 cm/s, the radial concentration gradient had completely disappeared within 4.4 cm. of the injection point.

1.3.4 REVIEW OF EXPERIMENTAL RESULTS

Effect of Gas Superficial Velocity.

In general, all the results show that the dispersion coefficient (calculated from a Peclet Number based on either column or bubble diameter) show a marked increase with increasing gas superficial velocity. Siemes and Weiss[98] found a 20-fold increase in the axial dispersion coefficient (2.5 to 50 cm^2/s) for a 5-fold increase in gas superficial velocity (1.5 to 7.5 cm/s). Both Argo and Cova[84] and Tadaki and Maeda[99] found that D_l was approximately constant (7 cm^2/s) until the superficial gas velocity was greater than 2.5 cm/s. Beyond this point D_l rose approximately linearly with superficial gas velocity ($D_l \simeq 60$ cm^2/s at $v_{gs} \simeq 6.5$ cm/s). Aoyama[98] observed a similar but less marked change in D_l as the superficial gas velocity was increased. The dispersion coefficient increased 20-fold for a 10-fold increase in v_{gs}.

Bischoff and Phillips[86] reported a rapid increase in D_l with v_{gs},

Pe_l^{-1} increasing from 0.1 to 17.0 as the gas superficial velocity was changed from 2.4 to 10 cm/s. At $v_{gs} > 10$ cm/s, Pe_l^{-1} was observed to fall to a minimum value and then increase again. The transition point noted by these workers[86] ($v_{gs} \simeq 10$ cm/s) corresponds to the condition at which Siemes and Borchers[100] observed the onset of bubble coalescence.

The equation used by Ohki and Inoue[94] for correlating their data has already been introduced (see page 47). The same equation fits the results of Tadaki and Maeda[99], Kato[97] and Aoyama et al[98] to within about 5% at higher values of D_l and to within about 30% at low values.

Dal'man and Zhilyaeva[92] found very good agreement with Taylor's[87] model when operating with a single-phase system. They found a steady increase in D_l with increasing flow-rate (plotted as Reynolds Number), the transition between equations 1.85 and 1.87 occurring at a Reynolds Number of approximately 250. This transition was also noted by Levenspiel[101]. When operating with a gas-liquid system, the transition between the two equations occurred at a Reynolds Number between 1800 and 2100, depending on the liquid-phase velocity.

Effects of Column Diameter.

Tadaki and Maeda[99] noted an increase of about 50% in D_l (based on d_c) when the diameter of the column was increased from 4.2 to 6.3 cm.

Argo and Cova[84] observed a 20-fold increase in D_l when the column diameter was increased by a factor of 10. With a 45 cm. diameter column values of D_l from 1000 to 1750 cm^2/s were obtained. Fair[48], when using the same column under the same operating conditions, reported even higher values for D_l, of the order of 5000 cm^2/s.

Aoyama et al[98] noted that the value of D_l was almost proportional to column diameter to the power 1.5, at a fixed gas velocity. They also altered liquid physical properties, but the effect on D_l was relatively small.

Reith et al[83] have also found that column diameter has a significant effect on the dispersion coefficient, higher values of D_l being obtained with the larger columns throughout the flow range.

Effect of Liquid Velocity.

Dal'man and Zhilyaeva[92] noted that D_l was practically independent of the liquid velocity for values up to 4 cm/s, but then found a sharp increase in the dispersion coefficient for $v_{lt} > 4.0$ cm/s.

Reith et al[83] found that, when operating with a 5.1 cm. column D_l was greater during co-current flow than during counter-current flow. However, this difference disappeared when the column diameter exceeded 5.1 cm., and then liquid velocity appeared to have little effect on D_l.

Effect of Orifice Diameter.

When operating with a 5.0 cm. diameter column, Aoyama et al[98] found that the values of D_l obtained with porous plate gas distributors were about 100% greater than those with perforated plates. These results agree quite well with those of Tadaki and Maeda[99], who used perforated plate distributors of different designs.

Ohki and Inoue[94] found that D_l increased steadily with increasing gas superficial velocity when using a distributor with holes 0.2 cm. in diameter. Distributors with holes of other sizes led to more complicated behaviour at low gas flow-rates. For 8.0 and 16.0 cm. diameter columns, they noted that D_l showed a maximum value which was higher when distributors with a larger number of holes were used. They found that the critical flow-rate, corresponding to the maximum value of D_l, decreased slightly with a decrease in orifice diameter.

2. BUBBLE SIZES AND BUBBLE SIZE DISTRIBUTIONS

2.1. INTRODUCTION

When a gas is injected into a large pool of liquid through submerged, upward acting orifices, streams of bubbles are formed, the characteristics of which depend on various parameters. Of these characteristics the most important, and probably the most difficult to determine, is the size of the bubbles themselves. The size is required to determine the surface area available in the calculation of heat-transfer and mass-transfer rates, in such gas-liquid operations as fractionation, absorption, desorption and fermentation.

The behaviour of such equipment under commercial contacting conditions is extremely complex. Consequently many authors have turned away from the determination of bubble sizes in swarms and studied the factors affecting the size of bubbles formed at a single orifice. The diversity of the results obtained from these studies, as pointed out in Section 1, shows that even this simplified system is more complicated than was originally thought.

2.2. METHODS OF DETERMINING BUBBLE SIZES

There are several accepted methods of determining the sizes of bubbles rising either as a steady stream, or as a cloud, through a pool of liquid above stationary horizontal orifices. The majority of these methods are dependent upon light transmission, absorption or reflection, and the most widely employed technique is that of photography.

Two-phase flow is highly photogenic and most investigators in the field have, at one time or another, used photographic techniques. A great number of papers on two-phase flow, therefore, make reference to or report the use of photography. A more limited number of papers give details of the techniques actually used.[117 - 119]

In photographing two-phase flow it is usually necessary to distinguish in the image produced between two phases, both of which are colourless and in which the absorption of light is minimal. It is true that in many studies it is possible to add dyestuff to the liquid phase to render it absorbent to light, but such contamination of the liquid is always undesirable and the addition of dyestuffs is not possible in many instances. To produce a useful image, therefore, it is necessary that the interface between the phases can be distinguished. This can only be achieved as a result of the reflection and the refraction of light. These inherent limitations on the photography of interfaces form a background to all the techniques which have been used.

Although photographic methods can be used for single bubble studies or for investigating bubble-swarms systems, their main disadvantage lies in the fact that they cannot be used in a system (1) where there is no light transmission, such as emulsions and suspensions and (2) where the retaining walls of the system are opaque.

Two other methods relying on light transmission and absorption have been described by Vermeulen, Williams and Langlois[58] and Langlois, Gulberry and Vermeulen[107]. Vermeulen et alia[58] determined interfacial areas and drop diameters in a concentrated, dispersed system using a simple photo-electric cell outside the system to measure the amount of both transmitted and forward scattered light. Langlois et alia[107] designed and used a photo-electric probe which was actually immersed in the emulsion and then used to measure the total surface area by means of light transmission relative to clear fluids.

The theory behind both of these methods is that when a parallel beam of light is passed through a transparent suspension or dispersion, light is scattered by the particles of the dispersed phase by reflection, refraction and diffraction. The angular distribution and intensity of the scattered and transmitted light for dilute suspensions with no multiple scattering has been calculated by Mie[108]. Whilst both methods can be used for bubble swarms, they only measure the total surface area between the two phases. An average bubble size must then be calculated, knowing the volume of the apparatus and the hold-up. As a result no appreciation of the size distribution of the dispersed phase can be obtained.

The photo-electric cell used by Vermeulen et alia[58] has the advantage that it can be used in systems of single bubbles or bubble swarms, although again with the latter, only the average bubble size is determined; but it cannot be used with concentrated suspensions of solids, and neither Vermeulen's or Langlois' methods can be used if the containers of the two phases are non-transparent.

One method of overcoming this problem is to use radiography. In this technique X-rays for example are beamed through the two-phase system onto a sensitized plate. This method has the drawback that the equipment is cumbersome and is somewhat impractical to use.

Hayes, Hardy and Holland[24] devised a simple technique to determine the average size of bubbles rising from a single orifice by measuring the volumetric flow of gas and the frequency of bubble formation. The former was measured by a standard variable area flow meter and the latter by visual observation, at low frequency, and by means of a stroboscope at higher frequencies. This method does not permit measurement of bubble-size distribution, and some of its simplicity is lost if the bubbles themselves are not visible.

Brown and Craddock[109] devised a method for determining bubble-size distributions by actually capturing a large number of bubbles and measuring the individual volumes. The sampling was achieved by means of a capillary tube which was held under vacuum at one end. Knowing the length of a slug of gas formed by trapping a bubble and the previously measured cross-sectional area of the capillary, it is a simple matter to determine the diameter of the bubble either by assuming it to be spherical or by assuming a major to minor axis ratio. This method can be used, with care, in either single bubble or bubble cloud systems, whether the continuous phase is transparent or not. The major disadvantage of this technique is that a large number of bubbles must be collected and measured to ensure satisfactory results on statistical grounds.

Although by no means exhaustive, the above review indicates that there are a number of possible methods of determining bubble sizes and/or bubble size distributions, all of which have various limitations. With this in mind, it was decided to develop a convenient method for determining the sizes of individual bubbles rising from a single orifice immersed in a wide range of solutions and suspensions. At the outset it was also hoped that equipment might later be modified to study bubble-size distributions in bubble-columns and similar equipment.

2.3. DETERMINATION OF BUBBLE SIZE DISTRIBUTIONS

2.3.1 INTRODUCTION

The method that was devised to measure the individual sizes of bubbles rising from a single horizontally placed, sharp edged orifice overcomes many of the above problems. It is based on the resistance change of a volume of liquid during passage of a bubble; so it is, in fact, the volume of the bubble that is measured. The method measures the volume of every bubble, so a true representation is obtained; and, due to the fact that every bubble is measured, the frequency of formation of the bubbles is also obtained. The method can also be used when the continuous phase and/or the equipment is opaque.

2.3.2 THEORETICAL APPROACH

The method devised used a simple Wheatstone Resistance Bridge with two fixed volumes of liquid as two arms of the bridge (which are initially

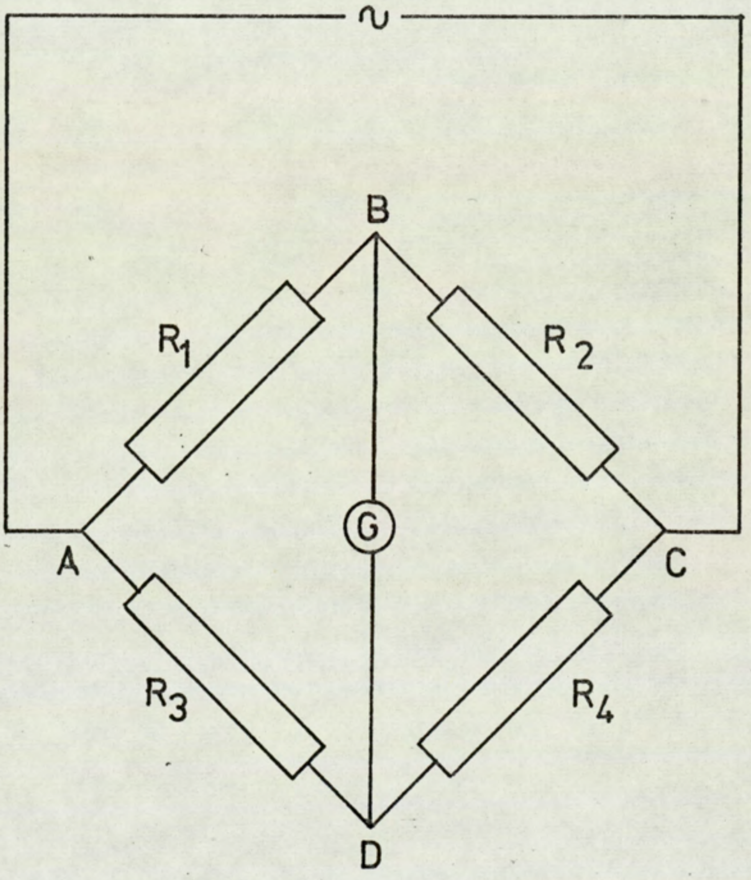

FIG 2.1
Wheatstone Bridge Circuit

balanced). As a bubble passes through one of these volumes it displaces some of the liquid and therefore alters the resistance. At this point the out-of-balance potential across the circuit is recorded and, since this is an indirect measure of the resistance change and therefore the volume change, the size of the bubble can be determined. The theoretical circuit is shown in Fig. 2.1 and comprises two resistances, R_1 and R_3, which are identical volumes of liquid, and two other resistances, R_2 and R_4, which are used to initially balance the system. Initially, with no current flowing through the galvonometer, the following condition is satisfied.

$$\frac{R_1}{R_3} = \frac{R_2}{R_4} \qquad 2.1$$

If, however, R_1 is altered to R_1^1 equation 2.1 has to be modified, since there is now a potential drop between B and D, which is directly proportional to the change in resistance, i.e.

$$(R_1 - R_1^{\,1}) \propto V_{BD} \qquad 2.2$$

where V_{BD} is the potential difference between B and D. Since $R_1^{\,1}$ is the resistance of a volume of liquid with a bubble in it and R_1 is that of the original volume of liquid, equation 2.2 is a measure of the bubble volume. The potential difference, V_{BD}, can then be related to bubble size by prior calibration of the equipment.

2.3.3 EXPERIMENTAL APPARATUS

Flow Apparatus

The general arrangement of the apparatus is shown in Fig. 2.2. The design of the apparatus was such that it was in two symmetrical halves, as is shown in Fig. 2.3.

The columns (9) and (10) were constructed from $^5/_8$" (1.6 cm) internal

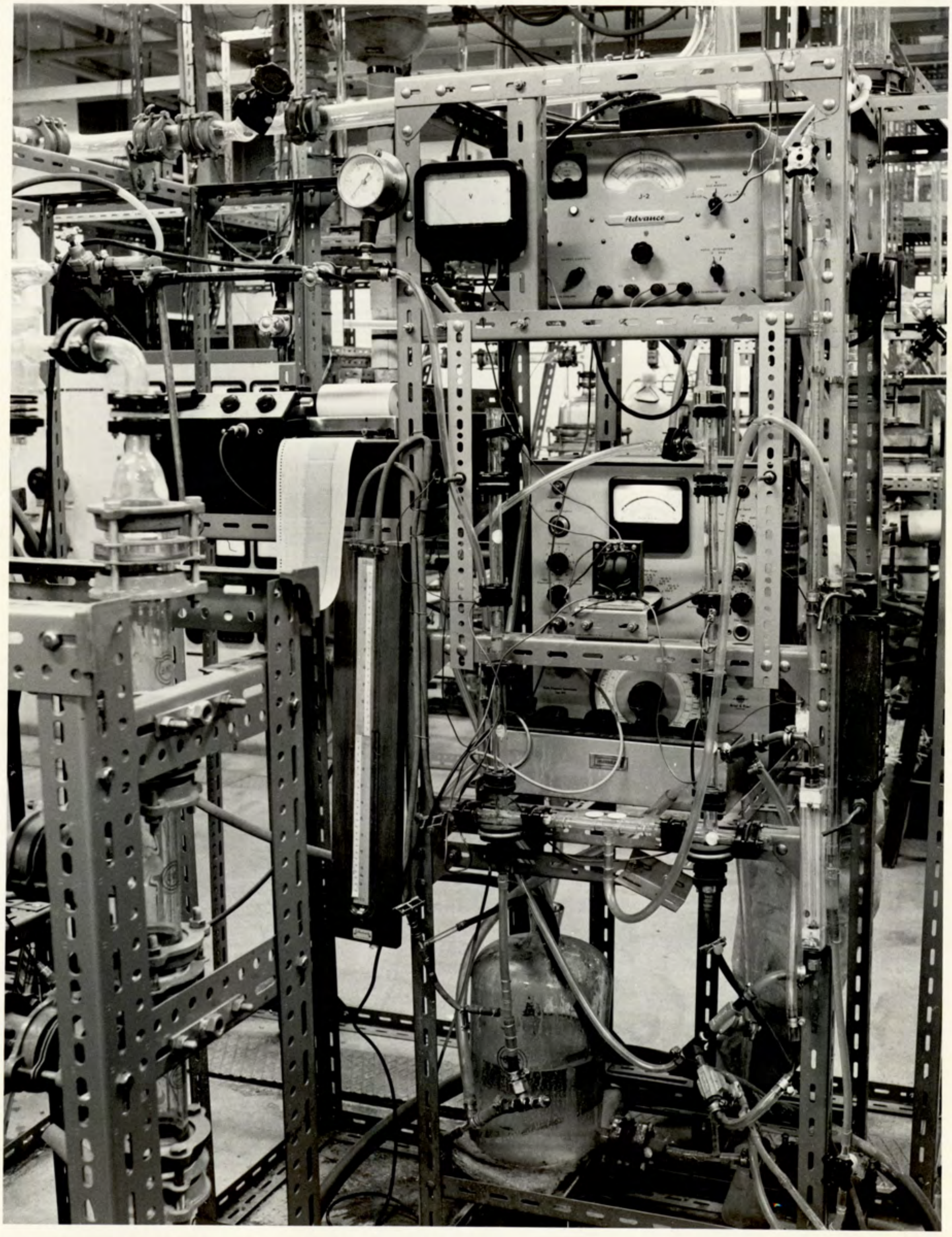

FIG 2.2
General Arrangement of Apparatus
(Resistance Method)

diameter Q.V.F. * glassware, and the interlinking pipework was $^3/_8$" (0.95 cm) internal diameter P.V.C. tubing. The measuring column (9) and the "dummy" column (10) were each built up of five sections: an inlet section made from a T-piece which was 4" (5.1 cm) in height; a calming section, 6" (7.65 cm) high; the measuring section which was 4" (5.1 cm) in height; a further 6" (7.65 cm) calming section; and an outlet section constructed from a T-piece 4" (5.1 cm) high. This gave a total column height of 24" (31.5 cm) and a liquid seal of 22" (31 cm).

The liquid circulation was from a 25 l. Aspirator (13) via a Stewart * centrifugal pump (14), capable of delivering 120 gal/hr against a 60 ft. head. A recirculation line and valve (16) were also fitted around the pump. The flow was regulated by this valve in conjunction with valve (15) and metered by a standard variable area meter (17), a Rotameter * 7K (Korunnite float). The liquid was then fed to a T-piece (18) situated centrally between the two columns. The return flow from the top of the columns was via two plastic drain lines (12), running side by side, back to the resevoir (13).

The gas supply was a $^1/_4$" B.S.P. tapping from the compressed air service main (1), through a $^1/_4$" Saunders * valve (A type) (2) to reduce the pressure. A pressure gauge (0 - 25 p.s.i.) (3) was fitted immediately upstream to the throttling valve to measure the pressure in the flow-meter (5). The air-flow was measured by a Fisher and Porter * variable area meter (5), type $^1/16$ - 08 - G, with a glass or stainless steel ball-float, depending on the flow-rate required: a by-pass line (4) was fitted around the meter. The flow of air was regulated by means of the needle valve (6). The pressure immediately upstream of the flow-meter was

---

* James Jobling (Q.V.F.) Ltd., Stoke-on-Trent, Staffs.
Stewart and Turner, Henley-on-Thames.
Rotameter Mfng.Co.Ltd., Croydon, Surrey.
Saunders Valves Ltd., Cwmbran, Mon.
Fisher and Porter, Workington, Cumberland.

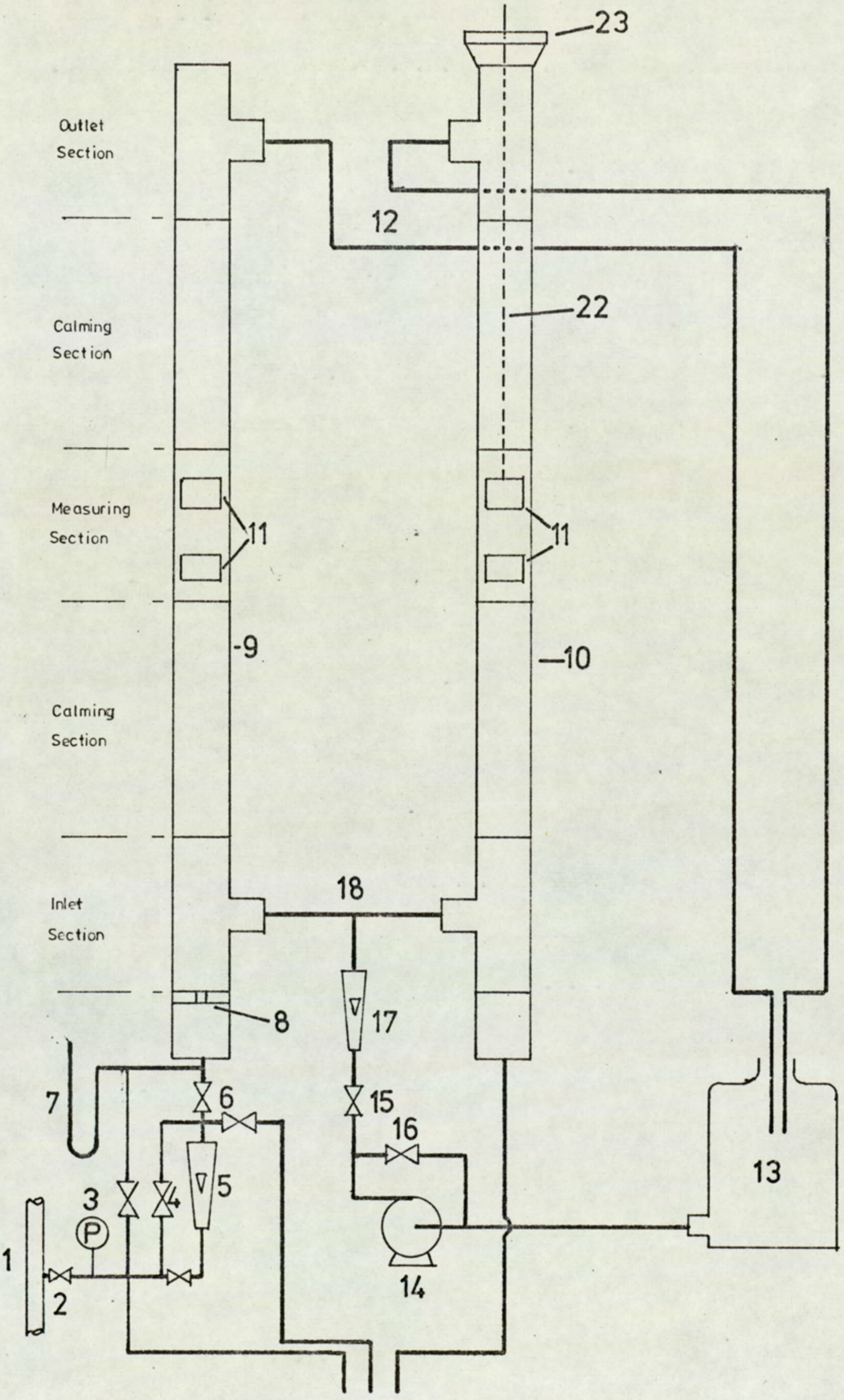

FIG 2.3
Flow Diagram
(Resistance Method)

measured by means of a 20" (49 cm) water-gauge manometer (7). The orifices (8) themselves were made from stainless steel sheet, $^{5}/_{64}$" (0.2 cm) thick by 1" (2.5 cm) diameter and drilled with one central hole: Table 2.1 shows the orifice diameters used, ranging in size from 0.037 cm to 0.253 cm.

Table 2.1 Orifice Diameters for Resistance Measurements.

Orifice No.	Dia. Cm.
1	0.253
2	0.201
3	0.198
4	0.147
5	0.117
6	0.101
7	0.094
8	0.075
9	0.037

The diameters of the orifices were measured, after drilling, by means of a travelling-microscope, and the arithmetic mean diameter was determined from four readings taken on each side of the orifice.

The "dummy" column, the air chamber beneath the orifice and the manometer tapping were all fitted with drain lines, constructed from rubber-tubing with Mohr clips. These drain lines are shown as (19), (20) and (21) on Fig. 2.3.

The Electrodes

The four electrodes, (11) and Fig. 2.4, were made up from platinum foil (0.5 mm thick, 1 cm wide and 5 cm long) that was rolled into a

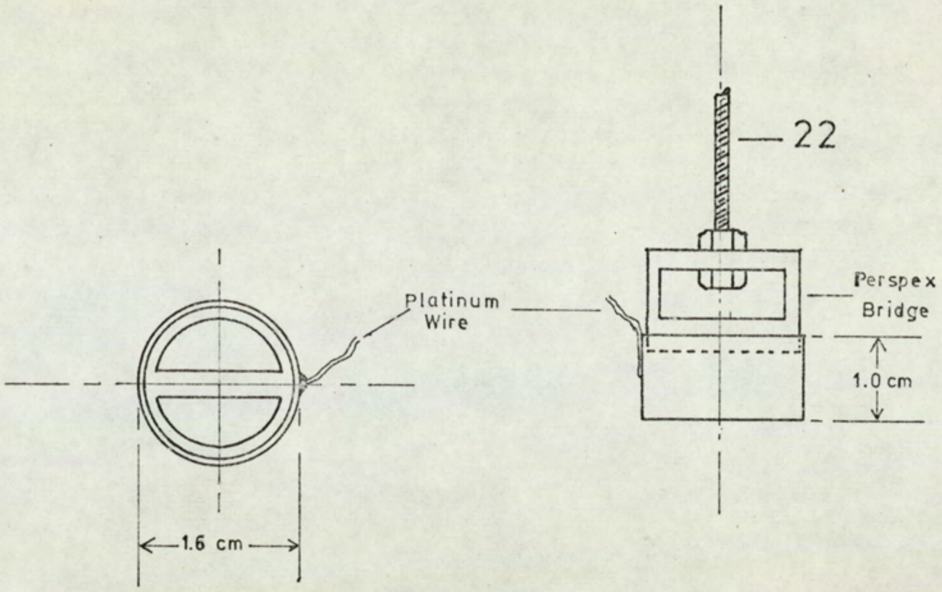

FIG 2.4
Electrodes

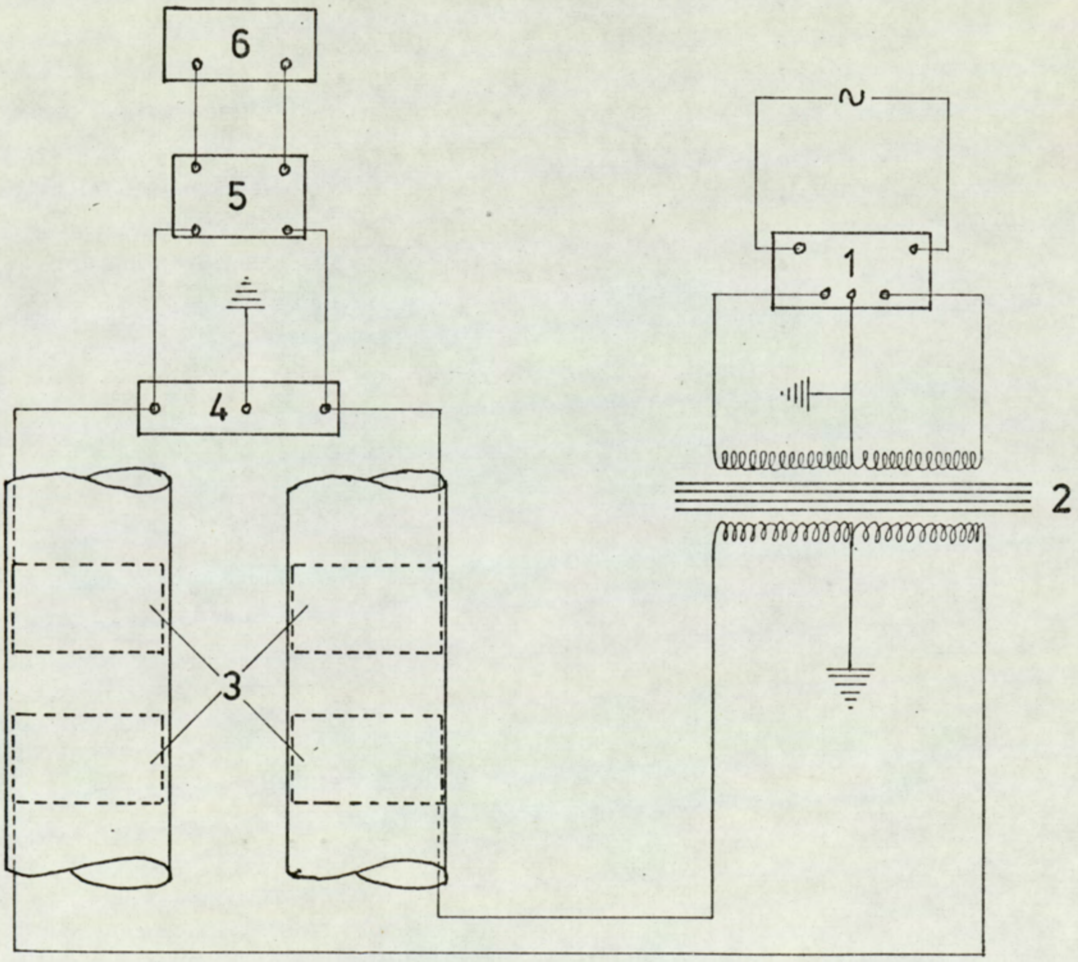

FIG 2.5
Schematic Wiring Diagram

cylinder so as to be a sliding-fit in the columns and then welded along the seams. Each electrode had a 2.5" (6.35 cm) length of 20 S.W.G. platinum wire welded to it and this was fed out of each end of the measuring section of the columns between two gaskets. The top electrode in the "dummy" column had a perspex ring cemented to the top inside edge. A length of 8 B.A. screwed brass rod (22) was attached to this ring by locknuts. The upper end of this rod passed through a fixed perspex flange (23) situated about 1" (2.5 cm) above the top of the column and was used for adjusting the height of the electrode, in order to obtain an exact electrical balance after the electrodes had been inserted into the columns.

Electrical Apparatus

The electrical part of the equipment, shown diagrammatically in Fig. 2.5, consisted of an Advance * Type J 2, signal generator (1), operating off 240 volts, 50 Hz , mains supply and generating 12 volts at 500 Hz (sine wave). The high frequency was used to prevent any electrolysis taking place between the electrodes. This signal was fed to a specially designed transformer (2), described below. The divided, transformed signal was then fed to one of the immersed electrodes in each column, the volumes of liquid between the two pairs of electrodes acting as two of the resistances of the Wheatstone Bridge circuit. T he other two electrodes were connected to a Muirhead * decade resistance box (4) fitted with a central earth tapping: this arrangement provided the other two legs of the Wheatstone Bridge. The galvonometer (5) used to measure the potential difference between the two pairs of electrodes was a Bruel & Kjoer * Audio Frequency Analyser with a full-scale deflection of

* Advance Electronics Ltd., Bishops Stortford, Herts.
Muirhead-Addison Ltd., Beckenham, Kent.
Bruel & Kjoer Laboratories, Hounslow, Middlesex.

0.01 volts by 0.00001 divisions, which is a discrimination of 1 in 1000. This means that the smallest bubble that could accurately be detected would have a volume of 2.9 mm ^{3} (1.77 mm diameter), since the volume of liquid between the electrodes was 2900 mm ^{3}. The distance between the electrodes was fixed at approximately 1.5 cm as a result of empirical tests. It was found that if the distance was greater than 1.5 cm, the change in resistance when a bubble was present was too small to be accurately detected; and if the distance between the electrodes was less than 1.5 cm, the residence time of the bubble between the electrodes was too short compared with the response time of the recorder of about 0.02 s. When set at 1.5 cm the residence time of a bubble between the electrodes was approximately 0.04 s, thus providing a safety factor of 2. The frequency analyser response was in turn recorded by a Bruel & Kjoer variable chart-speed recorder (6).

The basic design and dimensions of the transformer are shown in Fig. 2.6 and the wiring is shown in Fig. 2.7. The transformer was used as a source of two identical voltages for each half of the Bridge circuit and was wired in the following way. Each half of the primary winding had exactly 200 full turns of enamel-insulated copper wire (23 S.W.G.) made up of eight layers, the first turn on each half being connected to the signal generator and the last turn on each half being joined together to earth. Between each series of turns was a single layer of P.V.C. insulating tape. One complete turn of copper foil which was connected to earth and covered with a further thickness of insulating tape was used over the top layer of P.V.C. tape (see Fig. 2.7 A).

The secondary winding was made up in a similar manner, each half of the Paxolin former having exactly 200 full turns of copper wire which were insulated between layers. The first turn of wire on each half of the secondary winding was connected to the electrodes and the last turns of each half of the secondary winding were joined together and earthed (see

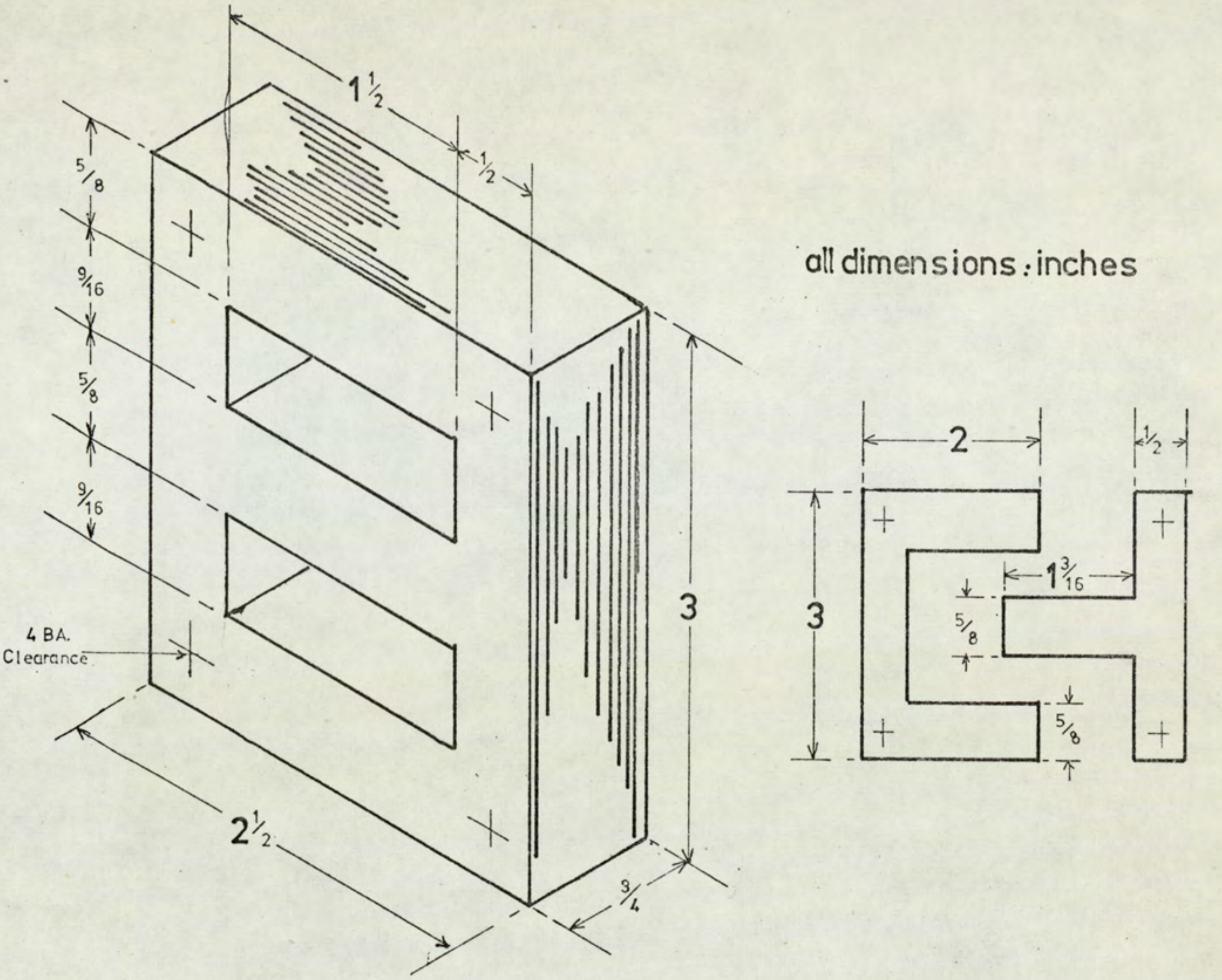

all dimensions: inches

2.6a Laminated core (full-size)

2.6c Laminates (half-size)

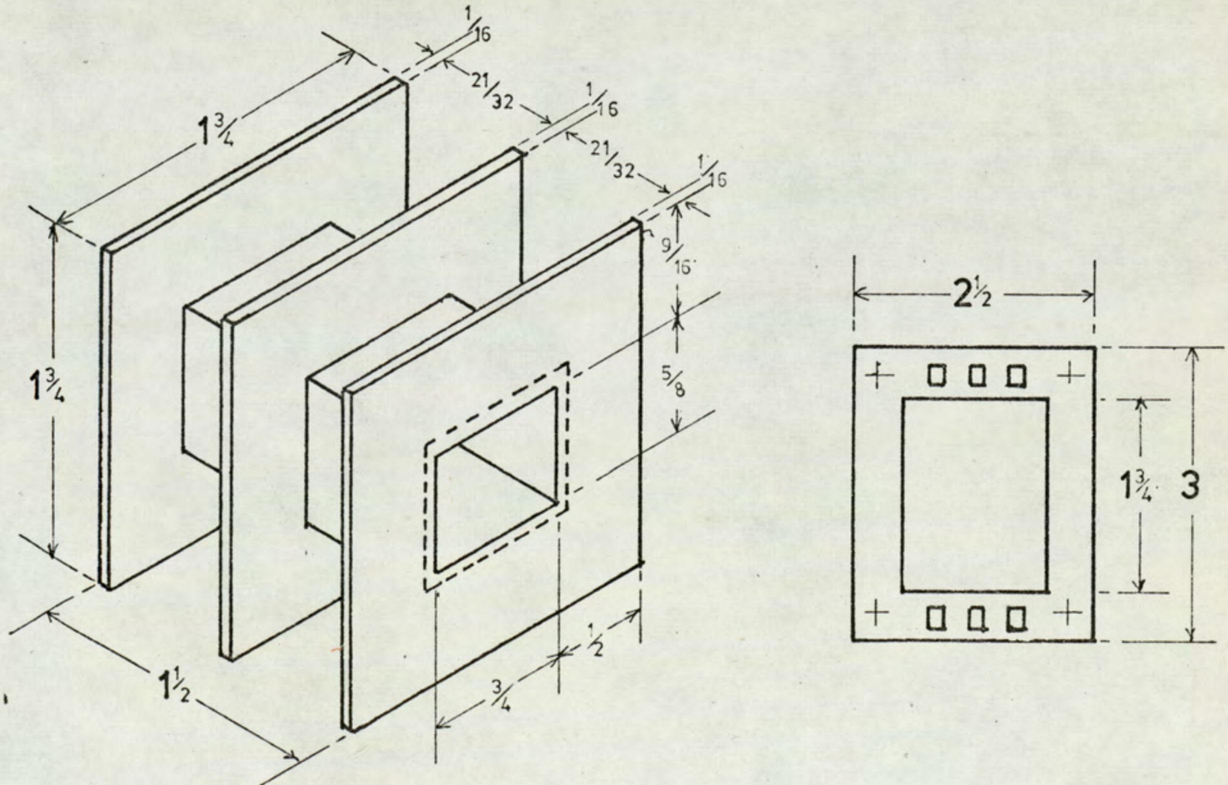

2.6b Winding former (full-size)

2.6d Laminate former (half-size)

FIG 2.6 Transformer Components

Fig. 2.7 B).

On both the primary and the secondary winding, the total number of turns and the number of turns per layer were identical, so that the resistance of each half of the transformer was the same. The supply voltage to the transformer was 12 volts, so that the voltage to each electrode was 6 volts. All electrical connections and wires used throughout the system were identical on each half of the equipment.

In order to carry out comparative measurements using the method of Brown and Craddock[109], a 1½" (3.8 cm) internal diameter column was built up from three sections of Q.V.F. glass tubing: the overall column height was 24" (64 cm) with a liquid seal of 20.5" (52.2 cm). The fluid pumping and recirculation circuit and the air metering system were similar to those shown in Fig. 2.8. The capillary tube was bent as shown and the immersed end was cone-shaped to facilitate the capture of the bubbles. The inside diameter of the capillary was determined by filling a measured length of the capillary with mercury, which was then withdrawn and weighed. It is then a relatively simple matter to calculate the internal cross-sectional area and diameter. The orifices used were 1⁷/8" (4.75 cm) diameter stainless steel discs, ³/16" (0.475 cm) thick and drilled with one central hole (see Table 2.2).

Table 2.2 Orifice Diameters for Capillary Measurements.

Orifice No.	Orifice Dia. cm.
1	0.141
2	0.099
3	0.079
4	0.036

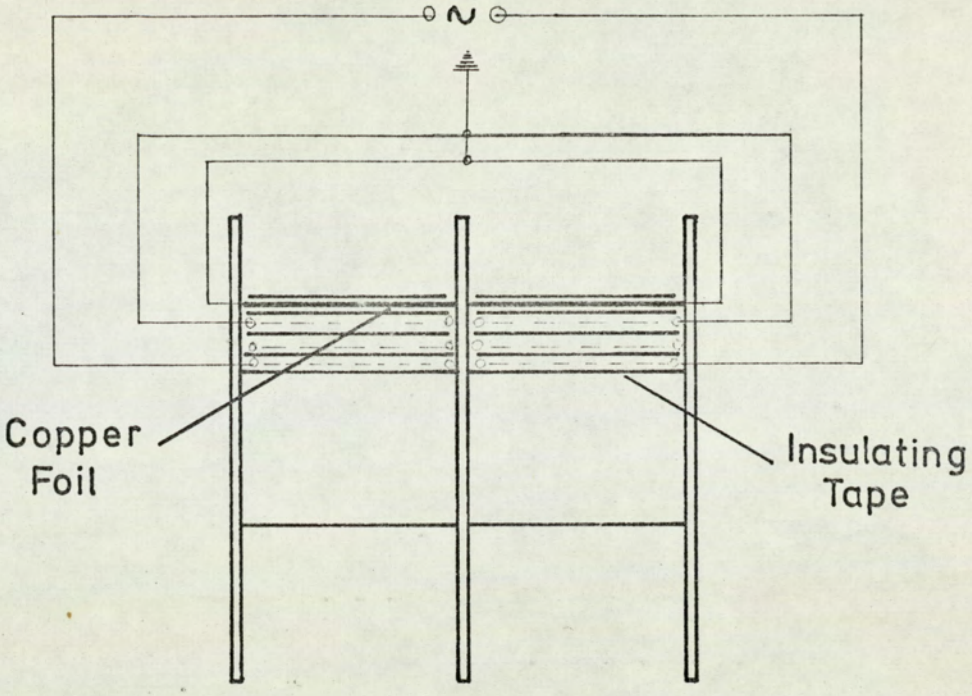

2.7a Primary Winding

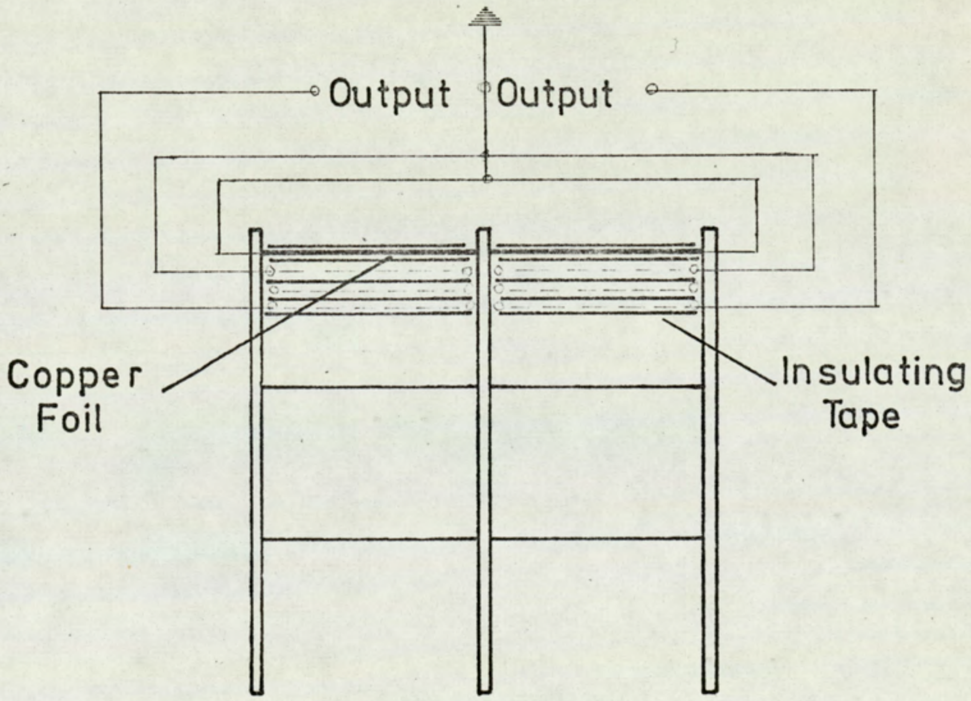

2.7b Secondary Winding

FIG 2.7

Transformer Windings

2.3.4 EXPERIMENTAL PROCEDURE

Capillary Method

Initial experiments were conducted in the larger ($1^1/2''$ dia.) column using the capillary method, which was set up as follows. Firstly, the air pressure in the chamber beneath the orifice was set high enough to prevent weeping through the orifice. Secondly, the liquid circulation-pump was started and the flow-rate set to give the desired liquid velocity. The air-supply needle-valve was then opened slowly until a steady stream of bubbles was being formed at a frequency of approximately 2 - 3 bubbles per second. When both air and liquid rates were steady, the cone-shaped end of the capillary was inserted to a depth of 12" (30.5 cm) inside the column and a slight negative pressure put on it: this had the effect of drawing bubbles along the capillary tube. When several bubbles were in the measuring section, the vacuum was turned off and the lengths of the slugs of air measured. This procedure was repeated until 100 bubbles had been trapped and measured. Since the cross-sectional area of the capillary was known, the diameter of the bubble could easily be determined, assuming the bubbles to be spherical.

For statistical purposes the lengths of the air-slugs were grouped into classes differing by 1 mm, the corresponding equivalent bubble diameter being calculated for each class. The number frequency of bubbles within any one class was then determined and the mean bubble size calculated from

$$\frac{\sum_{i=1}^{i=00} n_i \; d_{bi}}{\sum_{i=1}^{i=00} n_i} = \bar{d}_b \qquad 2.3$$

where n_i is the number of bubbles occuring with a diameter d_{bi} and $\overline{d}_b$ is the mean bubble diameter. This procedure was then repeated for each of the orifices, keeping the frequency of bubble generation approximately the same.

Resistance Method

The experimental procedure for the measurement of bubble sizes by means of the resistance method can be divided into six sections, viz:

1) Setting the liquid flow
2) Electrical balancing
3) Calibration
4) Setting the air flow
5) Measurement of bubble frequency and size
6) Analysis of results

1) Setting the liquid flow - This was done in a similar manner to that described for the capillary method. Firstly, a slight positive pressure was created in the chamber beneath the orifice plate to prevent any liquid weeping through the orifice. The pump was then switched on and the liquid flow-rate adjusted by means of the valves (15) and (16) (see Fig. 2.3) to give the desired liquid superficial-velocity.

2) Electrical balancing - When the liquid flow-rates were steady and before introducing air, the signal generator, analyser and recorder were switched on and allowed to warm up. The resistance of the "dummy" column (i.e. the volume of liquid between the electrodes) was then set equal to that of the measuring column by either raising or lowering the upper electrode until the analyser and recorder showed zero deflection.

3) Calibration - The system was calibrated by lowering a series of small plastic beads attached to fine threads below the electrodes and

then raising them at velocities similar to those expected for the bubbles. The deflections caused by the beads were then noted and related to bead size. The mean volume of the beads was measured by determining the volume of liquid displaced by several of them when put into a small measuring cylinder. This procedure was then repeated for different sizes of beads.

4) Setting the air flow - Since the bubble frequency was chosen as one of the parameters, this was set to the desired value at the start of each experiment. The frequency was varied from approximately one bubble per four seconds to five bubbles per second.

In the initial set of experiments the volume of the air chamber, V_c, below the orifice plate was fixed at 52.4 cm^3 which corresponds to a capacitance number, N_c, of 36.2 for the largest orifice and 0.772 for the smallest. In the second series of experiments the volume of the orifice chamber was reduced to a minimum consistent with stable bubbling by flooding the chamber with water. The air-volume remaining was estimated to be about 0.5 cm^3, which reduced the capacitance number by a factor of 100 for each orifice.

5) Measurement of Bubble Frequency and size - When a steady rate of bubbling had been achieved, the recorder chart-drive was switched on and up to about 200 deflections were measured. From the known chart-speed and the number of deflections an accurate determination of the bubble frequency could be made.

The bubble size was determined by comparing the length of the deflection with those recorded during the calibration procedure. Since the length of deflection was proportional to the volume of the bubble and the constant of proportionality was known from the calibration curve, the bubble diameter could be readily computed.

6) Analysis of Results - The size distribution of the bubbles

was determined in the following way. The lengths of the deflections were grouped into classes differing by 2 mm increments and the equivalent bubble diameter for each increment in length was calculated. The distribution of the bubble sizes was then estimated from the number of bubbles occuring within each class. Finally, the mean bubble diameter was found using equation 2.3.

In order to fit a series of curves to the size distribution, each distribution was "normalised", i.e. it was multiplied by a factor such that the number of bubbles in the modal size class equalled 100.

2.3.5 EXPERIMENTAL PROGRAMMES AND RESULTS ON AVERAGE BUBBLE SIZE.

Measurement of bubble sizes by the capillary method.

The conditions under which the control experiments were carried out are shown in Table 2.3. The operating temperature was 68°F. Since this series of experiments was used primarily to check the resistance method, the only parameter that was varied was the orifice diameter.

Table 2.3 Experimental Conditions.

Orifice No.	Orifice Dia. (cm)	Bubble Rate (Bubbles/s)	Liquid Flow (l/min)	Liquid Super-ficial Vel. (cm/s)	True Gas Flow (cm^3/min)	ΔP_o (mm H_2O)
1	0.141	2.5	6.85	1.0	10.0	6.8
2	0.099	2.3	"	"	8.0	7.5
3	0.079	2.6	"	"	6.4	10.7
4	0.036	2.5	"	"	3.0	15.5

The liquid flow rate was maintained constant throughout the tests and the rate of bubble formation was held approximately constant. The liquid phase used was tap-water and the liquid seal (height of liquid above the orifice)

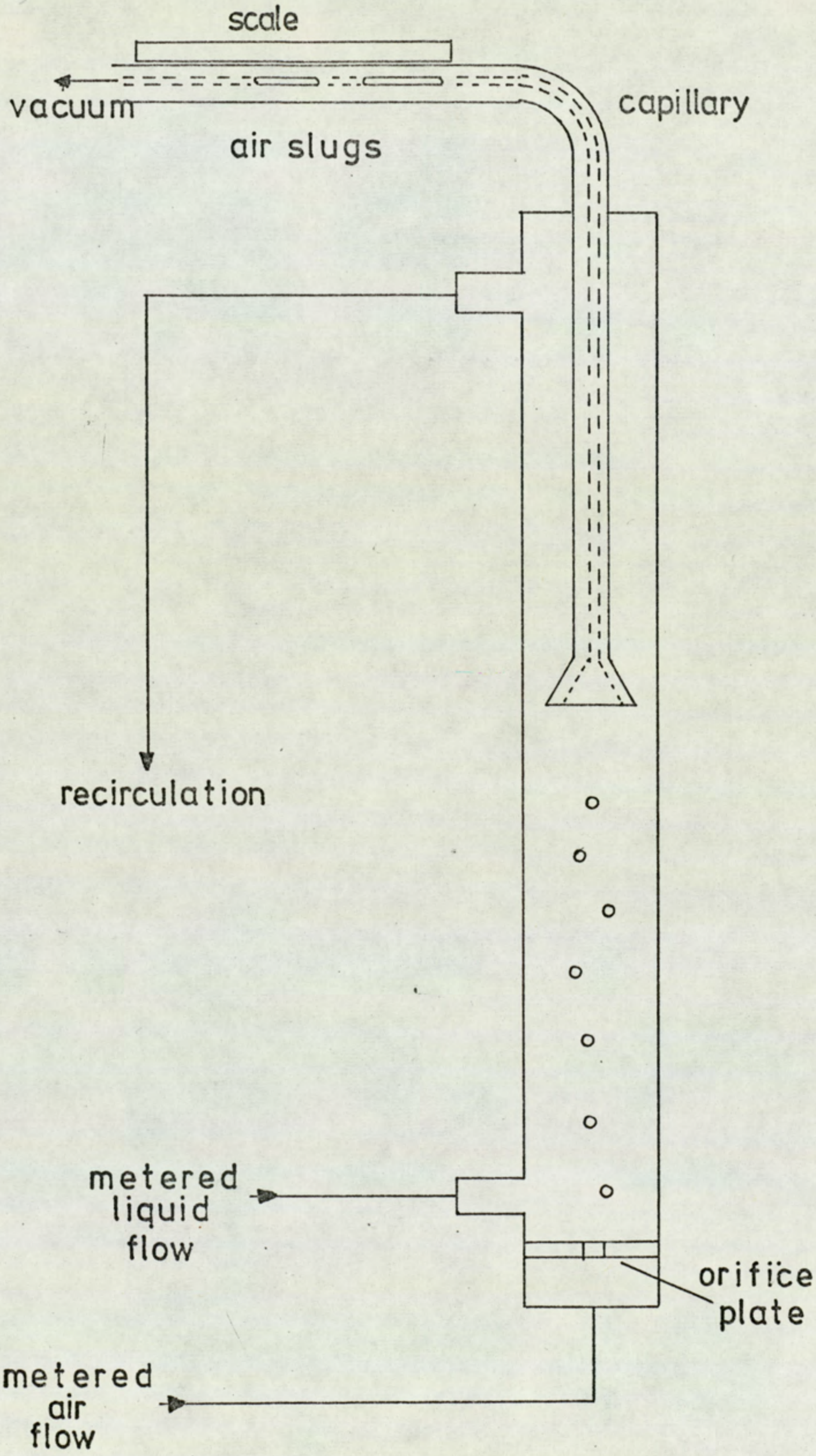

FIG 2.8
Schematic Flow Diagram
(Capillary Method)

was maintained at 22.5 " (57.2 cm), whilst the capillary tube was submerged to a constant depth of 12" (30.5 cm). The volume of the air chamber beneath the orifice plate was approximately 40 cm^3. The diameter of the measuring section of the capillary tube was found to be 0.1630 cm, so that the diameter, d_b, of a spherical bubble of the same volume as a slug of air of length, l, is given by:-

$$d_b = 0.736\, l^{\frac{1}{3}} \qquad 2.4$$

where d_b and l are both measured in cm.

The mean bubble diameters formed at a given orifice were calculated by means of equation 2.3. Table A.1 in Appendix A shows the detailed results, which are summarized in Figs. 2.9 and 2.10. Fig. 2.9 shows the true distribution, whilst Fig. 2.10 shows the distributions superimposed about a common mean value. For the sake of easy comparison in Fig. 2.9 all the distributions have been "normalised", i.e. multiplied by a factor so that the number of bubbles occuring within the modal class is 100. This enables a direct comparison of the frequency distribution curves to be made: this procedure was followed throughout the work. The "normalised" distribution figures are given alongside the actual measurements in Table A.1.

Table 2.4 shows the mean bubble diameter, as calculated from equation 2.3, with respect to the orifice diameter, and Fig. 2.11 shows the graphical relationship between them. As can be seen, there is a simple correlation between mean bubble diameter, $\bar{d}_b$, and orifice diameter, d_o, which can be written in the form : -

$$\bar{d}_b = B\, d_o^{\,k} \qquad 2.5$$

Analysis of the experimental data leads to the following expression

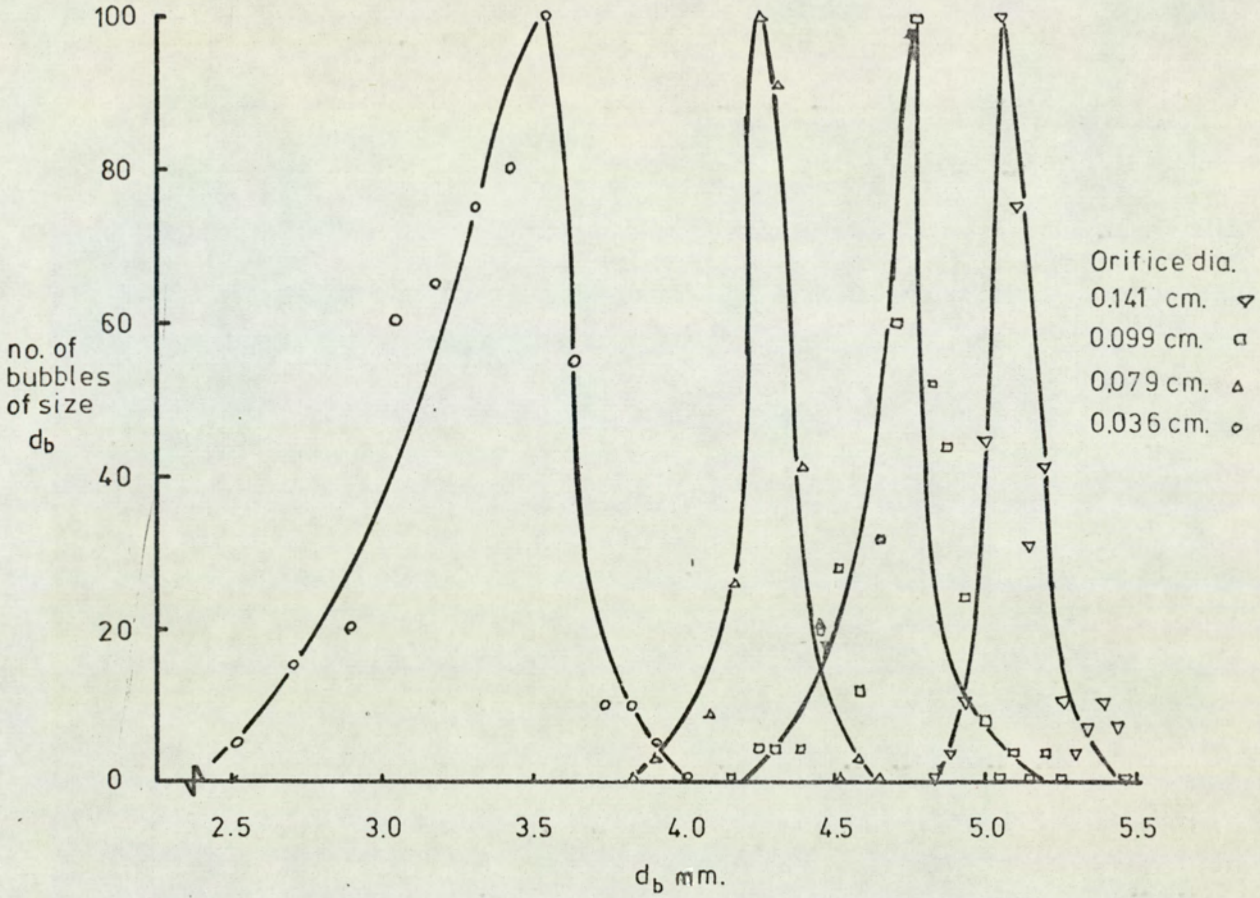

FIG 2.9 Bubble-size Distribution. (Capillary Method)

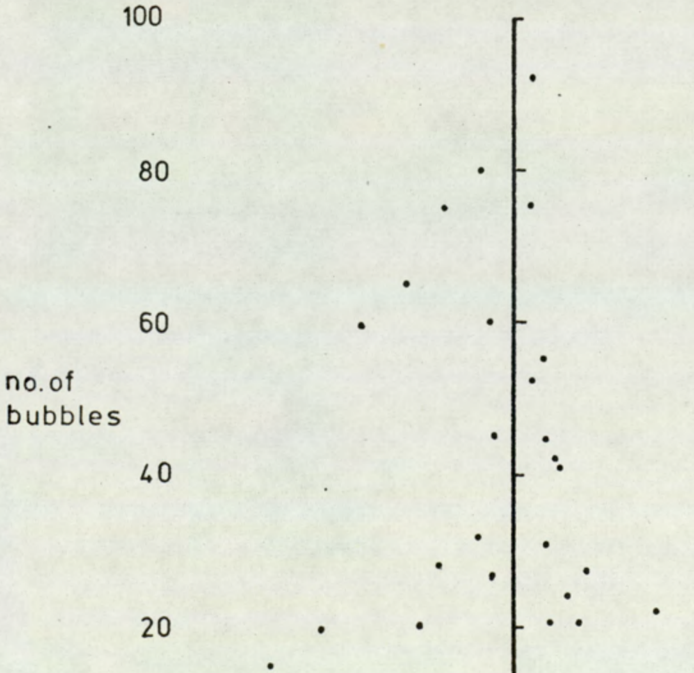

FIG 2.10 Distribution about a Common Mean.

with $\bar{d}_b$ and d_o in cm.

$$\bar{d}_b = 1.0\, d_o^{\frac{1}{3}} \qquad 2.6$$

Table 2.4 Mean Bubble Diameters (air/water)

d_o (cm)	$\bar{d}_b$ (cm)
0.141	0.509
0.099	0.473
0.079	0.427
0.036	0.334

Fig. 2.12 shows a graph of the measured gas flow-rate against the calculated flow-rate, derived from equation 2.7.

$$G_v' = 10\pi\, \bar{d}_b^{\,3}\, f \qquad 2.7$$

Where G_v' is the volumetric flow-rate (cm^3/min), f is the frequency of bubble formation (bubbles/s), and $\bar{d}_b$ (cm) is as defined by equation 2.3. The results of these calculations are listed in Table 2.5. As can be seen from Fig. 2.12 the agreement between the calculated and the measured values of the flow-rate is very good, showing that the method used to determine the mean diameter of the bubbles is reliable.

Table 2.5 Measured and Calculated Flow Rates.

Measured Flow Rate (cm^3/min)	Calculated Flow Rate (Eq. 2.7) (cm^3/min)
10	10.37
8	7.99
6.4	6.37
3.0	2.91

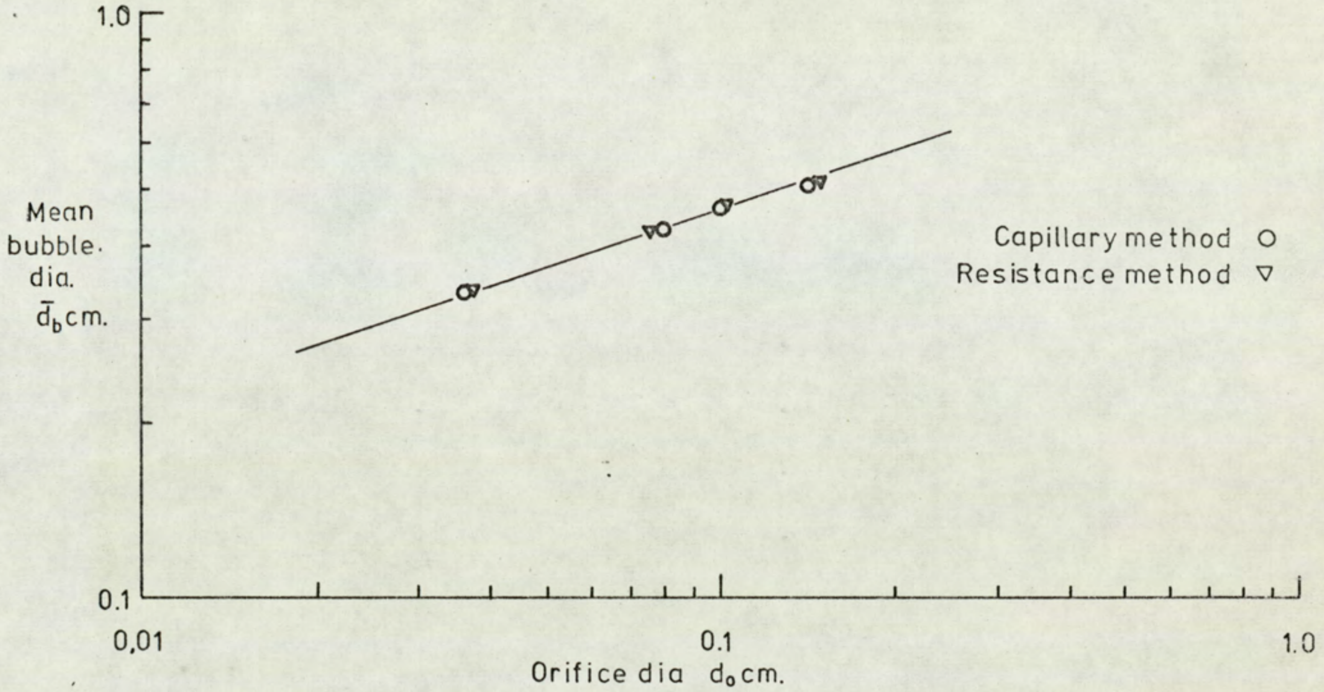

FIG. 2.11 Bubble diameter as a function of orifice diameter.

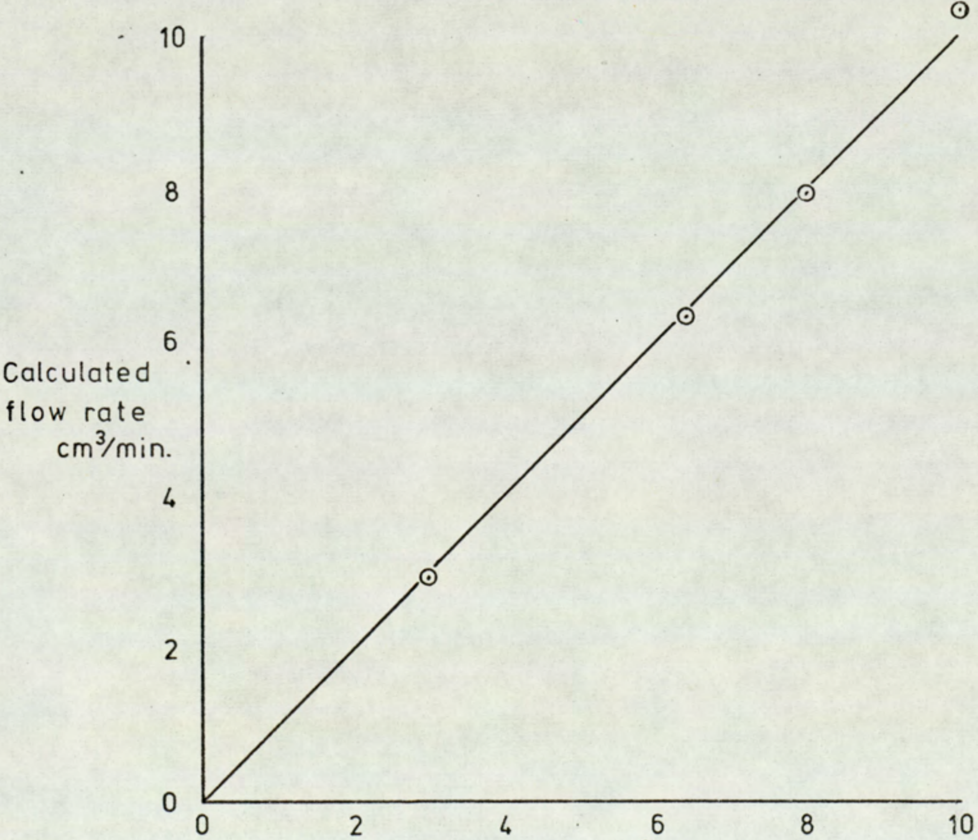

FIG 2.12 Comparison of measured and calculated flow rates.

Measurement of bubble sizes by resistance measurements.

The bubble-size and size-distribution measurements carried out with the resistance method are presented in three main sections corresponding to the liquid systems studied. Each main section is further subdivided to aid discussion of the effects of other parameters.

The three main sections are headed:

Series 1. Tap-water.

This series was used to assess the reliability of the resistance method, using results from the capillary method as a basis. The volume of the air chamber beneath the orifice was held constant at its maximum value.

Series 2. Potassium Chloride solution (0.1N) in tap water.

This series of experiments was carried out to assess the effect of changing the liquid phase properties whilst using a translucent system.

Series 3. Yeast suspensions.

Yeast suspensions were chosen for study because (1) they are widely used in various commercial processes, (2) physical property data for such systems were available and (3) they are opaque.

The sub-sections are explained below: in effect they describe the experimental programme that was pursued.

1 A. The only parameter used with the air/water system was orifice diameter and this was only varied to a limited extent.

2 A. The orifice diameter was varied from 0.037 to 0.253 cm in nine steps (see Table 2.1)

2 B. The rate of bubble formation was varied in order to study the effect of gas flow-rate on bubble-size.

2 C. The volume of the air-chamber beneath the orifice plate was varied to determine the effect on bubble diameter.

3 A. The concentration of yeast in the suspension was varied from 5% to 30% (on a dry weight basis) in six steps. The 30% suspension was used only to get some idea of the effect of a Non-Newtonian fluid on bubble behaviour. The results for this particular suspension were not included in the final analysis of data, since the physical properties of yeast suspensions change considerably between 25% and 30% concentrations.

3 B. The orifice diameter was varied over a similar range of sizes as for the experiments with potassium chloride.

3 C. The volume of the air chamber was also varied to the same extent as in the tests with the potassium chloride solution.

Calibration of the Equipment.

Although the calibration experiments were carried out at the beginning and end of each set of experiments, the results and calibration curves have been set out together at this stage for the sake of convenience.

The measured values of the average length of the galvonometer deflections are given in Table A.2 in Appendix A. Also shown is the cube root of the deflection length, l_d, since the deflection is a measure of the volume of the bubble and is thus proportional to the cube of the bubble diameter, i.e.

$$d_b = B\, l_d^{\frac{1}{3}} \qquad 2.8$$

where B is the constant of proportionality which is dependent, among other things, on the electrical resistance of the liquid phase.

Fig. 2.13 shows the calibration for each liquid system. The equations used for determining the bubble diameters, which were obtained from Fig. 2.13, are as follows:

Water	$\bar{d}_b = 0.1600\, \bar{l}_d^{\frac{1}{3}}$	2.9
0.1N KCl	$\bar{d}_b = 0.1770\, \bar{l}_d^{\frac{1}{3}}$	2.10

5% Yeast $\bar{d}_b = 0.1932\ \bar{l}_d^{\frac{1}{3}}$ 2.11

10% Yeast $\bar{d}_b = 0.1998\ \bar{l}_d^{\frac{1}{3}}$ 2.12

15% Yeast $\bar{d}_b = 0.1802\ \bar{l}_d^{\frac{1}{3}}$ 2.13

20% Yeast $\bar{d}_b = 0.1941\ \bar{l}_d^{\frac{1}{3}}$ 2.14

25% Yeast $\bar{d}_b = 0.1941\ \bar{l}_d^{\frac{1}{3}}$ 2.15

30% Yeast $\bar{d}_b = 0.1966\ \bar{l}_d^{\frac{1}{3}}$ 2.16

$\bar{l}_d$ is the average deflection length measured over increments of 2 mm and $\bar{d}_b$ is in cm.

Series 1. Tap-Water

Four orifices only were used. The bubbling frequency was kept constant at approximately 2.5 bubbles/s, and the liquid superficial velocity at 1.0 cm/s. Ten bubbles from each orifice were measured. The results are given in detail in Table A.3 in Appendix A, and Table 2.6 provides a summary. Fig. 2.11 also shows the data along with that obtained by the capillary method. As can be seen from Fig. 2.11, equation 2.6 holds equally well for data obtained by both methods.

Table 2.6 Orifice Diameters and Measured Bubble Diameters (mean) for Air/Water System.

d_o (cm)	$\bar{d}_b$ (cm)
0.147	0.515
0.101	0.474
0.075	0.429
0.037	0.339

Series 2. Potassium Chloride Solution (0.1N) in Tap-Water

The results are shown graphically in Fig. 2.14 for different bubble

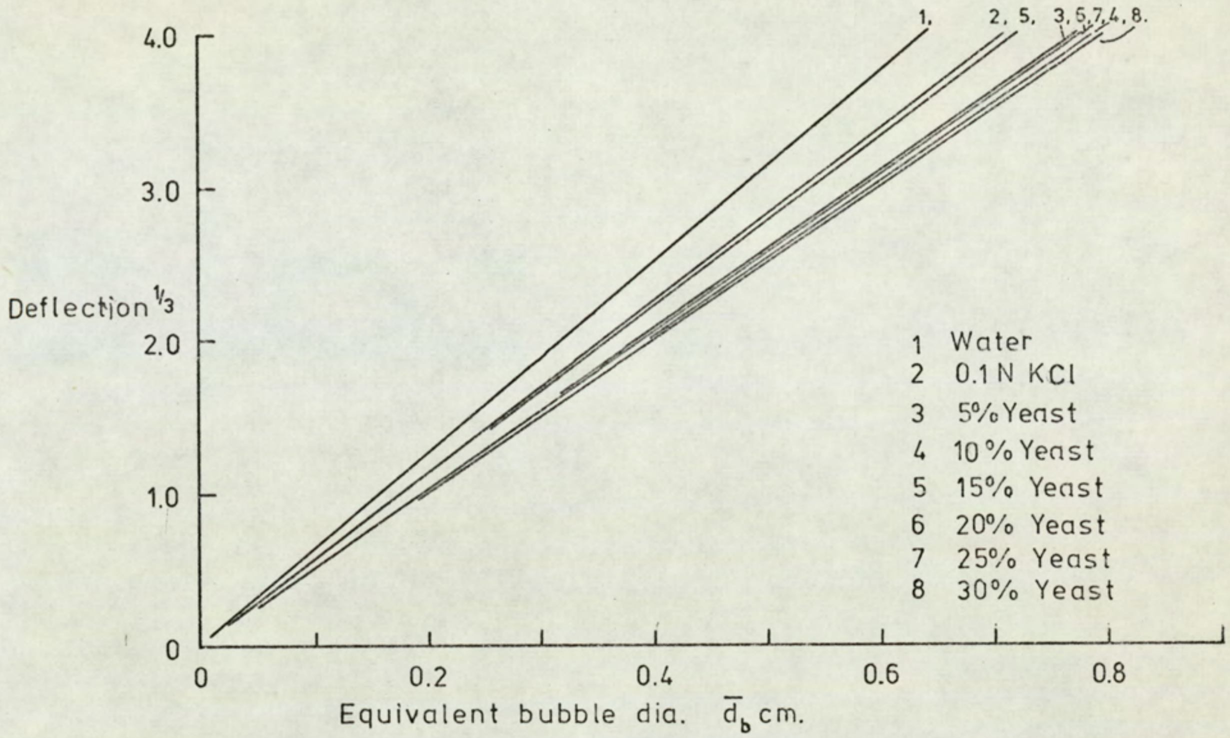

FIG 2.13 Calibration curves.
(Resistance method)

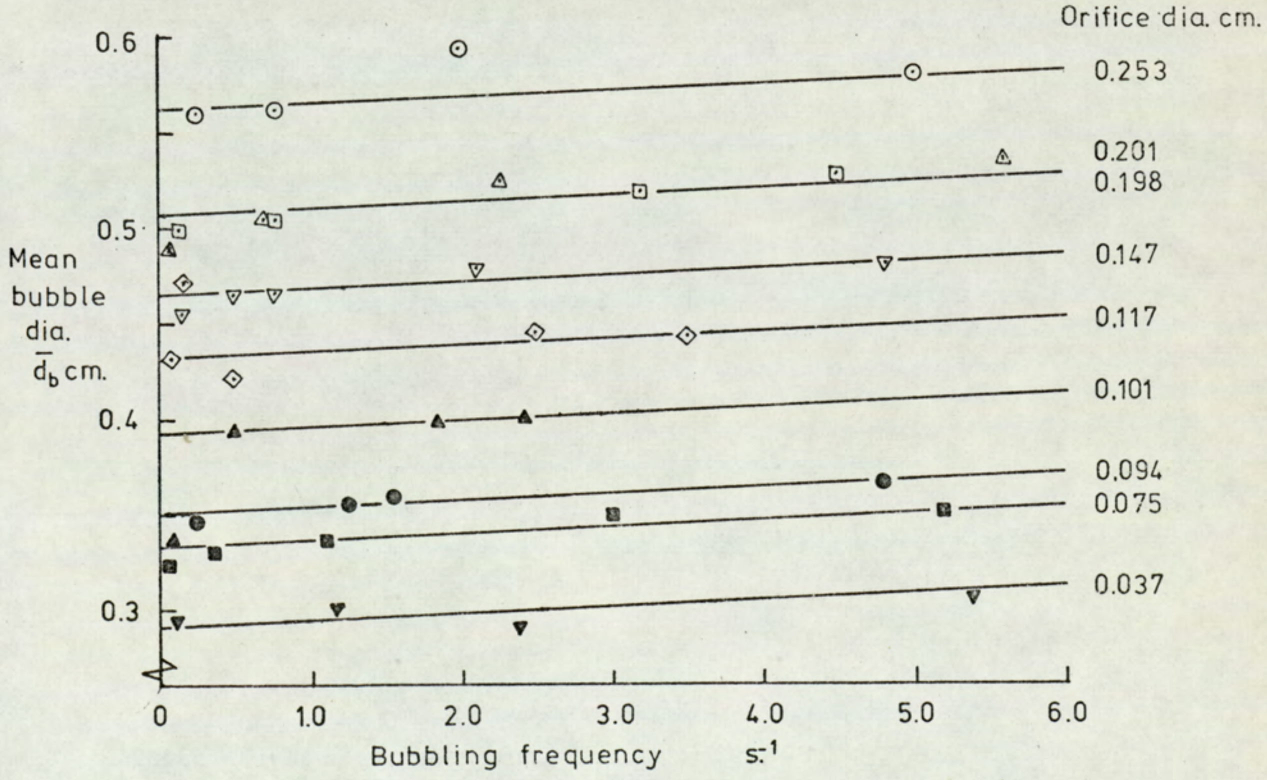

FIG 2.14 Bubble size as a function of gas flow (air/0.1N. KCl) min. air chamber volum

formation-rates and orifice diameters with the air-chamber beneath the orifice at minimum volume. These results are listed in full in Tables A.4 to A.12 in Appendix A, and a summary appears in Table 2.7.

The bubble formation-rate, the abscisca in Fig. 2.14, is in fact a measure of the flow-rate of the dispersed phase since

$$G_v = \frac{\pi}{6} f \bar{d}_b^{\,3} \qquad 2.17$$

Where G_v is the volumetric flow-rate (cm^3/s), f is the bubble frequency (bubbles/s) and $\bar{d}_b$ is in cm. As can be seen from Fig. 2.14 the mean bubble diameter increases linearly with the frequency over the range considered, although the effect of bubbling rate is not very great. The relationship between mean bubble diameter, for a given orifice diameter, and bubble formation-rate (see Fig. 2.15, the data for which was interpolated from Fig. 2.14) can be expressed in the following form:

$$\bar{d}_b = K \, d_o^{\frac{1}{3}} \qquad 2.18$$

where K is a constant dependent on the bubble formation frequency (see Fig. 2.16). From this plot the value of K was found to be given by the empirical relationship:

$$K = 0.881 \, f^{\,0.02} \qquad 2.19$$

By eliminating K between equations 2.18 and 2.19, an overall correlation between mean bubble diameter, bubble formation-rate or frequency, and orifice diameter is obtained:

$$\bar{d}_b = (0.881 \, f^{\,0.02}) \; d_o^{\frac{1}{3}} \qquad 2.20$$

This expression holds for the following conditions:

$$46 < Re_b < 1500$$

Where Re_b is the Bubble Reynolds Number, defined by Hughes et al [25] as

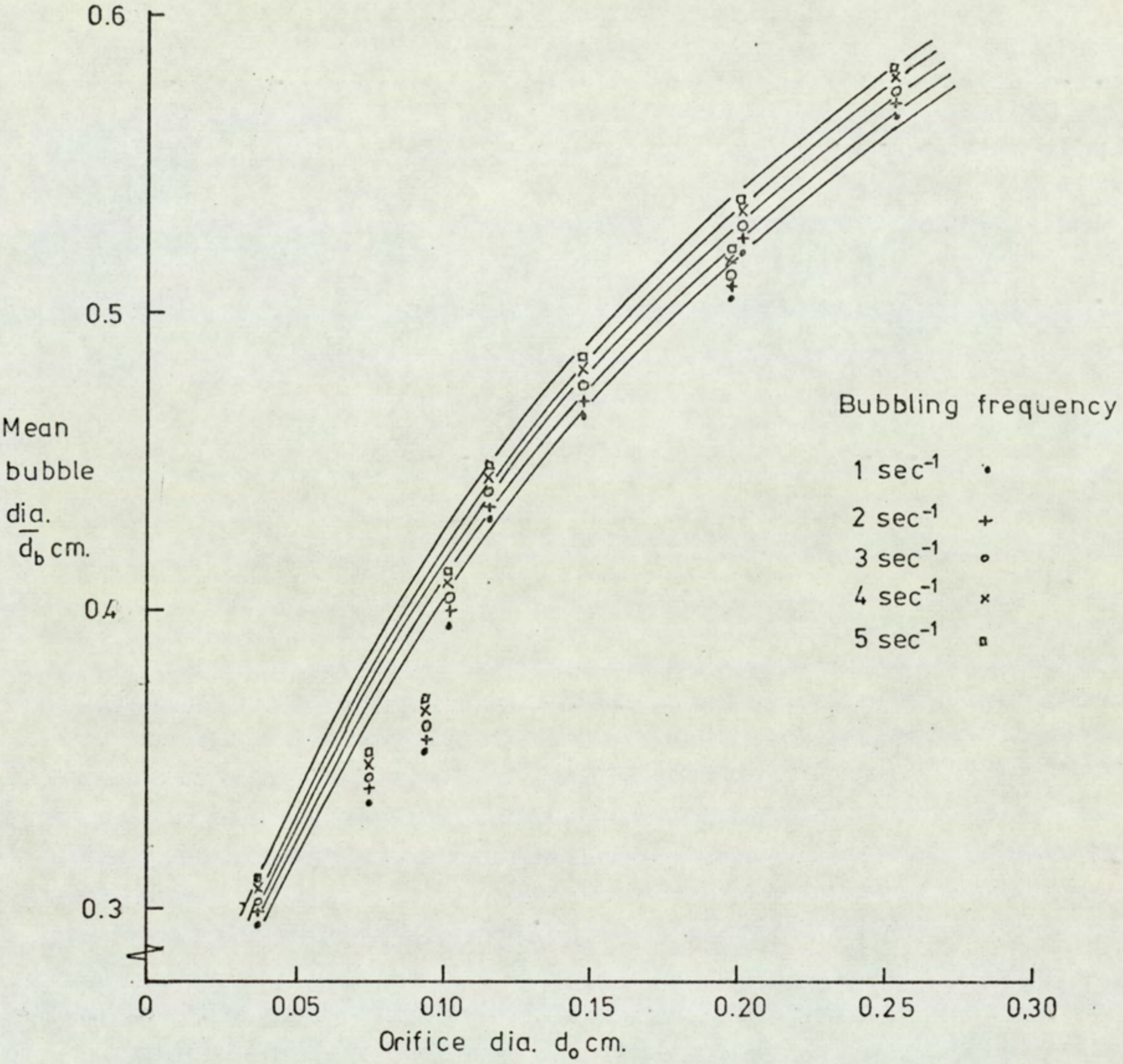

FIG 2.15 Bubble diameter as a function of orifice diameter for varying frequencies. (air/0.1 N. KCl)

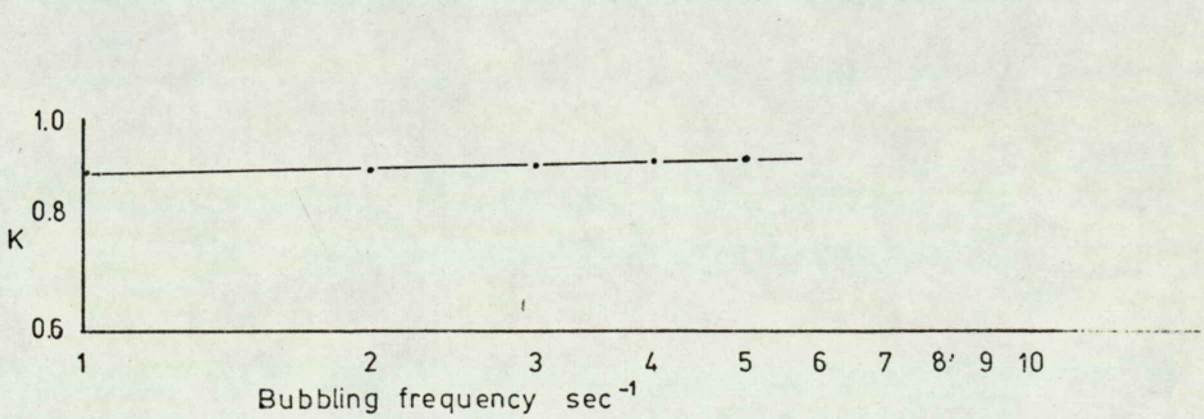

FIG 2.16 'K' (equation 2.18) "vs" bubbling frequency.

$$Re_b = \frac{\rho_l d_b v^*}{\mu_l} = \frac{2 d_b^4 \rho_l f}{3 \mu_l d_o^2} \qquad 2.21$$

where v^* is the mean gas velocity through the orifice.

When operating under conditions of maximum air-chamber volume, i.e. when the volume beneath the orifice was 52.4 cm^3, stable bubbling could not be maintained with an orifice diameter less than 0.147 cm. The reason for this phenomenon, which only occurs when operating with a single orifice, is multiple bubble formation.[1, 5, 36, 37] Since the chamber pressure is constant, the gas flow-rate must vary fractionally during the time of bubble formation: this results in the formation of one or more secondary bubbles, considerably smaller in size than the primary bubble. When these multiple bubbles did not coalesce but followed one another closely, it was impossible to obtain a meaningful deflection on the galvonometer. However, the results that were obtained are summarised in Table 2.7 and shown graphically in Fig. 2.17. Full details are given in Tables A.4 to A.7 inclusive in Appendix A. As can be seen from Fig. 2.17 the relationship between bubble formation-rate and bubble diameter for a given orifice diameter is not so systematic as for the results with the smaller air-chamber. Nevertheless there is a general increase in bubble diameter as the frequency, and thus the gas flow-rate, is increased. The reason for this more random pattern is not clear although it may be linked with the tendency for multiple bubbling to occur.

Fig. 2.17A shows the effect of the volume of the air-chamber on the bubble diameters, the values of which are all taken at a frequency of one bubble/s: the data for this figure were interpolated from Figs. 2.14 and 2.17. As can be seen, the effect of air-chamber volume is negligible for orifice diameters greater than 0.2 cm. Below this figure, the effect is slight although as orifice diameter decreases it becomes slightly greater.

As can be seen from Fig. 2.17A the relationship between mean bubble

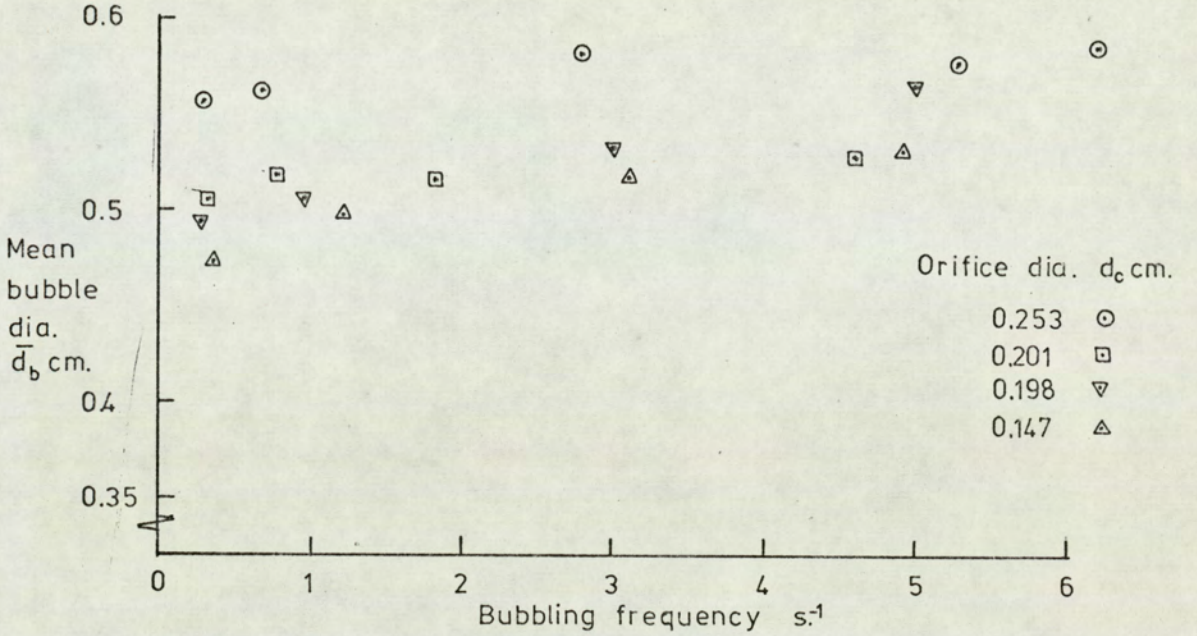

FIG 2.17 Bubble size as a function of gas flow (air/0.1N. KCl) max. air chamber volume.

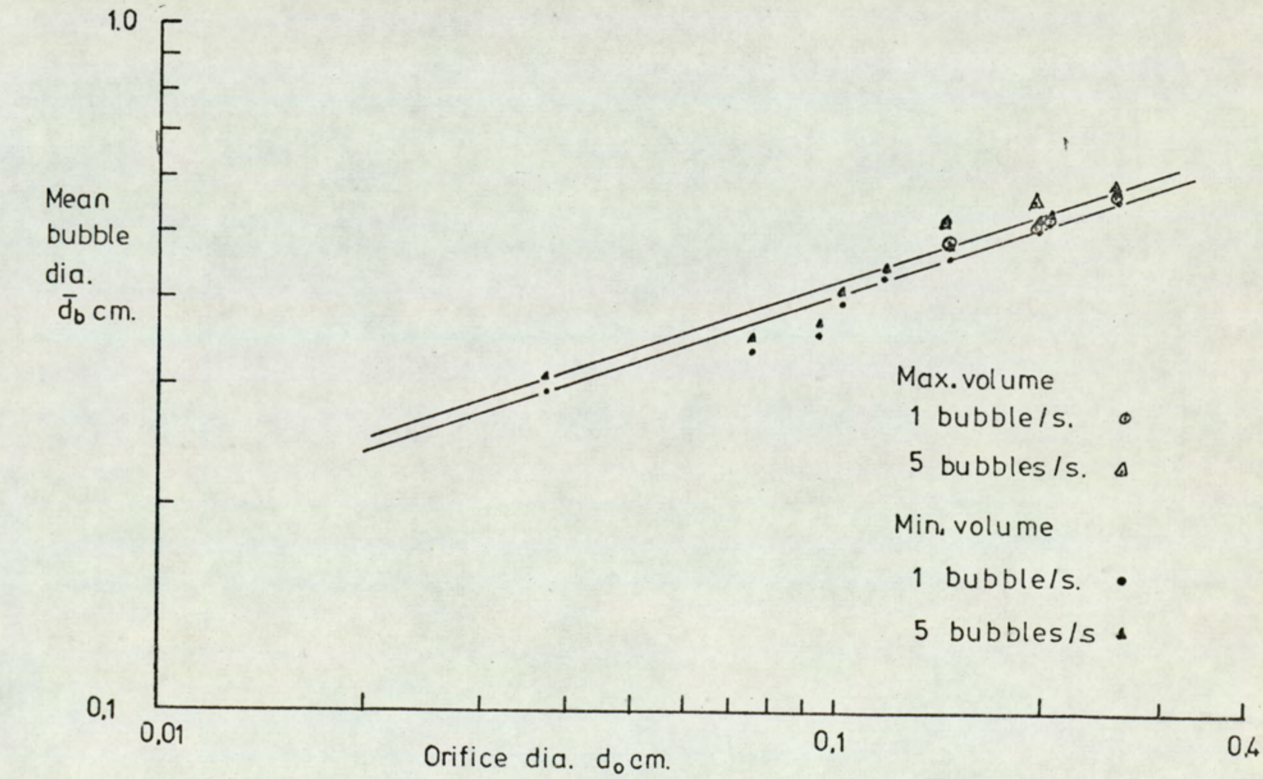

FIG 2.17a. Bubble sizes for frequencies of one and five bubbles/s. for both max. and min. air chamber volume.

SUMMARY OF RESULTS

Table 2.7

LIQUID PHASE : 0.1N KCl

GAS PHASE : AIR

Orifice Dia. cm.	Minimum Air Chamber Volume		Maximum Air Chamber Volume	
	Frequency Bubbles/s	Mean Bubble Dia. cm.	Frequency Bubbles/s	Mean d_b cm.
0.253	5.00	0.581	5.30	0.579
	2.00	0.596	2.80	0.581
	0.78	0.564	0.63	0.562
	0.26	0.562	0.29	0.559
0.201	4.50	0.528	4.60	0.528
	3.20	0.519	1.70	0.516
	0.77	0.506	0.78	0.518
	0.14	0.501	0.33	0.507
0.198	5.58	0.537	5.00	0.566
	2.28	0.526	3.00	0.531
	0.68	0.506	0.95	0.506
	0.09	0.490	0.26	0.494
0.147	4.80	0.480	4.90	0.533
	2.10	0.478	3.10	0.519
	0.77	0.466	1.20	0.499
	0.50	0.465	0.35	0.470
	0.17	0.458		

CONT'D ....

Summary of Results cont'd....

Orifice Dia. cm.	Minimum Air Chamber Volume		Maximum Air Chamber Volume	
	Frequency Bubbles/s	Mean Bubble Dia. cm.	Frequency Bubbles/s	Mean d_b cm.
0.117	3.50	0.441	No measurements could be obtained under these conditions because of the instability of bubble formation (see text)	
	2.50	0.444		
	0.50	0.420		
	0.16	0.471		
	0.09	0.430		
0.101	2.42	0.401		
	1.85	0.399		
	0.50	0.394		
	0.10	0.336		
0.094	4.80	0.367		
	1.55	0.360		
	1.25	0.357		
	0.23	0.346		
	0.11	0.338		
0.075	5.20	0.350		
	3.00	0.351		
	1.10	0.338		
	0.35	0.331		
	0.06	0.324		
0.037	5.40	0.307		
	2.40	0.291		
	1.18	0.302		
	0.12	0.295		

diameter and orifice diameter is similar to that obtained when using water (see equations 2.5 and 2.6). The exponent is the same, and the full expression is:

$$\bar{d}_b = 0.881\, d_o^{\frac{1}{3}} \qquad 2.22$$

at a bubbling frequency of one bubble/s, and

$$\bar{d}_b = 0.910\, d_o^{\frac{1}{3}} \qquad 2.23$$

at a bubbling frequency of five bubbles/s.

This is a variation of only 2% over a fivefold increase in flow-rate.

Series 3. Yeast Suspensions.

Since the frequency of bubble formation has only a small effect on bubble-size, it was not used as a parameter in this section of the experimental programme. The bubbling-rate was kept at about 1 - 2 bubbles/s: in fact the overall range was 0.715 to 2.43 bubbles/s, which accounts for a variation in bubble diameter of only 0.9%.

Six different yeast concentrations suspensions were used, the properties of which are shown in Table 2.8.

Table 2.8 Physical Properties of Yeast Suspensions.

Suspension No.	Dried Yeast gms.	Water gms.	Total Wt. gms.	% Yeast	*Density gm/cm^3	*Viscosity cP	Surface Tension dyne/cm
5Y	150	2850	3000	5.00	1.013	1.5	50.5
10Y	316	2850	3166	9.98	1.032	2.1	47.6
15Y	503	2850	3353	15.00	1.048	3.6	-
20Y	600	2400	3000	20.00	1.064	6.0	-
25Y	800	2400	3200	25.00	1.083	18.8	-
30Y	1030	2400	3430	30.03	1.099	-	-

* T hese measurements were obtained by Kilkarni[110].

The suspensions 10 Y and 15 Y were made up by adding extra yeast to the original suspension 5 Y. A completely fresh mixture was made up in the case of suspension 20 Y, and the most concentrated suspensions were again prepared by the addition of extra yeast. The yeast used was supplied by Hopkins and Williams * as Dried Bakers' Yeast in 500 gm lots. 2 kgm were obtained and thoroughly mixed to minimise variations in the yeast quality.

Throughout this series the circulating pump by-pass was used to regulate the flow of liquid, the downstream valve being fully open at all times (see Fig. 2.3). The mixing so achieved served to prevent the settling out of the yeast cells from the suspensions.

Again, as in the experiments with the potassium chloride solution, the volume of the air-chamber beneath the orifice was varied between the same two values.

The full experimental results are given in Tables A.13 - A.26 inclusive in Appendix A, whilst a summary is presented in Tables 2.9 and 2.10 and in Fig. 2.18.

As can be seen from Fig. 2.18, the slopes of the $\bar{d}_b$ vs d_o lines for $d_o > 0.14$ cm are the same as those for potassium chloride and water. Thus the relationship between orifice diameter and mean bubble size can be expressed as follows:

5% Yeast suspension

$$\bar{d}_b = 0.740\, d_o^{\frac{1}{3}} \qquad 2.24$$

10% Yeast suspension

$$\bar{d}_b = 0.675\, d_o^{\frac{1}{3}} \qquad 2.25$$

---

* Hopkins & Williams, Cheedwell Heath, Essex.

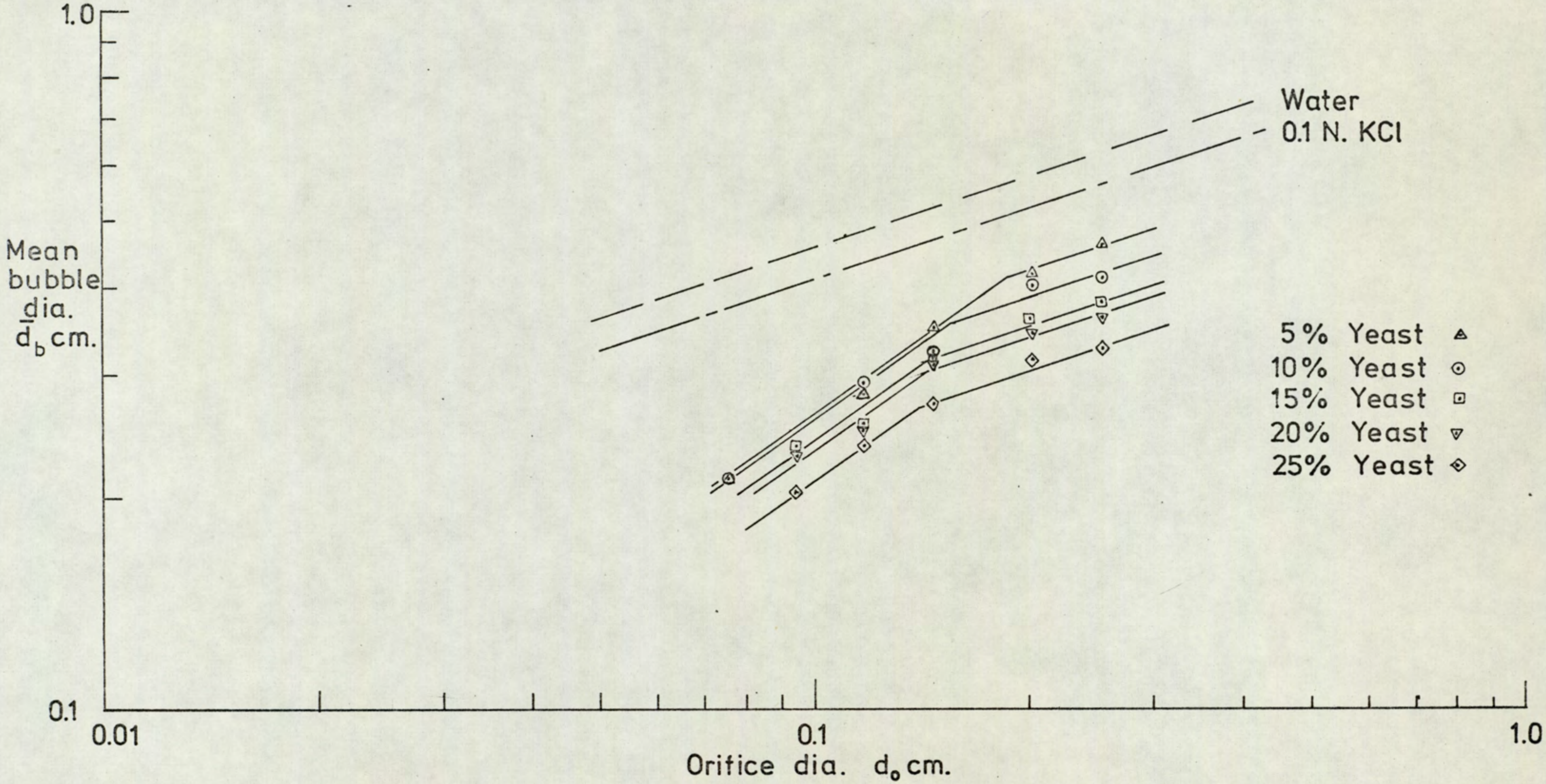

FIG 2.18 Bubble diameter as a function of orifice diameter (min. air chamber volume) for varying yeast concentrations.

15% Yeast suspension

$$\bar{d}_b = 0.615\, d_o^{\frac{1}{3}} \qquad 2.26$$

20% Yeast suspension

$$\bar{d}_b = 0.580\, d_o^{\frac{1}{3}} \qquad 2.27$$

25% Yeast suspension

$$\bar{d}_b = 0.530\, d_o^{\frac{1}{3}} \qquad 2.28$$

The major effect of increasing the concentration of yeast in the suspension is to decrease the bubble size formed at a given orifice.

Table 2.9 Bubble Diameters, air/yeast suspension (min.chamber volume)

% Yeast / Orifice Dia.cm.	5%	10%	15%	20%	25%	30%
	Bubble Dia. cm.					
0.253	0.468	0.416	0.382	0.365	0.330	0.387
0.201	0.421	0.404	0.364	0.342	0.320	0.383
0.147	0.367	0.322	0.321	0.316	0.274	0.322
0.117	0.284	0.296	0.256	0.254	0.241	0.309
0.094	-	-	0.240	0.233	0.206	0.287
0.075	0.214	0.214	-	-	-	-

Table 2.10 Bubble Diameters, air/yeast suspension (max.chamber volume)

% Yeast / Orifice Dia.cm.	5%	10%	15%	20%	25%	30%
		Bubble Dia. cm.				
0.253	0.510	0.458	0.400	0.380	0.361	0.399
0.201	0.437	0.414	0.364	0.345	0.342	0.397
0.147	-	-	-	0.328	0.332	0.385
0.117	-	-	-	-	0.320	-

Increasing the quantity of yeast in the suspension obviously changes the physical properties (see Table 2.8). The density is not greatly affected but marked changes in viscosity and surface tension occur. As the surface tension decreases, so the triple angle of contact decreases. This in turn decreases the bubble size. It is also a factor leading to the formation of rigid bubbles. The effect of viscosity on bubble formation has not been studied in great depth but it is generally accepted that the effect at low gas flow rates is negligible. It seems that the main effect of viscosity occurs after the bubble has detached, either causing or hindering coalescence. At higher gas flow rates the effect of viscosity is greater when it is linked with inertial effects of the liquid.

The effect of the upstream gas-chamber volume has been studied by several workers[2, 5, 7, 22, 24] who distinguish two distinct cases: (1) constant pressure situation corresponding to an infinitely large reservoir and (2) the case of constant gas-flow. In the latter case smaller bubbles are to be expected from a given orifice, since the pressure drop across the orifice fluctuates and causes the bubble to be released a little prematurely. This behaviour is confirmed by the results shown in Tables 2.9 and 2.10. The effect of air-chamber volume is less marked in the case of multiple orifices. With several orifices, the pressure fluctuations and the gas flow-rate variations mentioned earlier are smoothed out.

Another factor which must be considered is the presence of solid particles in the liquid phase. Because of their effect on the physical properties of the suspensions, they must influence the bubble formation and detachment mechanisms. Another effect, viz. partial blockage of the orifice, will also become increasingly important as the particle diameter to orifice diameter ratio increases.

Intuitively one would expect bubble sizes to be smaller than usual.

This phenomenon possibly accounts for the more rapid change in $\bar{d}_b$ which is observed with all the yeast suspensions at smaller orifice diameters. This does not occur with either water or potassium chloride solution as the liquid phase.

The results obtained with the 30% yeast suspensions do not follow the expected trend, probably because the liquid phase was non-Newtonian. For this reason, the experimental results were not fully analysed. Considerably more work needs to be done with non-Newtonian systems before any conclusions can be drawn.

2.3.6 EXPERIMENTAL RESULTS ON BUBBLE SIZE DISTRIBUTION.

Theory.

Figures 2.19 to 2.23 inclusive show the "normalised" frequency distribution curves of the bubbles formed at a given orifice. Mitropolskij[111] has suggested that an expression of the form

$$y\,(z_i) \;=\; K^1 \left(1 + \frac{z_i}{l_1}\right)^{q_1} \left(1 - \frac{z_i}{l_2}\right)^{q_2} \qquad 2.29$$

where

$$\frac{q_1}{q_2} \;=\; \frac{l_1}{l_2} \qquad 2.30$$

can be fitted to such curves. In equation 2.29 $y\,(z_i)$ is the frequency of species z_i, where z_i is the displacement about the mean ($z_i = 0$), l_1 and l_2 are the limits set for the distribution and K^1 is the frequency at $z_i = 0$ (see also Fig. 2.24) From equation 2.29 it can readily be shown that

$$q_2 \;=\; \frac{\ln y\,(z_i) \;-\; \ln K^1}{\frac{l_1}{l_2}\;\ln\left(1 + \frac{z_i}{l_1}\right) + \ln\left(1 - \frac{z_i}{l_2}\right)} \qquad 2.31$$

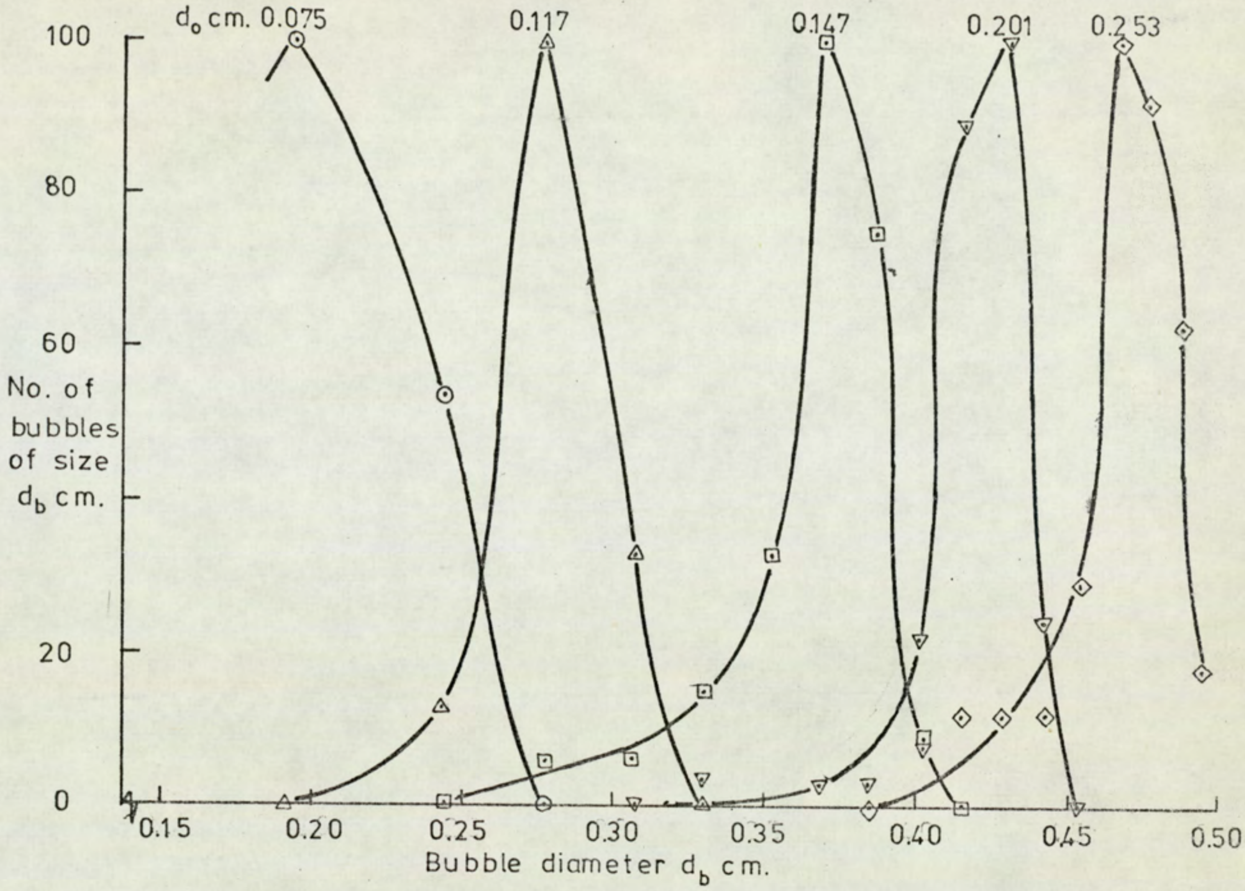

FIG 2.19 Bubble size distribution (5% yeast).

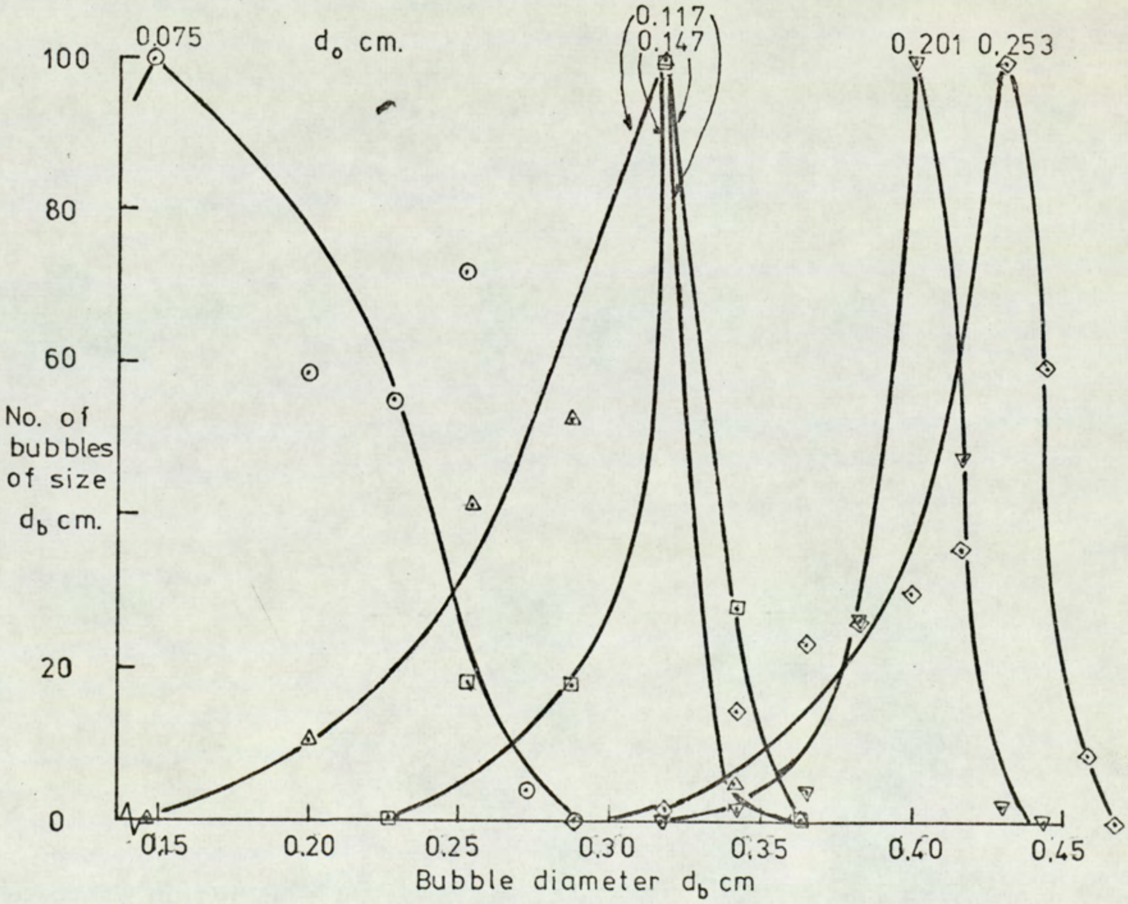

FIG 2.20 Bubble size distribution (10% yeast).

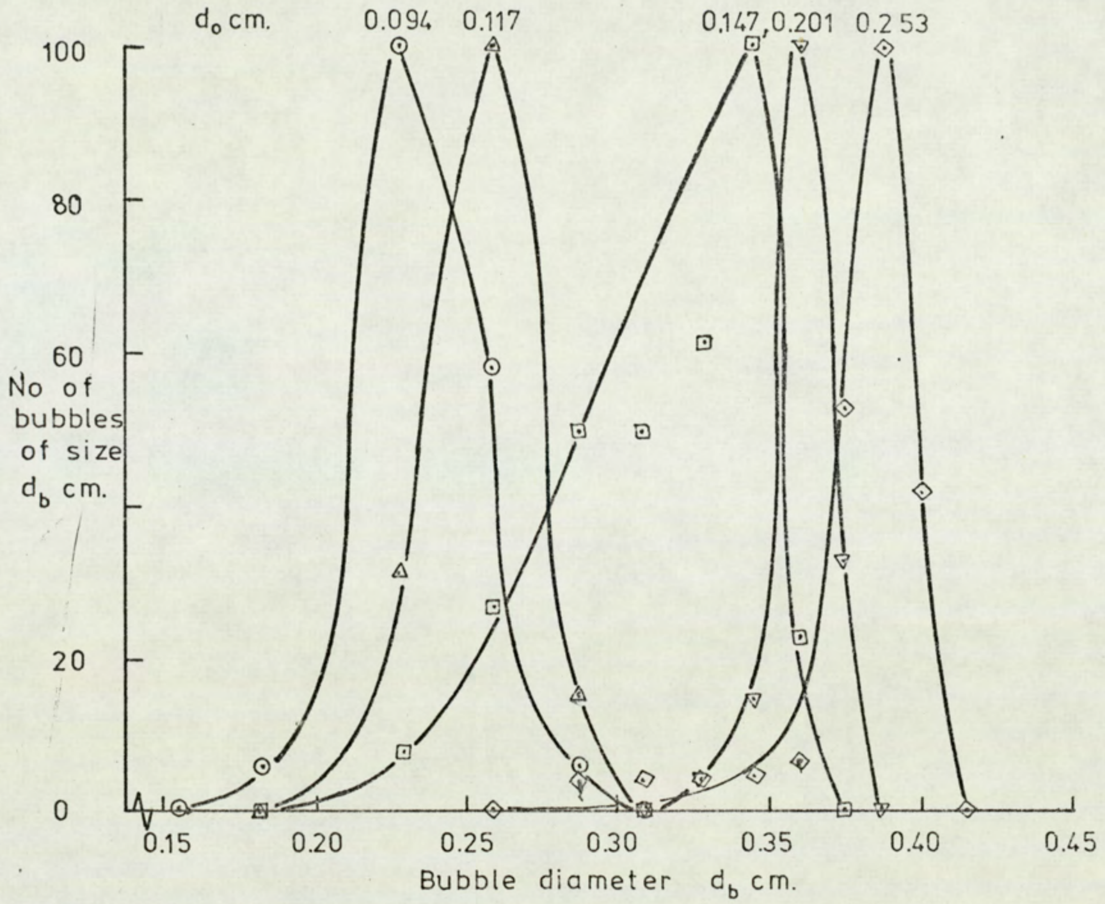

FIG 2.21 Bubble size distribution (15% yeast).

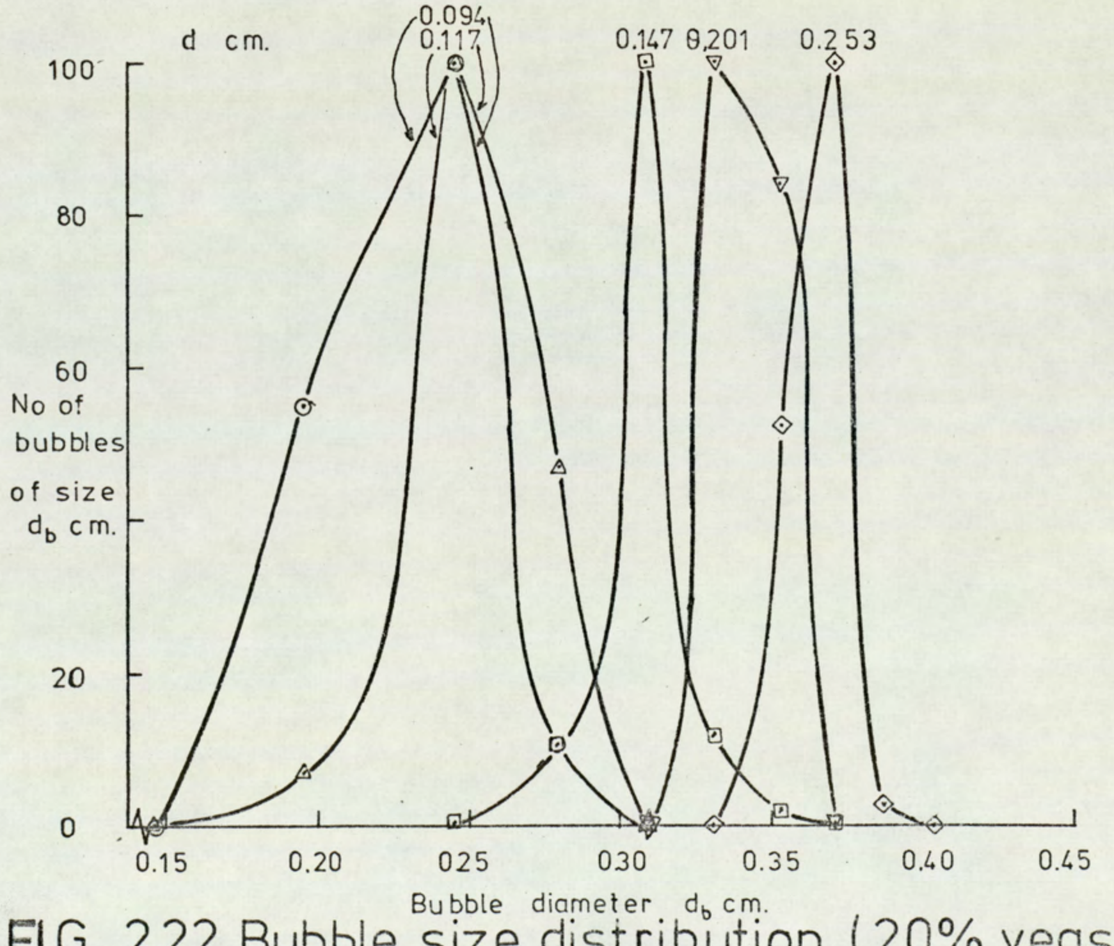

FIG 2.22 Bubble size distribution (20% yeast).

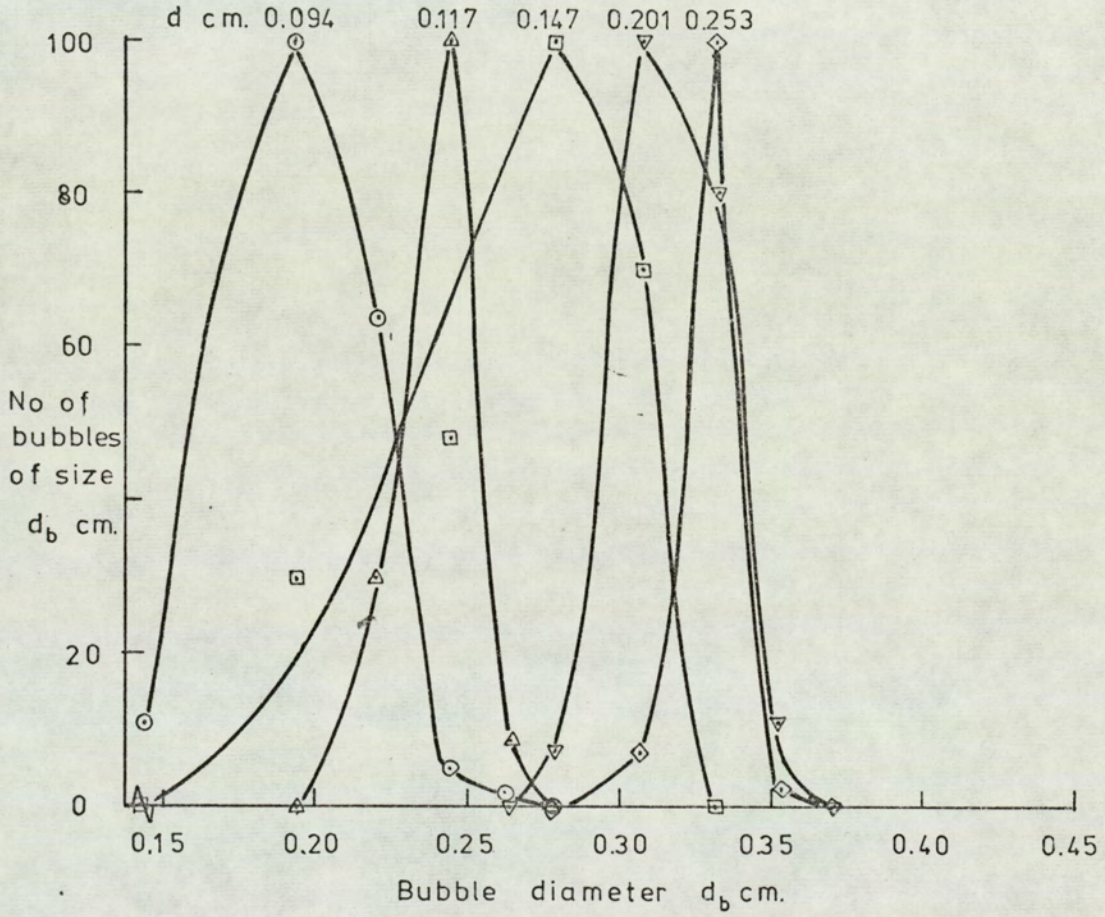

FIG 2.23 Bubble size distribution (25% yeast).

After determining the frequency distribution curve for the

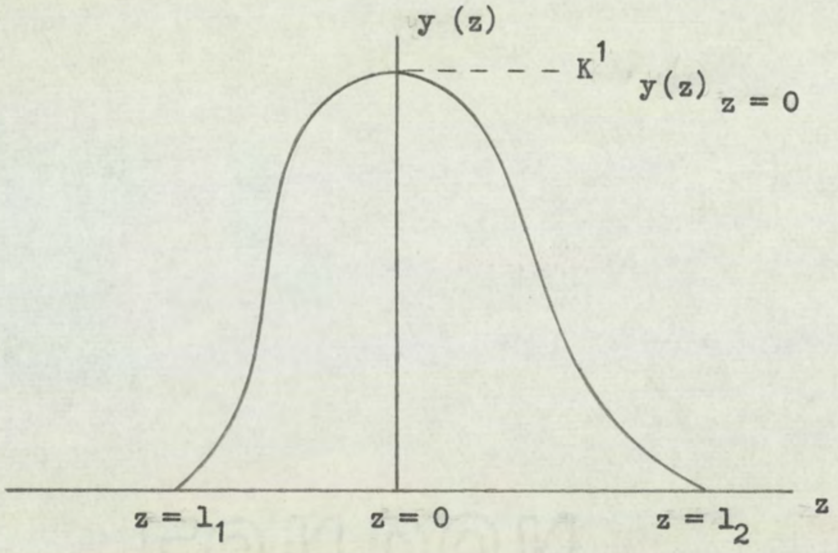

Fig. 2.24 Nomenclature used in size distribution calculations

experimental results a fitness test was applied.

Method of Determining the Distribution Frequency Curves.

Since the bubble diameter at which the maximum number of bubbles was counted was close to the calculated mean bubble diameter, this point was taken as $z = 0$. The differences between the calculated $\bar{d}_b$ and bubble diameter at the mean of the distribution are shown in Fig. 2.25. The maximum error in assuming that the two diameters are identical is 7·0%. However, neglecting the two extreme points of the remaining points on the curve, 85% lie within the limits $\pm$ 3·5%. This is considered to be satisfactory agreement and within experimental error.

Initially, for each set of yeast concentrations, the mean value of the bubble diameter, i.e. the value of $\bar{d}_b$ at which the greatest number of bubbles occurred, was designated as $z = 0$. The frequencies of occurrence, $y(z_i)$, were then tabulated at values of $\pm z_i$, the displacement from the mean (see Tables A.28 to A.32 in Appendix A); and these figures were put into one table for each concentration (see Tables A.33 to A.37 - columns 1 and 2). The values of l_1 and l_2, i.e. the values of z_i at which $y(z_i)$ is zero, were then nominated by inspection of the curves. With this information, it is then possible to calculate the two values $(1 + \frac{z_i}{l_1})$ and $(1 - \frac{z_i}{l_2})$ for each value of z_i (see columns 3 and 4 Table A.33). An initial value of q_2 was then estimated using equation 2.31 and values of z_i and $y(z_i)$ taken from any one set of data. Having found q_2, the value of q_1 was determined from equation 2.30. Having obtained the parameters required in equation 2.29, frequency distribution values, $y(z_i)$, were then calculated using the distribution equation (see column 5 Table A.33) and the fitness test applied. If this was not satisfied, a new value of q_2 and q_1 were obtained and the process repeated.

This procedure was repeated for each suspension concentration.

Results.

The results of these calculations are listed in Tables A.33 to A.37 in Appendix A. Comparisons between the experimental and computed data are shown in Figs. 2.26 to 2.30 inclusive, the solid lines representing the calculated size-distribution curves, whilst the experimental values are shown as points.

The calculated expressions which best satisfied the experimentally determined distributions are as follows:

5% Yeast Suspensions

$$y\,(z_i) = 100\left(1 + \frac{z_i}{1.00}\right)^{7.5}\left(1 - \frac{z_i}{0.40}\right)^{3.0} \qquad 2.32$$

10% Yeast Suspension

$$y\,(z_i) = 100\left(1 + \frac{z_i}{1.09}\right)^{15}\left(1 - \frac{z_i}{0.47}\right)^{5.0} \qquad 2.33$$

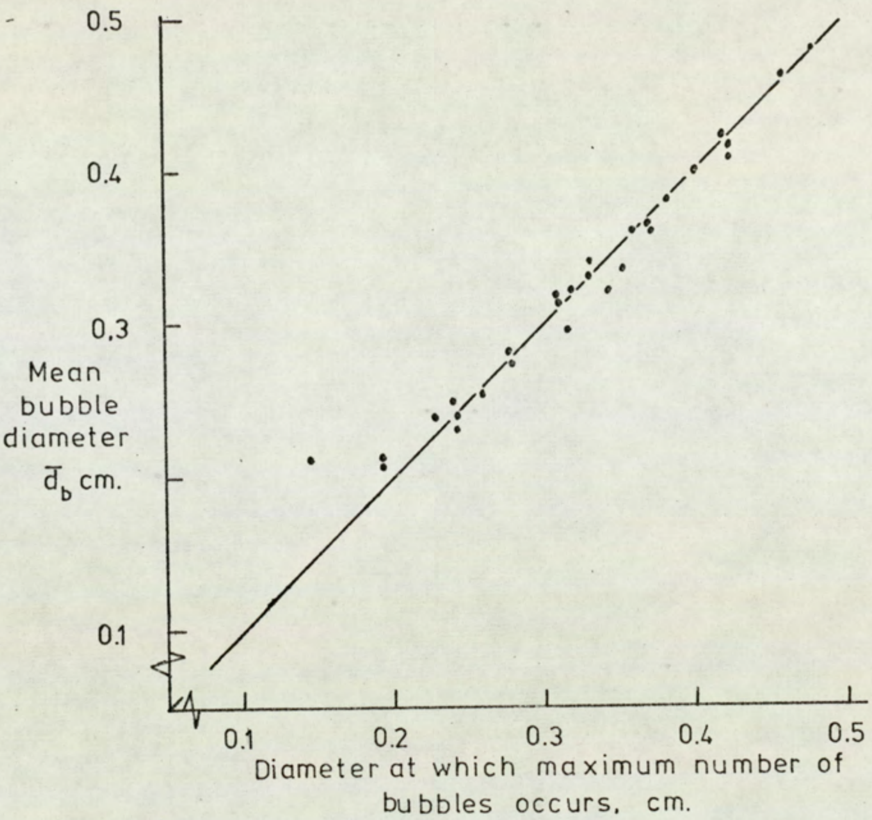

FIG 2.25 Comparison of calculated and modal bubble diameters.

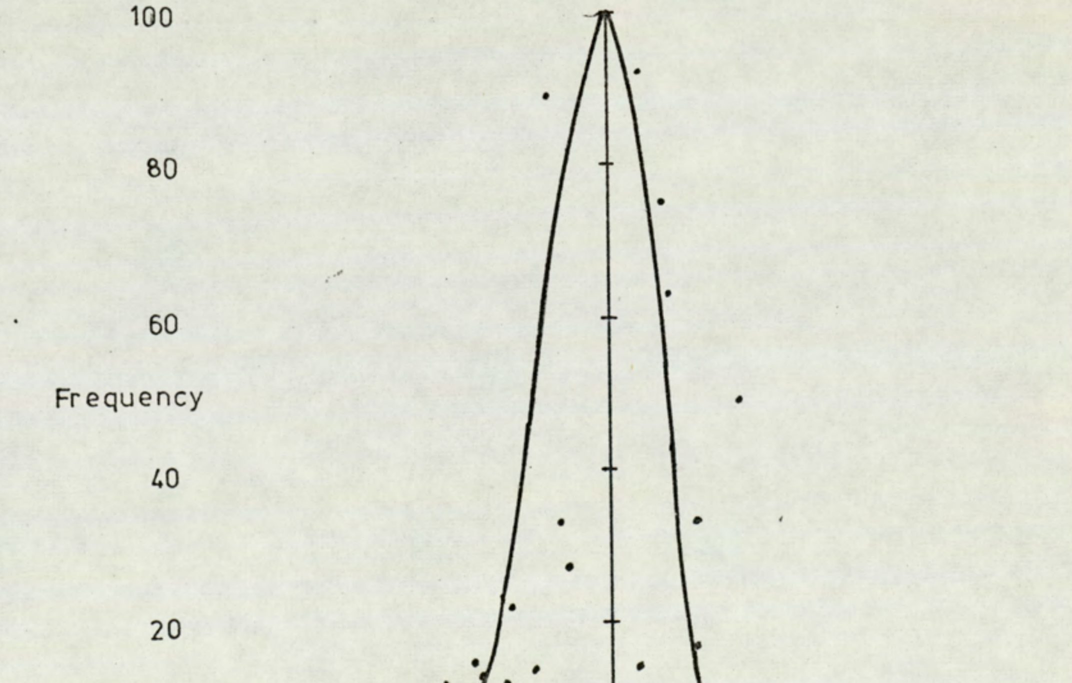

FIG 2.26 Comparison of distributions (5% yeast).

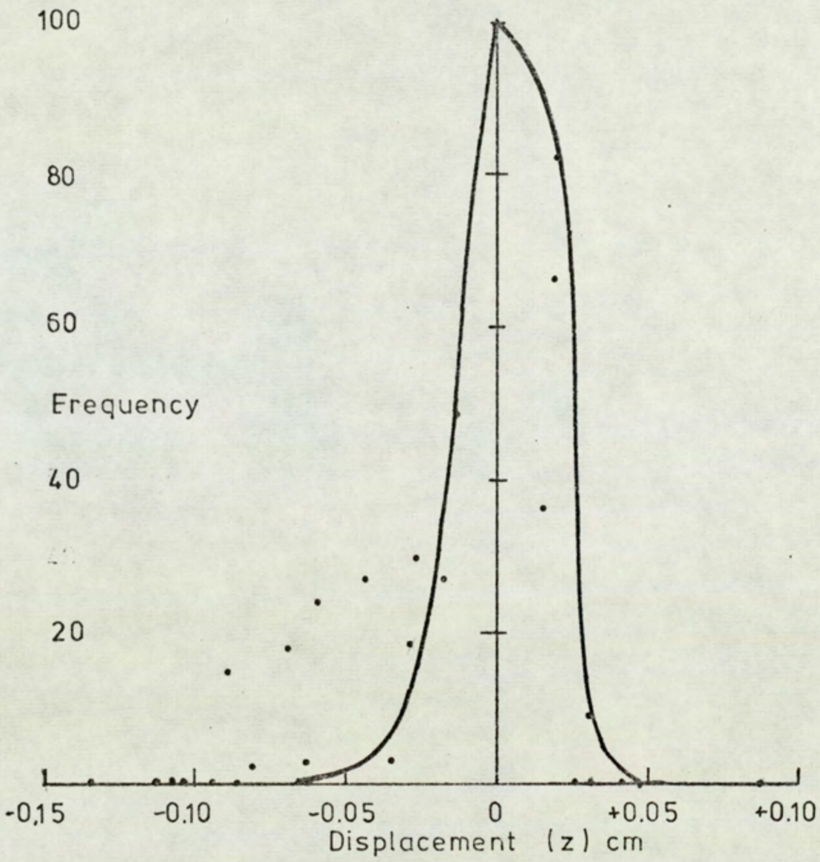

FIG 2.27 Comparison of distributions (10% yeast).

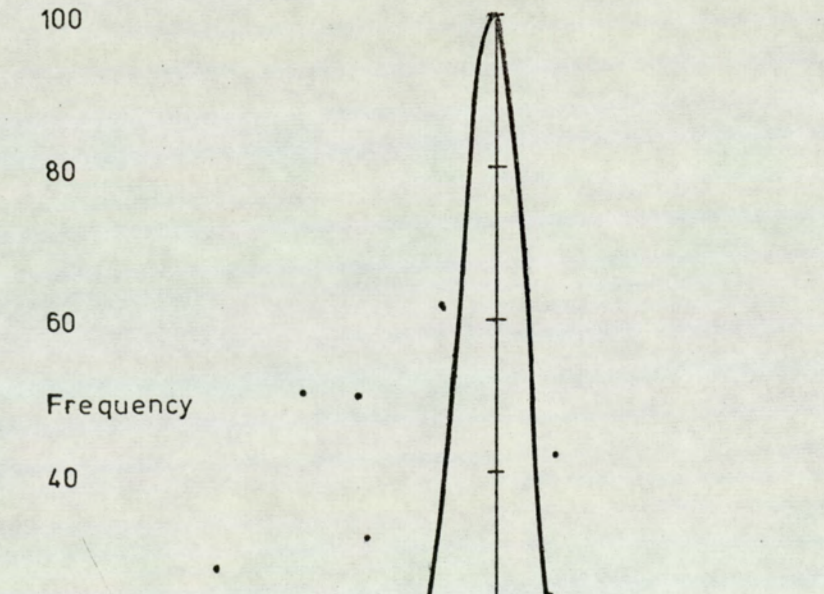

FIG 2.28 Comparison of distributions (15% yeast).

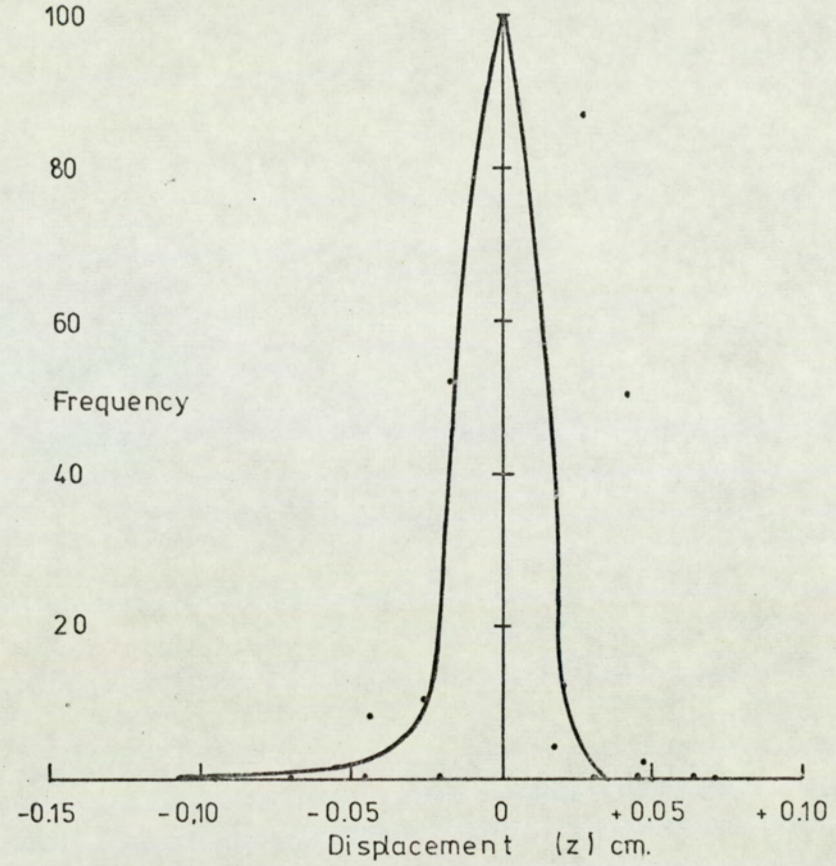

FIG 2.29 Comparison of distributions (20% yeast).

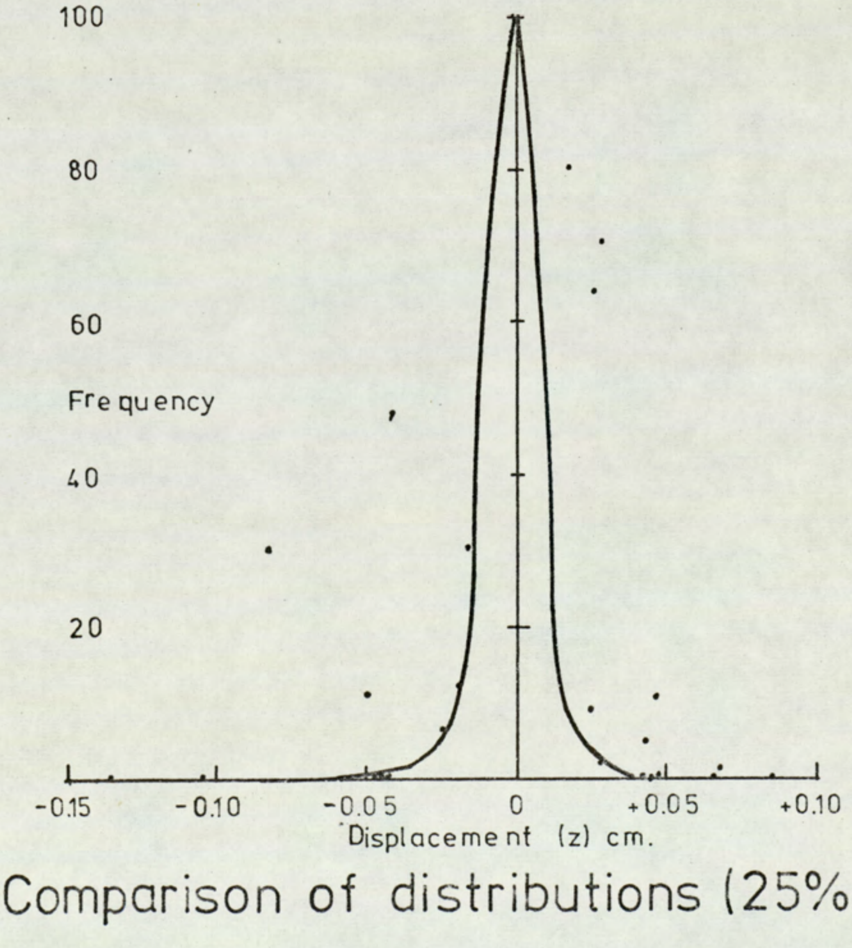

FIG 2.30 Comparison of distributions (25% yeast).

15% Yeast Suspension

$$y(z_i) = 100\left(1 + \frac{z_i}{1.10}\right)^{22} \left(1 - \frac{z_i}{0.40}\right)^{8.0} \qquad 2.34$$

20% Yeast Suspension

$$y(z_i) = 100\left(1 + \frac{z_i}{1.08}\right)^{29} \left(1 - \frac{z_i}{0.40}\right)^{10.0} \qquad 2.35$$

25% Yeast Suspension

$$y(z_i) = 100\left(1 + \frac{z_i}{1.08}\right)^{36} \left(1 - \frac{z_i}{0.40}\right)^{13.0} \qquad 2.36$$

A summary of the results is given in Table 2.11 which lists the values of l_1, l_2, q_1 and q_2 for each concentration of yeast.

Table 2.11 Values of l_1 l_2 q_1 and q_2

Conc'n. % Dry Wt.	l_1	l_2	q_1	q_2
5	1.00	0.40	7.5	3.0
10	1.09	0.47	15.0	5.0
15	1.10	0.40	22.0	8.0
20	1.08	0.40	29.0	10.0
25	1.08	0.40	36.0	13.0

From Table 2.11 it can be seen that the values of l_1 and l_2 can be assumed to be constant, within the limits of experimental error, with a mean value of l_1 equal to 1.07 and l_2 equal to 0.414. The values of q_1 and q_2 have been plotted against concentration in Fig. 2.31 which shows that they are both linearly dependent on concentration. The constant of proportionality is 1.44 in the case of q_1 and 0.52 in the case of q_2, i.e

$$q_1 = 1.44\,C \qquad 2.37$$

and

$$q_2 = 0.52\ C \qquad 2.38$$

where C is the % concentration of yeast, on a dry weight basis. Using equations 2.32 - 2.38, the distribution of bubble sizes for any yeast concentration can be written

$$y\ (z_i) = 100\ \left(1 + \frac{z_i}{1.07}\right)^{1.44C} \left(1 - \frac{z_i}{0.414}\right)^{0.52C} \qquad 2.39$$

In order to describe the relationship between the mean bubble diameter and orifice size for different suspensions, it was anticipated that an equation similar in form to 2.5 would be suitable, with the constant B as some function of the concentration, C.

This latter relationship was found by plotting the constants in equations 2.24 to 2.28 against the concentration (see Fig. 2.32). This gave rise to the equation

$$B = \frac{1.12}{C^{0.22}} \qquad 2.40$$

The final correlation for yeast suspensions is

$$\bar{d}_b = 1.12\ C^{-0.22}\ d_o^{\frac{1}{3}} \qquad 2.41$$

Due to the similarity in behaviour of air bubbles in yeast suspensions and in potassium chloride solutions, it is perhaps reasonable to assume that a modified form of equation 2.20 would suffice to determine the effect of gas flow-rate on mean bubble diameter.

2.3.7. CONCLUSIONS

The major conclusion that can be drawn from the preceding work is that the diameters of bubbles generated in a steady stream from a horizontal,

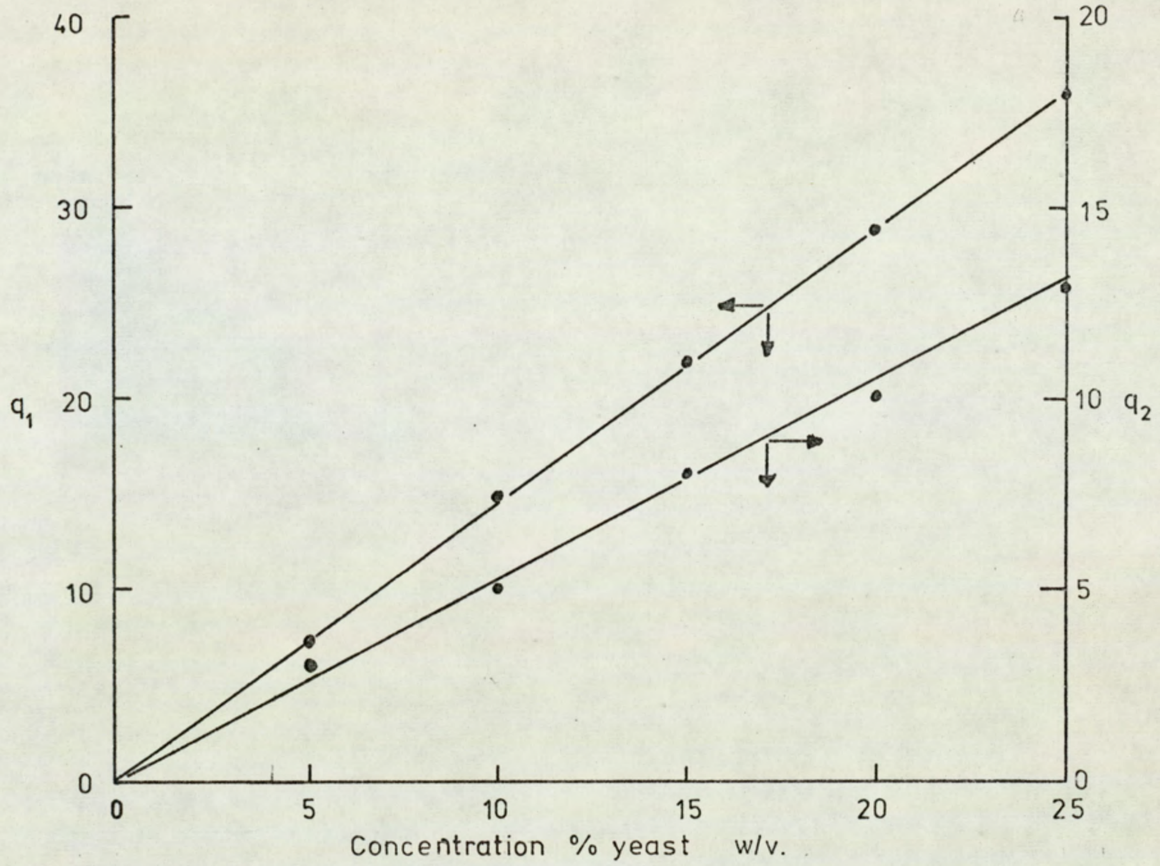

FIG 2.31 Relation between q_1, q_2, and concentration.

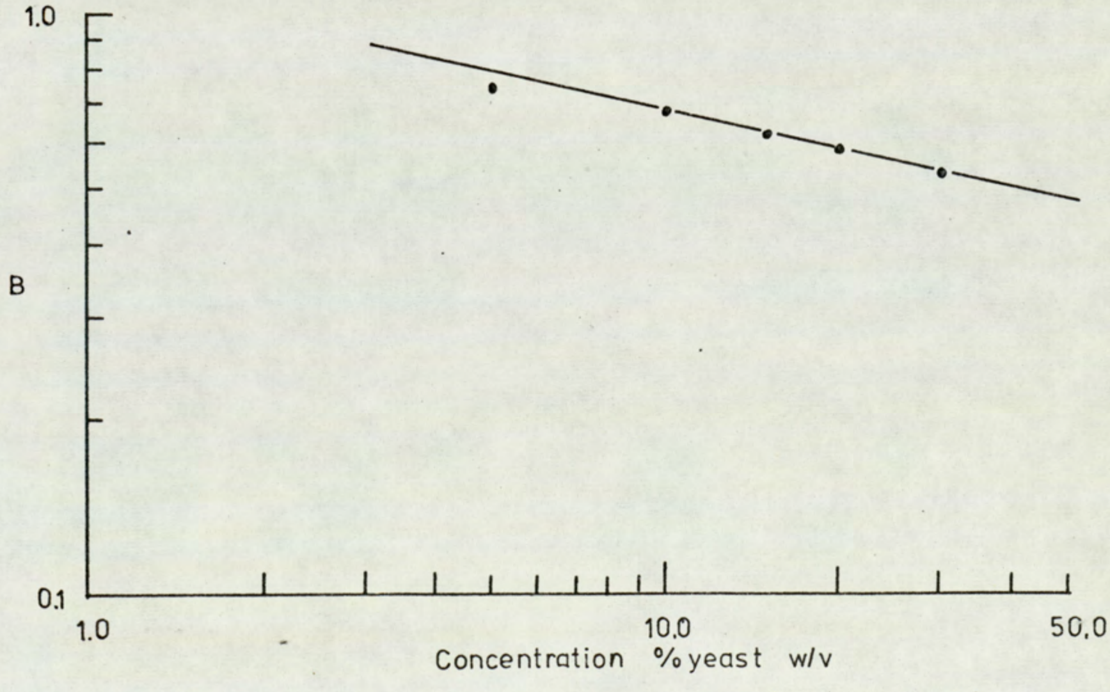

FIG 2.32 Relation between 'B' (eqn. 2.5) and yeast concentration.

circular, smooth-edged orifice are strongly dependent upon orifice diameter and weakly dependent upon gas-rate for a given set of liquid properties. At a given bubble generation the relationship is of the form:

$$\bar{d}_b = B\, d_o^{\,k} \qquad 2.5$$

Section 1. Tap Water

The only conclusion that can be drawn from this section is that the bubble diameter and orifice diameter are related by the following expression:

$$\bar{d}_b = 1.0\, d_o^{\frac{1}{3}} \qquad 2.6$$

Section 2. Potassium Chloride Solutions

The correlation for mean bubble diameter is:

$$\bar{d}_b = (0.881\, f^{0.02})\, d_o^{\frac{1}{3}} \qquad 2.20$$

This correlation was found to hold good for values of Re_b:

$$46 < Re_b < 1500$$

although for one case; that of the maximum flow-rate through the smallest orifice (0.037 cm.) a bubble Reynolds Number of approximately 4000 was calculated.

The range of orifice diameters for which equation 2.20 is valid is 0.037 cm. (0.048% free area) to 0.253 cm. (2.5% free area). These figures represent a flow-area variation of approximately 50 times.

The effect of the air-chamber volume beneath the orifice cannot really be defined, since only two values were studied; but over a change in

Capacitance Number of a factor of 10 for each orifice used, the diameter of the issuing bubbles was only varied slightly and this effect would be lost as soon as a multiple-holed orifice was used.

Section 3. Yeast Suspensions

It was found that equation 2.5 also described the effect of orifice diameter on bubble diameter when operating with yeast suspensions as the liquid-phase. The value of K was found to be dependent on the concentration (and thus the physical properties) of the suspension (equation 2.41). The limits over which this equation can be applied are not so wide, and range from $d_o = 0.253$ cm. to $d_o \simeq 0.15$ cm. (a flow-area change of 3 times).

Over the lower range of the orifice diameters, $d_o \simeq 0.15$ cm. to $d_o \simeq 0.075$ cm. (a flow-area variation of 4 times) the exponent of d_o altered and equation 2.5 becomes:

$$\bar{d}_b = K_1 \, d_o^{\frac{2}{3}} \qquad 2.42$$

where K_1 again is dependent on the properties of the liquid-phase.

The cause of this steepening of the curve at $d_o = 0.15$ cm. is probably, as mentioned earlier, that the ratio of yeast particle diameter to orifice diameter is becoming sufficiently large to alter the geometry of the orifice.

The effect of varying the Capacitance Number is insignificant, an average increase in $\bar{d}_b$ of 6.3% (compared to 4% when operating with KCl solutions) for an air-chamber volume change of 10 times. The Capacitance Number was not calculated due to lack of data.

Due to the similarity in behaviour between the bubble formation in potassium chloride and in yeast suspensions, one can assume that the variation of bubble-size with bubbling frequency is very similar. This means that a modified form of equation 2.20 could be used to predict this effect.

Bubble-Size Distributions

Theoretically one would not expect bubble sizes to vary when all the conditions are steady. Obviously this state of affairs cannot be attained in practice and slight variation in operating conditions are bound to be met. The variations can include such factors as:

1) Slight changes in pressure in the air-space beneath the orifice, causing premature or delayed bubble release,

2) Slight variation in air-supply pressure, causing alteration in flow of gas.

3) Alteration of ambient temperature affecting both air and liquid-flows.

4) The liquid circulation around the periphery of the orifice could alter fractionally, thus changing the turbulence effects on bubble release.

5) Variation in liquid pumping-rate, caused by voltage fluctuations or cavitation in the pump.

6) Differences in physical properties of the liquid-phase, due to incomplete mixing.

None of the above factors would have a great effect, either singly or collectively, on the bubble diameters, but as can be seen from the size-distribution graphs, all the bubble diameters for a given set of conditons fall within a narrow field which is evenly spread either side of the mean value.

The bubble-size distributions are very well described by the equation:

$$y\,(z_i) \;=\; K^1 \left(1 + \frac{z_i}{l_1}\right)^{q_1} \left(1 - \frac{z_i}{l_2}\right)^{q_2} \qquad 2.29$$

where q_1 and q_2 are dependent upon the physical properties of the liquid-phase.

By using equations 2.41, 2.29 and 2.42 and a modified form of equation 2.20, a full description of bubbling from single circular-holed orifices in yeast suspensions can be obtained.

The method of determining bubble-size distributions that has been developed is accurate and reproducable and has the major advantage that it can be employed in opaque systems or when using suspensions.

It should be possible to develope the technique further to include a measure of the bubble rise velocity and to determine bubble sizes in very low voidage bubble swarms.

Having developed the technique, a more thorough investigation should now be carried out into the effects of parameters, such as liquid viscosity, liquid density and surface tension effect, acting singly and together (as they do in yeast suspensions) and the effect of solid particles distributed in the liquid-phase.

3. BUBBLE - SWARM SYSTEMS

3.1. INTRODUCTION

Having studied the various factors involved in the formation of a stream of bubbles rising from a single orifice, the behaviour of bubble swarms in water and yeast suspensions was then investigated. The initial work was carried out in a small-scale apparatus, mainly to gain experience with this type of system.

After some experimentation and familiarisation with the small-scale equipment, work was continued with two larger columns, 6" and 12" in diameter. For convenience, the preliminary experiments and the more detailed studies with the large columns are described in separate sub-sections.

3.2. INITIAL STUDIES WITH THE SMALL-SCALE COLUMN

3.2.1 INTRODUCTION

The experiments carried out with the small-scale column, which was $1\frac{1}{2}$" (3.8 cm) in diameter, included measurements of the bubble-size distribution of bubble swarms generated from two types of gas distributor, viz. perforated and porous plates. A photographic method was used for this purpose.

The parameters included in the experimental programme were gas hold-up, liquid superficial velocity and gas-distributor design. By manipulating the gas flow-rate, gas hold-up was varied between about 5% and 20% by volume. Only two values of the liquid superficial velocity were used, viz. 0.06 and 0.34 cm/s. Details of the gas distributors used will be found in Table 3.1. Birmingham tap-water was used as the liquid phase throughout the work.

3.2.2 EXPERIMENTAL APPARATUS

Flow Equipment

The general layout of the apparatus is shown diagrammatically in Fig. 3.1: it was similar to that described in Chapter 2.

The liquid phase was contained in the reservoir (1), a 25 l aspirator, and was circulated by means of a Stewart centrifugal pump (2) with a pump recirculation-line and control-valve (3). The liquid-flow to the column was controlled by two valves (3) and (4) and measured by a Rotameter (size Metric 7 with Koranite float) (5). The liquid entered the column by means of a pipe-hose connector and an equal 'T'-piece in the base of the column (6). The column itself (7) consisted of sections of $1^1/2"$ (3.8 cm) nominal bore Q.V.F. glass tubing, mounted vertically. Each end was fitted with a $1^1/2"$ equal 'T'-piece (6) and (8) and a reducing pipe-hose connector (15). The bottom connector was used for the introduction of the gas-phase and also for holding the gas distributor in place, whilst the top connector was used only for a cover. The liquid phase left the column at the 'T'-piece (8) and returned to the reservoir by means of a flexible pipe (9).

The air supply was from a compressed-air service-main (10), via a valve (11) used to regulate the pressure and a flow control-valve (12). The volumetric flow was measured by a Rotameter (size Metric 10A with a Duralamin float) (14) and the metering pressure was found from the gauge(13).

The pressure in the air-chamber immediately below the gas distributor (17) was measured by means of a mercury manometer (16).

The total column height was 48" (122 cm), and the height of the liquid-seal was 38.5" (97.8 cm). All the connecting pipework between the reservoir and the column and between the air flow-meter and the column was of $^3/8"$ (0.9 cm) i.d. P.V.C. tubing.

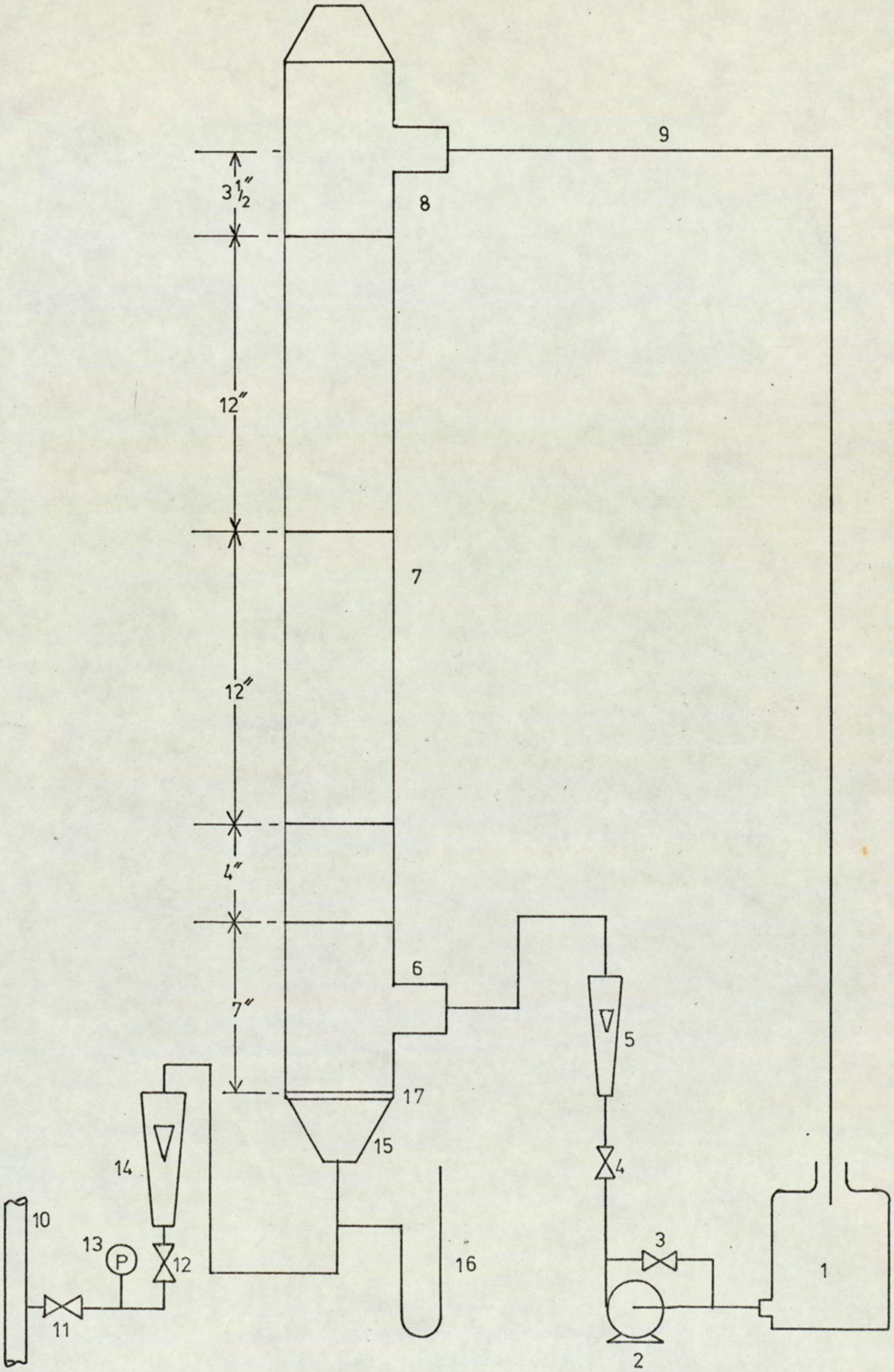

FIG 3.1 Flow diagram for initial small-scale tests.

Distributors

The four distributors are described in Table 3.1. The perforated plates were made up from mild-steel discs, 2" (5.1 cm) diameter by 18 gauge (0.12 cm), with 0.5 mm holes drilled as shown in Fig. 3.2 A and 3.2 B. These distributors were held in place by clamping between two gaskets, item (17) in Fig. 3.1. The porous plates were stainless steel sinters, 2" (5.1 cm) diameter by $^1/_4$" (0.64 cm) thick and were obtained from A. Gallenkamp & Co.Ltd. * The porosities are shown in Table 3.1. These discs were held in place simply by clamping directly between the two faces of the Q.V.F. glass sections at (17) using a U-shaped circular gasket to seal the exposed edge.

Table 3.1 Gas Distributors.

Distributor	Type	Hole Size (cm)	No.of Holes	% Free Area
A_4	Perforated Plate	0.05	125	2%
A_1	"	0.05	63	1%
P_1	Porous Plate	100 - 120 μ	-	-
P_2	"	40 - 60 μ	-	-

Photographic Apparatus

A Miranda reflex camera was used with Kodak Panatomic-X 35 mm film. The lighting arrangements are shown in Fig. 3.3. The camera-subject distance was approximately 12" (30.5 cm). The aperture-setting and shutter-speeds were determined for each set of operating conditions by means of a Weston photo-electric lightmeter.

The lighting arrangements used were decided upon after studying the available methods. Incident illumination, where the direction of lighting

---

* A. Gallenkamp & Co.Ltd., Christopher St., London E.C.2.

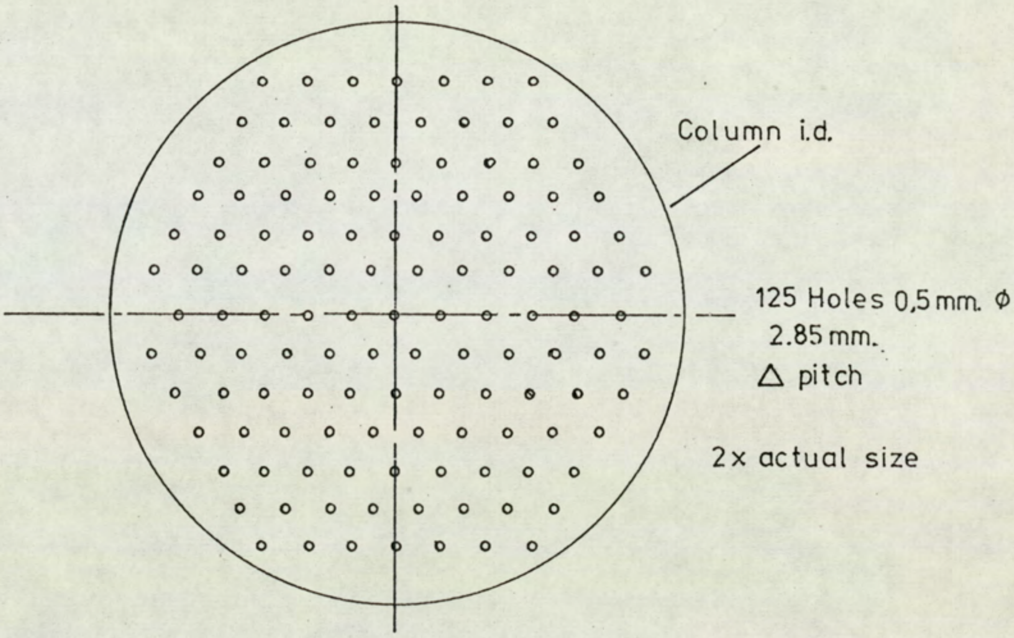

FIG 3.2a Distributor A_4.

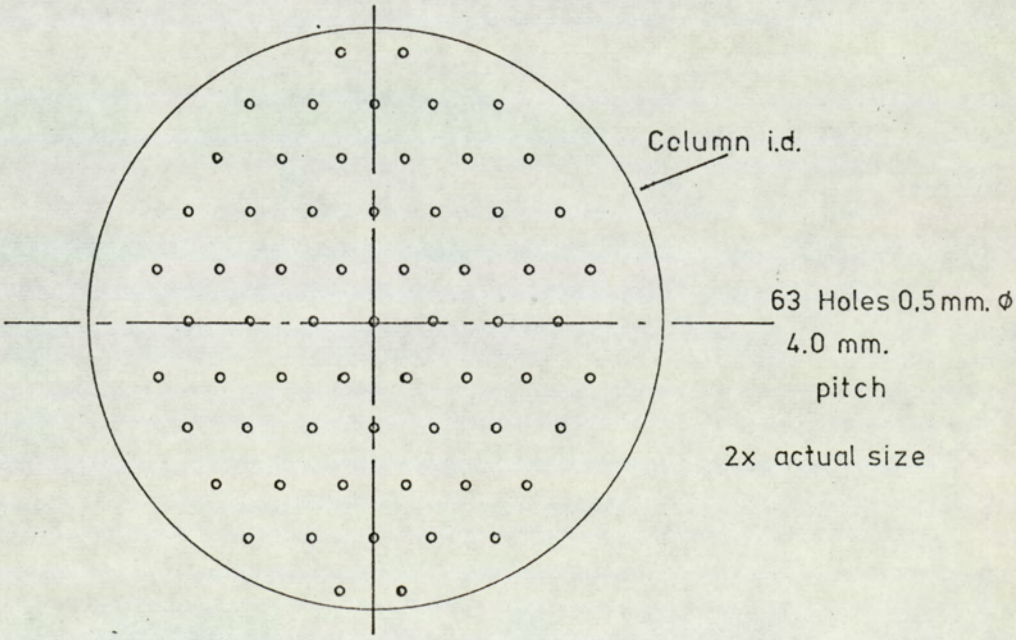

FIG 3.2b Distributor A_1.

FIG 3.2 Gas distributors.

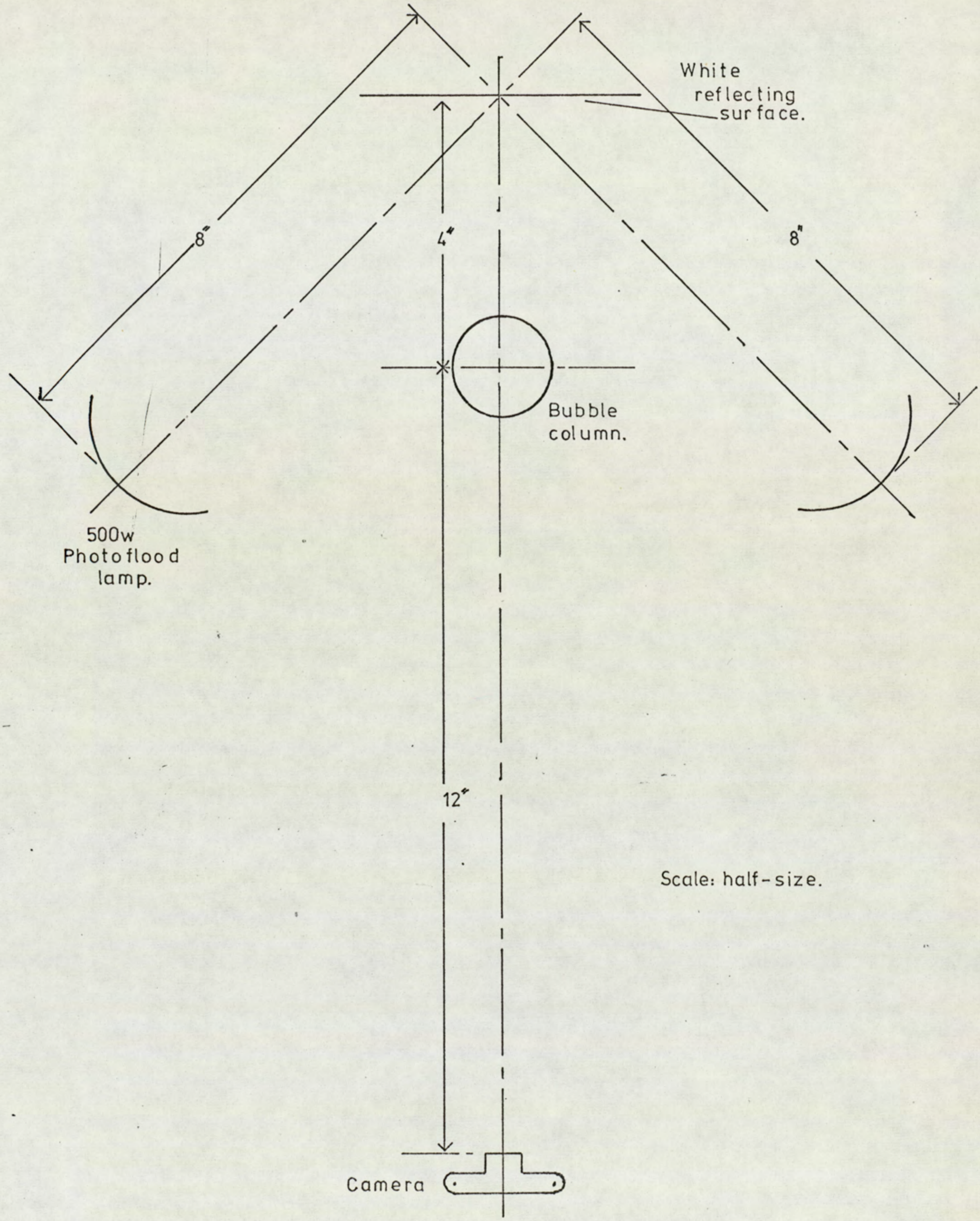

FIG 3.3 Photographic arrangement.

is approximately the same as the viewing direction, can only produce images by reflection: since reflection is small when the angle of the interface to the illumination and camera direction is within the critical limits, the method is relatively insensitive. Very oblique incident illumination will give rise, however, to strong specular reflections at steep leading wave fronts and provide a sensitive method for detection. Unfortunately with this type of illumination it is all too easy to pick up unwanted reflections from the apparatus itself. In general transmitted illumination is preferable for two-phase flow studies.

3.2.3 EXPERIMENTAL PROCEDURE

The procedure used was similar to that employed during the study of bubble formation at single orifices. T he air was turned on before the liquid recirculation was started, to prevent any weeping of liquid through the gas distributor. The gas and liquid flow-rates were then set to the required values, and, after the system had reached a steady state, readings of flow-rates, pressures, and total two-phase height were recorded. Any photographs that were required were taken at this stage. The air and liquid control valves were then shut off rapidly and the true liquid height measured.

The bubble-size distributions were obtained from enlarged prints of the bubble-swarm photographs. The bubble-diameter data were grouped into nine size ranges, the mean bubble diameter of each range being taken as the arithmetic mean of the limits of that range. For purposes of comparison, the mean bubble diameter obtained from the size distribution curve was used: the same method was employed in analysing the data for single bubbles (see Chapter 2, Section 2.3.4).

Table 3.2 Experimental Conditions and Data.

Expt. No.	Distributor	Air-Rate S.T.P. l/min.	Liquid Rate l/min.	ΔP Total mm Hg	2-Phase Ht.cms.	True Liquid Ht.cms	Gas Hold-up ϵ	$\frac{G_v}{L_v}$
1	A_4	2.5	0.045	73	98.0	92.5	5.6	55.2
2	"	2.3	0.23	73	98.3	94.0	4.4	10.2
3	"	4.2	0.045	70	97.5	87.0	10.8	94.1
4	"	4.2	0.23	70	98.6	89.0	9.7	18.5
5	"	5.9	0.045	68	98.0	81.1	17.2	130.8
6	"	5.7	0.23	68	98.3	84.0	14.5	24.6
7	"	7.6	0.045	64	97.5	75.4	22.7	168.3
8	"	7.4	0.23	64	98.7	76.9	22.1	32.3
9	A_1	2.1	0.045	72	97.8	93.0	4.9	47.4
10	"	2.1	0.23	72	98.4	94.1	4.4	8.9
11	"	3.2	0.045	69	97.7	88.5	9.4	70.7
12	"	3.1	0.23	70	98.1	90.3	8.0	13.5
13	"	4.7	0.045	66	98.0	81.8	16.5	105.4
14	"	4.7	0.23	65	98.4	84.4	14.2	20.3
15	"	7.8	0.045	64	97.8	72.8	25,6	174.0
16	"	7.8	0.23	68	98.5	77.0	21.8	34.2
17	P_2	2.2	0.045	87	99.5	94.2	5.3	48.8
18	"	2.2	0.23	91	100.4	95.1	5.3	9.5
19	"	3.3	0.045	88	100.0	90.0	10.0	73.5
20	"	3.5	0.23	88	100.6	91.5	9.0	15.1
21	"	5.3	0.045	86	100.0	84.8	15.2	117.4
22	"	5.3	0.23	87	100.6	86.3	14.2	23.1
23	"	6.8	0.045	85	100.0	79.7	20.3	150.6
24	"	6.8	0.23	85	100.5	81.9	18.5	29.5
25	P_1	1.6	0.23	88	100.0	98.4	1.6	7.1
26	"	3.3	0.23	89	100.8	89.4	11.3	14.4
27	"	5.0	0.23	89	100.7	80.5	20.1	21.5
28	"	3.5	0.23	91	100.8	86.1	14.6	15.4

3.2.4 EXPERIMENTAL RESULTS

The conditions used in the experiments and some of the data are shown in Table 3.2: detailed results will be found in Table B.1 in Appendix B. Fig. 3.4 shows the effect of the superficial gas-velocity on hold-up for the two liquid velocities used, and in Fig. 3.5 the total pressure-drop across the column is plotted as a function of the superficial gas-velocity.

The statistical results are given in full in Table B.2 in Appendix B and the bubble-size distributions are shown graphically in Figs. 3.6 to 3.11 inclusively. Table 3.3 lists the values of the mean bubble diameters: these are averaged figures for each distributor type. The data is also presented graphically in Fig. 3.12 as a function of the mean bubble diameter calculated, using equation 2.6.

Table 3.3 Calculated and Measured Bubble Diameters.

Distributor	d_o cm.	Measured d_b cm.	Calculated d_b cm.
A_4	0.05	0.360	0.368
A_1	0.05	0.491	0.368
P_1	0.011	0.222	0.222
P_2	0.005	0.139	0.171

3.2.5 DISCUSSION

The measured values for mean bubble-diameter are similar in magnitude to those obtained for single bubbles in Chapter 2. It will be noted, however, that the distributions are all skewed to the right and show very few bubbles with a diameter less than the mean. One possible explanation is that in the case of the bubble-swarms coalescence was taking place.

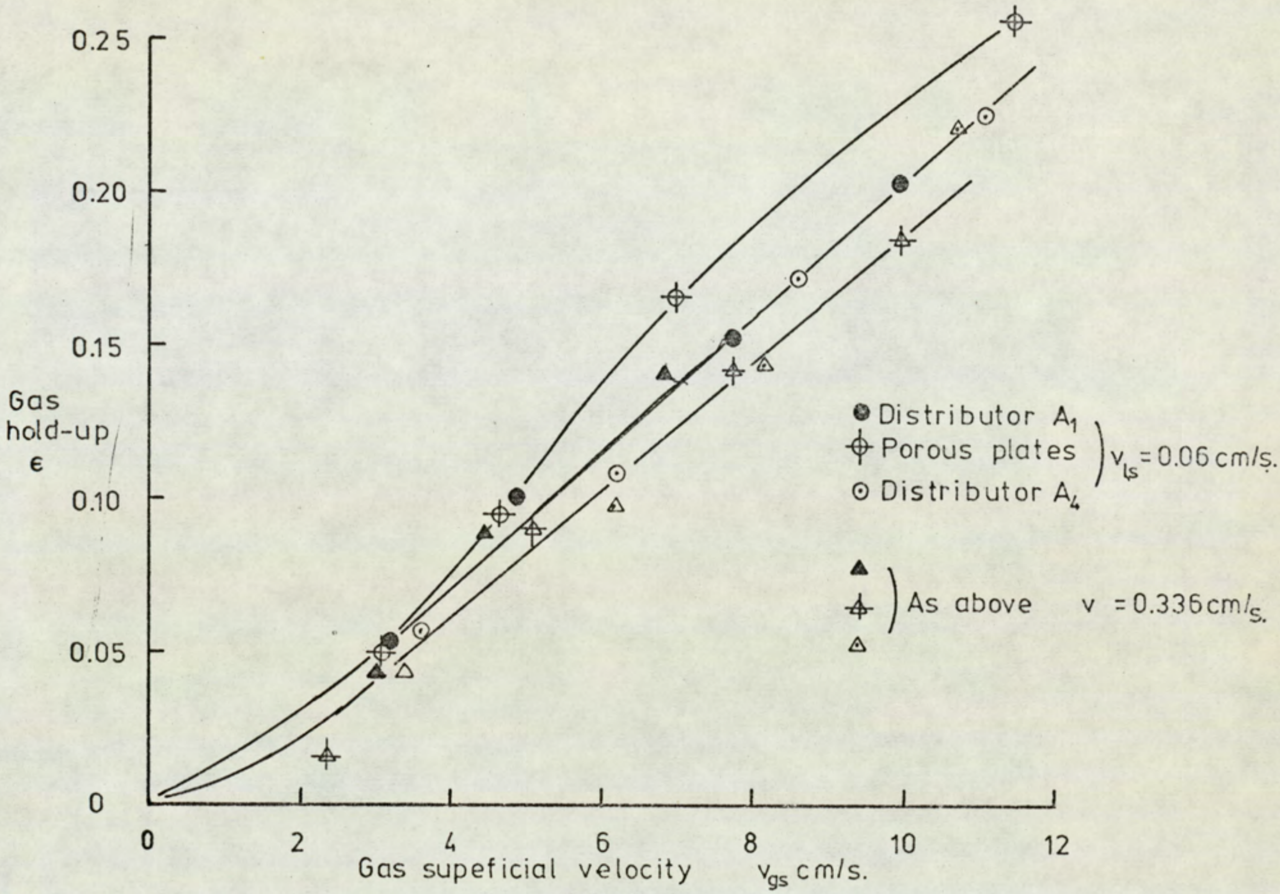

FIG 3.4 Gas hold-up: 1½" column, air/water.

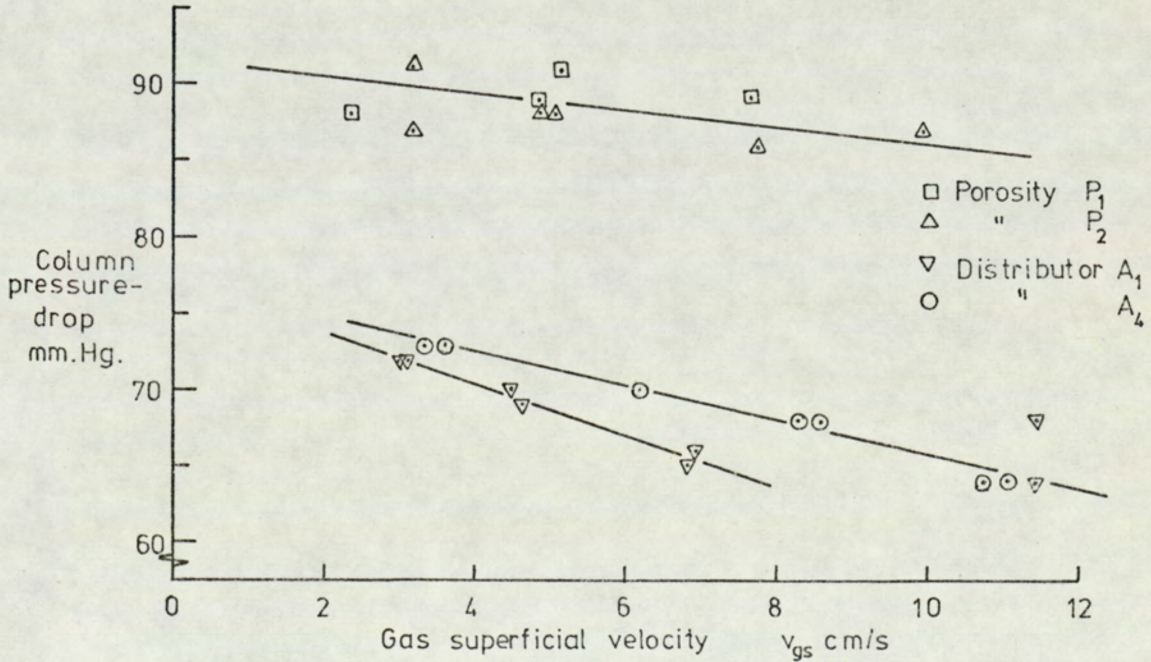

FIG 3.5 Column pressure drop: 1½" column, air/water.

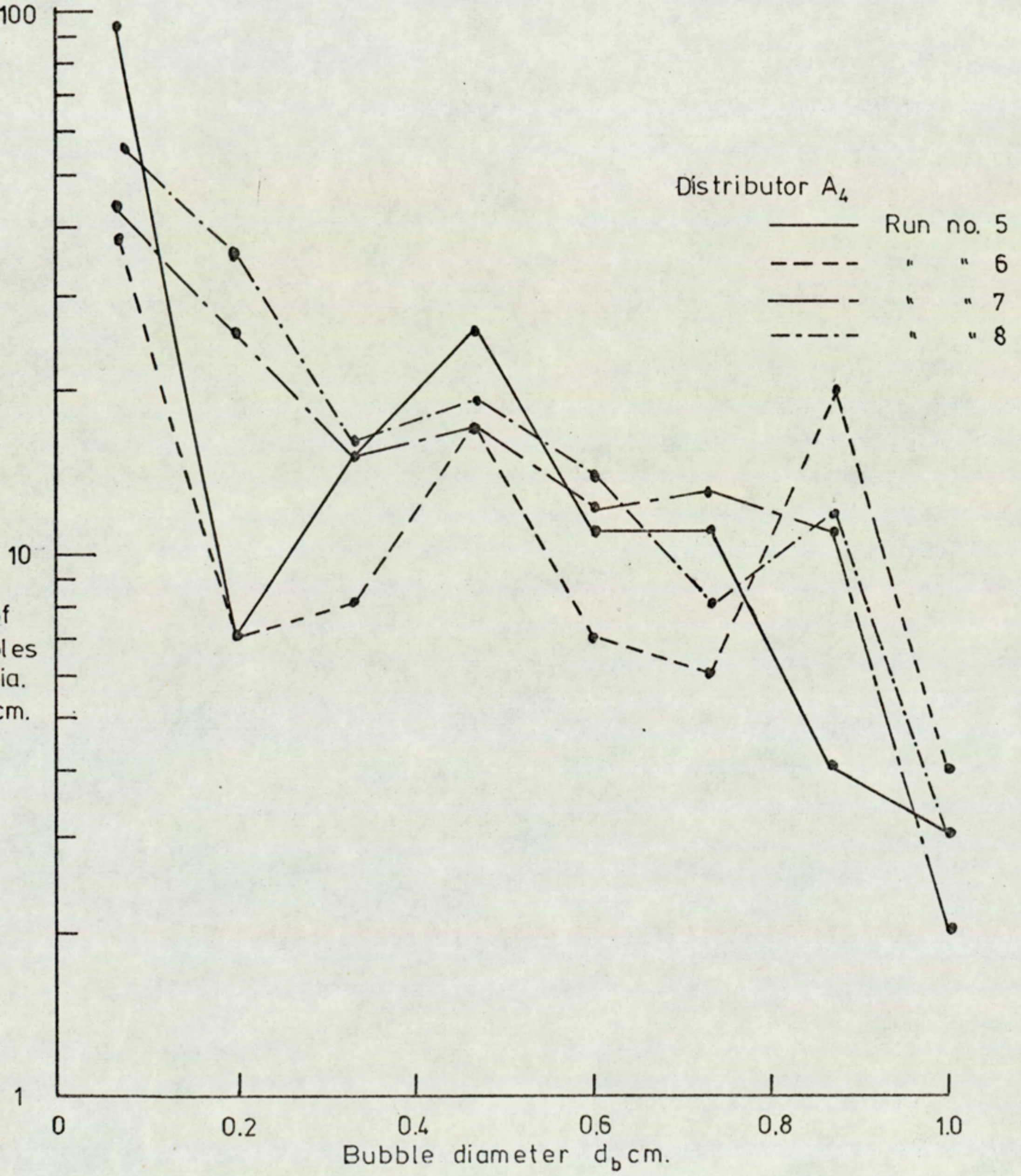

FIG 3.6 Bubble-size distributions.

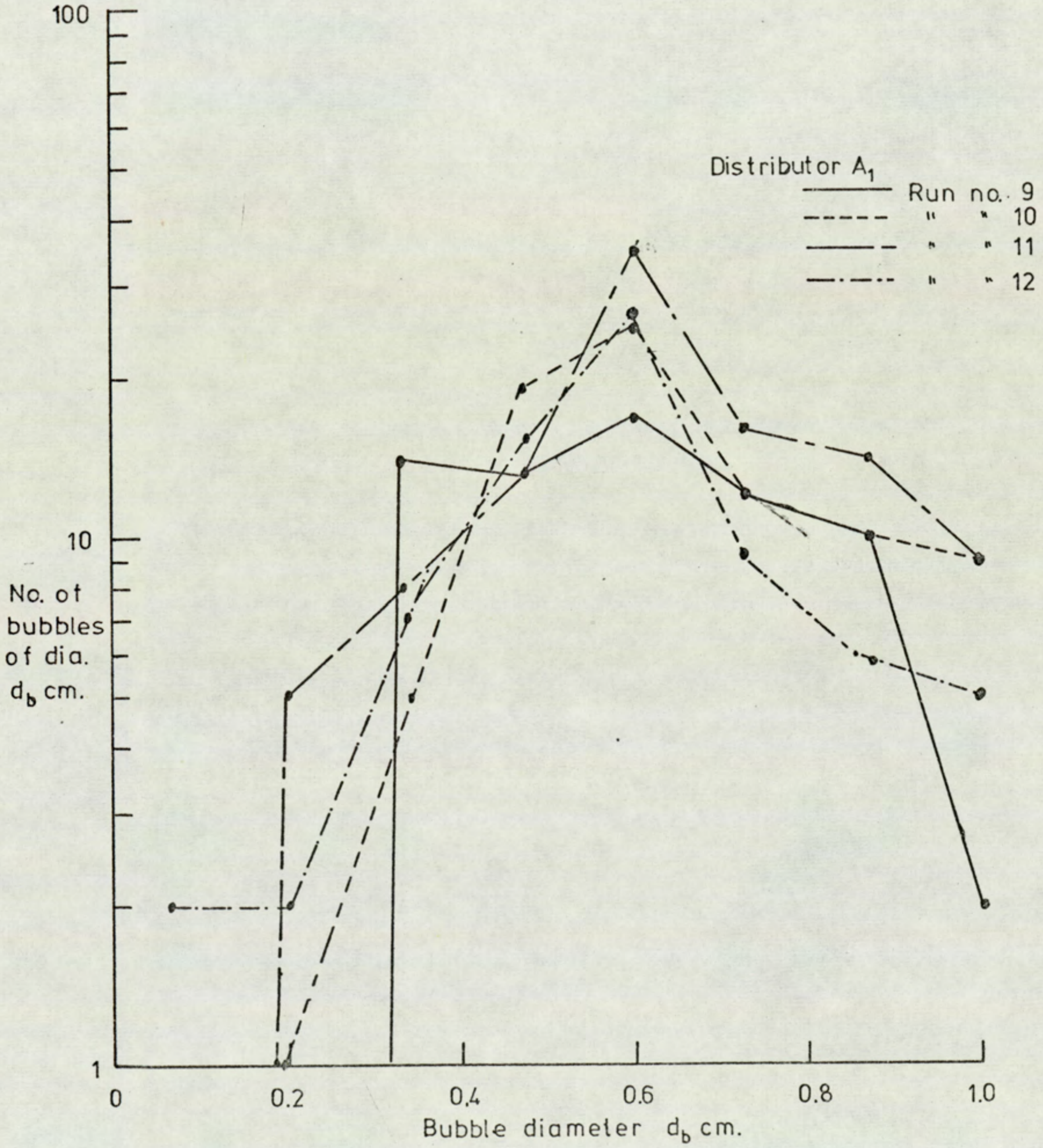

FIG 3.7 Bubble-size distributions.

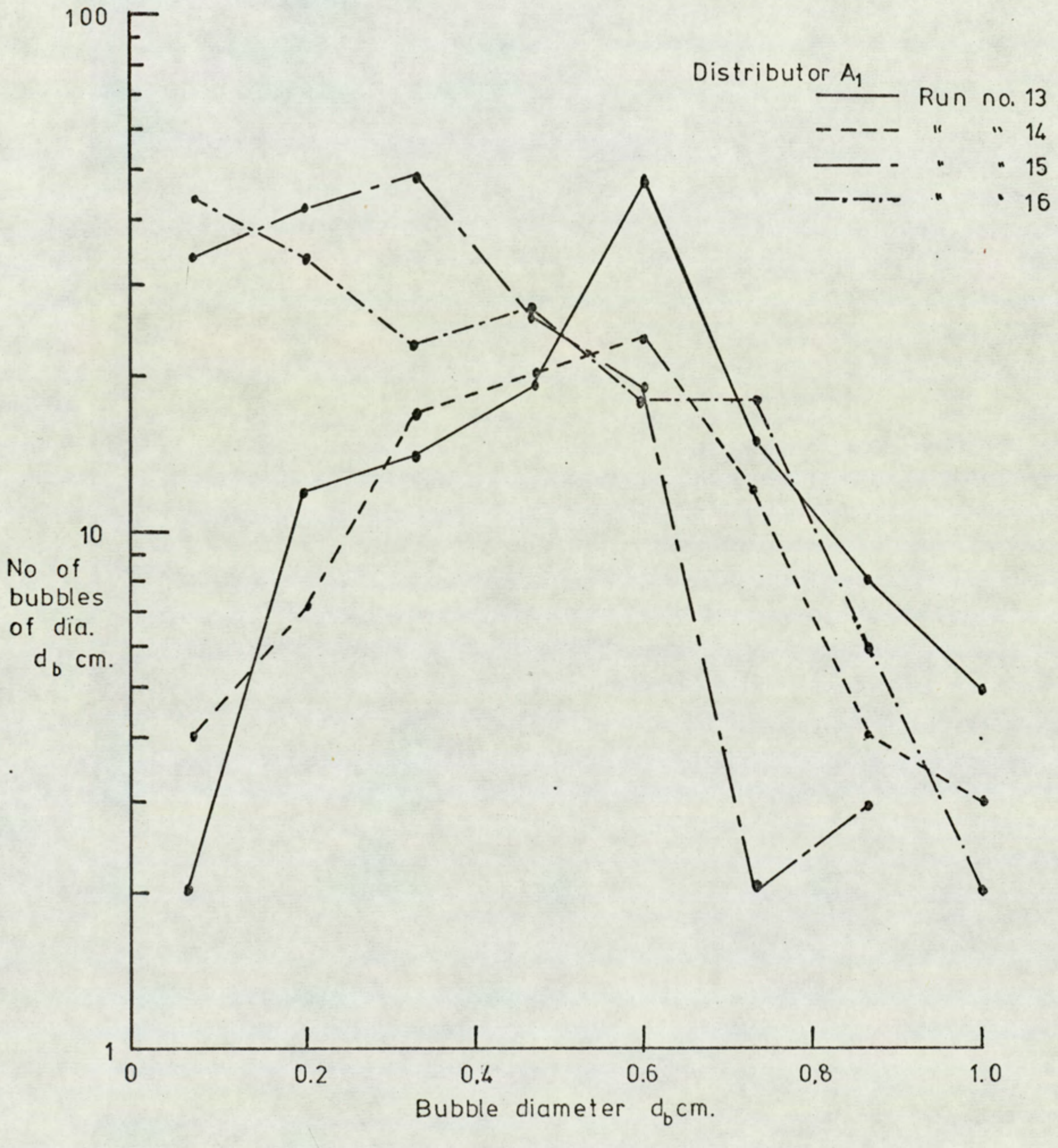

FIG 3.8 Bubble-size distribution

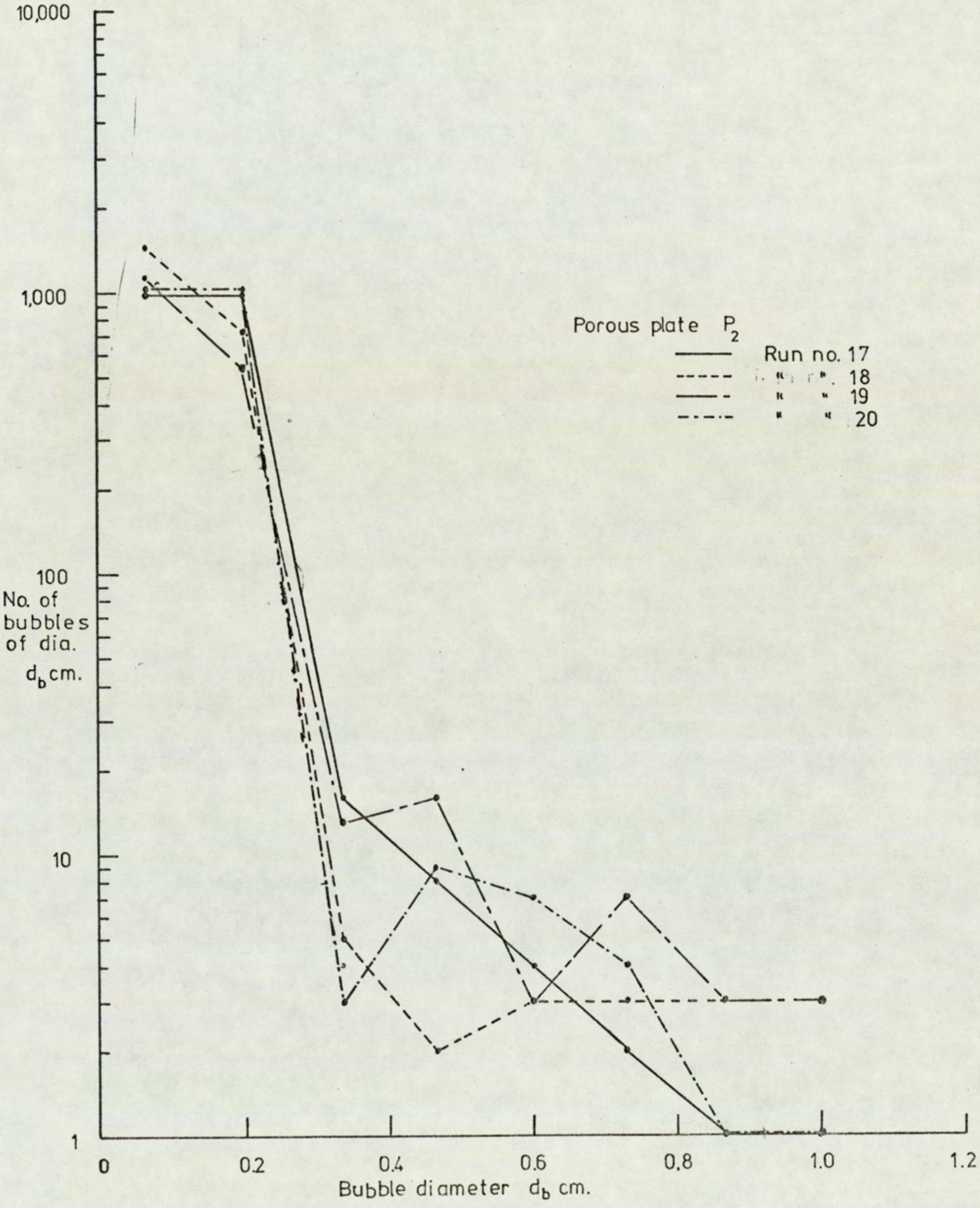

FIG 3.9 Bubble-size distribution.

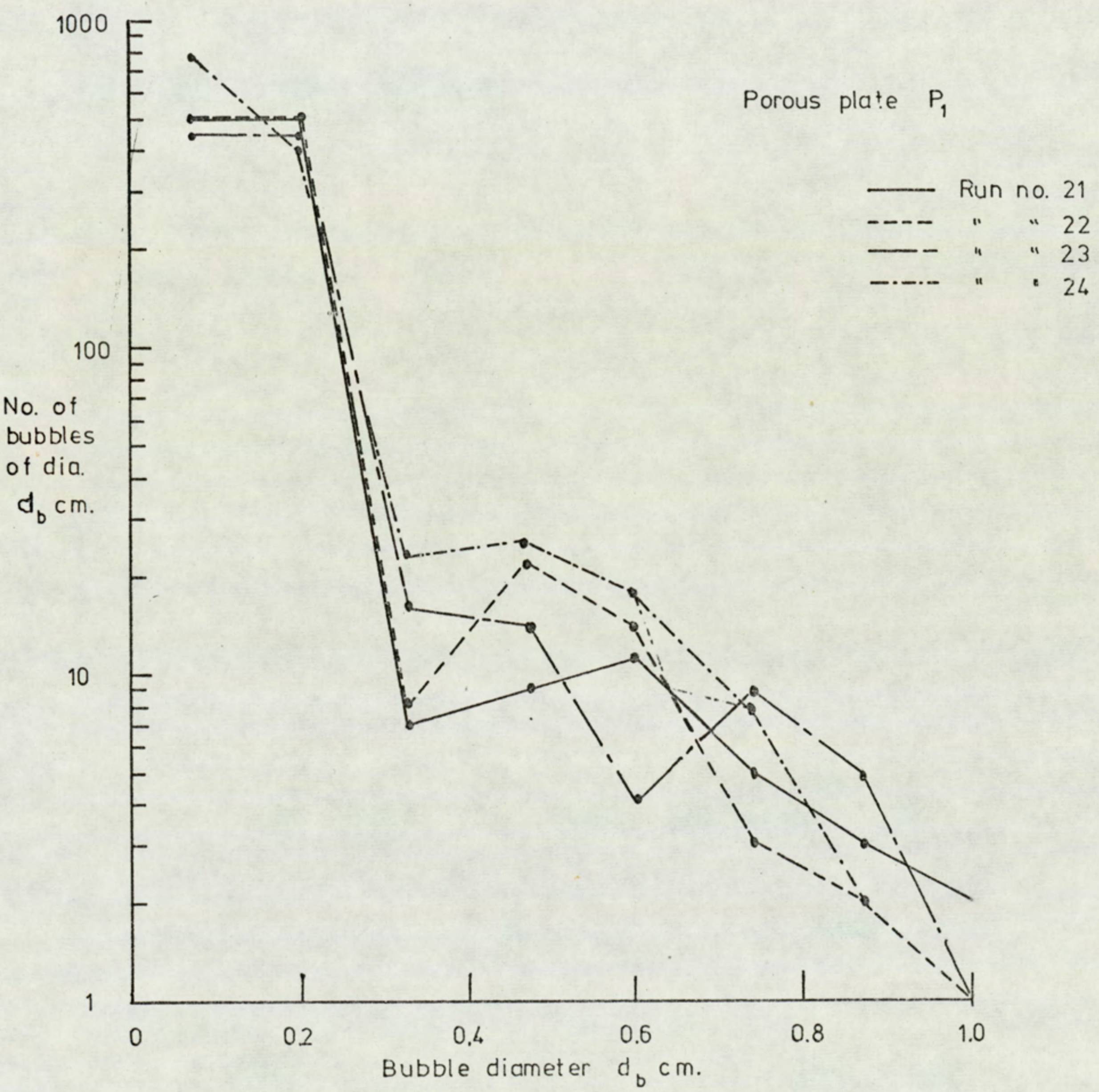

FIG 3.10 Bubble-size distributions.

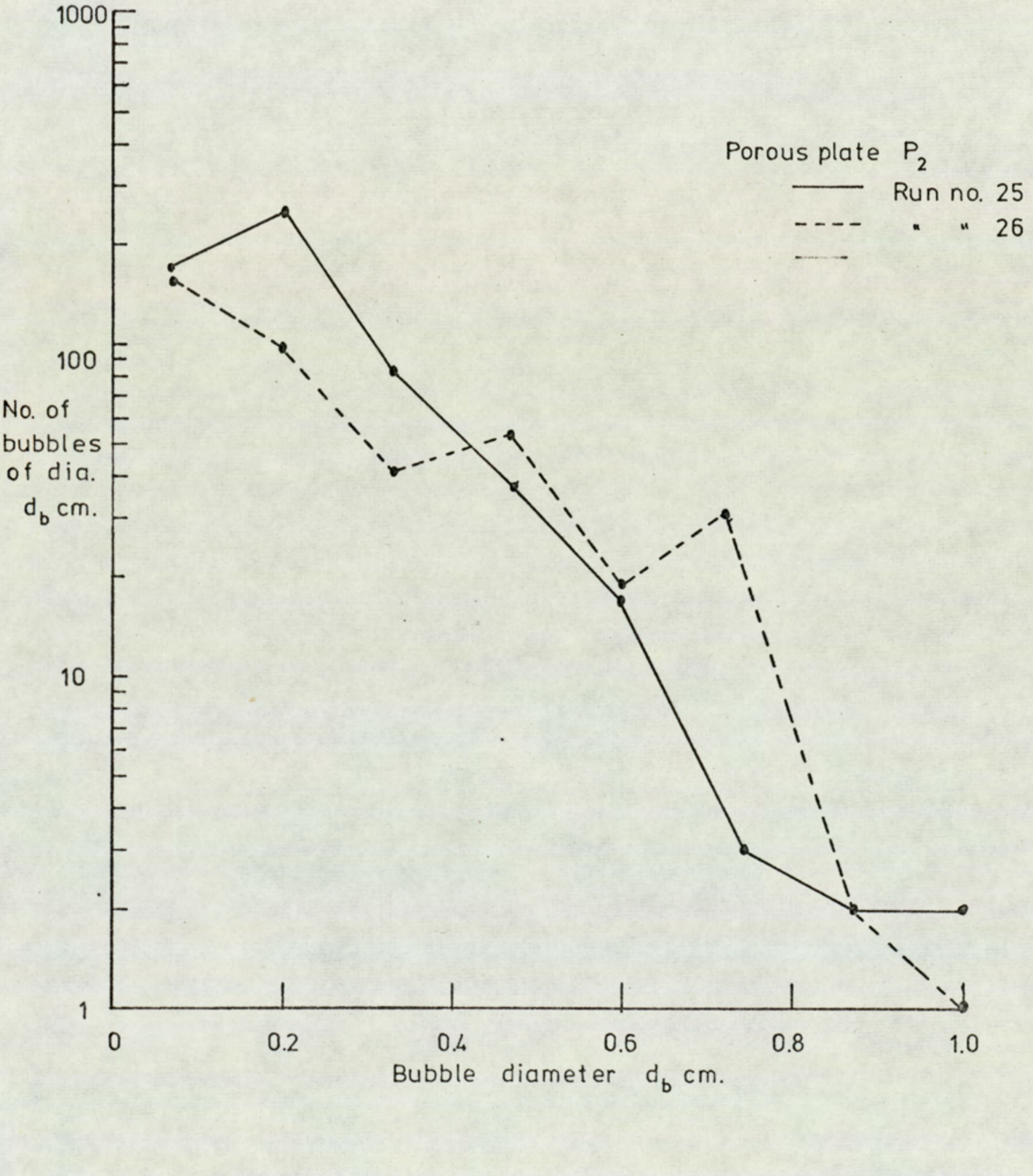

FIG 3.11 Bubble-size distributions.

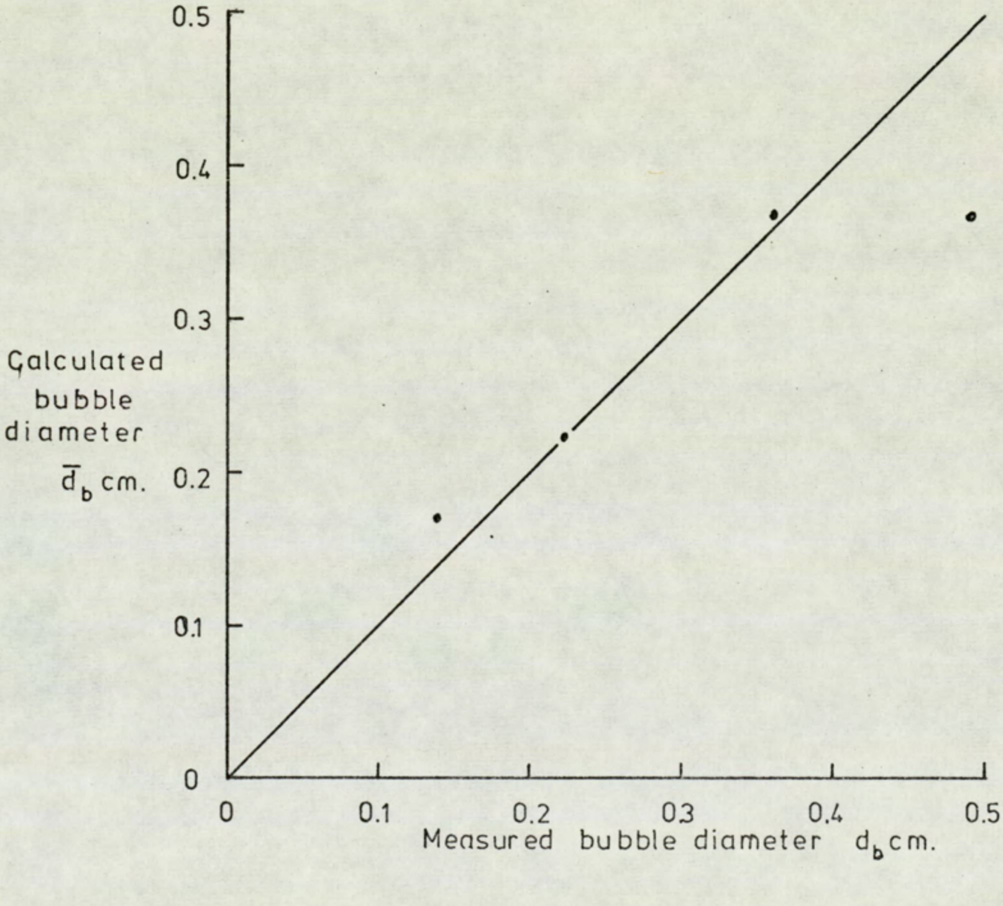

FIG 3.12 Comparison of calculated and measured bubble diameters.

Another arises from the method used for analysing the experimental data: usually the bubbles were only classified into one or two size ranges below the mean diameter, whereas in the single bubble studies much smaller size increments were used.

The results obtained with distributor A_1 require additional comment. The flow area of this distributor was in fact only half that of distributor A_4. This would cause the velocity through the orifices, and thus the Bubble Reynolds Number, to be much higher. In both cases the Reynolds Numbers were considerably greater than those encountered in the experimental work on single bubbles, viz:

$$5{,}790 < Re_b < 19{,}050 \qquad \text{for distributor } A_4$$

and

$$10{,}470 < Re_b < 38{,}800 \qquad \text{for distributor } A_1$$

The orifice Reynolds Number, which defines the flow-rate of gas through the orifices, is in the following ranges:

$$52 < Re_o < 172 \qquad \text{for distributor } A_4$$

$$94 < Re_o < 350 \qquad \text{for distributor } A_1$$

This means that although the bubbles are in so-called turbulence, the actual flow through the orifices is in the transition zone for distributor A_1, whereas the flow is in the laminar region for distributor A_4. This difference in Reynolds Numbers between distributor A_1 and A_4 is most likely the cause of the bubbles formed by the former distributor being larger than those formed by the latter at comparable flow-rates.

The relationship between gas hold-up and gas superficial velocity appears to be roughly linear over the range of values studied. The liquid velocity has only a slight effect, an increase in velocity decreasing the gas hold-up for a given gas flow-rate. Both these trends are confirmed by the results of previous workers.

3.3 LARGE SCALE TWO - PHASE STUDIES

3.3.1 INTRODUCTION

The work carried out in this section included a study of the effect of both gas and liquid flow-rates on gas hold-up and bubble-swarm velocity. Also included as parameters were column diameter and the porosity of the distributor, which were decided upon partially as a result of the effects noted in the previous section. A further parameter studied was the effect of the continuous phase physical properties. These were altered by using yeast suspensions of varying concentration, which increased the viscosity and decreased the surface tension of the liquid phase as well as including a third, semi-solid phase.

3.3.2 EXPERIMENTAL APPARATUS

Initially three column diameters were chosen, viz. 3" (7.6 cm), 6" (15.2 cm) and 12" (30.4 cm).

After some experimental work had been carried out in the 3" column it was found that consistent results could not be obtained. This was thought to be due to wall effects since the ratio of column diameter to bubble diameter was approximately 15. This figure has been quoted by several workers as a limiting value for wall effects, and the results that were obtained seem to confirm this. Consequently the programme of work was altered to include only the 6" and 12" diameter columns.

Basically the equipment consisted of two vertical columns fed co-currently with air and the liquid-phase. The two-phase system produced by this arrangement was deaerated and the liquid-phase returned to reservoirs from which it was recirculated.

For convenience the equipment is described under three headings:

1. Equipment common to both columns (This includes the storage tanks, liquid-phase pumping and metering systems and the air supply and metering systems).

2. The 6" diameter column.

3. The 12" diameter column.

1. Equipment common to both columns

A schematic layout of the liquid-recirculation and air-supply systems is given in Fig. 3.13. Figs. 3.14 and 3.15 show the storage tanks and take-off points, and the air entry section to the column respectively. The air entry section shown in Fig. 3.15 is for the 6" column and was similar to that used on the 12" column.

Referring to Fig. 3.13, the liquid reservoirs (1) consisted of two, 100 gal. tanks, 3'-0" (91.5 cm) in diameter by 3'-0" (91.5 cm) deep, manufactured from 10-gauge stainless steel, with removeable lids. The liquid was fed to the columns by means of a Q.V.F. rotating vane pump (3) (100 gals/hr), and the flow was metered by a bank of three Rotameters (4) (metric 24 XG. 35 G and 65 G, each with a stainless steel float), capable of giving a liquid flow-rate of 0 to 200 l/min. This represents a possible liquid superficial velocity of 0 to 4.6 cm/s for the 12" column. The Rotameters were each fitted with P.T.F.E. lined diaphragm valves downstream and stainless-steel ball-valves upstream. These two types of valves were used for flow regulation and rapid shut-off respectively. Immediately downstream of the metering system a return line (6) was fitted to enable the liquid-phase to be circulated when necessary. The return-lines (7) from the tops of the two columns were linked together and could be fed to either storage tank (8) A second Q.V.F. pump (10) (75 gal/hr) was used purely to transfer the liquid, either from one tank to another by the valve arrangement (11), or to maintain the solids in suspension in the

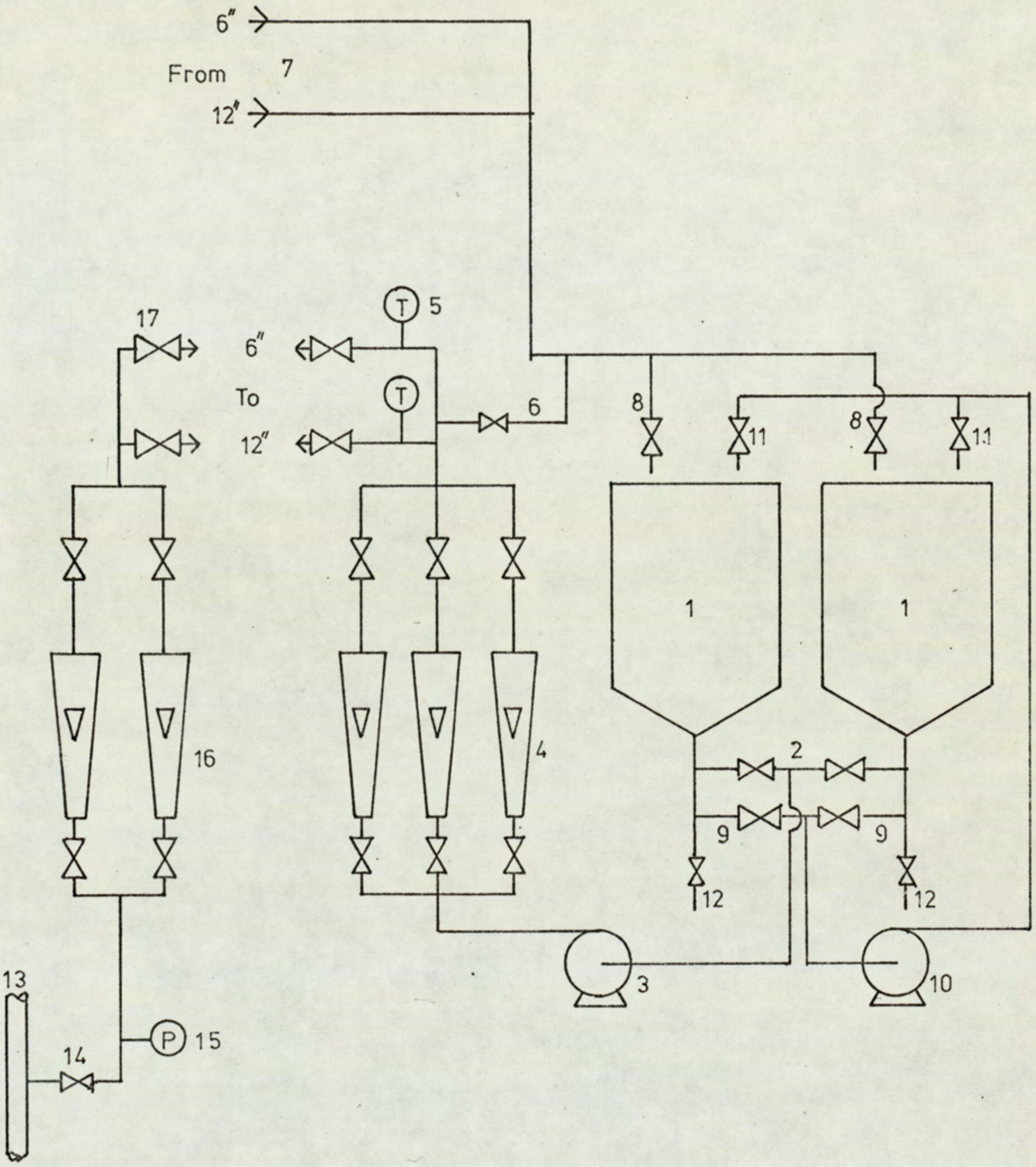

FIG 3.13 Schematic flow diagram of equipment common to both the 6″ and 12″ columns.

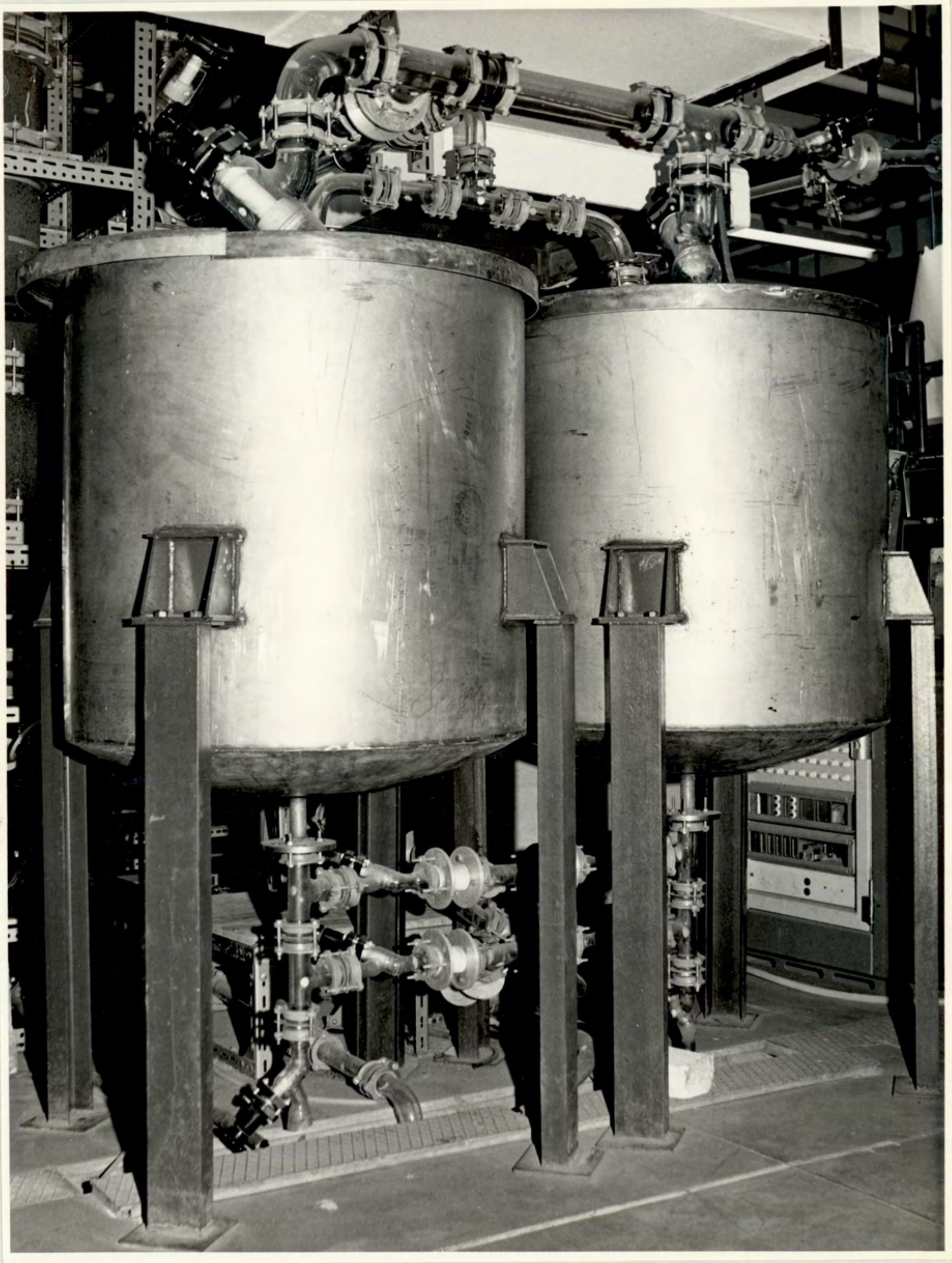

FIG 3.14 Liquid phase storage tanks.

liquid-phase. By means of the take-off systems (2) and (9) the two liquid circulating pumps could draw liquid from either or both tanks. All the liquid-side pipework comprised standard $1^{1}/2"$ (3.8 cm) Q.V.F. glassware and valves or 1" (2.5 cm) o.d. stainless steel tubing fitted with suitable couplings.

The gas supply (13) was obtained from a compressed air service-main via a 1" (2.5 cm) n.b. 'T'. This was fed directly to the metering section via a control valve (14), used to regulate the flow and pressure at the meters. The metering section consisted of two Rotameters, a Metric 24 and a Metric 47, both with duralamin floats, enabling the flow-rate to be measured from 0 to 500 l/min at S.T.P. The metering-pressure was measured by the calibrated pressure gauge (15). The flow-control was similar to that used on the liquid phase, i.e. P.T.F.E. lined diaphragm valves downstream and ball-valves upstream. From the metering section two $1^{1}/2"$ (3.8 cm) n.b. Q.V.F. lines led to the air-chambers below the gas-distributors in the two columns.

The air-chambers beneath the distributors (see Fig. 3.15 and 3.16 B) (5) were made up in the same way for each column. This design was arrived at after visually studying the bubbles rising from the distributor plates and was found to give the most even gas distribution. The volumes of the two chambers to the first restriction upstream, were approximately 5,000 cm^3 for the 6" column, and approximately 17,000 cm^3 for the 12" column. Since the flow-area for the 12" distributor was three times that for the 6" distributor, these volumes gave the same capacitance number (see Figs. 3.18 A and 3.21 A) The pressure in this gas chamber was measured by means of a mercury manometer (see Fig. 3.16 (19)).

The gas hold-up was estimated from the height of liquid in the side-tube (8) (Fig. 3.16). This consisted of a length of $^{1}/4"$ (0.63 cm) o.d. glass-tubing, fitted alongside a scale. The upper end was open to atmosphere and the lower end was connected to a length of $^{1}/4"$ (0.63 cm) o.d.

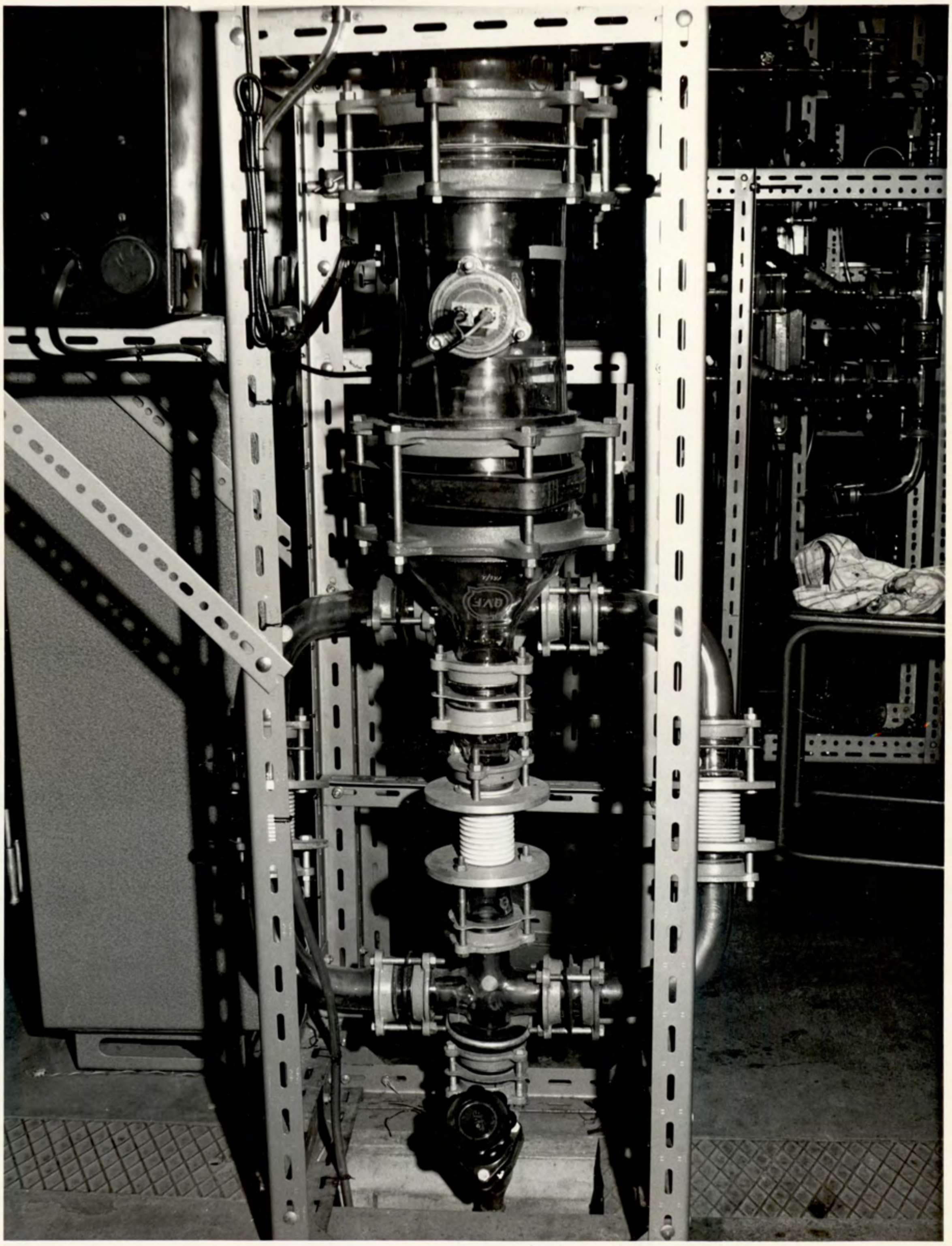

FIG 3.15 Air inlet section - 6" column.

copper tubing, which passed inside the column through a sealed 'T'-piece and terminated about 1" (2.5 cm) above the distribution plate. This method of measuring hold-up was found to be quite accurate, the error being $<1\%$ at a gas hold-up of 5% and $< 2\%$ at 20% gas hold-up.

2. The 6" diameter Column

This column was made up of standard lengths of Q.V.F. 6" (15.25 cm) bore pipe (see Figs. 3.16 and 3.17). The liquid was pumped into the column through a $1^1/2$" (3.8 cm) pipe-section (1), a control valve (16) and a liquid-distributor (2). The two lowest sections (9) and (10) of the column comprised an unequal 'X'-piece and an unequal 'T'-piece, the side-arms all being $1^1/2$" (3.8 cm) bore. The side-arms on section (9) were used for the liquid entry and a conductivity probe (see Chapter 4), whilst the side-arm on section (10) was used for the tube employed in hold-up measurements.

The three sections comprising (11), (12) and (12A) made up the major part of the column. The lower of the two 24" (61 cm) sections was fitted with a square perspex box (18) which was filled with water and used for photographing the contents of the column. Sections (13) and (14) of the column were again unequal 'T'-pieces with $1^1/2$" (3.8 cm) side arms. The lower one (13) was used as an insertion point for a conductivity probe (see Chapter 4), whilst the upper one (14) served as the liquid off-take point (3). The top of the column consisted of a section (15) for containing any foam and a domed vent cap, which was covered with fibre-glass (7).

The air-inlet system to the column (4) consisted of a 1" (2.5 cm) n.b. mild-steel pipe, control valve (17), glass inlet section (5), and the distributor plate (6). The latter was clamped between the adjoining faces of the Q.V.F. sections.

The overall column height, from the gas distributor plate, was

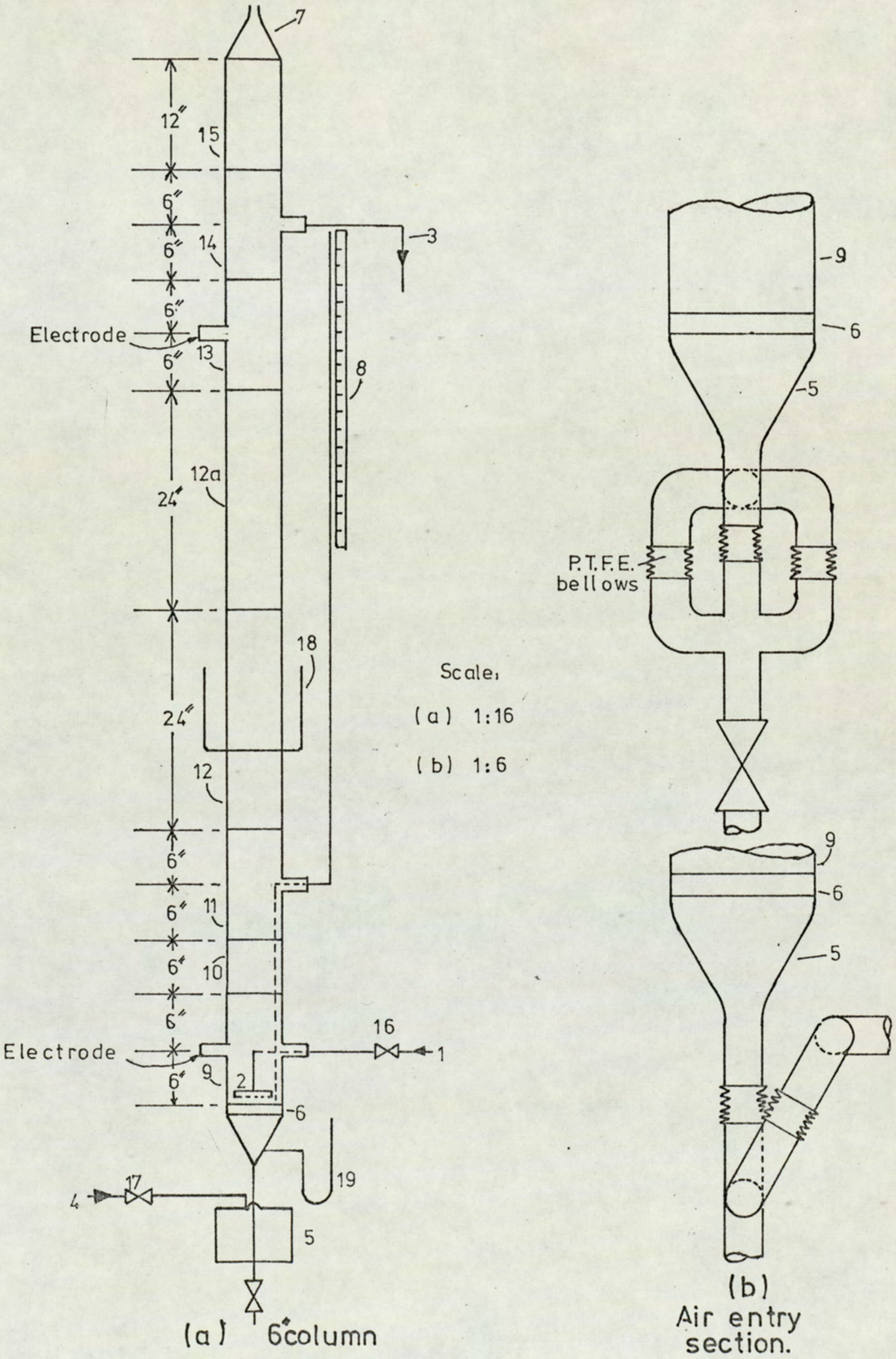

FIG 3,16 Construction of the 6" column.

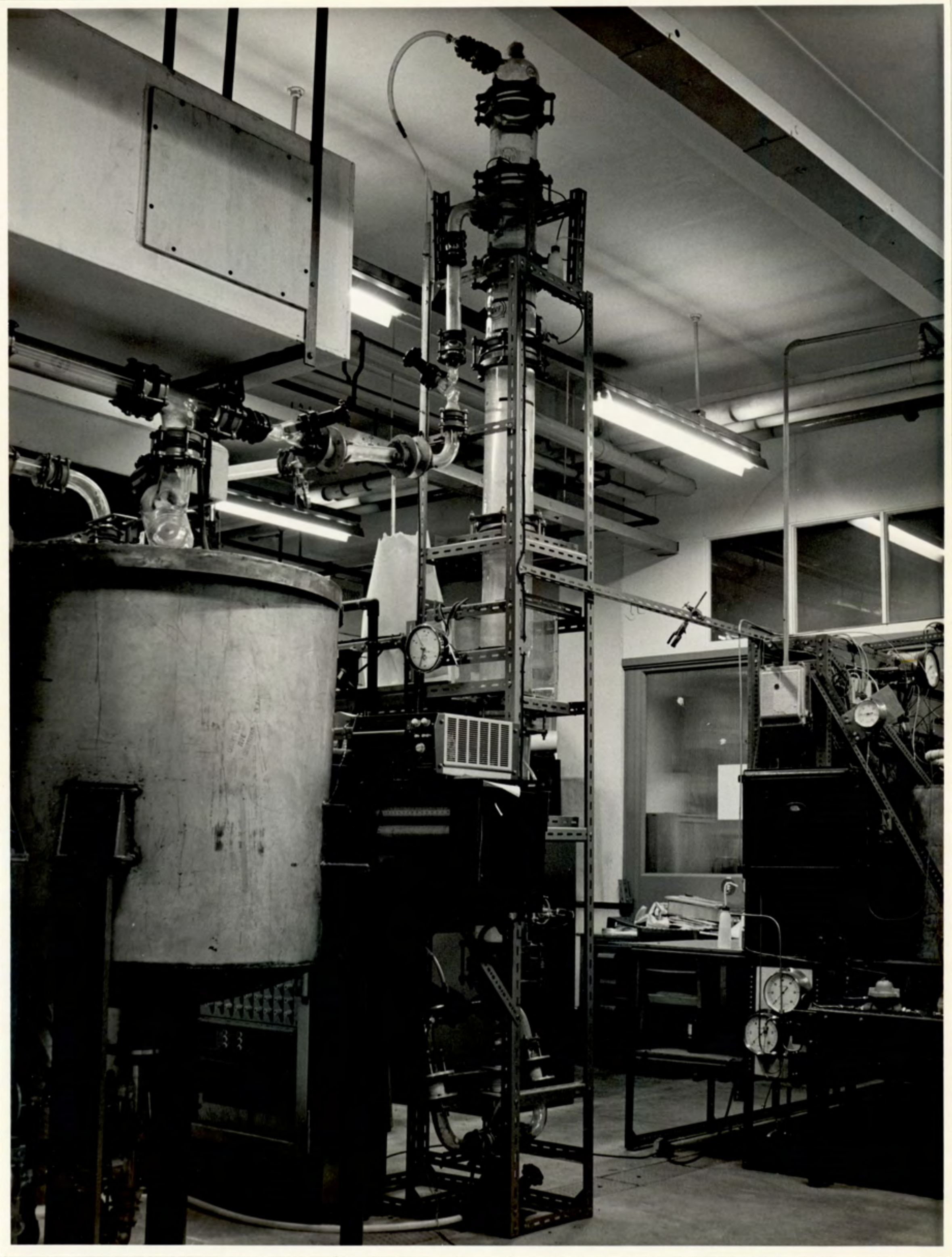

FIG 3.17 General view of the 6" column.

126" (320 cm) and the liquid seal was 96" (244 cm).

The air-distributor plates consisted of three perspex plates, cut as shown in Fig. 3.18 A, and fitted with stainless-steel sinters of various porosities. The sinters were clamped between the two outer perspex plates, as shown in Fig. 3.18 (Section A - A^1) The porosities of these sinters are shown in Table 3.4.

The liquid-distributor was constructed from $^1/2$" (1.3 cm) o.d. copper tubing, brazed up and drilled, as shown in Fig. 3.18 B. The distribution ring itself was situated $1^3/4$" (4.9 cm) above the gas-distributor plate. The design was chosen so as to minimise turbulence in the neighbourhood of the gas-distributor and to achieve uniform distribution of the liquid phase.

Table 3.4 Porosities of the Stainless Steel Sinters.

Porous Plate Sinter	Porosity μ
P_1	100 - 120
P_2	40 - 50
P_3	20 - 30

3. <u>The 12" diameter Column</u>

This was built up in a similar manner to the 6" column (see Fig. 3.19 and 3.20). The liquid-distributor was constructed as shown in Figs. 3.21 B and 3.23. The clearance between the distributor ring and the gas-distributor plate was $1^1/2$" (3.8 cm) in this case.

The overall height of the column was 129" (328 cm) and the liquid seal was 96" (244 cm), the same as the 6" column.

The air-distributor was made up from three perspex plates, as shown in Figs. 3.21 A and 3.22. The only difference between this distributor and

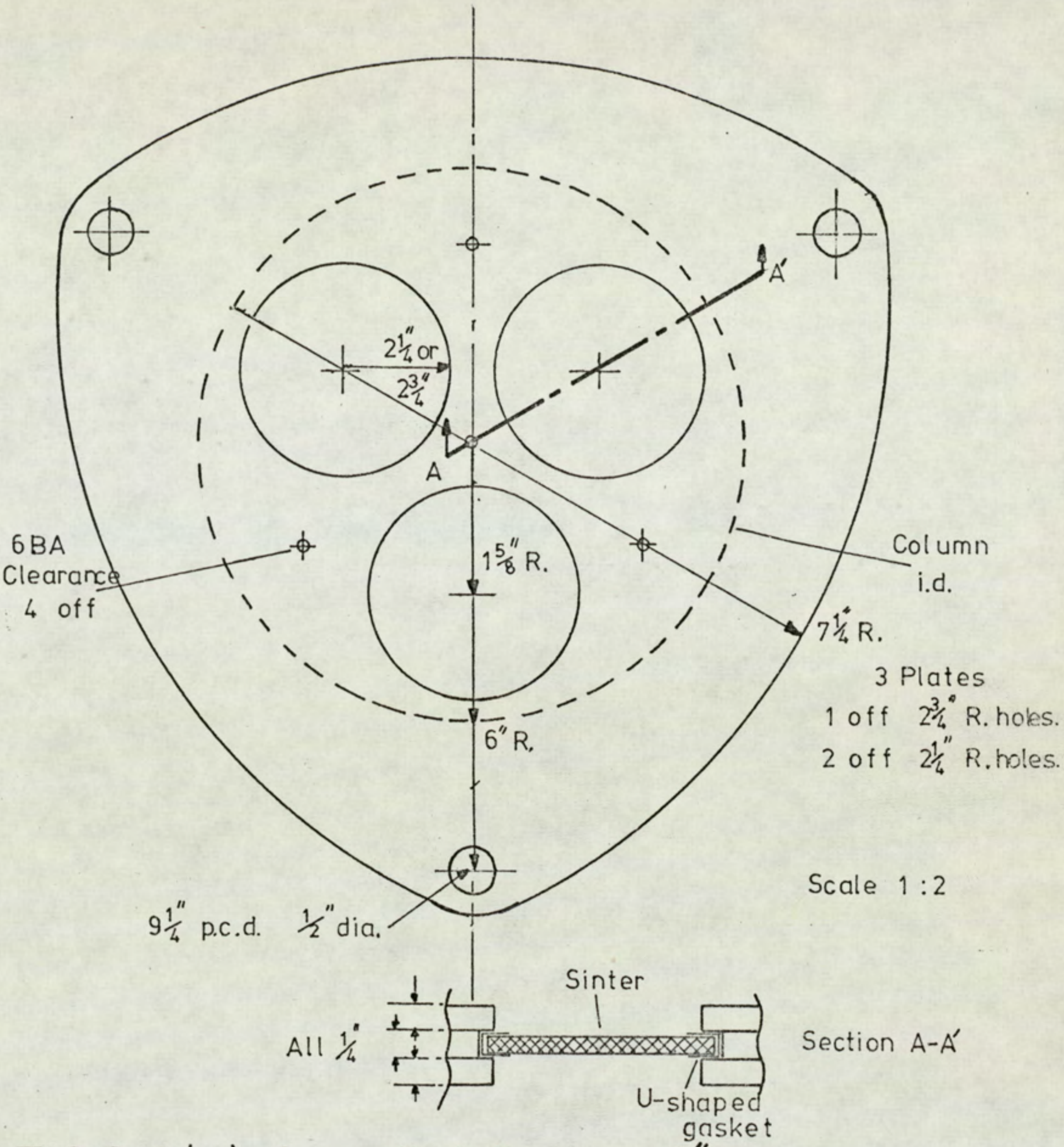

FIG 3.18 (a) Gas distributor 6" column.

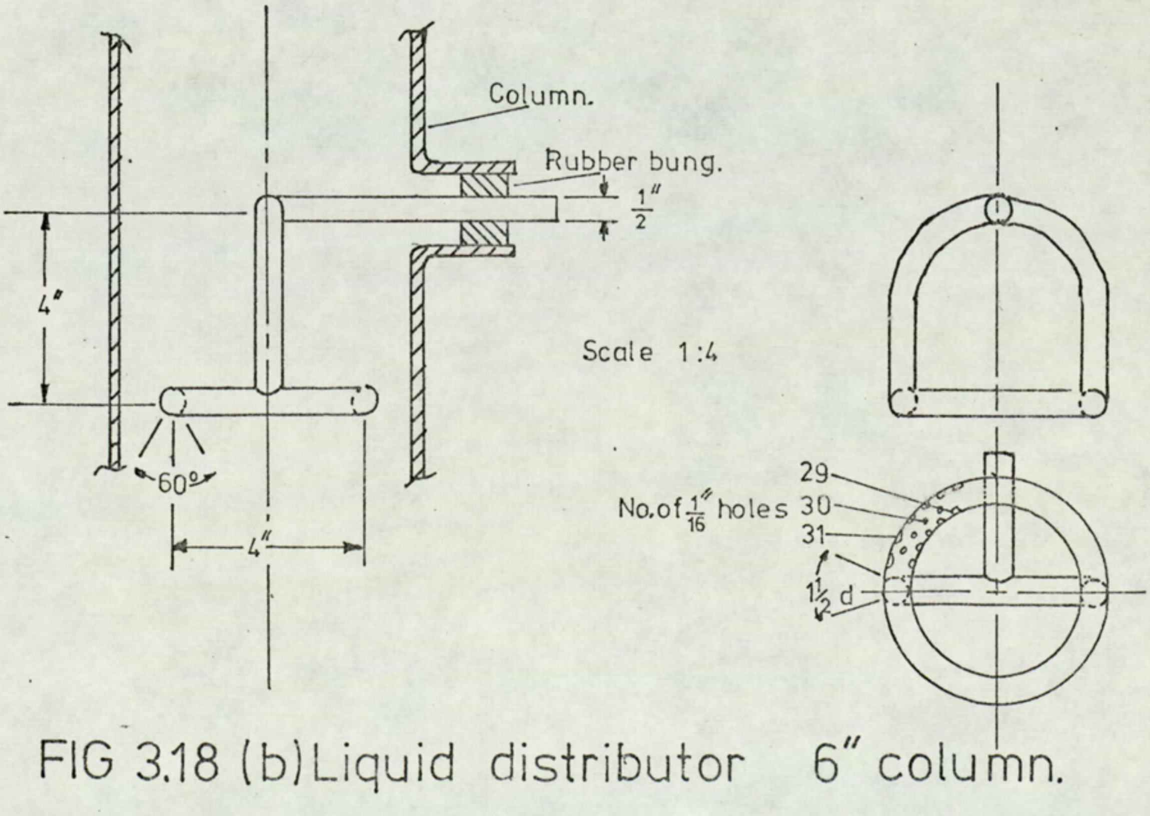

FIG 3.18 (b) Liquid distributor 6" column.

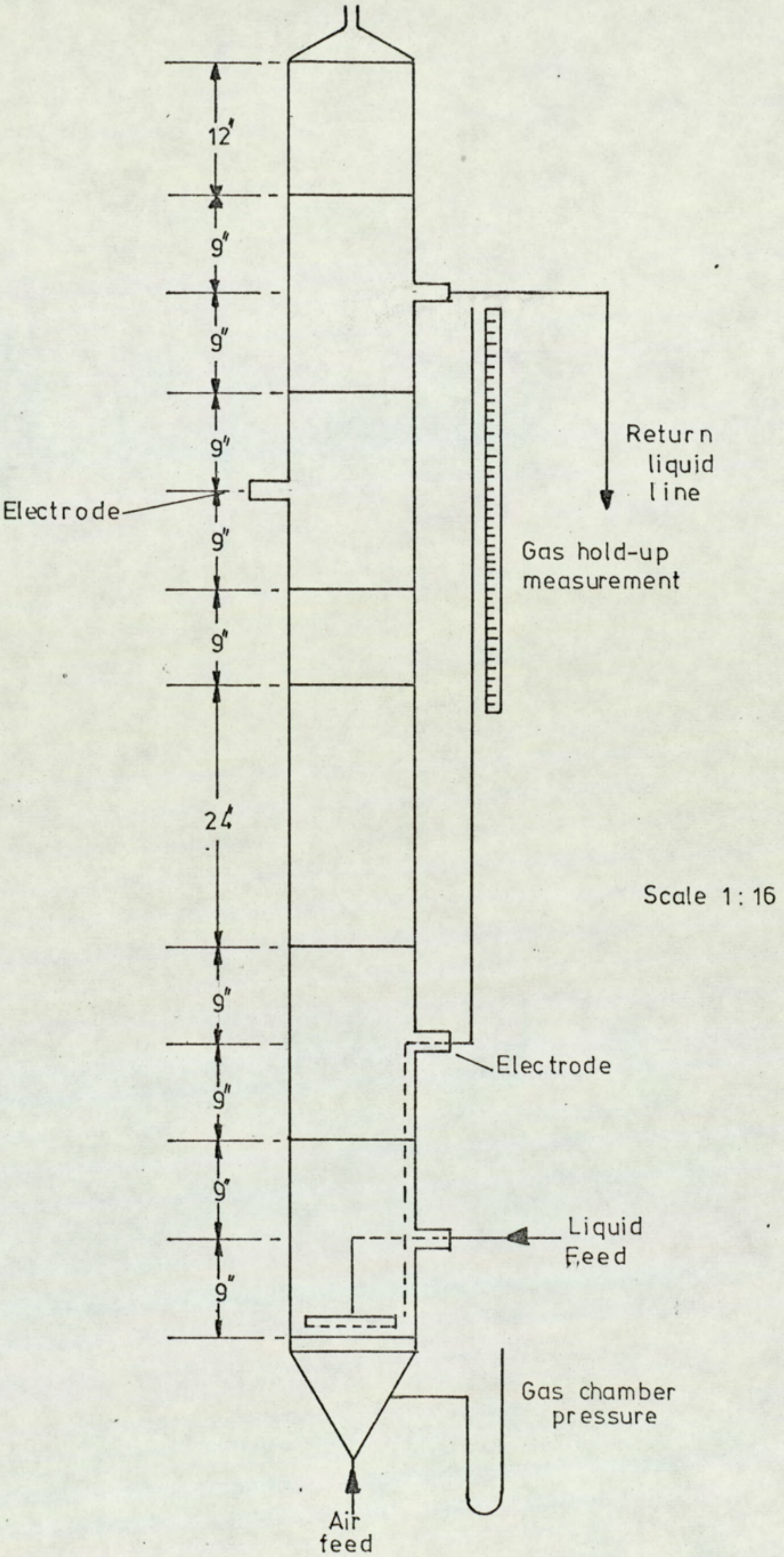

FIG 3.19 Construction of the 12" column.

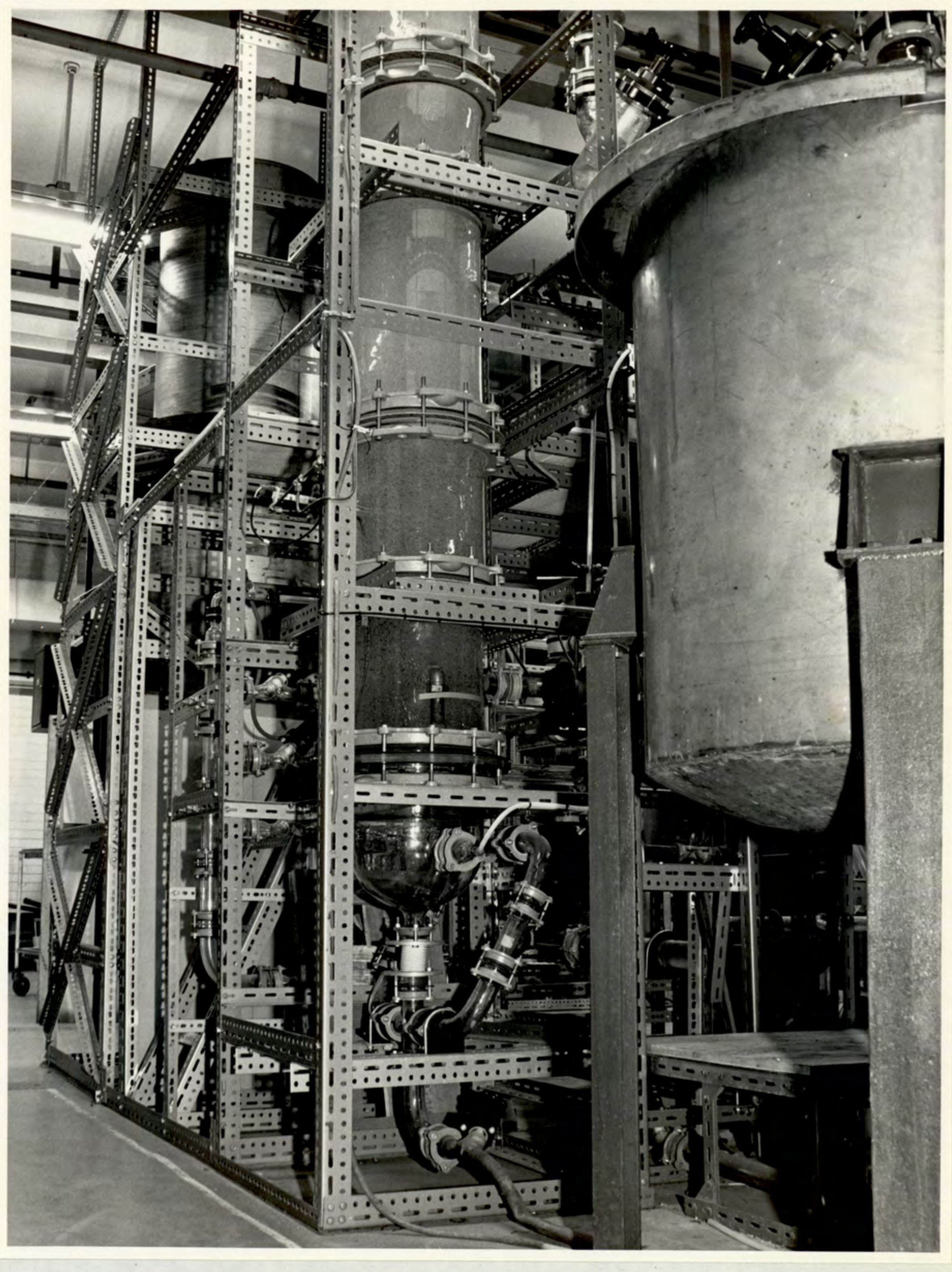

FIG 3.20 General view of the 12" column.

that used for the 6" column was that it contained 9 sintered metal discs instead of 3. The original intention was to have had 12 discs, so that at any given superficial velocity the volumetric flow-rate per disc was constant. However, this was not possible because of the geometry of the distributor plates. The flow areas of the two gas-distributors were:
11·9 sq.in. (77.0 cm^2) and 42.1% free area, for the 6" distributor;
35·7 sq.in (231.0 cm^2) and 31.5% free area for the 12" distributor.

3.3.3 EXPERIMENTAL PROCEDURE AND PROGRAMME

The experimental work carried out on the two large columns can be divided into three sections, all of which are closely integrated:

1. Pressure drop measurements
2. Bubble swarm velocity measurements
3. Gas hold-up measurements

1. Pressure drop

The total pressure drop across the column was measured during each individual test. In addition, a series of experiments was carried out to determine the dry pressure drop across the gas distributors at various flow-rates in both the 6" and the 12" columns.

In the latter series, the sintered metal discs were first cleaned in nitric acid, washed, thoroughly dried and inserted into the appropriate column. The air-flow was then turned on and the pressure-drop across the distributor measured by means of a mercury manometer for the full range of air flows available. This was repeated for the various porosities in both the 6" and the 12" columns. The flow metering pressure was also noted, so that the air flow-rates could be converted to standard conditions.

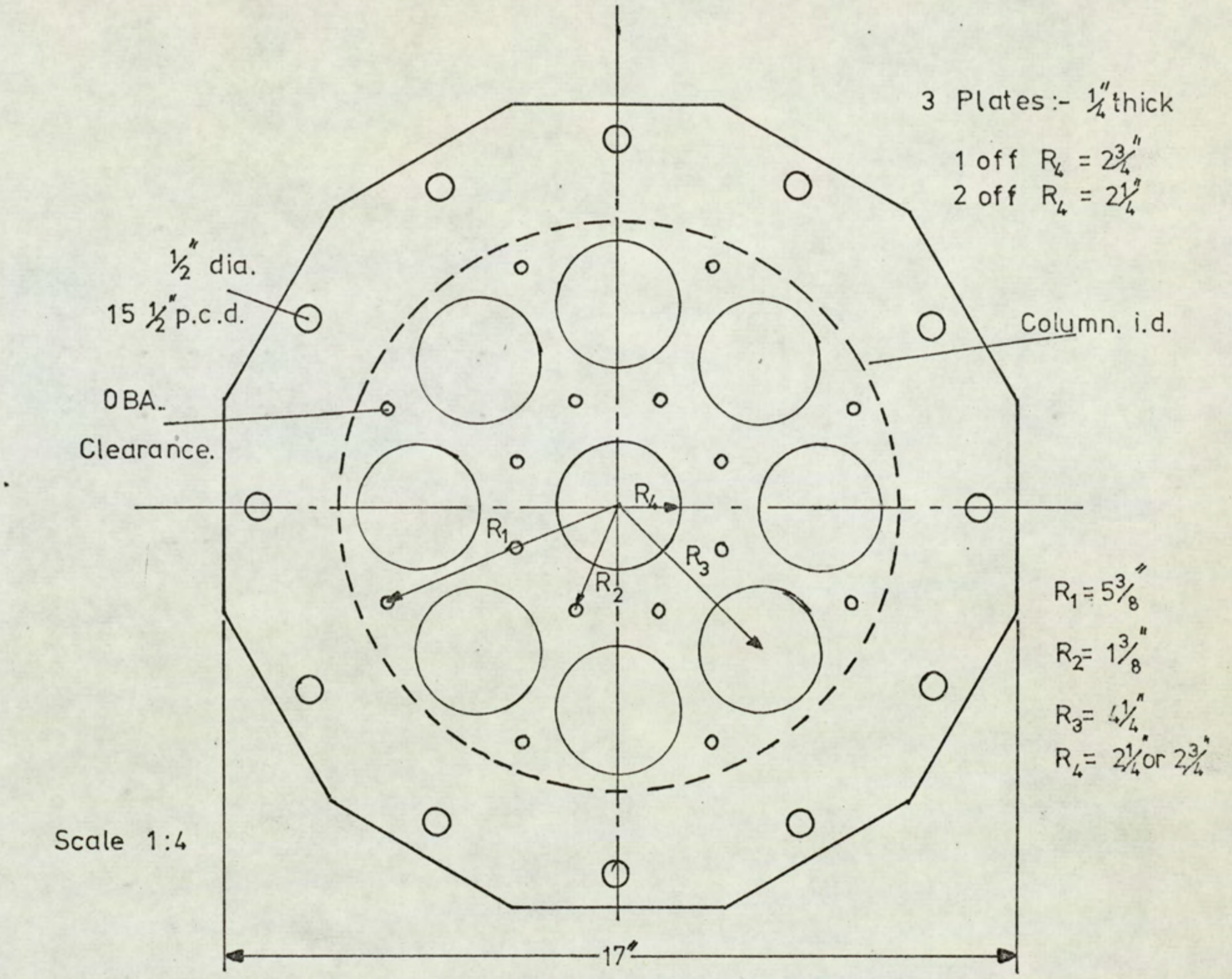

FIG 3.21 (a) Gas distributor 12" column.

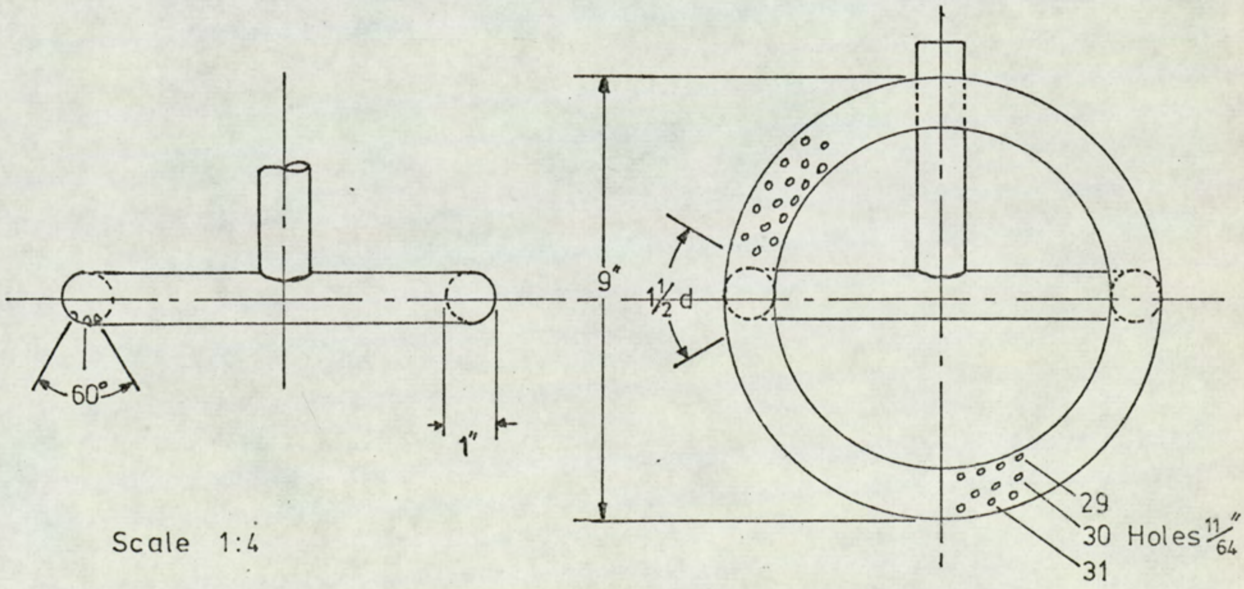

FIG 3.21 (b) Liquid distributor 12" column.

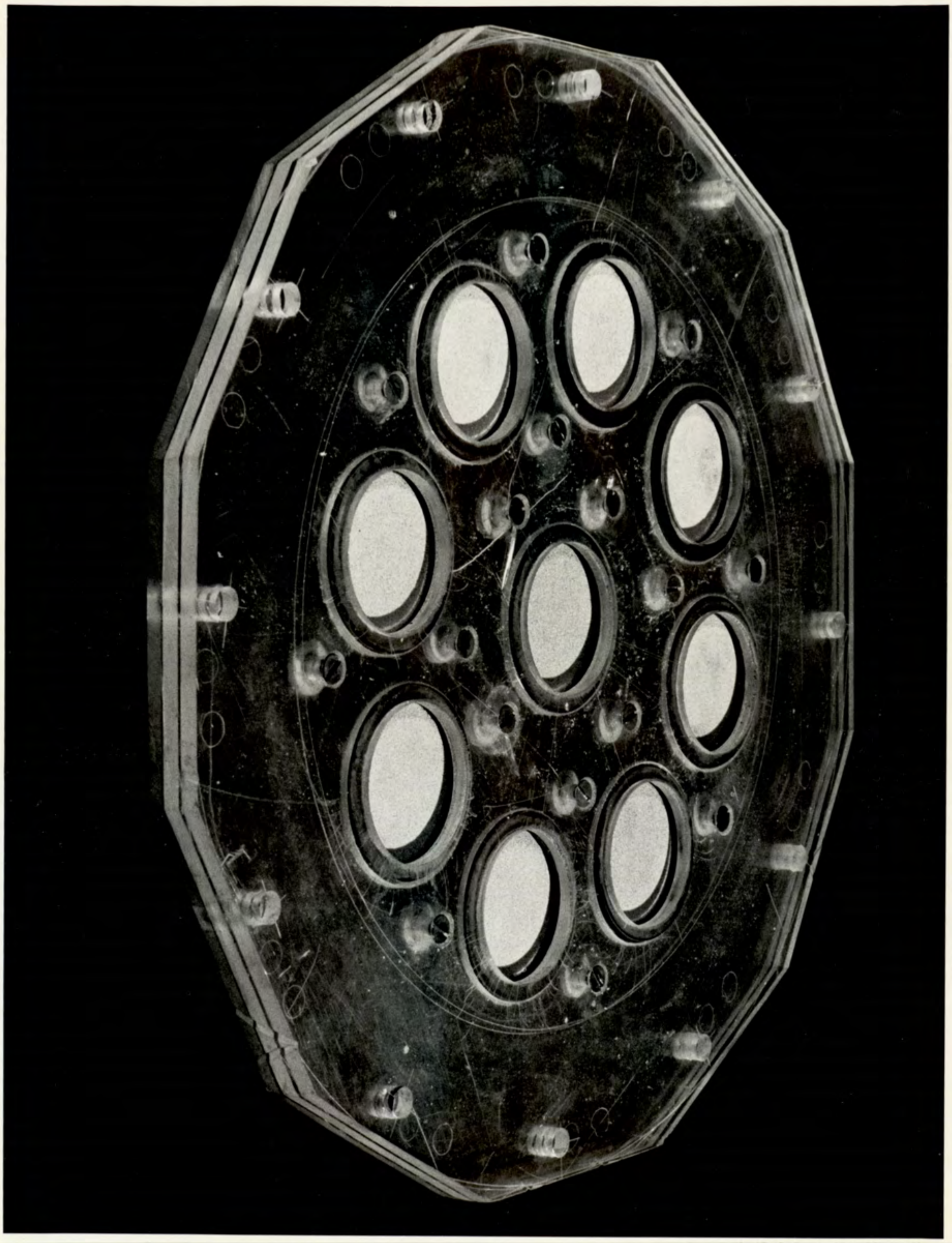

FIG 3.22 General view of the gas distributor for the 12" column, (complete).

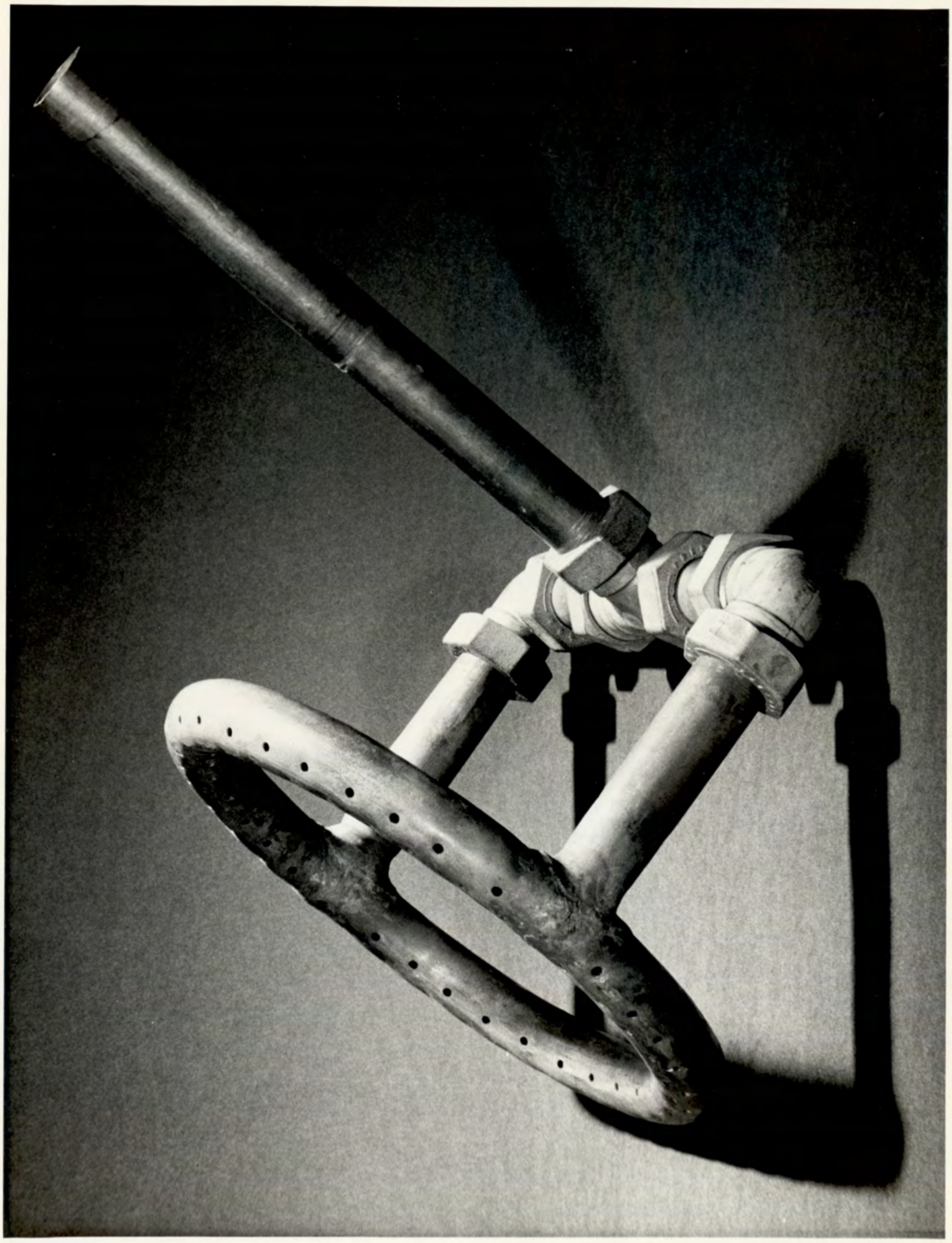

FIG 3.23 General view of the liquid distributor for the 12" column, (complete).

2. Bubble-Swarm Velocities

The general procedure for starting up the equipment when operating with both phases was the same as that outlined in Chapter 2. Firstly, the air-flow was started at a low rate, followed by circulation of the liquid phase. The liquid superficial velocity was then set to the desired rate and the air flow-rate adjusted until the required hold-up was obtained. At this stage the flow-rate, gas hold-up and pressure drops were noted.

Table 3.5 Experimental Conditions for Bubble-Swarm Velocity Determinations (6" Column)

Liquid Superficial (cm/s) Velocity	Fractional Gas Hold-up	Distributor Disc Porosity
0	0.05	1, 2, 3
0	0.10	1, 2, 3
0	0.15	1, 2, 3
0	0.20	1, 2, 3
0.5	0.05	1, 2, 3
0.5	0.10	1, 2, 3
0.5	0.15	1, 2, 3
0.5	0.20	1, 2, 3
1.0	0.05	1, 2, 3
1.0	0.10	1, 2, 3
1.0	0.15	1, 2, 3
1.0	0.20	1, 2, 3
2.6	0.05	2, 3
2.6	0.10	2, 3

Table 3.6 Experimental Conditions for Bubble-Swarm, Velocity Determinations (12" Column)

Liquid Superficial Velocity (cm/s)	Fractional Gas Hold-up	Distributor Disc Porosity
0	0.05	2
0	0.10	2
0	0.15	2
0.8	0.05	2
0.8	0.10	2
0.8	0.15	2
1.0	0.05	2
1.0	0.10	2
1.0	0.15	2
2.0	0.05	2
2.0	0.10	2

The air flow was then shut off by means of the quadrant valve, which gave an almost instantaneous cut-off of air, whilst the liquid-flow remained unaltered. The rise velocity of the bubble-swarm was then measured between two marks, 100 cm apart, on the column. This was repeated five times for each condition. The results were found to be very reproducible, mainly because the bubble-swarm/clear liquid interface had very good definition.

Details of the experimental programme followed with the 6" and 12" columns are shown in Tables 3.5 and 3.6 respectively. As can be seen in Table 3.6, no measurements were taken with the 12" column at gas hold-ups greater than 15%. This was because of limitations in the air-supply system.

3. Gas Hold-up

The starting procedure has already been described. When the desired values of air-flow and liquid-flow rates were obtained and the equipment was at steady state, the air flow-rate, the air metering pressure, the liquid-flow, the total column pressure drop and the gas hold-up were recorded.

The conditions under which the experiments were carried out are listed in Tables 3.7 to 3.10 inclusive. With the yeast suspensions it was

Table 3.7 Experimental Conditions for Hold-up Measurements.

Liquid phase : Water
Column diameter : 6"

Liquid Superficial Velocity (cm/s)	Fractional Gas Hold-up	Distributor Disc Porosity
0	0.05	1, 2, 3
0	0.10	1
0	0.20	1, 2, 3
0.5	0.025	2
0.5	0.050	1, 2, 3
0.5	0.075	2
0.5	0.100	1, 2, 3
0.5	0.200	1, 2, 3
1.0	0.05	1, 2, 3
1.0	0.10	1, 2, 3
1.0	0.20	1, 2, 3
2.6	0.025	2
2.6	0.050	1, 2, 3
2.6	0.075	2
2.6	0.100	1, 2, 3

not possible to operate at high gas hold-ups: for even when using silicone anti-foam agents, so much foam was generated that no estimate of hold-up could be made. Also, even with the extra column section to aid degassing, foam was frequently observed leaking from the top of the columns at relatively low gas flow-rates.

Table 3.8 Experimental Conditions for Hold-up Measurements.

Liquid phase : Water
Column diameter : 12"

Liquid Superficial Velocity (cm/s)	Fractional Gas Hold-up	Distributor Disc Porosity
0	0.05	3
0	0.175	3
0.8	0.025	2
0.8	0.050	2, 3
0.8	0.075	2
0.8	0.100	2, 3
0.8	0.140	2
0.8	0.150	3
1.0	0.05	3
1.0	0.10	3
1.0	0.15	3
2.0	0.025	2
2.0	0.050	2, 3
2.0	0.075	2
2.0	0.100	2
2.0	0.130	2

The yeast used was obtained from Ansell's Brewery *: it was a non-flocculent strain of Saccharomyces cerevisiae, typical of the brewing yeasts used in the U.K. The yeast was obtained fresh from the filter presses after fermentation and contained approximately 75% by weight of water. The suspensions were made up as follows. In the case of the 10% Yeast suspension, 400 lb. (880 kg) of pressed yeast were added to one of the storage tanks and 600 lb. (1,320 kg) of tap water added. The yeast quantity was determined by weighing whilst the water was added, by means of a hose-pipe, to help disperse the yeast. The volume of water was determined by filling the tank to a predetermined depth. The

Table 3.9 Experimental Conditions for Hold-up Measurements.

Liquid phase : 5% and 10% Yeast
Column diameter : 6"

Liquid Superficial Velocity (cm/s)	Fractional Gas Hold-up	Distributor Disc Porosity	Yeast $^{W}/_{V}$ %
0.5	0.025	2	5, 10
0.5	0.045	2	5
0.5	0.050	2	10
0.5	0.075	2	5, 10
0.5	0.100	2	5, 10
2.6	0.025	2	5, 10
2.6	0.050	2	5, 10
2.6	0.075	2	5, 10
2.6	0.100	2	5, 10
2.6	0.125	2	10

---

* Ansell's Brewery, Gosta Green, Birmingham.

suspension was then circulated by means of the smaller pump until it was judged to be completely mixed. After conducting the experiments with the 10% suspension, it was then watered down to form a 5% suspension. This

Table 3.10 Experimental Conditions for Hold-up Measurements.

Liquid phase : 5% and 10% Yeast
Column diameter : 12"

Liquid Superficial Velocity (cm/s)	Fractional Gas Hold-up	Distributor Disc Porosity	Yeast % W/V
0.8	0.025	2	5, 10
0.8	0.050	2	5, 10
0.8	0.075	2	5, 10
0.8	0.100	2	5
0.8	0.125	2	5
2.0	0.025	2	5, 10
2.0	0.050	2	5

was again carried out by filling the tanks to a predetermined depth, followed by recirculation of the suspension. During experimental work with the yeast suspensions the recirculation pump was left running at all times, to maintain an even suspension.

3.3.4 EXPERIMENTAL RESULTS

1. Pressure Drop Measurements over the Distributor

The results of these experiments are set out in full in Tables B.3 and B.4 in Appendix B. Since two Rotameters were used, the measurements overlap for some gas flow-rates. This helped to minimise errors that would otherwise appear in the flow-rate measurement when operating at the extreme ends of the Rotameter scales. The values of the dry pressure drops listed in Tables B.3 and B.4 are the mean values of two runs in each case, one with increasing flow-rate and the other with decreasing flow-rate.

The data are presented graphically in Figs. 3.24 and 3.25, from which the following correlations were obtained.

6" diameter Column.

Porosity 1. $$\Delta P_{1D} = 0.0079\,G_v = 0.0875\,v_{gs} \qquad 3.1$$

Porosity 2. $$\Delta P_{2D} = 0.013\,G_v = 0.145\,v_{gs} \qquad 3.2$$

Porosity 3. $$\Delta P_{3D} = 0.054\,G_v = 0.59\,v_{gs} \qquad 3.3$$

12" diameter Column.

Porosity 2. $$\Delta P_{2D} = 0.0044\,G_v = 0.195\,v_{gs} \qquad 3.4$$

Porosity 3. $$\Delta P_{3D} = 0.0148\,G_v = 0.667\,v_{gs} \qquad 3.5$$

Where ΔP_{1D}, ΔP_{2D} and ΔP_{3D} are the respective dry pressure drops in cm of mercury when operating with distributors of porosities 1, 2 and 3, G_v is the volumetric air flow-rate (l/min) at standard conditions and v_{gs} is the gas superficial velocity in cm/s.

As can be seen from both the tables and the graphs, the corresponding values for the 6" diameter column are approximately three-quarters the value for the 12" diameter column. The explanation for this is that the gas flow area for the 12" column is four times the flow area of the 6" diameter column, whilst the distributor flow areas are in the ratio of 3 : 1 and the pressure drop is proportional to the flow area for a given flow rate.

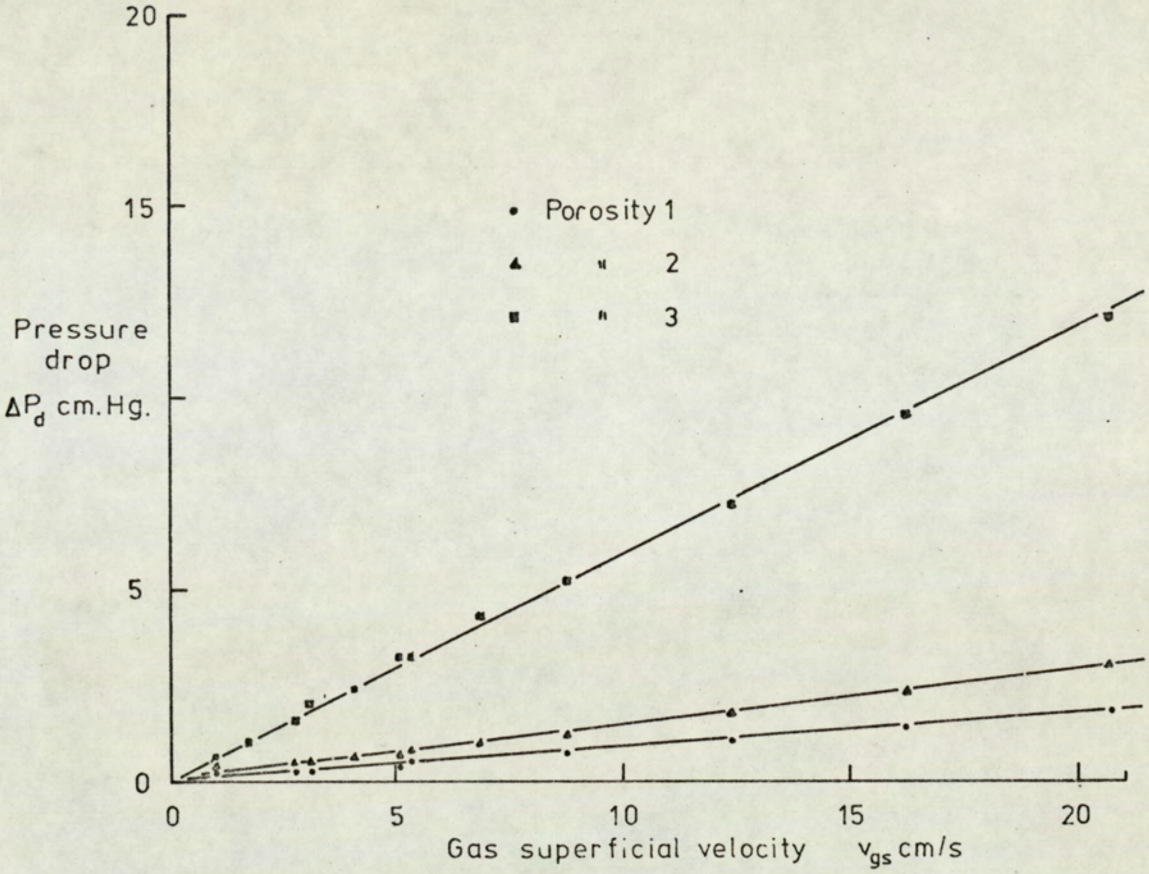

FIG 3.24 Distributor (dry) pressure drop, 6" column.

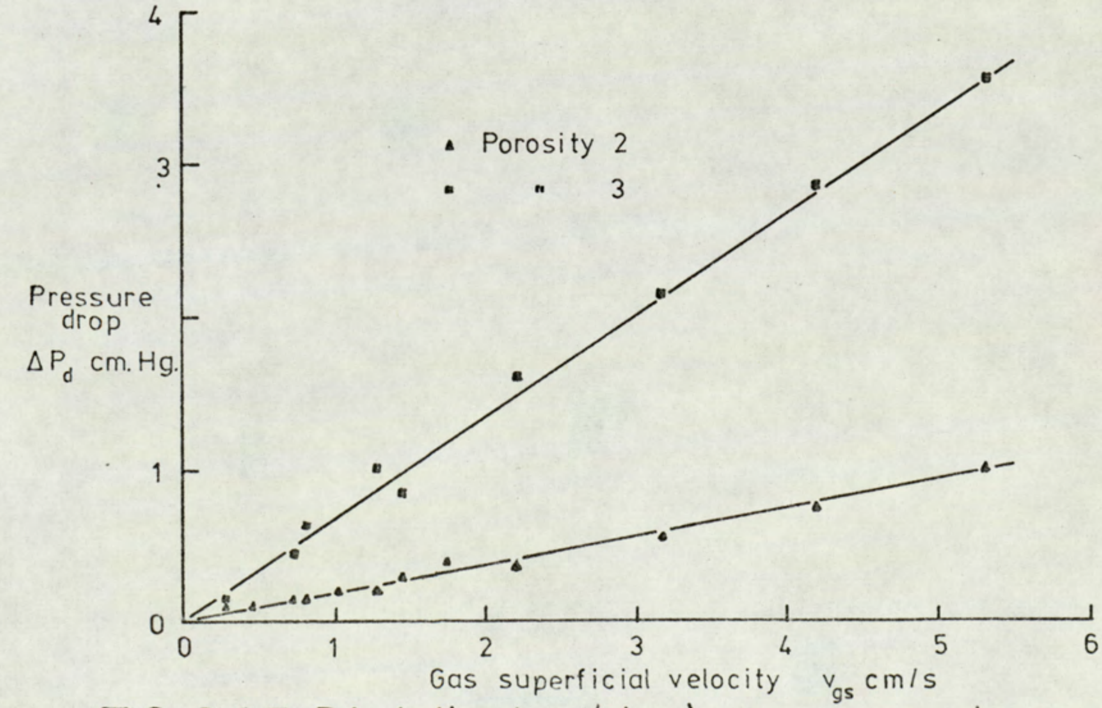

FIG 3.25 Distributor (dry) pressure drop, 12" column.

2. Bubble-Swarm Velocity Measurements

The experimental results from this series of tests are shown in Tables B.5 and B.6 in Appendix B. The figures for the gas superficial velocity and the bubble-swarm velocity are the mean figures calculated from at least four runs for each value of hold-up.

Fig. 3.26 shows the bubble-swarm velocity as a function of gas superficial velocity for the 6" diameter column. From the graph it appears that the bubble-swarm velocity, v_{bs}, is only slightly dependent upon the distributor porosity, since there is no systematic variation with porosity. Fig. 3.27 shows the term $(v_{bs} - v_{ls})$ as a function of gas superficial velocity, where v_{ls} is the liquid superficial velocity and v_{bs} is the mean value of the velocity for all the distributors. From Fig. 3.27 the following relationship was obtained.

$$(v_{bs} - v_{ls}) = 20.8\, v_{gs}^{-0.1527} \qquad 3.6$$

where the velocities are in cm/s.

Data from the 12" diameter column were treated in a similar manner. Table B.6 lists the results for the bubble-swarm velocities also presented graphically in Fig. 3.28 as a function of gas superficial velocity. Fig. 3.29 shows the expression $(v_{bs} - v_{ls})$ as a function of gas superficial velocity. From Fig. 3.29 it can be seen that there is more scatter about a line drawn through the experimental points. However, when data for both the 6" and the 12" columns were plotted on the same graph (Fig. 3.30) and equation 3.6 was superimposed, a reasonable fit was obtained.

The gas hold-up data recorded during measurement of the bubble-swarm velocities were also used for purposes of correlation. Another method of correlating the bubble-swarm velocity is against gas hold-up, itself a function of gas superficial velocity. Figs. 3.31 and 3.32 show the bubble-swarm velocities as a function of gas hold-up. The values of v_{bs} used in

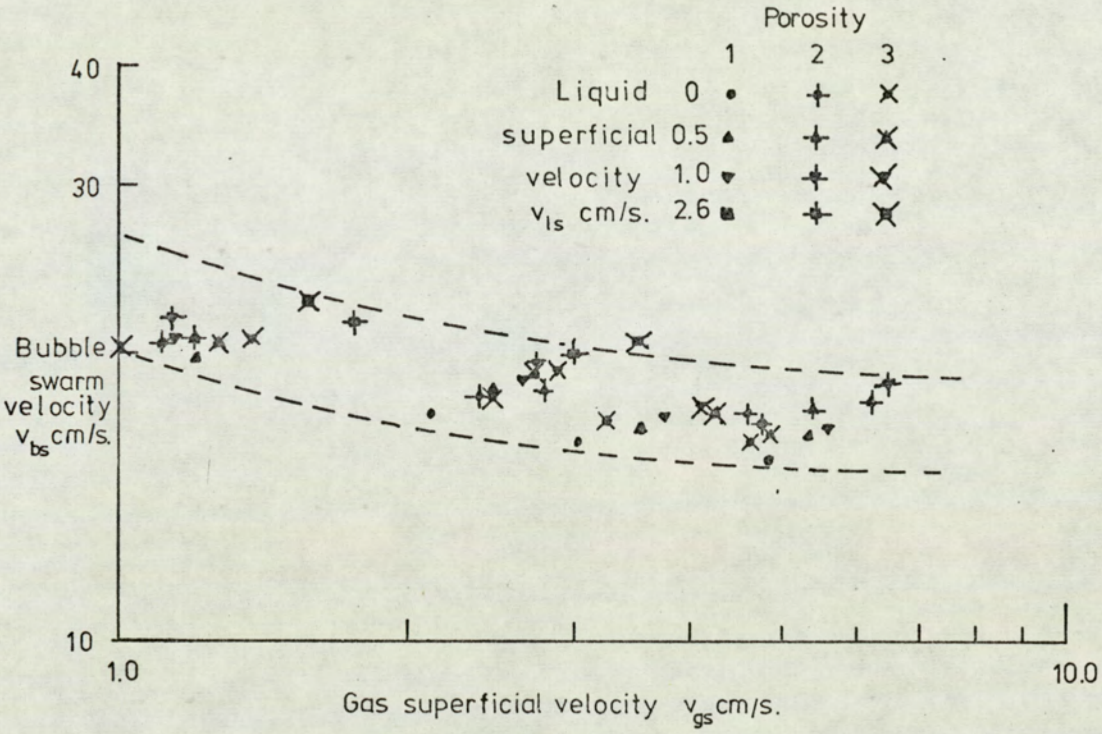

FIG 3.26 Bubble-swarm velocities, 6"column.

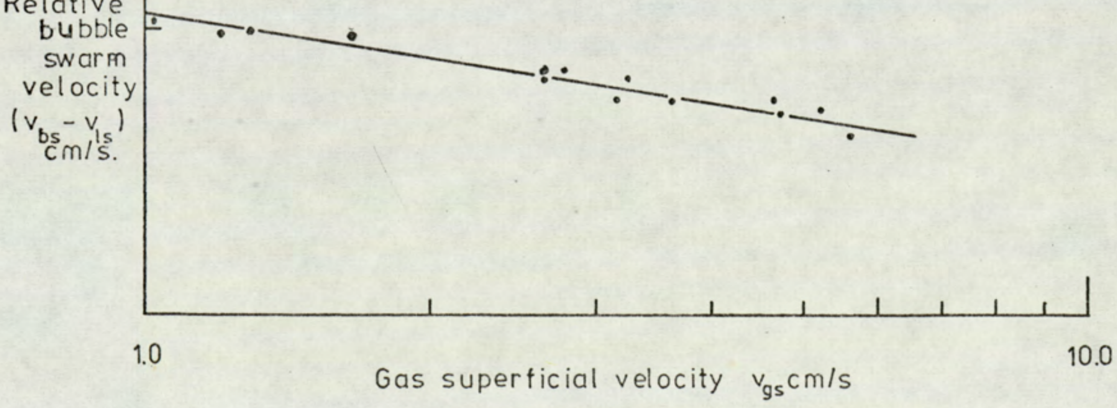

FIG 3.27 Relative bubble-swarm velocities, 6" column.

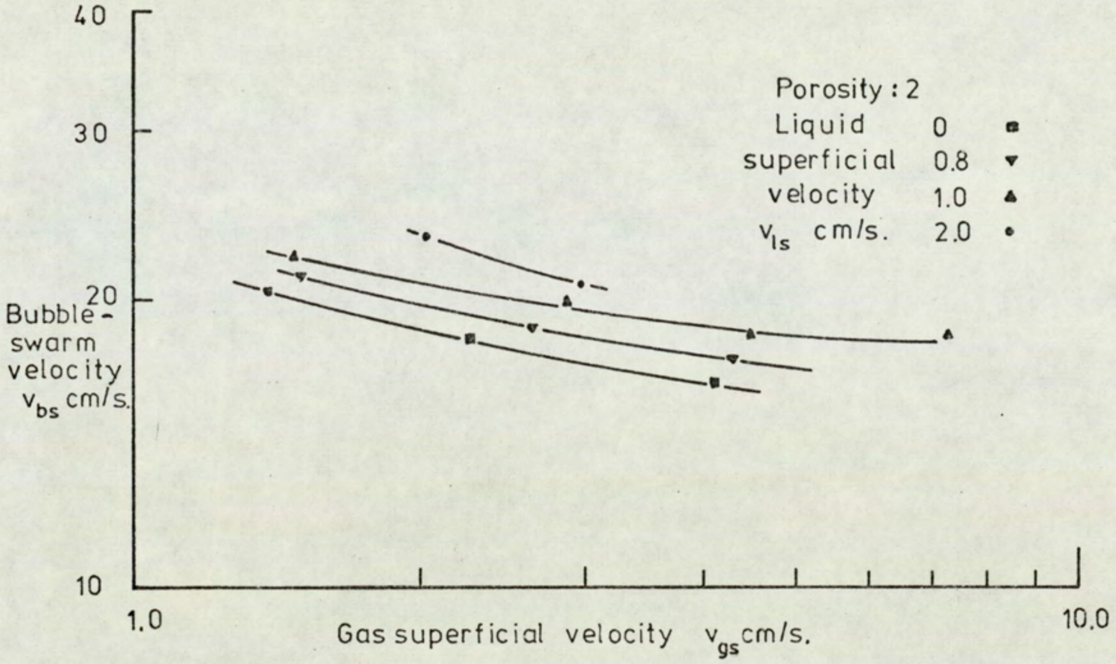

FIG 3.28 Bubble-swarm velocities, 12" column.

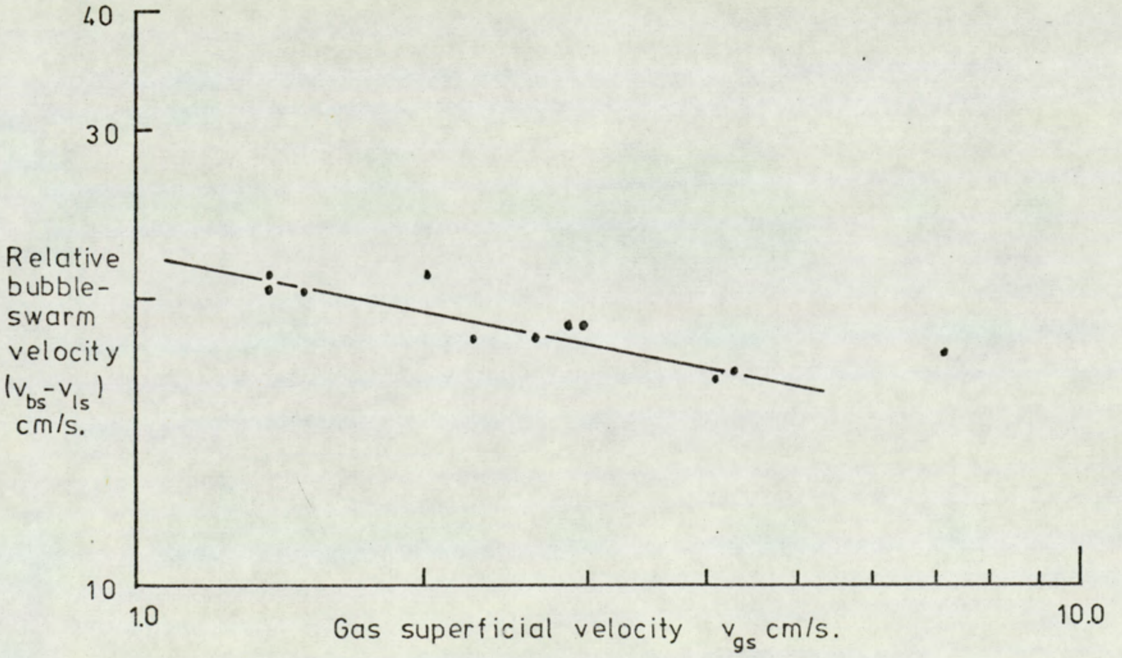

FIG 3.29 Relative bubble-swarm velocities, 12" column.

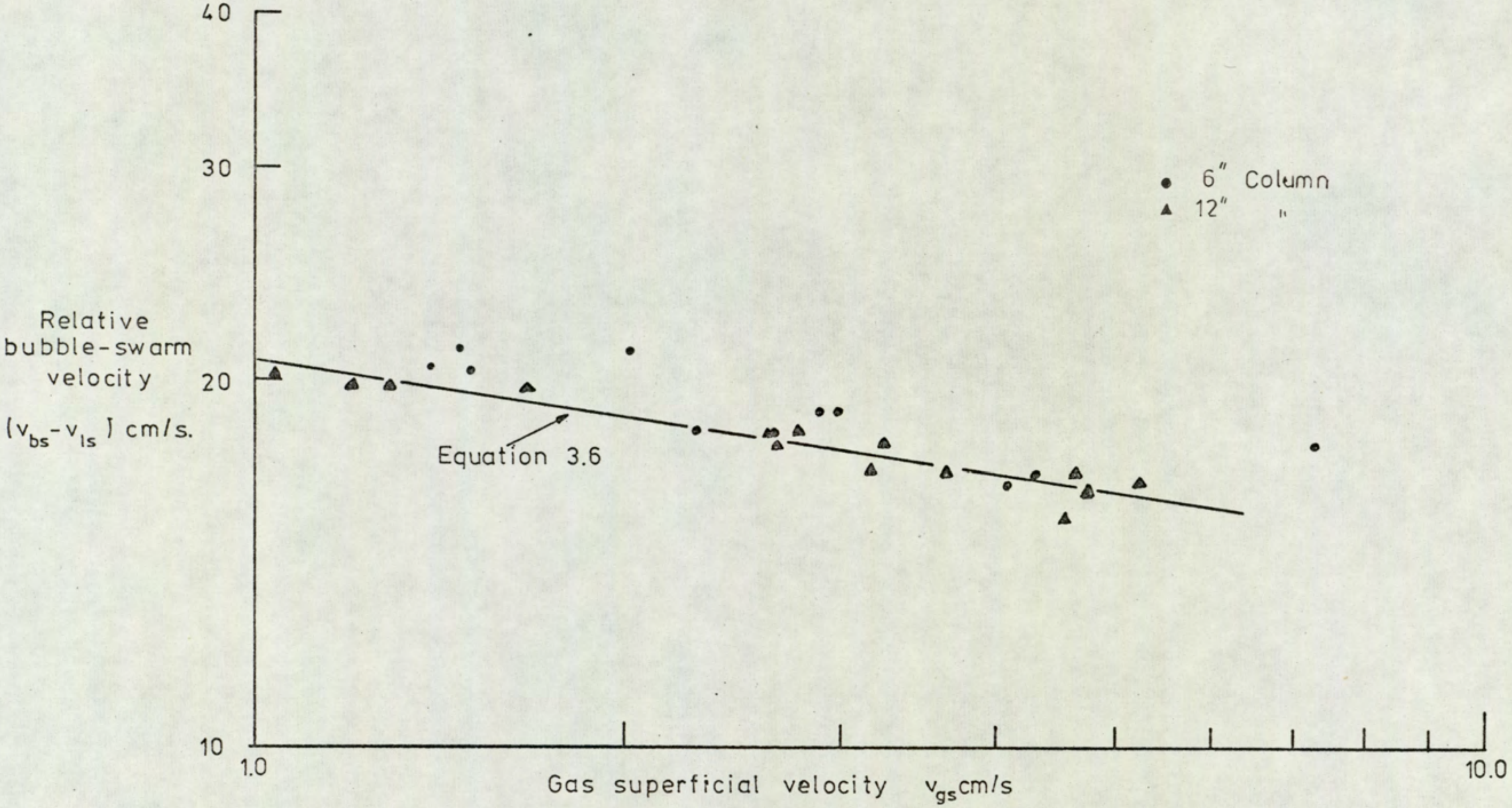

FIG 3.30 Relative bubble-swarm velocities 6″ and 12″ columns.

these two figures are again the means of velocities for all the distributors, since with the available data it is not possible to state categorically the exact effect that porosity has on the swarm velocity.

From Figs. 3.31 and 3.32 v_{bs} can be seen to be a function of gas hold-up of the form:

$$v_{bs} = B\epsilon^{k} \qquad 3.7$$

where k = - 0.16 for the 6" column and - 0.19 for the 12" column.

Fig. 3.33shows a plot of the constant B against v_{ls}. The resulting linear relationships can be put in the form:

$$\text{6" Column} \qquad B = 0.58\, v_{ls} + 12.4 \qquad 3.8$$

$$\text{12" Column} \qquad B = 0.81\, v_{ls} + 11.8 \qquad 3.9$$

Equation 3.7 can now be rewritten to give the following correlations:

$$\text{6" Column} \qquad v_{bs} = (0.58\, v_{ls} + 12.4)\epsilon^{-0.16} \qquad 3.10$$

$$\text{12" Column} \qquad v_{bs} = (0.81\, v_{ls} + 11.8)\epsilon^{-0.19} \qquad 3.11$$

These two equations give a much better agreement than the general equation (3.6) which was formulated in an endeavour to summarise the data for both the 6" and the 12" columns. It should be noted that equation 3.6 cannot be used in conjunction with either 3.10 or 3.11 to give accurate predictions. There is a slight difference in the values of bubble-swarm velocity for the 6" and the 12" diameter columns which can be put down to two factors:-

1. The wall effects, which if applicable in this size of column would vary slightly, the 6" column having the greater wall effect.

2. The gas hold-up for similar gas superficial velocities is not quite the same for the two columns, and since the bubble-swarm velocity is partially dependent upon gas hold-up, there is bound to be some variation.

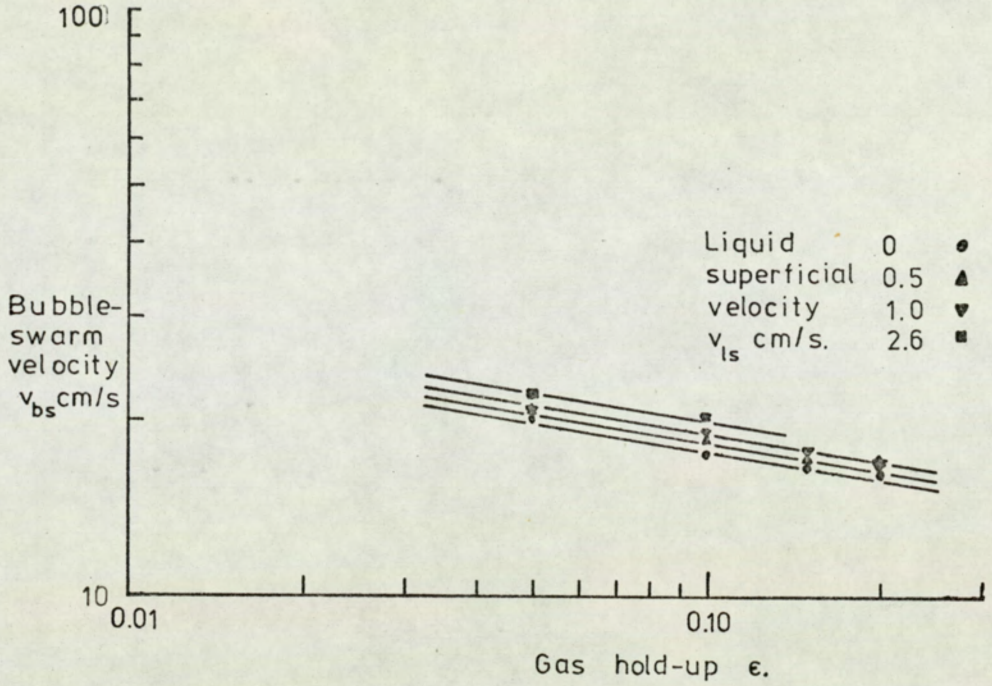

FIG 3.31 Bubble-swarm velocities, 6" column.

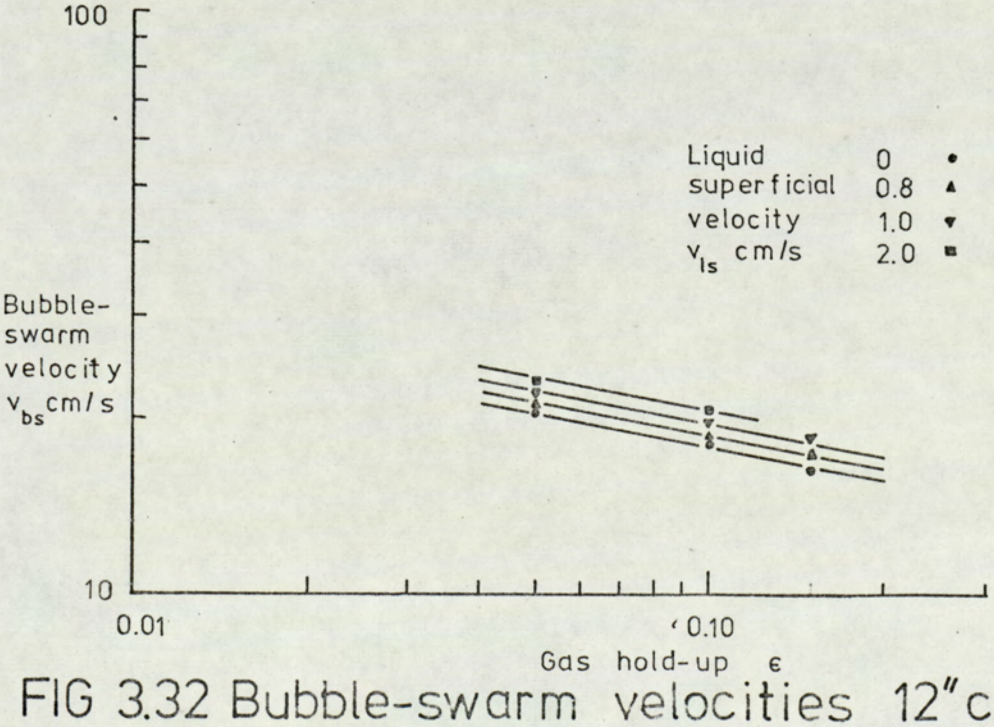

FIG 3.32 Bubble-swarm velocities 12" column.

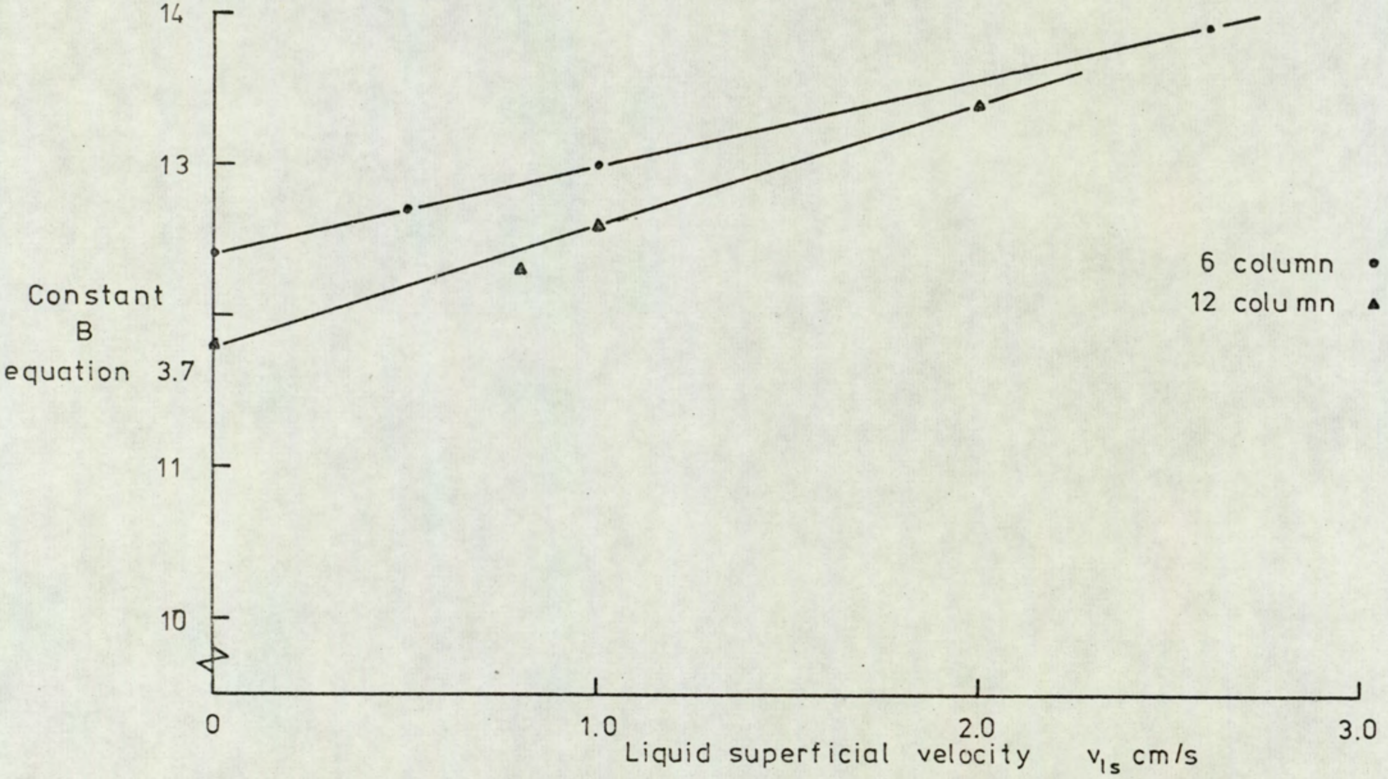

FIG 3.33 Graph of 'B' (eqn. 3.7) against liquid superficial velocity both columns.

Although the data used in obtaining these equations have been taken as mean values for all three distributor porosities, there does seem to be a slight dependence of v_{bs} on the porosity, and hence the bubble diameter. With the available data it is very difficult to determine this effect since the value of v_{bs} rises as the porosity decreases from 1 (mean pore diameter 0.011 cm) to 2 (mean pore diameter 0.0045 cm) and then falls as the pore size is further reduced from porosity 2 to porosity 3 (mean pore diameter 0.0025 cm).

At present there is insufficient data to explain this phenomena, but it seems likely that there is interaction between the bubbles, since as the bubble size varies the interbubble distance must also vary to give the same gas hold-up.

3. Gas Hold-up Measurements

6" Diameter Column (Tap Water)

Fig. 3.34 shows the 6" diameter column under varying conditions of gas hold-up at zero liquid velocity. Fig. 3.35 shows the 6" diameter column under the same conditions of hold-up with a liquid superficial velocity of 2.6 cm/s. A general observation, which is borne out by the following experimental results, is that the volume of gas required to produce a given hold-up increases as the liquid superficial velocity increases.

Tables B.7 to B.10 inclusive, in Appendix B, list the results of the measured hold-up and superficial gas-velocities when operating the 6" diameter column. The values of the gas superficial velocities have all been corrected to standard conditions. Three distributor porosities were used: Tables B.7 to B.9 inclusive show the results obtained in this series of experiments and also those obtained in the bubble-swarm measurements. Table B.10 lists the mean values of the measured superficial

(a) $\epsilon = 0.025$ (b) $\epsilon = 0.05$

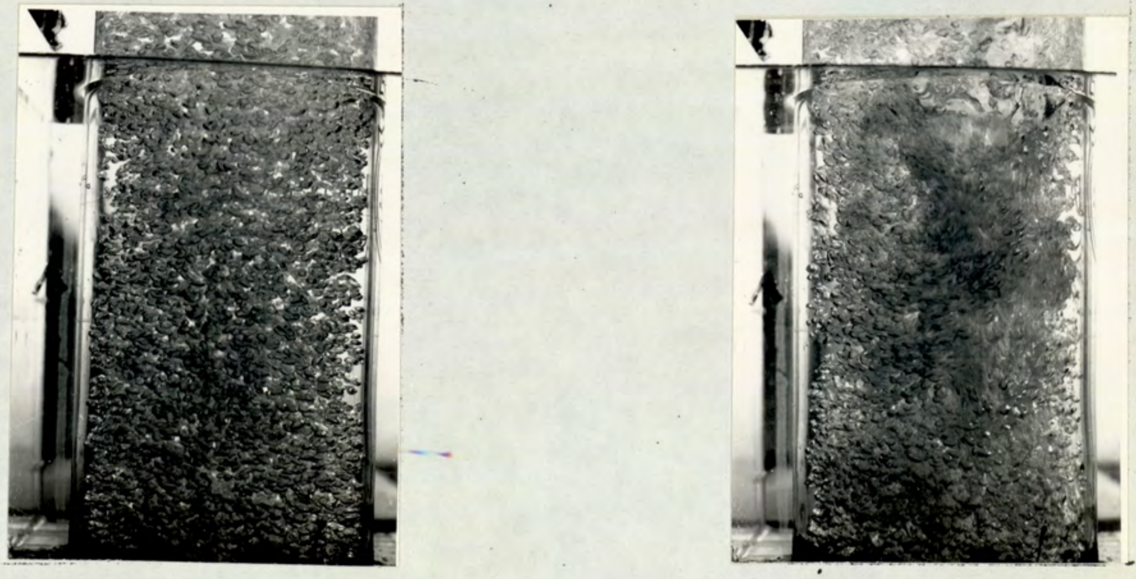

(c) $\epsilon = 0.10$ (d) $\epsilon = 0.20$

FIG 3.34 The 6" column under various gas hold-up conditions, ($v_{ls} = 0$).

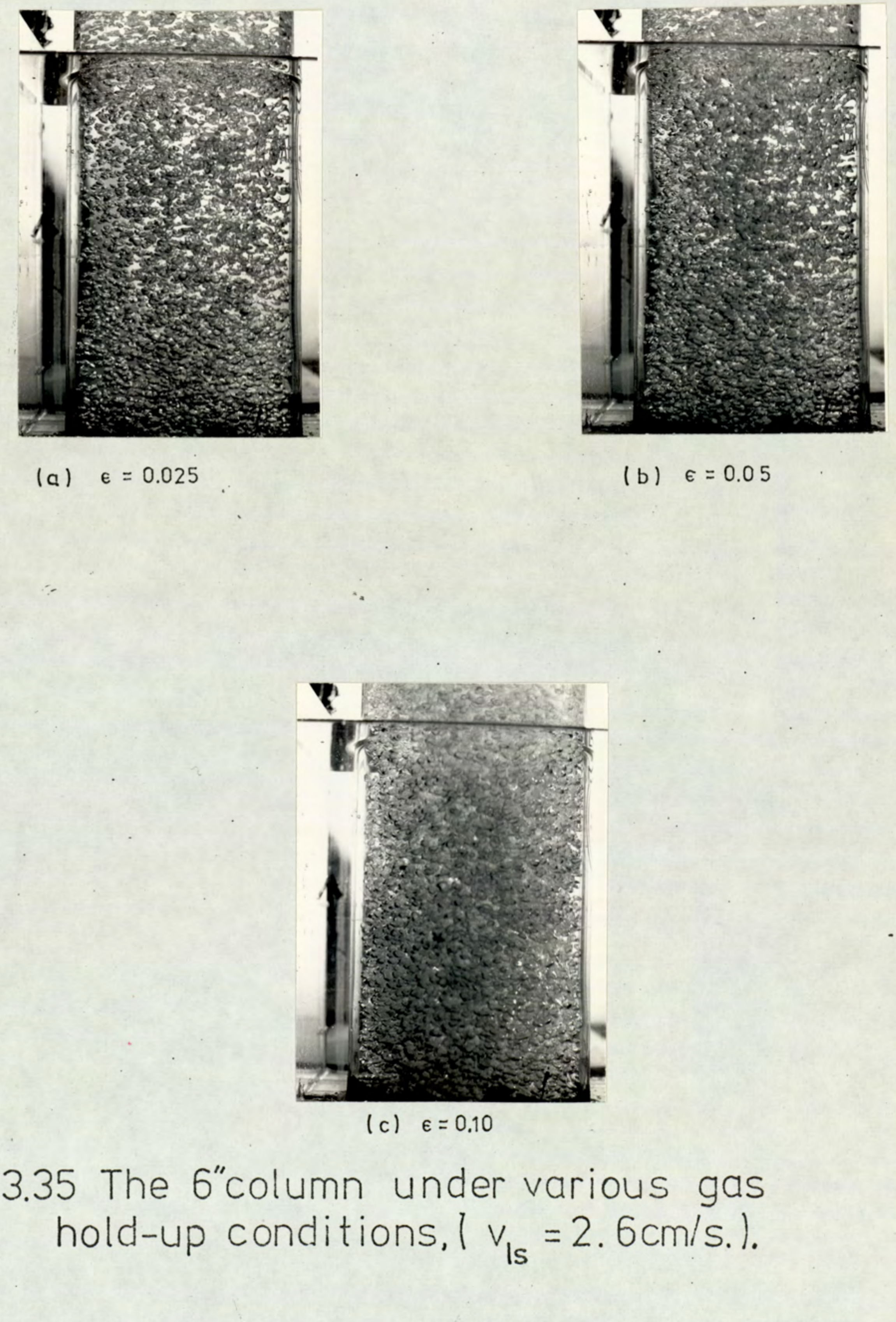

(a) $\epsilon = 0.025$

(b) $\epsilon = 0.05$

(c) $\epsilon = 0.10$

FIG 3.35 The 6"column under various gas hold-up conditions, ($v_{ls} = 2.6$ cm/s.).

velocities for each distributor porosity. Figs. 3.36 to 3.39 inclusive present these data graphically, each Figure showing the results at either zero or a finite value of liquid superficial velocity.

Since the effect of distributor porosity is only slight and insufficient data is available to correlate any effect, Table B.11 lists the mean values of v_{gs} calculated from the data obtained for each distributor porosity, P_1 P_2 and P_3. These data are represented graphically in Fig. 3.40.

From this last figure it can be seen that a series of plots can be used to represent the effect of gas superficial velocity on gas hold-up for fixed values of the liquid superficial velocity. These curves can be expressed in the following form :

$$\epsilon = k_{\epsilon} \cdot v_{gs} \qquad 3.12$$

where ϵ is the fractional gas hold-up. Using Fig. 3.40 the following correlations were developed:

$$v_{ls} = 0 \qquad \epsilon = 0.041\ v_{gs} \qquad 3.13$$

$$v_{ls} = 0.5 \qquad \epsilon = 0.0385\ v_{gs} \qquad 3.14$$

$$v_{ls} = 1.0 \qquad \epsilon = 0.0350\ v_{gs} \qquad 3.15$$

$$v_{ls} = 2.6 \qquad \epsilon = 0.0315\ v_{gs} \qquad 3.16$$

where velocities are in cm/s.

Fig. 3.41 shows the result of plotting values of k_{ϵ} against v_{ls}, the liquid superficial velocity. The following equation can be used to describe the results:

$$k_{\epsilon} = 0.35\ v_{ls}^{(-\ 0.105)} \qquad 3.17$$

By combining equations 3.12 and 3.17 an expression is obtained for

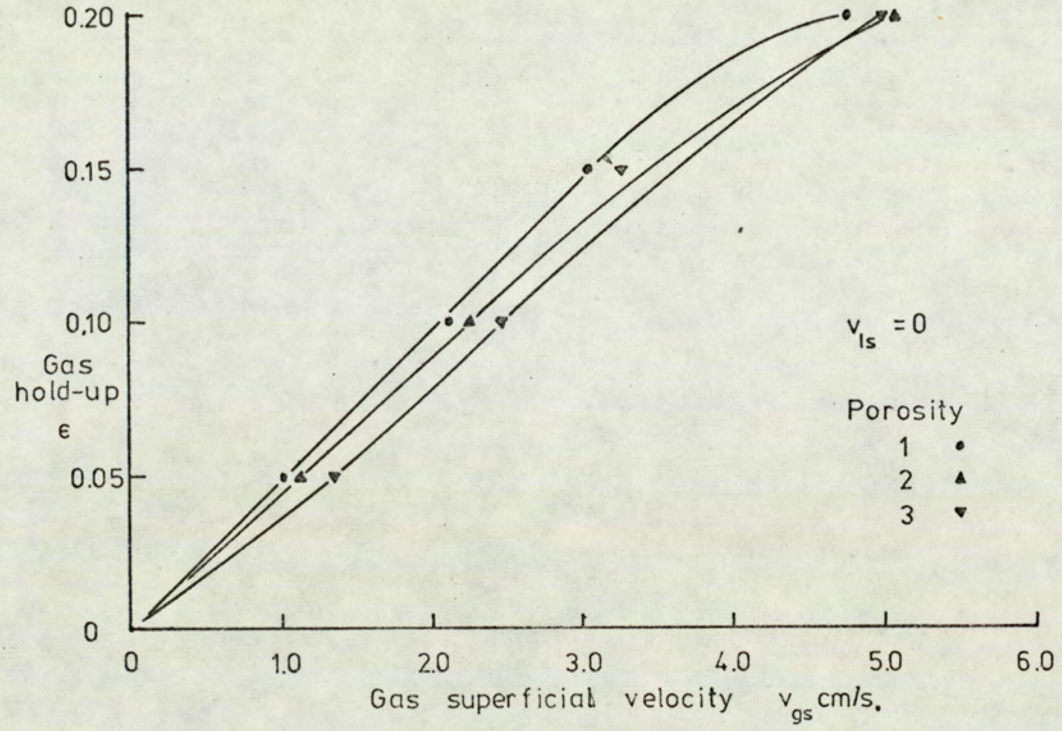

FIG 3.36 Gas hold-up, 6″ column, $v_{ls}=0$.

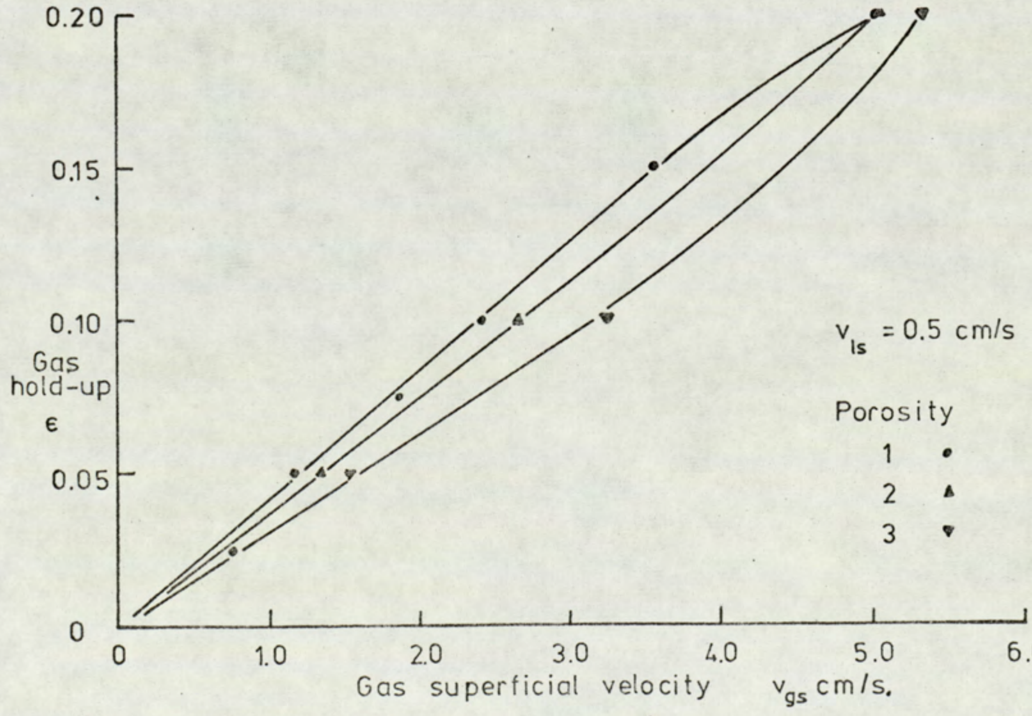

FIG 3.37 Gas hold-up, 6″ column, $v_{ls}=0.5$ cm/s.

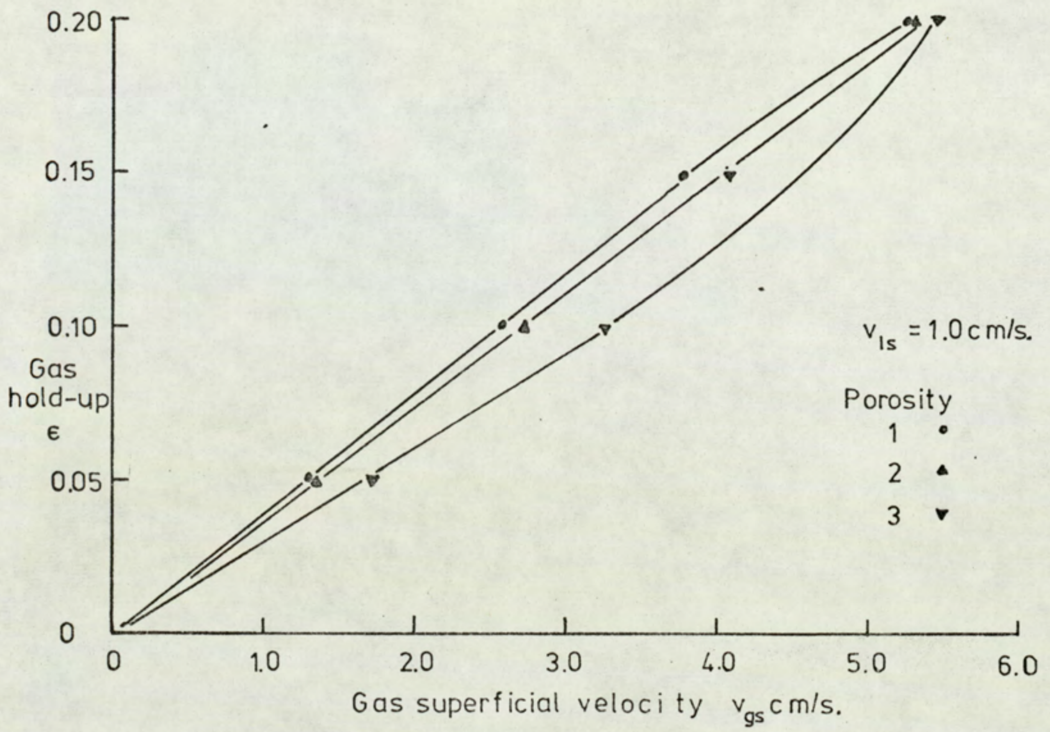

FIG 3.38 Gas hold-up, 6" column, v_{ls} =1.0 cm/s.

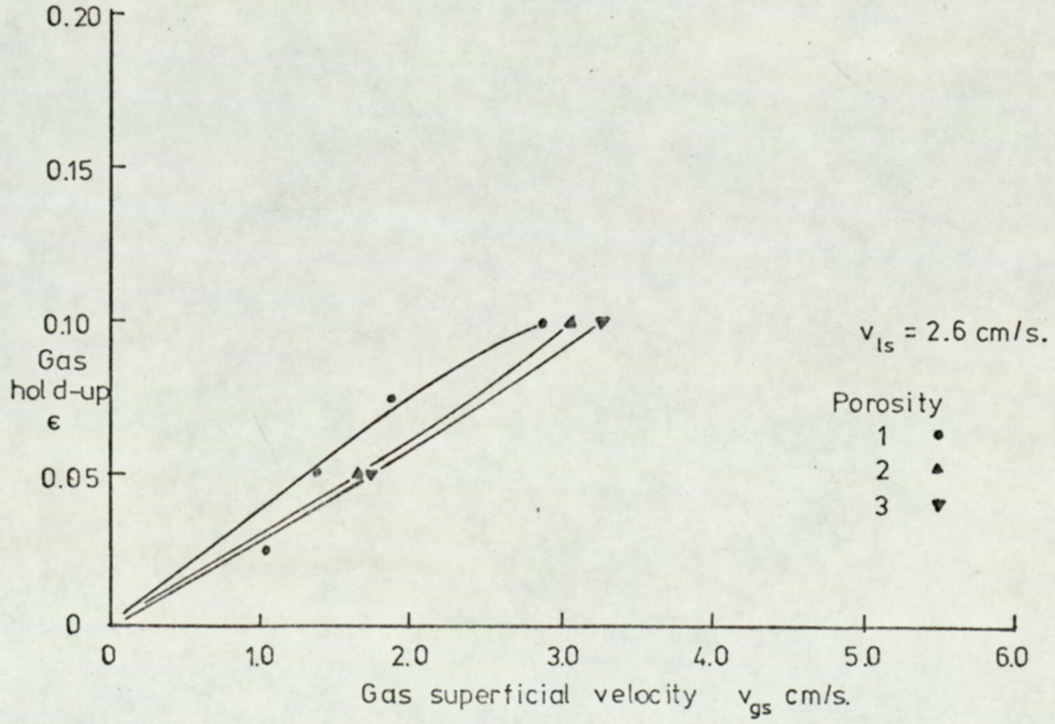

FIG 3.39 Gas hold-up, 6" column, v_{ls}=2.6 cm/s.

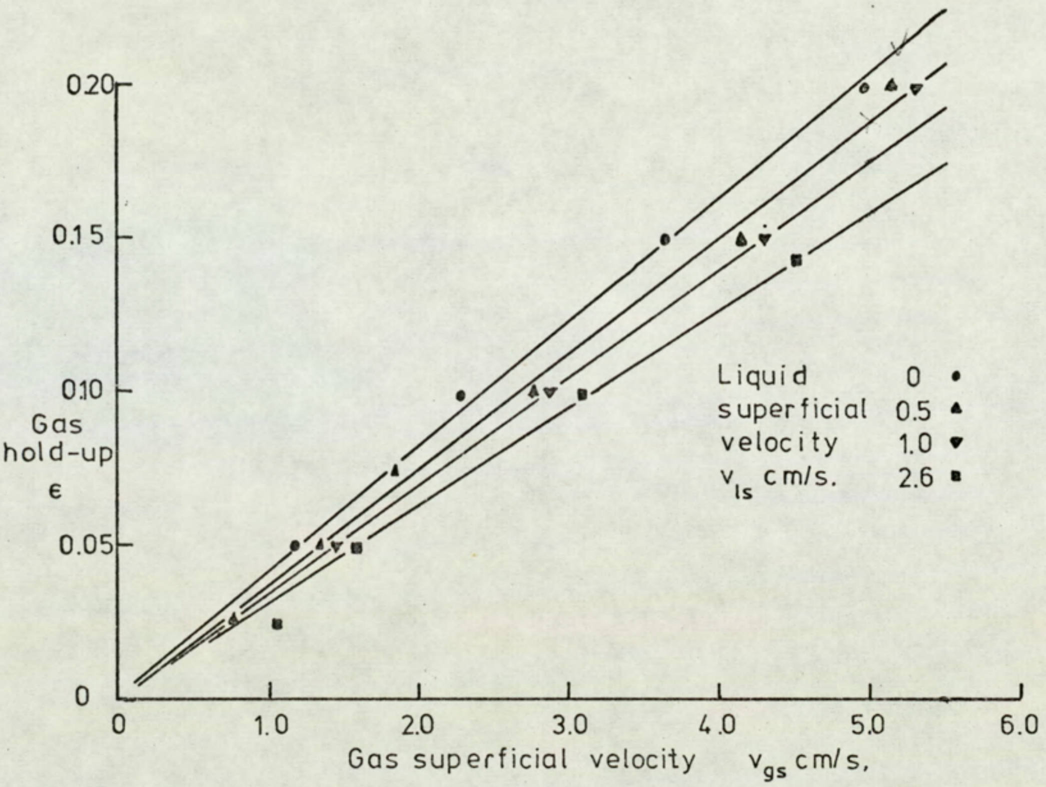

FIG 3.40 Gas hold-up, 6" column, all liquid velocities.

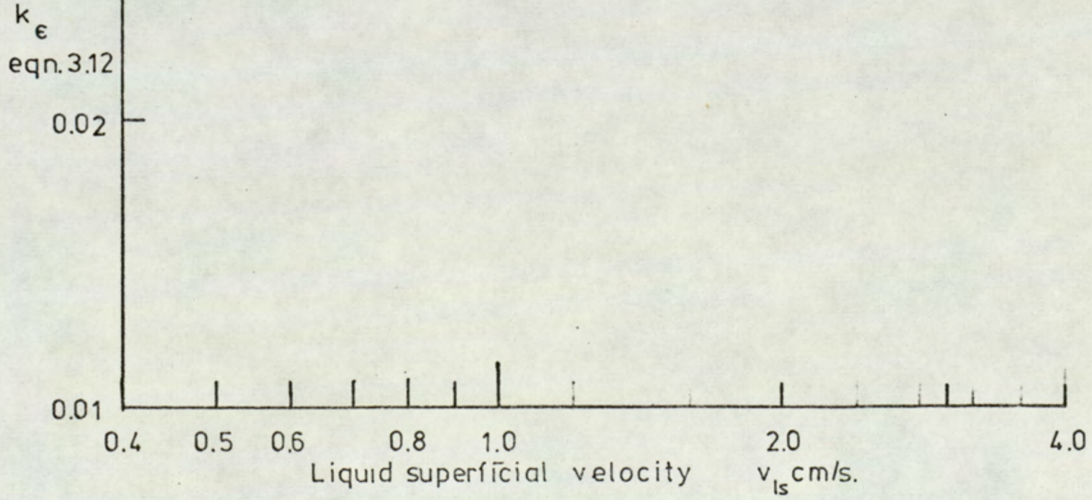

FIG 3.41 Graph of k_ϵ (eqn. 3.12) against liquid superficial velocity.

gas hold-up in terms of v_{ls} and v_{gs}:

$$\epsilon = 0.35\, v_{ls}^{(-0.105)} \cdot v_{gs} \qquad 3.18$$

Table B.12 lists the relative superficial velocity v_{Rs} as a function of the gas hold-up, as a mean of the three porosities used. Fig. 3.42 represents this data graphically, for which the following type of expression can be written:

$$\epsilon = k_{\epsilon}\, v_{Rs} + K \qquad 3.19$$

In this case the constants can be evaluated to give the following correlation:

$$\epsilon = 0.034\, v_{Rs} + 0.0416 \qquad 3.20$$

Equation 3.20 holds for the following conditions:

1. Column diameter - 6"
2. Liquid phase - tap water
3. Gas phase - air
4. $0 \leqslant v_{Rs} \leqslant 5.0$ cm/s
5. $0.025 \leqslant \epsilon \leqslant 0.20$
6. $0.126 \leqslant \bar{d}_b \leqslant 0.222$ cm

The term v_{Rs} was used since this work was aimed at producing, among other factors, design data for two-phase fermentation systems. The relative superficial velocity term is an easily determined factor which can be measured in isolation from the column itself.

Table B.13 in Appendix B shows the pressure-drop that can be accounted for by factors other than the hydrostatic head and the pressure-drop across the dry distributor. The two columns of figures represent the total pressure-drop ΔP_{TOT} minus the hydrostatic head pressure ΔP_H

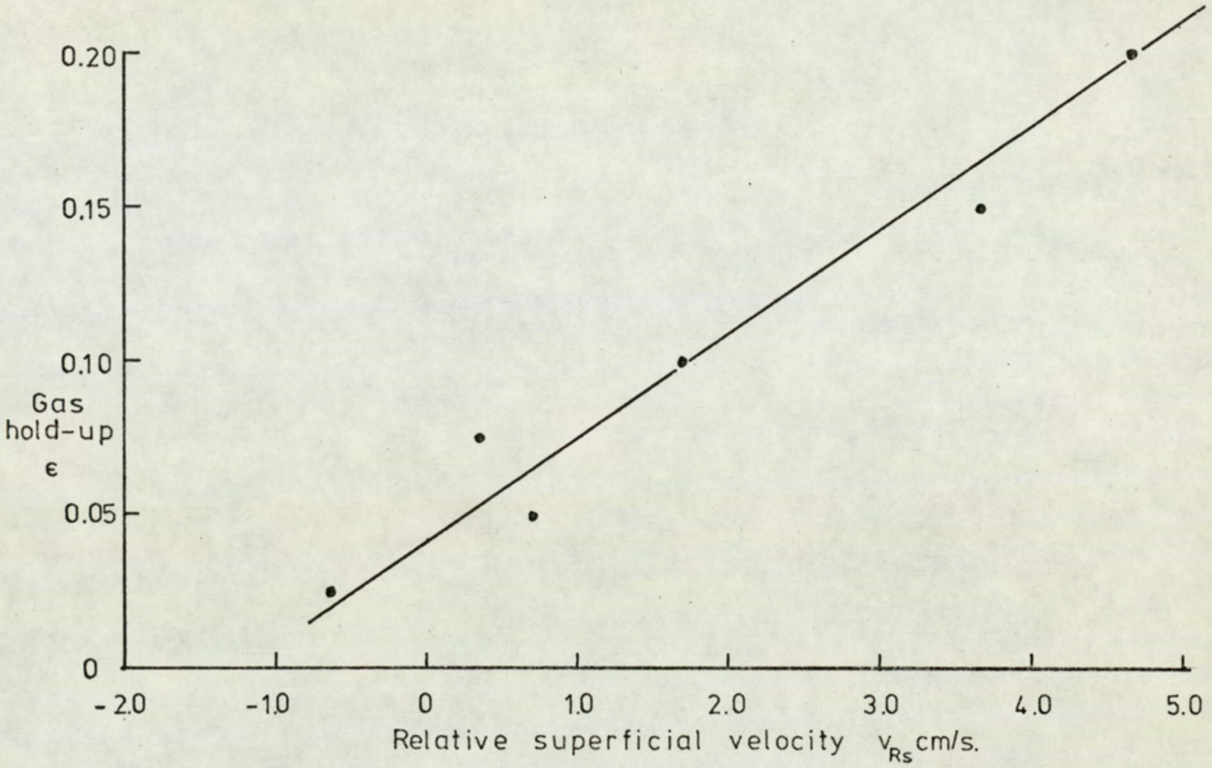

FIG 3.42 Gas hold-up as a function of relative superficial velocity.

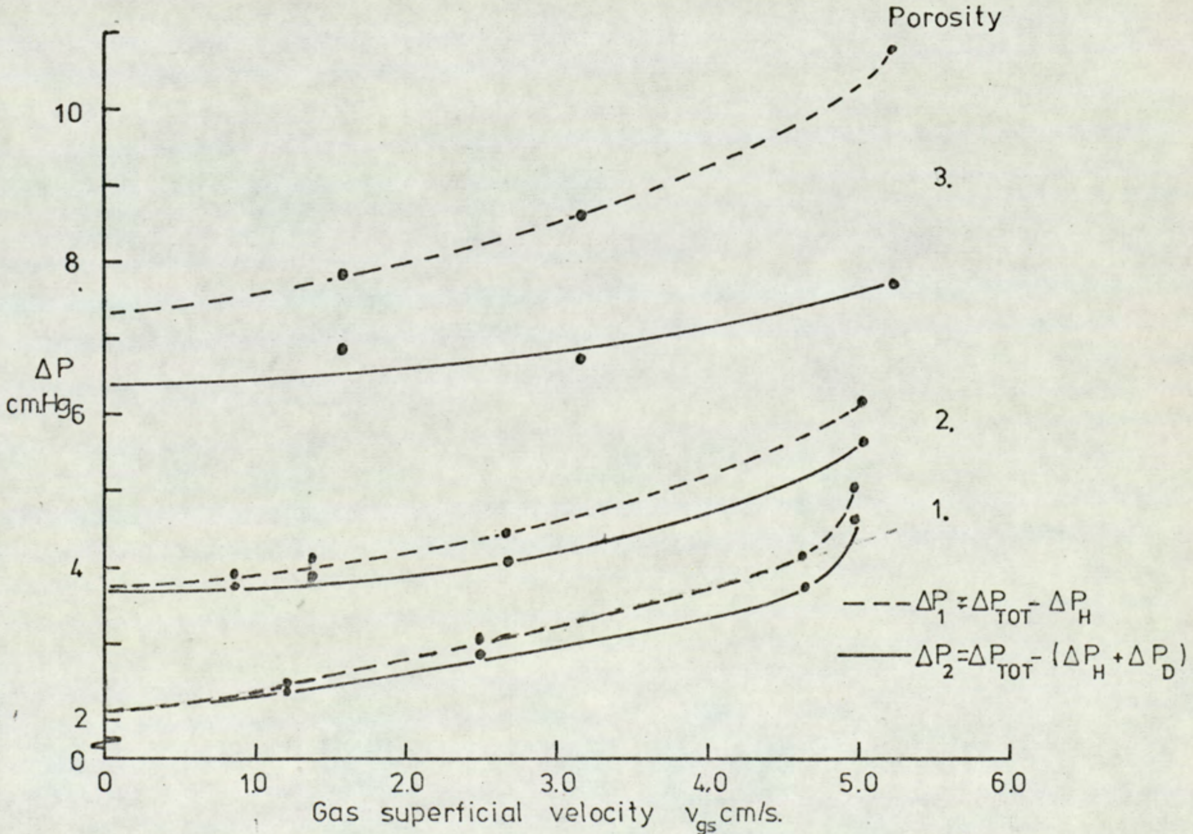

FIG 3.43 Column pressure drops, (6" column).

and $\Delta P_{TOT} - (\Delta P_H + \Delta P_D)$, where ΔP_D is the dry pressure-drop across the distributor.

The data are interpolated in Fig. 3.43, where the solid line represents $\Delta P_{TOT} - (\Delta P_H + \Delta P_D)$ and the dotted line represents $(\Delta P_{TOT} - \Delta P_H)$. The reason that both the lines were plotted was to enable the extrapolation to zero flow to be determined more easily. As can be seen, each pair of lines tends to converge as the gas superficial velocity decreases. At v_{gs} equals zero, the pressure-drop is that required to just prevent the liquid phase draining through the distributor: this is designated ΔP_W, the wet pressure-drop. The value of the pressure-drop above this datum is that due to wall friction and work done in the column, ΔP_F.

12" Diameter Column (Tap Water)

The results for the 12" column with water as the continuous phase have been analysed in a similar manner to those for the 6" column.

The experimental data are set out in Tables B.14 and B.15: Table B.16 combines data from both tables. The data are also represented graphically in Figs. 3.44 to 3.47 inclusive. As can be seen, the variation of hold-up with gas superficial velocity is approximately linear for values of ϵ less than 0.10, and the effect of porosity, and presumably bubble diameter, is relatively small.

Fig. 3.48 shows the mean values of v_{gs} for both distributor porosities plotted against gas hold-up. The plots suggest that for values of v_{gs} less than about 3 cm/s an expression similar to equation 3.12 can be applied. The following correlations were obtained:

liquid superficial velocity $v_{ls} = 0$ $\qquad \epsilon = 0.044\ v_{gs}$ $\qquad$ 3.21

$v_{ls} = 0.8$ $\qquad \epsilon = 0.038\ v_{gs}$ $\qquad$ 3.22

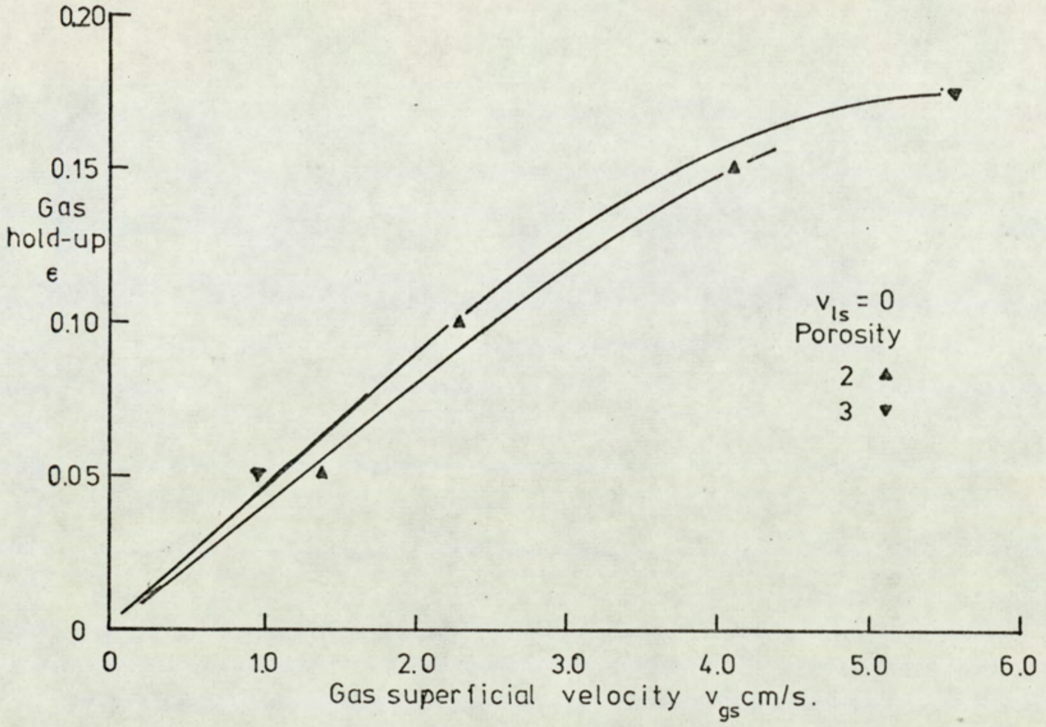

FIG 3.44 Gas hold-up, 12" column, $v_{ls}=0$.

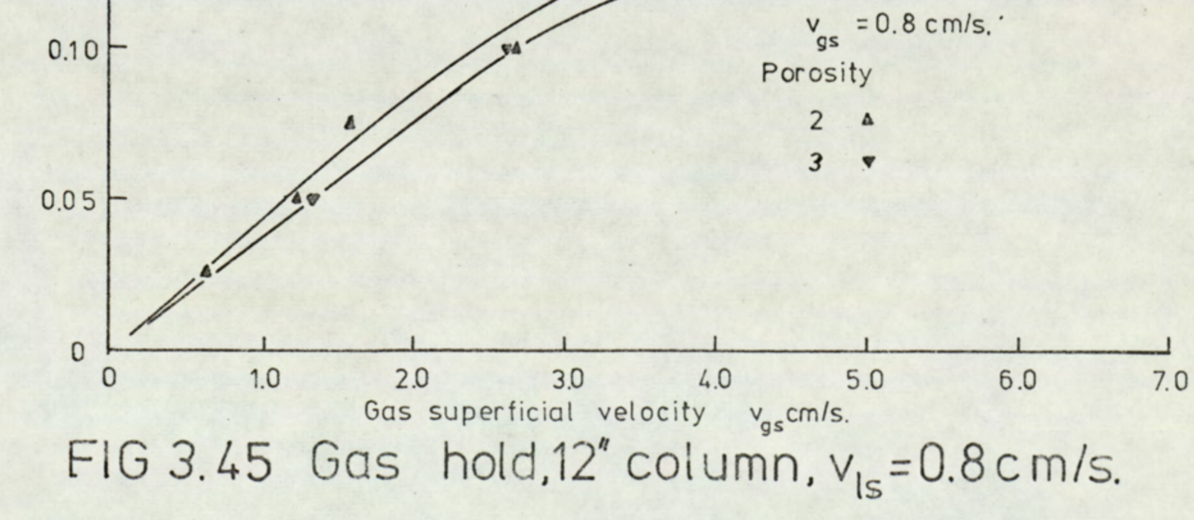

FIG 3.45 Gas hold, 12" column, $v_{ls}=0.8$ cm/s.

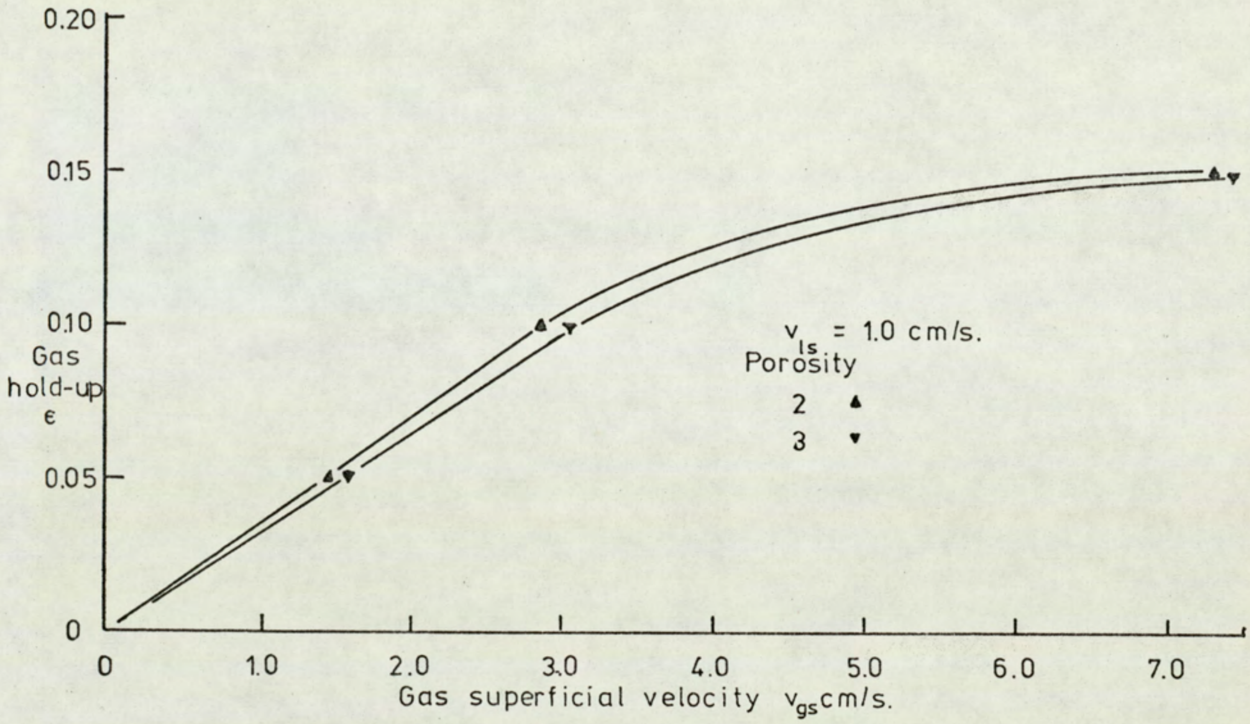

FIG 3.46 Gas hold-up, 12" column, v_{ls} = 1.0 cm/s.

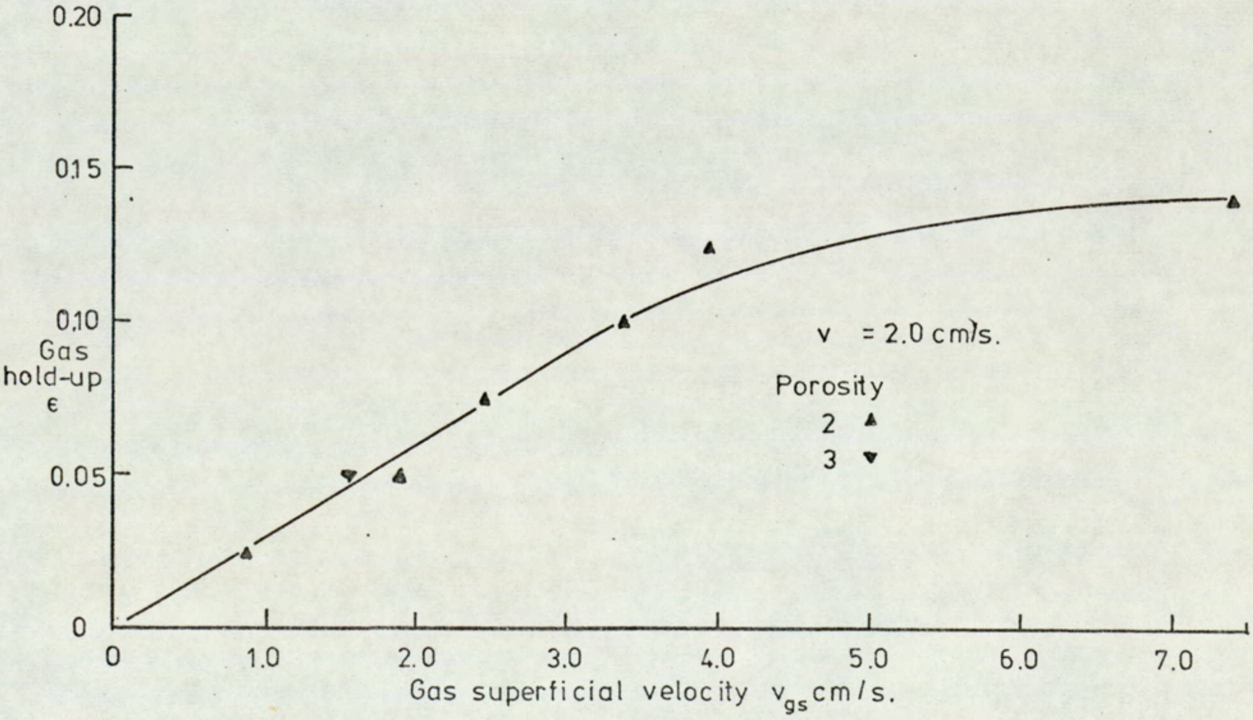

FIG 3.47 Gas hold-up, 12" column, v_{ls} = 2.0 cm/s.

$$v_{ls} = 1.0 \qquad \epsilon = 0.34\, v_{gs} \qquad 3.23$$

$$v_{ls} = 2.0 \qquad \epsilon = 0.029\, v_{gs} \qquad 3.24$$

where v_{ls} and v_{gs} are in cm/s and ϵ is the fractional gas hold-up. Clearly the superficial liquid velocity has an effect on ϵ : for a fixed value of v_{gs}, ϵ decreases as v_{ls} increases.

On plotting the values of k_ϵ against v_{ls} (Fig. 3.49) a roughly linear relationship is seen to hold. Consequently the data can be described empirically by the equation:

$$\epsilon = (0.044 - 0.0080\, v_{ls})\, v_{gs} \qquad 3.25$$

This holds for the following conditions:

1. Liquid phase - tap water
2. Gas phase - air
3. $0 \leqslant v_{ls} \leqslant 2.0$ cm/s
4. $0 \leqslant \epsilon \leqslant 0.10$

Table B.18 in Appendix B lists the values of the mean relative superficial velocities, $(v_{Rs} = v_{gs} - v_{ls})$, as a function of gas hold-up: These are represented graphically in Fig. 3.50. An equation similar to 3.19 can be used to summarise the combined data for the two distributors, viz.

$$\epsilon = 0.028\, v_{Rs} + 0.045 \qquad 3.26$$

The effect of distributor porosity seems to be greater in Fig. 3.50, but this is due to the method of plotting the data.

The above equation holds for the following conditions:

1. Liquid phase - tap water
2. Gas phase - air
3. Column diameter - 12"

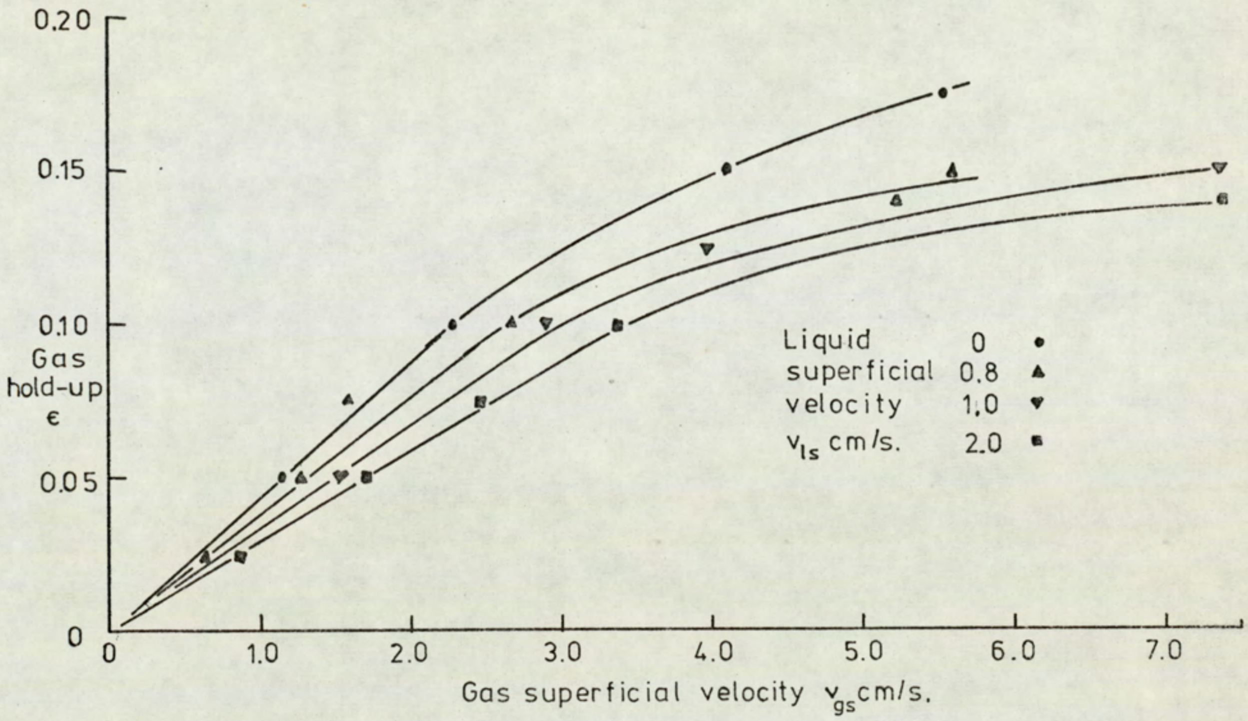

FIG 3.48 Gas hold-up, 12" column, all liquid velocities.

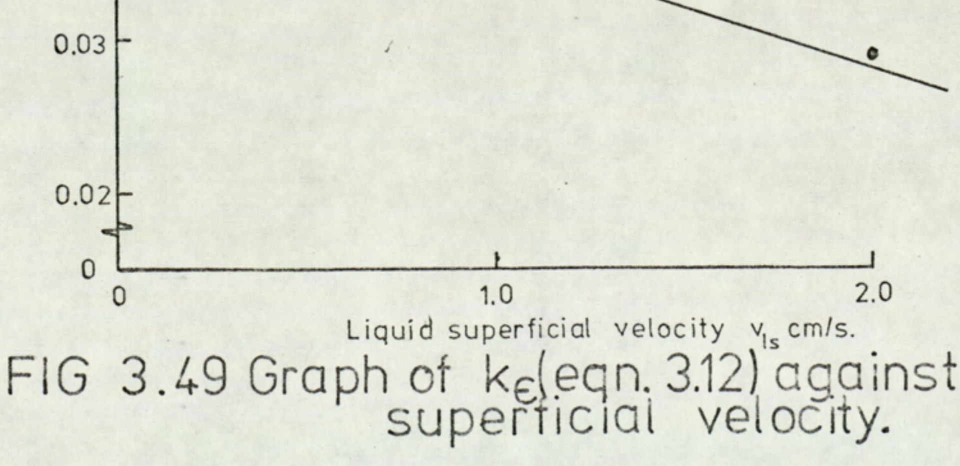

FIG 3.49 Graph of k_ϵ (eqn. 3.12) against liquid superficial velocity.

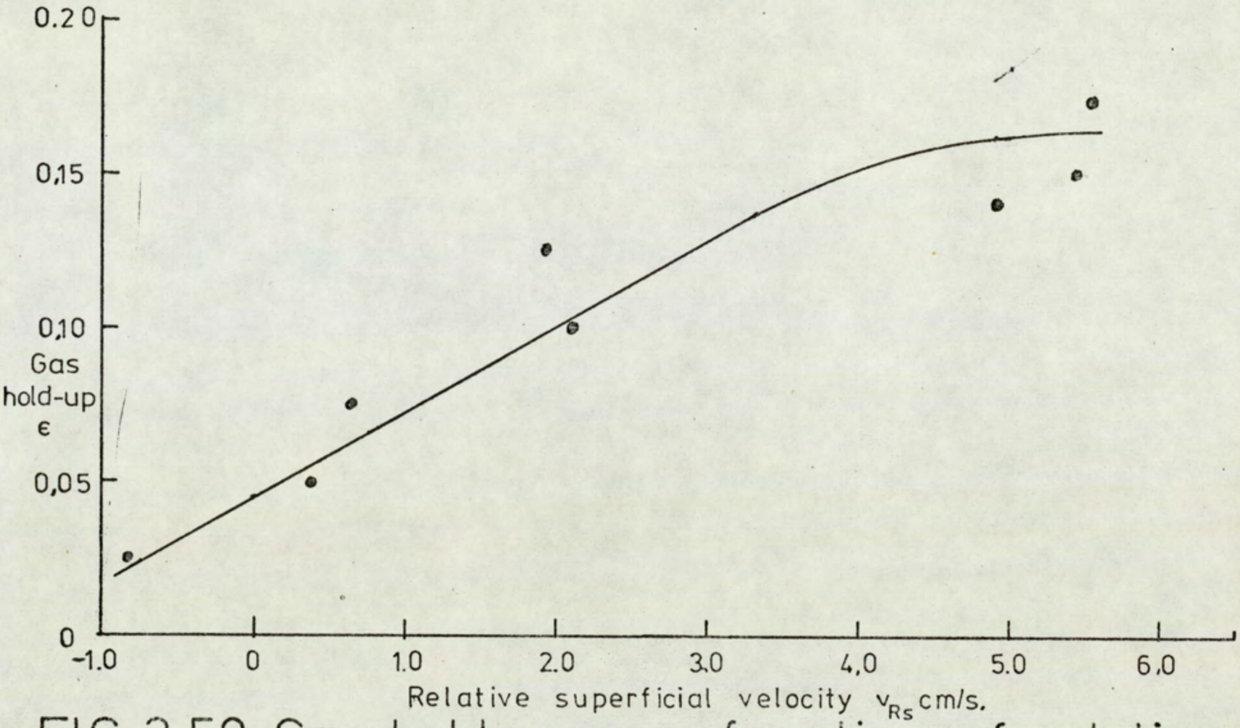

FIG 3.50 Gas hold-up as a function of relative superficial velocity.

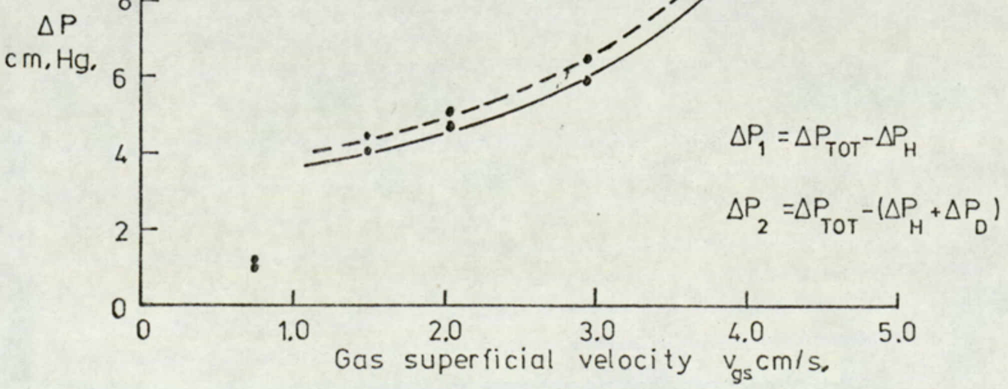

FIG 3.51 Column pressure drops,(12"column).

4. $0 \leqslant v_{gs} \leqslant 4.5$ cm/s

5. $0 \leqslant v_{ls} \leqslant 2.0$ cm/s

6. $0.025 \leqslant \epsilon \leqslant 0.11$

7. $0.126 \leqslant d_b \leqslant 0.171$ cm

For gas hold-ups greater than 0.10, a linear relationship with v_{gs} no longer holds. There is evidence of increased coalescence and a tendency towards slug flow in this region.

Table B.19 lists the values of the pressure-drops derived from the measured total pressure-drop ΔP_{TOT} , the pressure due to the hydrostatic head, ΔP_H , and the pressure-drop across the dry distributor, ΔP_D . These data are represented graphically in Fig. 3.51: only values for the distributor, P_2 , are plotted.

6" and 12" Diameter Columns (Yeast Suspensions)

The results from the experiments with the yeast suspensions are presented in a similar manner to those with water. However, correlation of the data along the same lines has not been possible, partly because there is need for more data and partly because, as will be seen, the results do not follow the same pattern.

Table B.20 in Appendix B shows values of the gas superficial velocities for various gas hold-ups and liquid superficial velocities for both 5% and 10% yeast suspensions when operating with the 6" column. These data are presented graphically in Fig. 3.52. Table B.21 and Fig. 3.53 show similar results obtained with the 12" diameter column.

As can be seen from Figs. 3.52 and 3.53, the liquid superficial velocity has the opposite effect in the two columns. In the 6" column increasing the liquid velocity increases the hold-up for a given gas superficial velocity, whilst in the 12" column the gas hold-up drops for an increase in liquid superficial velocity for a given gas flow-rate.

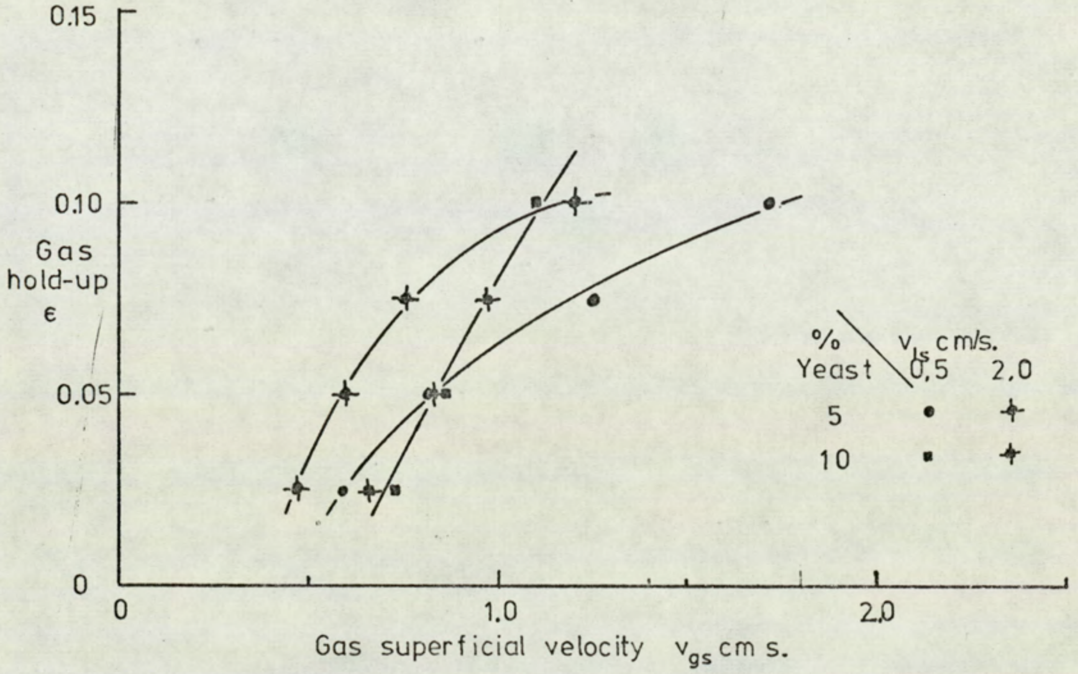

FIG 3.52 Gas hold-up, 6" column, 5 and 10% yeast suspensions.

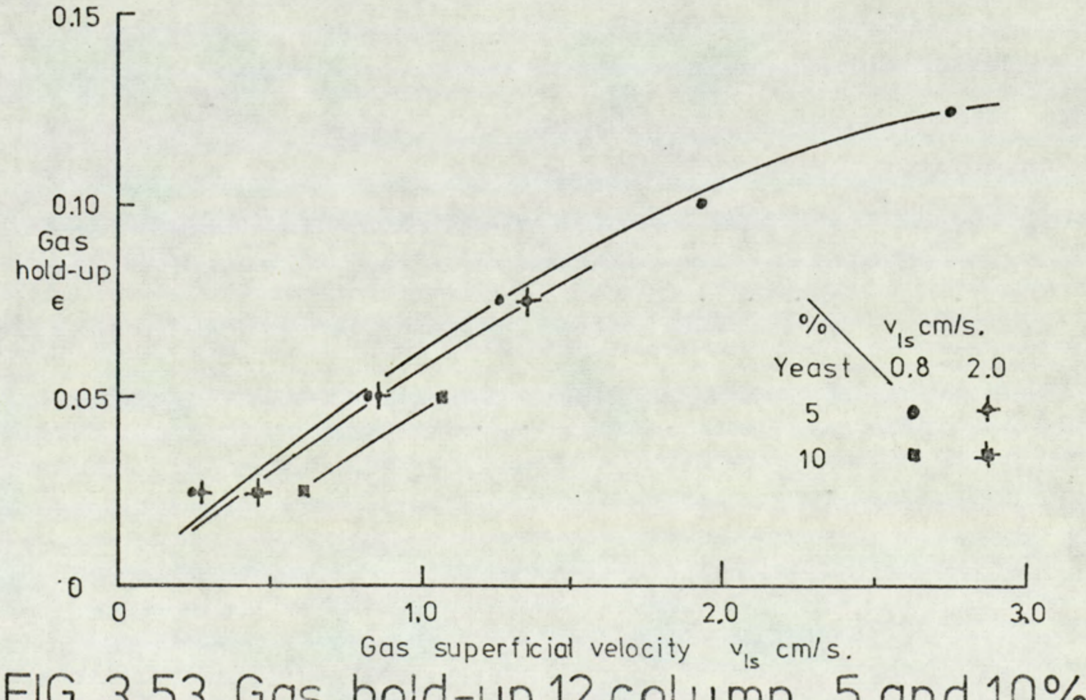

FIG 3.53 Gas hold-up, 12 column, 5 and 10% yeast suspensions.

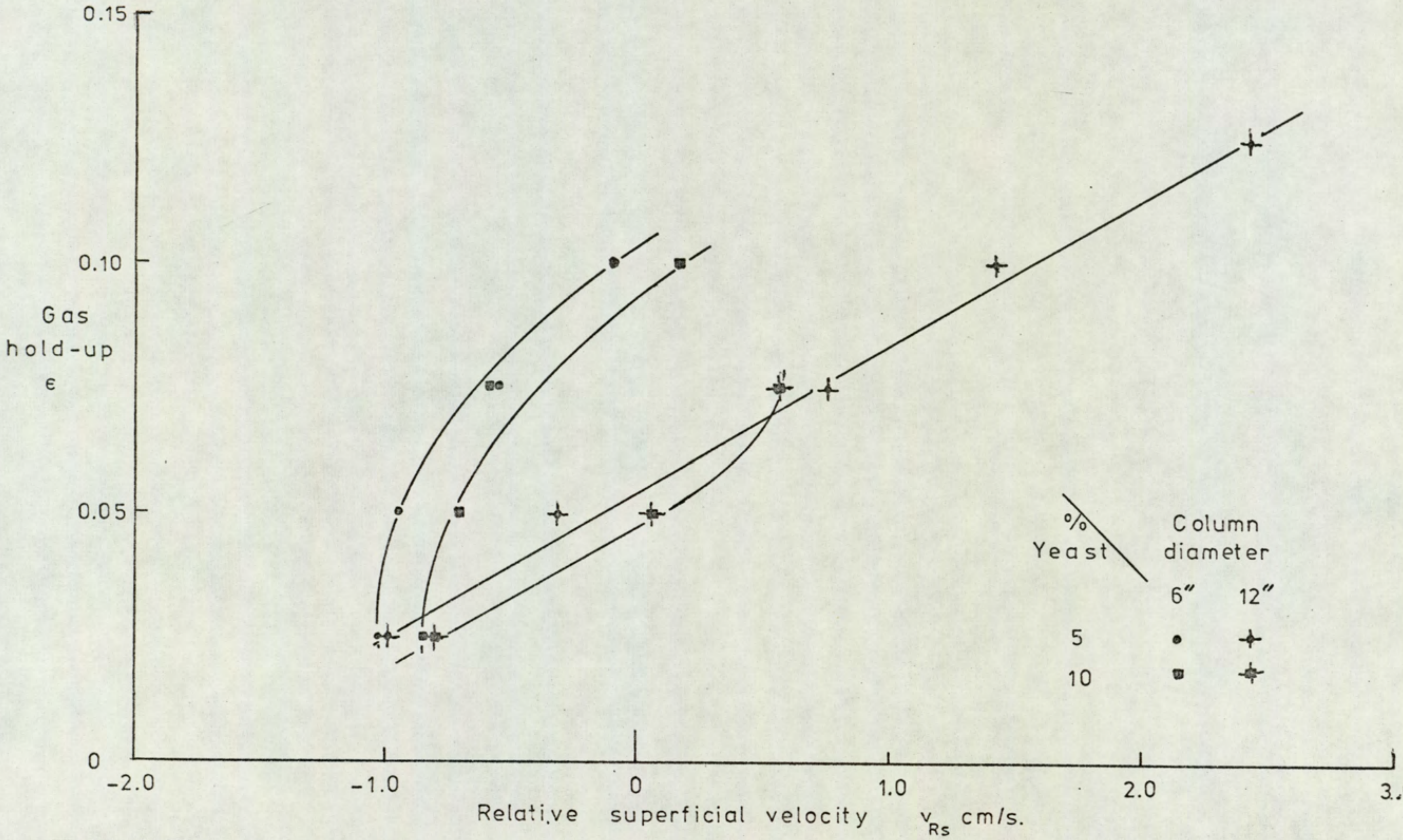

FIG 3.54 Gas hold-up as a function of relative superficial velocity, (6″ and 12″ columns, 5 and 10% yeast suspensions).

In Tables B.22 (6" column) and B.23 (12" column) the gas flow-rate and liquid velocity are expressed in terms of the relative superficial velocity, v_{Rs}. The data from both these tables are plotted in Fig. 3.54.

Finally, the pressure-drops, both measured and derived, are listed in Table B.24 and shown graphically in Figs. 3.55 (6" column) and 3.56 (12" column). Both the 12" and the 6" diameter columns show similar shaped curves for the derived pressure-drops as a function of superficial gas velocity. In both cases the pressure-drops are less than when operating with water as the liquid-phase.

3.3.5 QUALITATIVE ASSESSMENTS.

1. 6" Column. Air / 5% W/V Yeast.

In general very small bubbles were observed close to the walls and there was considerable foaming. At a gas hold-up of 2.5% there was approximately 30 cm of cellular foam at the top of the column and this increased steadily as the gas hold-up rose until, at a hold-up of greater than 10%, the foam was coming out of the air vent at the top of the column (about 60 cm above the liquid take-off point).

When operating at the higher liquid velocity the amount of foam produced was considerably less. Again very small bubbles were observed near the wall of the column and the liquid-phase appeared to be moving downwards.

2. 6" Column. Air / 10% W/V Yeast.

At low gas and liquid flow-rates there was a negligible amount of foam formed. Again very small bubbles (1 to 3 mm diameter) were observed and there seemed to be no variation in size throughout the column.

At a gas hold-up of 10% a cellular foam was formed that was about 7 to 8 cm deep, and comprised of cells measuring approximately 0.2 cm

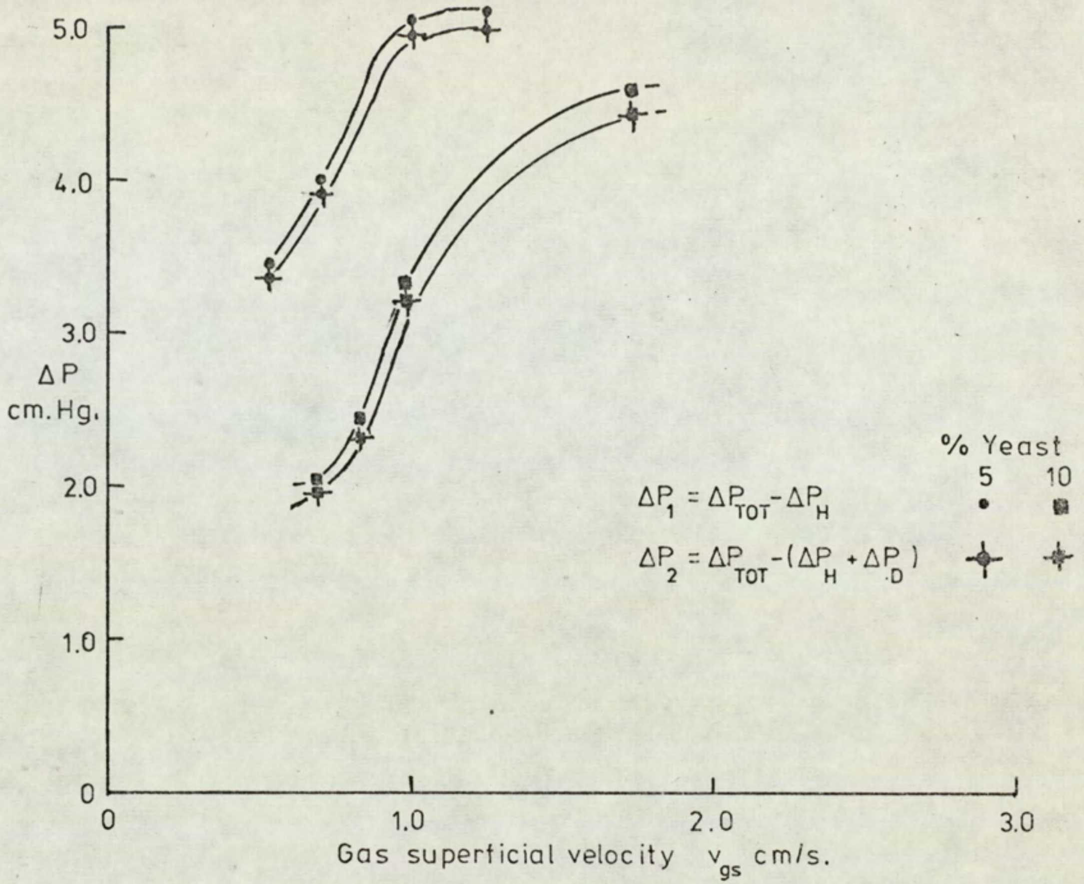

FIG 3.55 Pressure drops, 6" column, 5 & 10% yeast.

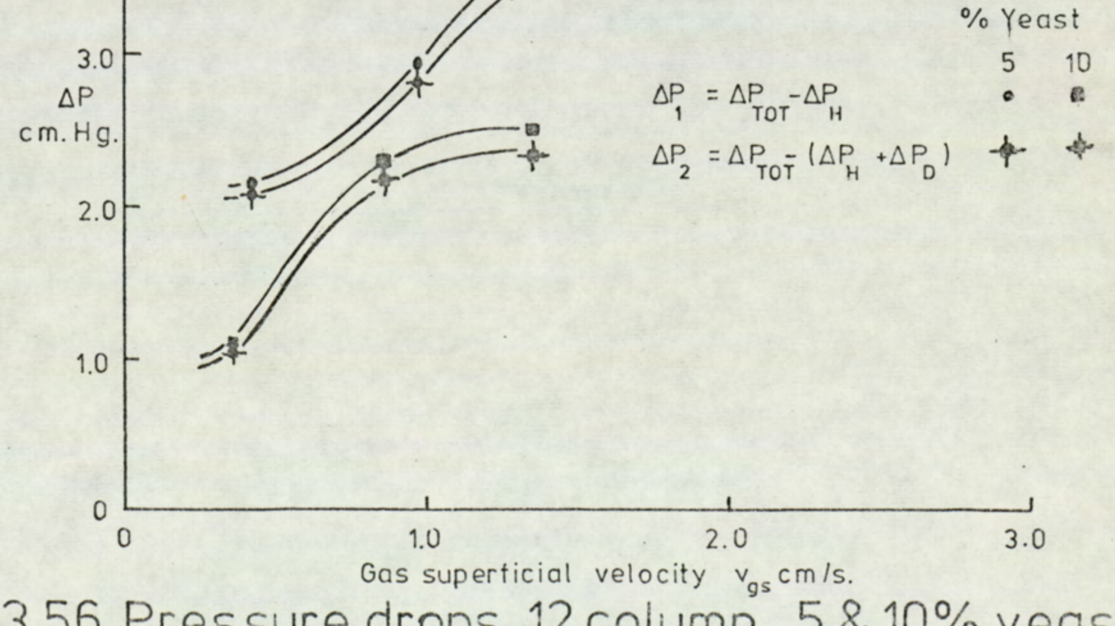

FIG 3.56 Pressure drops, 12 column, 5 & 10% yeast.

across at the liquid surface to about 2 cm across at the upper surface of the foam.

At higher liquid flow-rates the pattern was much the same, although at the lower gas rates the cells of the foam were much smaller (approximately 0.5 to 1.0 mm, and about 2.5 cm deep). The movement of bubbles at the wall of the column seems almost random, although there is a general upward trend.

At a gas hold-up of 10% and a liquid superficial velocity of 2.6 cm/s some slugging appeared to be occurring, although there was no real evidence of this at the bottom of the column. When the hold-up was increased to 14% there was a considerable amount of coalescence taking place and bubbles of about 2 to 3 cm diameter were breaking at the top of the column. In this case there was very little foam and by the movement of the liquid surface at the top of the column there was some slugging taking place.

3. <u>12" Column.</u> <u>Air / 5% W/V Yeast</u>.

At low gas and liquid flow-rates there were no visible bubbles at the walls of the column, but there was approximately 10 cm of foam with 1 to 2 cm cells.

As the gas flow was increased, the column seemed to behave more like an air/water system, apart from the foaming which was now about 20 cm deep but still comprised of 1 to 2 cm cells. The bubbles appear similar to those formed in water at similar gas and liquid flow-rates, except that they seem to be slightly smaller. As the gas hold-up increased, the depth of foam increased and the movement of the bubbles became more turbulent until, at a gas hold-up of about 12.5%, there was a certain amount of slugging occurring. At this value of gas hold-up, the majority of bubbles that could be seen seemed to be about 2 to 4 mm diameter, whilst some appeared to be as large as 1.25 cm. There was about 18 to 20 cm of very mobile foam and the top of the column seemed to be erupting as the larger bubbles broke the surface.

When the liquid velocity was increased there was no visible effect on the bubble sizes, but their movements increased rapidly. At low gas flow-rates there was approximately 15 to 18 cm of foam, which increased to about 45 cm depth as the gas flow-rate increased to give a hold-up of 5%. At this higher hold-up the bubbles seemed to be about 1 to 2 mm diameter, although bubbles up to 1.0 cm diameter were observed.

4. 12" Column. Air / 10% W/V Yeast.

At low gas hold-up (2.5%) and low liquid velocity, the column operated in a similar manner to a fluidised bed, with the bubbles making tracks through the fluid near the walls. As the gas hold-up was increased to 5% a foam, of about 25 cm depth, comprising of approximately 1.0 cm cells, was formed. The bubbles appeared to be 1 to 2 mm diameter at the bottom of the column, increasing to about 3 mm diameter at the top. When the gas hold-up was increased to 7.5%, the general observation was much the same; the only difference was that the foam was rising in peaks, as if some slugging was taking place.

There was little change in the performance of the column when the liquid velocity was increased, in fact the depth of foam decreased to about 2 to 3 cm.

3.3.6 CONCLUSIONS

Pressure Drop

The pressure-drop across a gas bubble column is made-up of the pressure-drop across the wet porous plate and the pressure-drop due to the hydrostatic head. The pressure-drop across the dry porous plate is proportional to the gas flow-rate, the constant of proportionality being dependent on the diameter of the pores and the percentage free area available for flow. The pressure-drop across the wet distributor is much higher (as much as 5 to 10 times). This phenomenon can be explained by the fact that at low gas-rates only a few of the pores are open to the passage of gas; but as the gas-flow increases, the pressure-drop increases and additional pores open. This reserve of pores results in only a slight increase in pressure-drop as the gas-rate is initially increased. At a gas superficial velocity of approximately 4 to 5 cm/s the majority of the pores are open, resulting in a rapid increase in pressure-drop with a relatively slight increase in v_{gs}.

In the case of yeast suspensions this phenomenon is reversed, with a relatively high pressure-drop occurring up to a gas superficial velocity of about 2 cm/s, after which the pressure-drop tends to level out. This can be explained by the fact that the pores can now be blocked by solid particles as well as by the liquid, which results in the higher initial pressure-drop to remove this blockage. At a gas superficial velocity of approximately 3 cm/s, the majority of the pores are now clear of liquid and solid matter and the pressure-drop levels off. It is to be expected that if v_{gs} increased to about 5 cm/s and greater, then the pressure-drop would start to increase rapidly again, as in the case with water as the liquid-phase.

Bubble-Swarm Velocity

It was found that the rise velocity of a swarm of bubbles (relative to the liquid) was a power function of the gas superficial velocity, although the dependency was not very strong. It would appear from this that the rise velocity in bubble swarms is only slightly less than that of single bubbles and although "hinderance" occurs, its effect is not very great.

The slight difference in the power functions (equations 3.10 and 3.11) for the 6" and 12" column shows that even with a column diameter of 6"

($^{d_c}/d_b > 30$) the wall does have a slight effect.

Gas Hold-up

1. Effect of Distributor Porosity.

In general, it would seem that decreasing the porosity of the distributor, i.e. generating smaller bubbles, causes the gas hold-up to decrease for a corresponding value of gas superficial velocity. This decrease was not always systematic and the effect was greatest at gas hold-ups of 0.10 to 0.15; outside this range the effect of porosity diminished.

2. Effect of Liquid Velocity

In all cases except the 5% yeast suspension in the 6" column, an increase in liquid velocity decreased the gas hold-up at a corresponding value of v_{gs}. This is to be expected, since the gas-phase is being removed from the column more quickly as the liquid-phase velocity increases. It is interesting to note that the effect of liquid superficial velocity is additive in the case of air/water systems in both the columns and also in the case of the yeast suspensions. This effect appears to be reversed in the 6" column when operating with 5% yeast suspension.

3. Effect of Column Diameter.

It was found that a higher gas superficial velocity was required to give the same gas hold-up at values of $v_{gs} > 3$ cm/s. In fact the hold-up in the 12" column levelled out at a value of ~ 0.15 at values of $v_{gs} > 7.0$ cm/s, when operating with air/water systems. This effect was also noted, though not so strongly, when operating with air/yeast suspensions.

4. Effect of Liquid Properties.

The hold-up measurements taken with the yeast suspensions show extremely complex behaviour in the 6" column. In fact it would appear that a finite value of v_{gs} (~ 0.5 cm/s) is required before any measurable hold-up is encountered.

At present the phenomenon is unexplained but it is most likely that it is a function of the relationship between the solid particles and the liquid. It is thought that wall effects may be much greater when operating with suspensions.

5. Effect of Gas Superficial Velocity.

In general, increasing gas superficial velocity increases the gas hold-up to a greater or lesser extent, dependent upon the other factors described.

In most cases, air/water (6" and 12" columns), air/5% and 10% yeast (12" column) and air/10% yeast (6" column) gas hold-up increases linearly with gas superficial velocity, up to the following values of ϵ and v_{gs}.

Air/water (6" column)

$$\epsilon > 0.20 \qquad v_{gs} > 5.5 \text{ cm/s}$$

Air/water (12" column)

$$\epsilon \simeq 0.10 \qquad v_{gs} \simeq 2.5 \text{ cm/s}$$

Air/yeast suspension (6" column)

extremely complex

Air/yeast suspension (12" column)

$$\epsilon \simeq 0.10 \qquad v_{gs} \simeq 2.3 \text{ cm/s}$$

The presence of solid particles and/or the change in physical properties when operating with yeast suspensions causes mugh higher gas hold-ups for corresponding gas flow-rates.

Referring to equation 1.76, values of K can be determined as follow

Air/water (6" column)

$$25 \leqslant K \leqslant 32.5$$

Air/water (12" column)

$$22.5 \leqslant K \leqslant 35.0$$

Air/yeast (12" column)

$$17.5 \leqslant K \leqslant 22.5$$

Slugging appears to take place at much lower values of v_{gs} when operating with microbial systems. No quantitative measures of this were taken however.

Having established the experimental procedure and the effects of the various parameters, it would be advantageous to carry out a more detailed study of gas hold-up in microbial systems in the following way:

1. Measurement of hold-up at positions throughout the columns.
2. Possible study of the systems with flocculent yeast suspensions.
3. Variation of particle dimensions.
4. Wider variations of distributor types and sizes.

4. LIQUID-PHASE MIXING IN TWO-PHASE COLUMNS

4.1. INTRODUCTION.

Having studied gas bubbles singly (Chapter 2) and in swarms (Chapter 3), an investigation of the effect of bubble swarms on mixing in the liquid-phase of bubble columns was carried out.

The equipment used was basically the same as that described in previous chapters. The parameters chosen for study were also similar to those used in Chapter 3.

An initial qualitative study was carried out by injecting dye into the system. This was considered necessary to assess the magnitude of the effects caused by various parameters on mixing. To this end colour cine film was taken during the tests.

Having made a qualitative assessment of the mixing, the apparatus was adapted for the use of a "one-shot" tracer input with two downstream measurement points. The concentration profiles were determined by measuring the conductivity of injected potassium chloride solution. The data were analysed, using the dispersed plug-flow model.

4.2. THEORETICAL ASPECT OF TRACER INJECTION.

The liquid-phase mixing in tubular reactors has received much attention in recent years (see Chapter 1). The most popular methods for handling experimental data have been based on dispersion models. To use the various equations, it is necessary to know the so-called dispersion coefficient for the system. The usual method of determining these is through stimulus-response experiments.

There are several methods of introducing the tracer into the system, viz. as a pulse, step-change or sinusoidal signal. Of these, the pulse or delta-function input is probably the easiest to handle, from the view-point of analysis, although the injection of a perfect delta-function input is impossible in practice. However, this difficulty can be overcome as is shown later. The step-change or sinusoidal input is rather awkward to handle and is equally difficult to introduce into the system.

Levenspiel and Smith[106] have shown that the variance of a measured concentration curve, resulting from injection of a pulse of tracer across a plane in a flow-system, can be used to measure the dispersion coefficients. For a perfect delta-function input and a double-infinite system (see Fig. 4.1a) they showed that

$$\sigma^2 = \frac{2}{Pe} + \frac{8}{Pe^2} \qquad 4.1$$

Where σ^2 is the variance of the residence time distribution curve and Pe is the Peclet Number. By definition:

$$Pe = \frac{vl_m}{D_l}$$

where v is the mean velocity in the measuring section in an axial direction, l_m is the length of the measuring section and D_l is the axial dispersion coefficient. Van der Laan[112] extended this treatment to finite vessels (see Fig. 4.1b) using the boundary conditions discussed by Wehner and Wilhelm[113]. Now a perfect delta-function is impossible to achieve in practice, but Aris[114] and Bischoff[115] showed that this restriction could be removed (see Fig. 4.1c), if response measurements were made at two points in the system. Bischoff and Levenspiel[116] have considered the case shown in Fig. 4.1d as well as the three previous ones; these cover all situations in which measurements are made inside the vessel.

By solving the boundary-value problem for the three system sections (viz. entry, measuring and exit) using the equation:

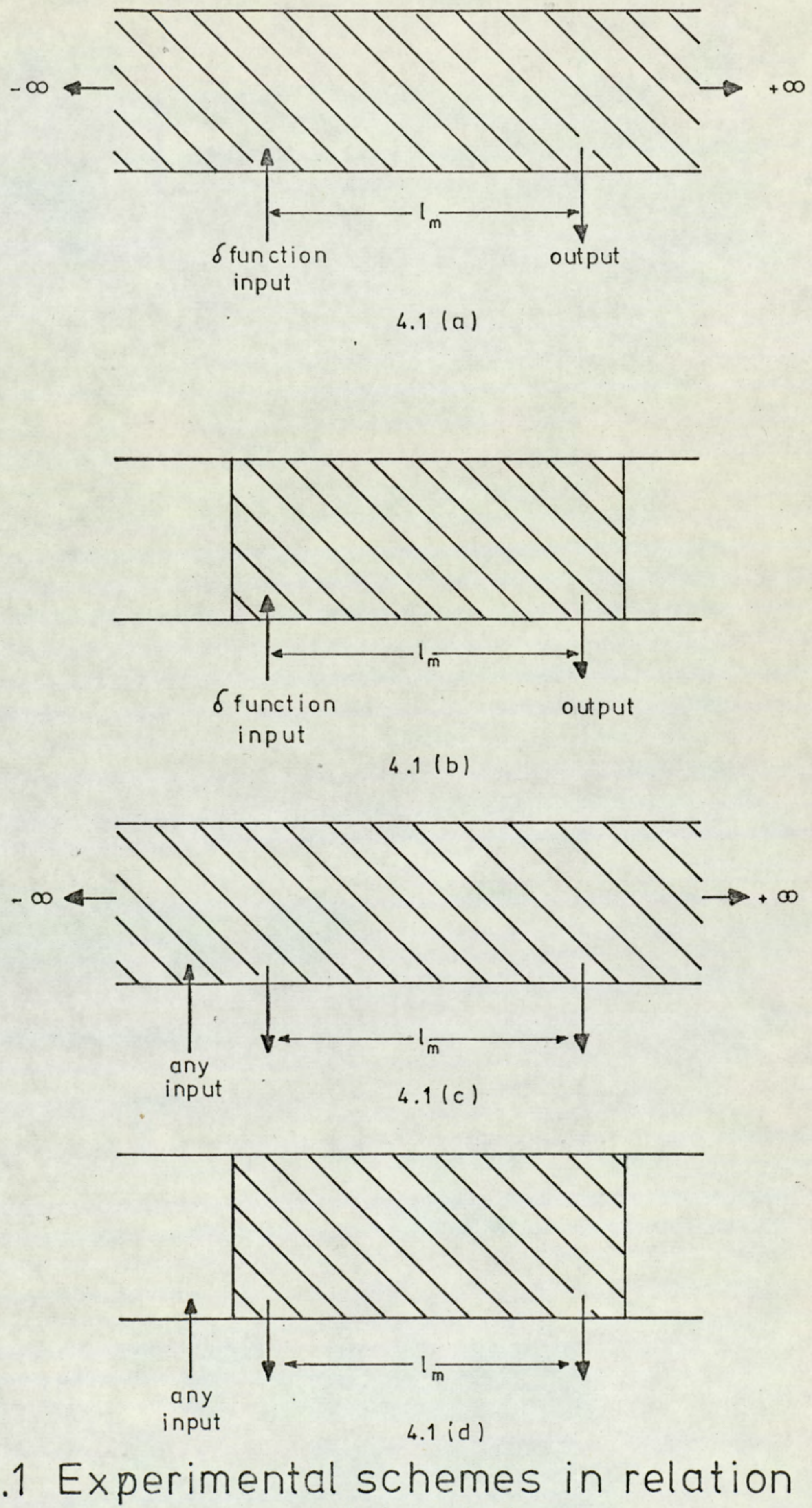

FIG 4.1 Experimental schemes in relation to axial mixing.

$$\frac{\partial c}{\partial t} + v\,\frac{\partial c}{\partial l} = D_l\,\frac{\partial^2 c}{\partial l^2} + S + r_c \qquad 4.2$$

where C is the concentration, l is the axial distance from the injection point, t is time, S and r_c are the source and reaction terms; expressions of the following type are obtained:

$$\Delta\sigma^2 = \sigma_2^2 - \sigma_1^2$$

$$= \frac{2}{Pe} + \frac{1}{Pe^2}\left[f\,(Pe_{entry}\,,\; Pe_{exit}\,,\; Pe) \right] \qquad 4.3$$

where σ_1^2 and σ_2^2 are the variances measured at the two output points and Pe_{entry} and Pe_{exit} are the Peclet Numbers measured immediately before and immediately after the measuring section. When the two outputs are within the measuring section, equation 4.3 reduces to:

$$\Delta\sigma^2 = \sigma_2^2 - \sigma_1^2 = \frac{2}{Pe} \qquad 4.4$$

$$\text{since} \qquad Pe_{entry} = Pe_{exit} = Pe \qquad 4.5$$

The only problem that now remains is to determine the error in neglecting the second term of equation 4.3 for the case of a real system with end-effects. Bischoff and Levenspiel[116] have computed such errors and have produced working data for their estimation.

4.3. QUALITATIVE STUDIES.

The preliminary studies of mixing were divided into two parts, viz. visual and filmed observations, and were carried out to determine the approximate magnitude of the liquid-phase mixing that occurs in a bubble-column.

4.3.1 VISUAL OBSERVATIONS

Two parameters only were investigated in this section of the work using the 6" column and two tracer-injection positions. The liquid superficial velocity was set at either 0.5 or 2.6 cm/s and the fractional gas hold-up was either 0 or 0.025. In each case the tracer was injected into the liquid-phase just before it entered the column.

Two further experiments were then carried out, using the same liquid velocities and a gas hold-up fraction of 0.025, but with the tracer injected at the top of the column.

The tracer material used was saturated $KMnO_4$ solution. The volume of tracer injected was 50 cm^3.

The results of these investigations are set out below.

Table 4.1 $v_{1s} = 0.5$ cm/s $\epsilon = 0$

mean residence time 8.1 min.

time t (min)	Observations
0	Tracer injected with liquid stream.
3.0	Tracer reaches height of 213 cm.
3.5	Tracer begins to flow out of column (height of 244 cm.) and is starting to clear at base of column.
9.0	Column clear to height of 213 cm.
10.0	Column clear of tracer material.

Table 4.2 $v_{1s} = 2.6$ cm/s $\epsilon = 0$

mean residence time 1.6 min.

time t (min)	Observations
0	Tracer injected with liquid stream.
1.5	Tracer reaches height of 213 cm. and the bottom 15 cm. of the column is clear.
5.0	Column clear of all tracer material.

In both these cases the tracer-front appeared to be quite flat, except close to the walls of the column. This suggests that the radial mixing is complete and that a modified plug-flow model could be used to define the system.

Table 4.3 $v_{ls} = 0.5$ cm/s $\epsilon = 0.025$

mean residence time 8.1 min.

time t (min)	Observations
0	Tracer injected with liquid stream.
0.5	Tracer reaches top of column (244 cm)
10.0	Tracer becoming very diffuse at the bottom of the column.
13.0	Bottom 15 cm. of the column is clear.
19.0	Column clear of all tracer material.

Table 4.4 $v_{ls} = 2.6$ cm/s $\epsilon = 0.025$

mean residence time 1.6 min.

time t (min)	Observations
0	Tracer injected with liquid stream.
0.2	Tracer reaches top of column (244 cm)
4.5	Column clear to height of 15 cm.
8.0	Column clear of all tracer material.

As can be seen by either increasing the liquid-flow or by introducing air, or both, the mixing occuring in the column is substantially increased.

Two further experiments were carried out by injecting the tracer into the top of the column. The results were as follow:-

Table 4.5 $v_{ls} = 0.5$ cm/s $\epsilon = 0.025$

mean residence time 8.1 min.

time t (min)	Observations
0	Tracer material added to top of column.
2.0	Tracer reaches the base of column.
2.0	Tracer material behaves as in Table 4.3.

Table 4.6 $v_{ls} = 2.6$ cm/s $\epsilon = 0.025$

mean residence time 1.6 min.

time t (min)	Observations
0	Tracer added to top of column.
0.2	Tracer reaches depth of 180 cm.
0.2	Tracer material behaves as in Table 4.4.

As can be seen from Table 4.6, the higher liquid velocity prevented the tracer material from reaching the bottom of the column, but the general trends are as before.

4.3.2 FILMED OBSERVATIONS

For these tests the tracer material was injected into the top of the column and the camera was panned downwards to follow the tracer movement. The film used was Kodak Echtachrome E.F. (A.S.A. 125). The column was illuminated by reflection off a strip of white card, about 60 cm. wide by 200 cm. long, placed behind the column. The light from four 500 watt. photo-flood lamps was directed onto the card. The conditions under which the film was taken are shown in Table 4.7, and the results obtained from analysing the films are given in Tables 4.8 to 4.13 inclusive.

Table 4.7 Flow Condition for Cine Filmwork.

Run No.	Gas Hold-up Fraction ϵ	Liquid Superficial Velocity cm/s	Film Speed f.p.s.
1	0.075	0.5	64
2	0.075	"	64
3	0.075	"	32
4	0.100	"	25
5	0.100	"	25
6	0.100	"	64

The height datum line in the following tables is the bottom of the column, i.e. the gas distributor.

Table 4.8 Runs 1. $v_{ls} = 0.5$ cm/s $\epsilon = 0.075$

Film Speed = 64 f.p.s. Mean residence time 8.1 min.

time t sec.	Observations
t = 0	Tracer occupying top 15 cm. of column. (ht.= 228 cm)
t = 0.5	Tracer reaches top probe (ht. = 213 cm.)
t = 1.9	Tracer reaches ht. of 196 cm.
t > 1.9	Tracer front very diffuse and cannot be defined.

Table 4.9 Run 2. $v_{ls} = 0.5$ cm/s $\epsilon = 0.075$

Film Speed = 64 f.p.s. Mean residence time 8.1 min.

time t sec.	Observations
$t = 0$	Tracer occupying top 15 cm. of column (ht. = 228 cm)
$t = 0.6$	Tracer reaches top probe (ht. = 213 cm.)
$t > 0.6$	Tracer front very diffuse.

Table 4.10 Run 3. $v_{ls} = 0.5$ cm/s $\epsilon = 0.075$

Film Speed = 32 f.p.s. Mean residence time 8.1 min.

time t sec.	Observations
$t = 0$	Tracer occupying top 10 cm. of column (ht. = 233 cm)
$t = 1.1$	Tracer reaches top probe (ht. 213 cm.)
$t = 12.8$	Tracer reaches bottom probe (ht. = 15 cm.)

Table 4.11 Run 4. $v_{ls} = 0.5$ cm/s $\epsilon = 0.10$

Film Speed = 25 f.p.s. Mean residence time 8.1 min.

time t sec.	Observations
$t = 0$	Tracer occupying top 15 cm. of column (ht. = 228 cm)
$t = 1.6$	Tracer reaches top probe (ht. = 213 cm.)
$t = 10.5$	Tracer reaches bottom probe (ht. = 15 cm.)

Table 4.12 Run 5. $v_{1s} = 0.5$ cm/s $\epsilon = 0.10$

Film Speed 25 f.p.s. Mean residence time 8.1 min.

time t sec.	Observations
t = 0	Tracer occupying top 15 cm. of column (ht. = 228 cm)
t = 1.2	Tracer reaches top probe (ht. = 213 cm.)
t = 9.8	Tracer reaches bottom probe (ht. = 15 cm.)

Table 4.13 Run 6. $v_{1s} = 0.5$ cm/s $\epsilon = 0.10$

Film Speed 64 f.p.s. Mean residence time 8.1 min.

time t sec.	Observations
t = 0	Tracer occupying top 10 cm. of column (ht. = 234 cm)
t = 0.5	Tracer reaches top probe (ht. = 213 cm.)
t = 8.8	Tracer reaches bottom probe (ht. = 15 cm.)

When these results are studied in conjunction with the observed results, it can be seen that an increase in hold-up increases the mixing in the column quite considerably. There is some spread in the results but this is to be expected, since a) the time intervals are quite small and b) the tracer front was often difficult to define. In general the coloured/clear liquid interface was fairly flat across the diameter of the column throughout its downward movement. The only part that wasnot was around the periphery of the column. This could have been due to wall effects, or to some effect of filming through the curved glass of the column.

4.4. QUANTITATIVE STUDIES.

4.4.1 EXPERIMENTAL EQUIPMENT

The basic apparatus consisting of the two columns, storage tanks, liquid recirculation systems and gas-distributor systems, was as described in 3.3.2. Additional equipment was added for the injection of the tracer and the measurement of the tracer concentration.

Tracer Injection System

From the preliminary investigations (see 4.3.1 and 4.3.2) it was decided to introduce the tracer into the liquid/tracer-stream just before entry to the column. A short section of the liquid inlet-line was removed and replaced with an equal, $^{5}/8''$ (1.6 cm.) dia., Q.V.F. 'T'-piece: Fig. 4.2 shows the injection arrangement for the 6" column. The same insert was made on the 12" column, using an equal $1^{1}/2''$ (3.8 cm.) 'T'-piece. The dimensions of these injection sections were chosen so that the liquid-flow was highly turbulent, thereby ensuring that the tracer was well mixed. With a superficial liquid velocity in the columns of 1 cm/s, the Reynolds Numbers for the inlet sections were 14,700 and 19,400 for the 6" and 12" column respectively.

The injector itself (see Fig. 4.2) was a 50 ml glass syringe with a stainless-steel plunger fitted with a three-way cock and a piece of copper tubing, $^{1}/4''$ (0.6 cm.) o.d. x 9" (23 cm.) This tubing could pass through a seal in the 'T'-piece and projected into the centre of the liquid-flow area. The lower end of the tube was closed-up slightly to give a hole of approximately $^{1}/8''$ (0.3 cm.) diameter, and was placed at right angles to the main liquid-flow, thus aiding the mixing of the tracer. The purpose of the three-way cock was to enable tracer material to be drawn from the reservoir and injected into the liquid without removing the syringe.

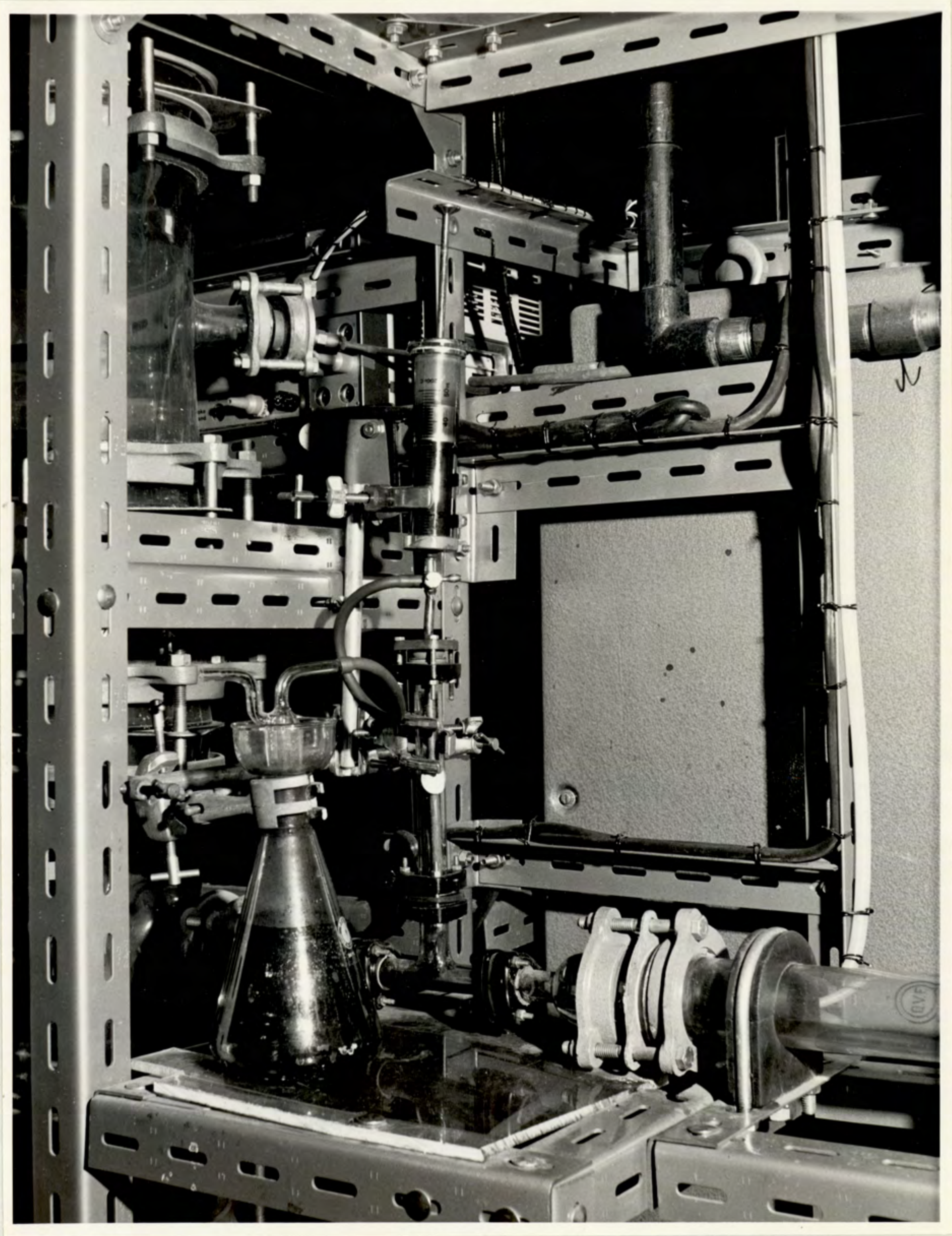

FIG 4.2 Injection system, 6" column.

The tracer used was a 2 N solution of KCl in Birmingham tap-water: usually 25 ml quantities were injected. This concentration and injected volume were chosen after carrying out several experiments aimed at obtaining (1) a rapid injection and (2) sufficient change in conductivity to give a reasonable deflection on the indicator/recorder equipment.

Conductivity Probes

Using the tracer concentration and volume mentioned previously, the range of concentration expected at the measurement points was from 0.0028N to 0.26N depending on liquid flow-rate. It was therefore decided to construct a probe to measure changes in concentration in the range 0.001 - 1.0N KCl.

The area of the electrode can be estimated from

$$a = \frac{l}{\chi R} \qquad 4.6$$

where a is the electrode area (cm^2), R is the probe internal resistance (ohms) and χ is the specific conductivity. The distance l was chosen as 0.5 cm. since it is advantageous to select a high inner probe resistance: this ensures that the voltage drop dependent on capacitance is several times smaller than that dependent on resistance. With the frequency at 50 Hz and R = 1000 ohms, a is found to be 0.354 cm^2.

The electrodes were made of platinum foil, 0.5 mm thick by 0.6 cm. square, with 18 cm. lengths of platinum wire welded to them. The body of the probe (see Fig. 43) was made of $^3/8$" (0.9 cm.) i.d. Perspex tubing and was 6" (15.2 cm.) long. The electrodes themselves were mounted in a slot cut in the end of a piece of $^3/8$" (0.9 cm.) o.d. Perspex rod, 2" (5.1 cm.) long. This rod was drilled in such a way

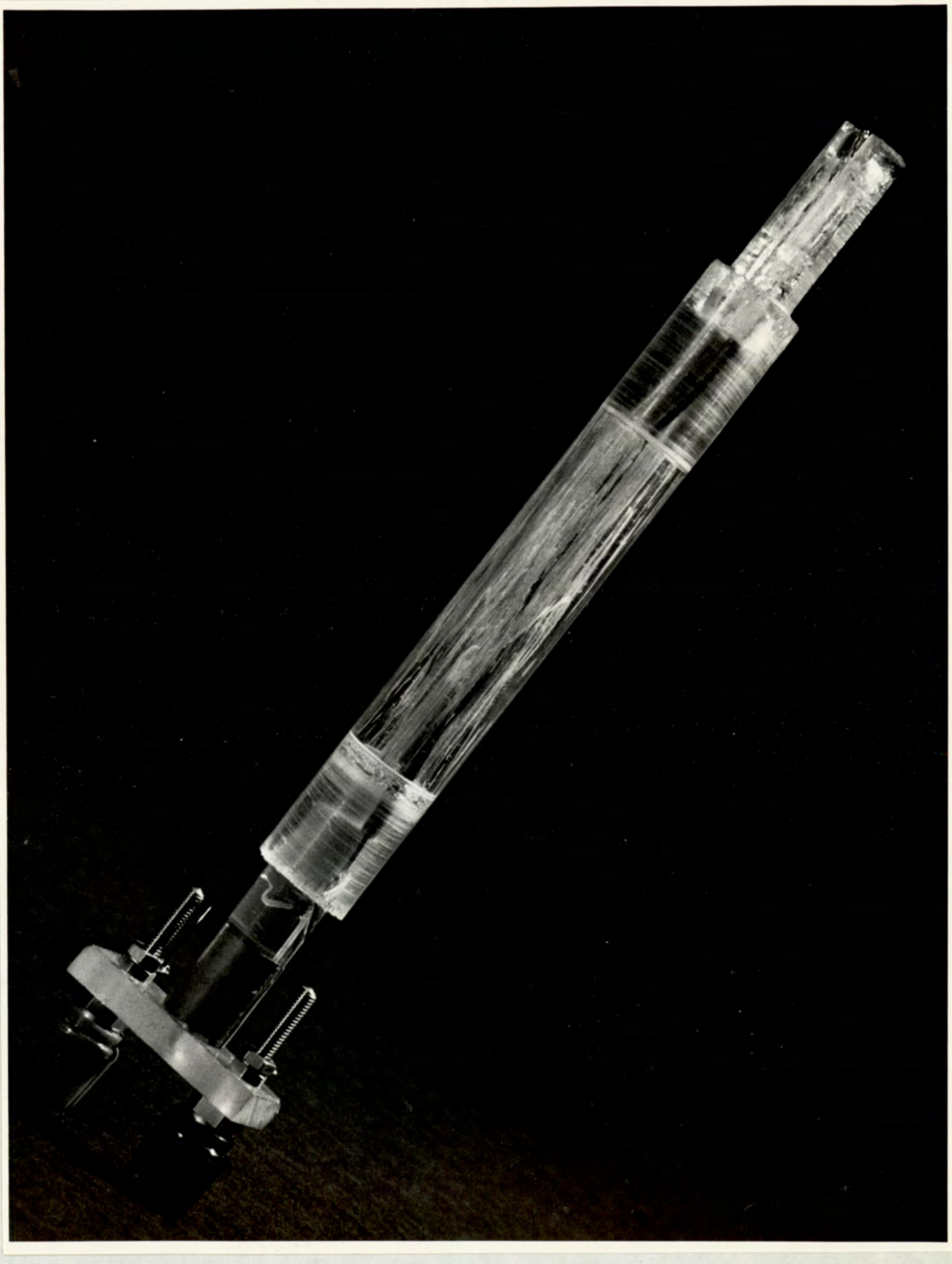

FIG 4.3 Conductivity probe.

that the leads from the electrode could pass into the body of the probe where they were connected to insulated copper-wire.

The slot housing the platinum electrode was cut such that the opposing faces were parallel and 0.6 cm. apart: when the platinum was glued in place, the distance between the faces was 0.5 cm. The other end of the probe body was made in a similar manner, from a $^3/8$" (0.9 cm) solid rod. This was grooved to take the two copper wires which were connected to two post terminals (see Fig. 4.3). All the joints and the holes for the wires were then sealed with Perspex cement to prevent leakage. Two such probes were made, and their cell-constants checked using conductivity measurements in KCl solutions of known concentration. The probes were accurately matched by trimming off small amounts of platinum until the two probes gave identical readings.

The positions of these probes in the two columns are as shown in 3.3.2 and the distances between the probes were 198 cm. and 130 cm. in the 6" and 12" columns respectively.

The electrical link between the probes and the conductivity meter was screened co-axial cable.

Conductivity Measuring System.

The system employed for measuring the tracer concentration at the two probe positions downstream of the tracer injection point consisted of two items of equipment, viz. 1) the conductivity meter and 2) the recorder.

The conductivity meter (see Fig. 4.4) was loaned by the Institute of Microbiology, of the Czechoslovak Academy of Sciences, Prague, where it had been designed and made. The original purpose of the equipment was to measure conductivity at several points during liquid flow over "Turbogrid" trays. The meter was capable of measuring conductivity at 9 points simultaneously and transmitting the output

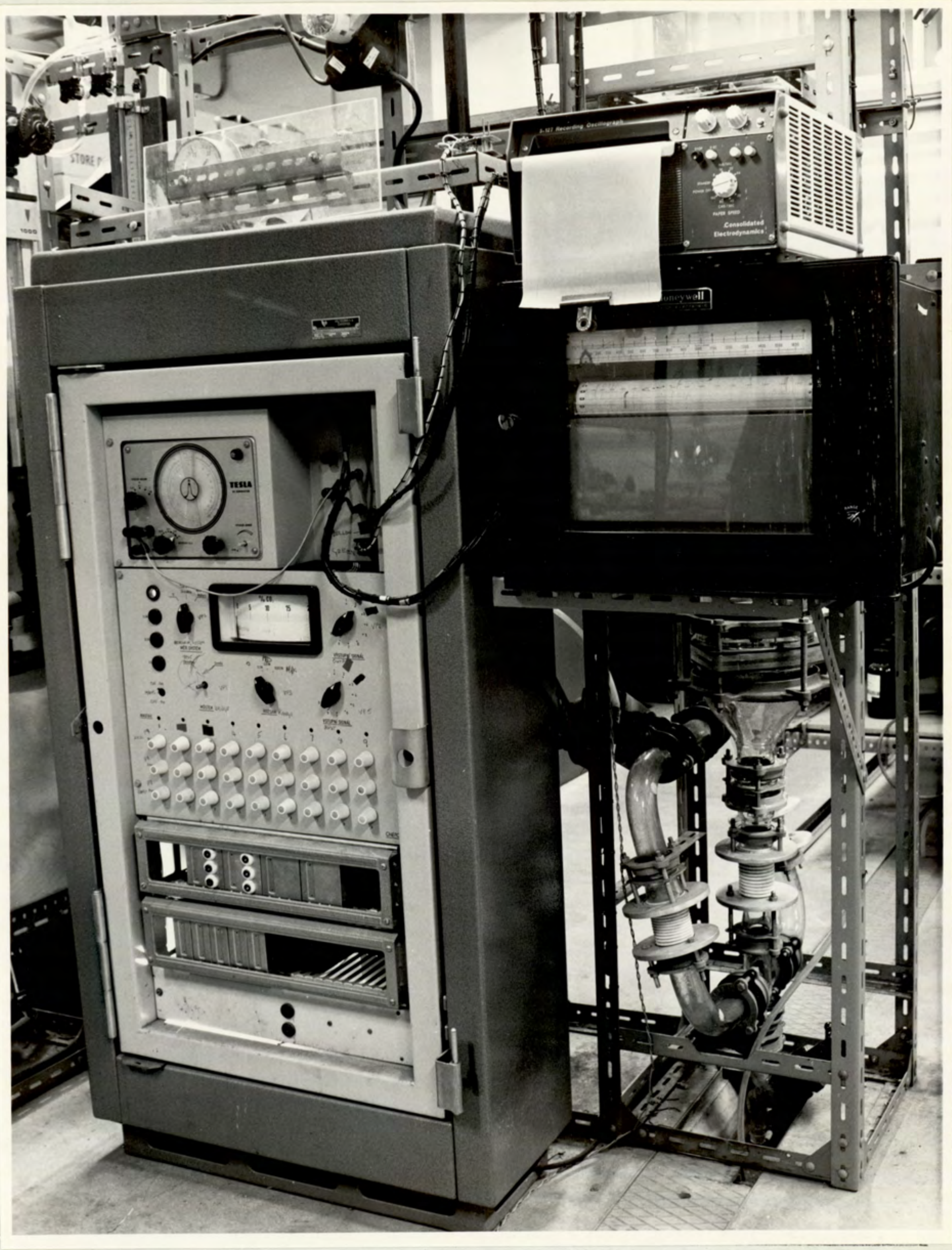

FIG 4.4 Conductivity meter and recorder.

signals to a multipoint recorder.

Each of the 9 measuring elements comprised a probe, a transducer and a measuring bridge. The transducer unit included a D.C. source; a current-source for supplying the measuring bridges, amplifiers and rectifiers; an adjusting circuit for calibration; and a thermostat. The measuring bridge was a standard Wheatstone Bridge for measuring the resistance changes of the probe.

The conductivity meter was temperature compensated with a temperature probe which was inserted into the liquid-phase pipeline. Each of the measuring systems had its own zero, midpoint and range settings, so that they could be individually calibrated.

The Recorder was a Consolidated Electrodynamics * Ultra Violet Recording Oscillograph (see Fig. 4.4). This was linked to the conductivity meter via suitable damping resistors. Two channels of the recorder were used and the polarity of one of the output signals from the conductivity meter was reversed, so that the two recorder-traces had base lines at opposite sides of the chart. This avoided confusion when analysing the "tail" of the traces. The recorder was calibrated using standard KCl solutions: the range of KCl solutions used was 0.001N to 1.0N. From these results a scale was drawn to enable the recorder charts to be read off easily.

4.4.2 EXPERIMENTAL PROCEDURE

The two-phase system was started up as described in Section 3.3.3. The conditions under which the dispersion coefficients were measured are as listed in Tables 3.7 to 3.10 inclusive.

When the system was operating steadily and after the instruments had warmed up (2 hours in the case of the conductivity meter), the

* Consolidated Electrodynamics (Bell & Howell Ltd.), Basingstoke, Hants.

recorder chart-drive was switched on. The recorder flash-timer, set at one-second intervals, was then switched on simultaneously with a stop-clock. After an interval of 10 seconds to allow a base-line to be detected, the tracer was injected into the inlet of the column. The time duration for the actual tracer-injection was approximately 0.75 s. The recorder was left running until the trace reached either the original datum line or the datum level corresponding to the concentration of the KCl when uniformly mixed throughout the whole system. In the latter case the tracer was extended to the original datum line by extrapolation from point-A (see Fig. 4.5) at the same gradient until the original datum line was met at point-B. This was done to enable the data to be handled more conveniently and since only the difference in variance was required and the two "tails" were similar, no error would be introduced by this method.

Several experiments were carried out to determine the extent of the radial mixing. These consisted of moving the probes outwards from the centre of the column during the tests and noting any change in the tracer concentration/time curve. Five repeat experiments, picked at random, were carried out to determine the reproducibility of the system as a whole.

4.4.3 ANALYSIS OF DATA

The form of the chart from the recorder is shown in Fig. 4.5. The concentration C_i was measured at a number of points t_i, the time interval between t_i and t_{i+1} being 0 - 1 min. From these measurements it is possible to calculate the various moments of the concentration/time distribution. Although only the second moment about the mean, i.e. the variance, was required to compute the dispersion coefficients, a computer programme was written to calculate the first four moments and various measures of the form of the distributions.

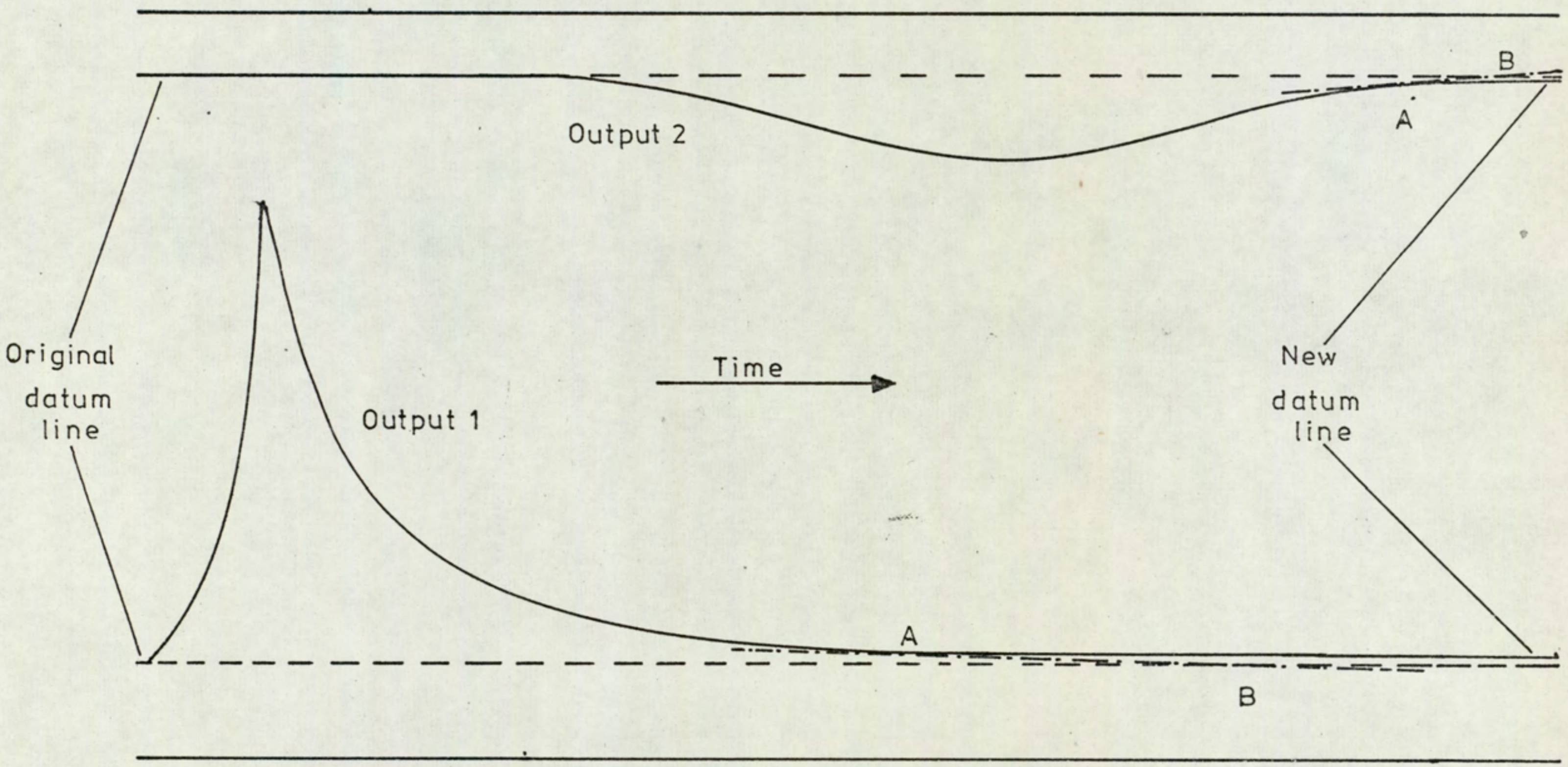

FIG 4.5 Recorder chart detail.

The programme (see Appendix C) is based on the following equations:-

$$C = f(t) \tag{4.7}$$

$$V_1 = \frac{\Sigma t_i C_i}{\Sigma C_i} \tag{4.8}$$

$$V_2 = \frac{\Sigma t_i^2 C_i}{\Sigma C_i} \tag{4.9}$$

$$V_3 = \frac{\Sigma t_i^3 C_i}{\Sigma C_i} \tag{4.10}$$

$$V_4 = \frac{\Sigma t_i^4 C_i}{\Sigma C_i} \tag{4.11}$$

where Σ represents the summation from $t = t_o$, the time of the tracer injection, to $t = t_{100}$, the time for 100% decay of the tracer concentration. The four moments were then calculated as follows:-

$$U_1 = V_1 \tag{4.12}$$

where U_1 is the mean of the distribution;

$$U_2 = V_2 - U_1^2 \tag{4.13}$$

where U_2 is the variance, σ^2 ;

$$U_3 = V_3 - 3V_2 U_1 + 2U_1^3 \tag{4.14}$$

and $$U_4 = V_4 - 4V_3 U_1 + 6V_2 U_1^2 - 3U_1^4 \tag{4.15}$$

where U_3 and U_4 are the third and fourth moments, which were then used in calculating the characteristic shape functions, α and β

where $$\alpha = \frac{U_3}{U_2^{1.5}} \qquad 4.16$$

$$\beta = \frac{U_4}{U_2^{2}} \qquad 4.17$$

These last two factors were calculated only because a computer was used and they could possibly be used if further work was carried out at a later date.

The variance was then expressed in "reduced time" units by dividing U_2 by the square of the mean residence time, t_r, which was obtained from the equation:

$$t_r = \frac{l_m}{60\, v_{1t}} \qquad 4.18$$

where l_m is the distance between the two measurement points (cm) and v_{1t} is the true liquid velocity (cm/s) expressed as a mean axial velocity between the two measuring points.

Knowing the variances of the curves at the two measuring points and assuming that the dispersed plug-flow model for an open vessel can be applied, the Peclet Number, Pe, can be readily computed from:

$$Pe = \frac{2}{\Delta \sigma_t^2} \qquad 4.19$$

where σ_t^2 is in reduced time units and is calculated from

$$\Delta \sigma_t^2 = \frac{\sigma_2^2 - \sigma_1^2}{t_r^2} \qquad 4.20$$

In this equation, σ_1^2 is the variance of the tracer concentration/time distribution from the first measurement point and σ_2^2 is the variance from the second measurement point. Finally, the dispersion coefficient can be extracted from Pe using the relationship:

$$D_l = \frac{v_{lt} \; l_m}{Pe} \qquad 4.20$$

where v_{lt} is the true liquid velocity in cm/s and D_l is in cm^2/s.

4.4.4 EXPERIMENTAL RESULTS.

The calculated moments for both output signals for all the experiments are listed in Tables C.1 to C.9 inclusive in Appendix C. From these the dispersion coefficients were calculated and are shown in Tables 4.14 to 4.17. In Tables 4.14 and 4.15, as can be seen, there seems to be no systematic variation in the dispersion coefficient with respect to varying porosity. Because of this and to aid comparison of the data, the dispersion coefficients measured for each porosity were averaged, and this average value is included in the last but one column of each table. Since the fractional gas hold-up and the gas superficial velocity are so closely related, either may be used for characterising system behaviour. In the graphical representation of the data D_l has been plotted as a function of fractional gas hold-up (see Figs. 4.6 to 4.9). Log-linear axes were used to enable all values of D_l to be included and compared.

The results of the attempted determination of radial mixing (see Sections 4.3.1 and 4.4.2) show that there was no significant concentration gradient radially across the column until the probe was within approximately $^1/_4$" (0.64 cm.) to $^1/_2$" (1.27 cm.) of the column-wall. This shows that, apart from a slight wall-effect, the radial mixing is complete in 6" and 12" columns operating under the conditions used in the experiments.

Table C.10 in Appendix C and Table 4.18 show the calculated moments and the dispersion coefficients for the five repeated experiments.

Table 4.14 Dispersion Coefficients.

6" Column. Liquid-phase water.

ϵ	v_{ls} cm/s	Dispersion Coefficients D_l cm^2/s				Mean v_{gs} cm/s
		Porosity 1	Porosity 2	Porosity 3	Average	
0	0.5				1.17	0
0.025	0.5	3.12			3.12	0.72
0.050	0.5	1.69	1.08	3.72	2.18	1.47
0.075	0.5	1.99			1.99	1.86
0.100	0.5	3.24	1.10	1.37	1.90	2.88
0.200	0.5	3.21	52.38*	1.67	2.44	5.10
0	1.0				4.73	0
0.05	1.0	3.61	7.14	12.87	7.87	1.61
0.10	1.0	13.48	22.91	5.16	13.85	2.93
0.20	1.0	17.43	30.55	3.04	17.01	5.10
0	2.6				12.27	0
0.025	2.6	189.5			189.5	1.06
0.050	2.6	183.5	213.2	144.0	180.2	1.52
0.075	2.6	462.4				2.89
0.100	2.6	54.42		36.9	45.66	2.98

* Slugging occurred

Table 4.15 Dispersion Coefficients.

12" Column. Liquid-phase water.

ϵ	v_{ls} cm/s	Dispersion Coefficients D_l cm^2/s			Mean v_{gs} cm/s
		Porosity 2	Porosity 3	Average	
0	0.8			10.08	0
0.025	0.8	0.75		0.75	0.62
0.050	0.8	1.61	13.85	7.73	1.13
0.075	0.8	2.46		2.46	1.59
0.100	0.8	4.40	6.94	5.67	2.68
0.140	0.8	2.76		2.76	5.24
0.150	0.8		5.09	5.09	6.88
0	1.0			1.40	0
0.05	1.0		7.63	7.63	1.56
0.10	1.0		19.21	19.21	3.04
0.15	1.0		26.78	26.78	7.37
0	2.0			78.79	0
0.025	2.0	218.6		218.60	0.94
0.050	2.0	66.11	134.2	100.10	1.61
0.075	2.0	46.50		46.50	2.45
0.100	2.0	42.54		42.54	3.78
0.135	2.0	196.80		196.80	3.93

Table 4.16 Dispersion Coefficients.

6" Column. 5% and 10% W/V Yeast.

Distributor Porosity 2.

ϵ	v_{ls} cm/s	5% W/V Yeast		10% W/V Yeast	
		D_l cm^2/s	v_{gs} cm/s	D_l cm^2/s	v_{gs} cm/s
0	0.5	1.00	0	3.38	0
0.025	0.5	0.41	0.59	1.91	0.73
0.050	0.5	0.83	0.81	3.14	0.85
0.075	0.5	1.12	1.25	3.70	0.97
0.100	0.5	0.47	1.71	1.79	1.10
0	2.6	217.6	0	21.5	0
0.025	2.6	322.2	0.46	227.4	0.66
0.050	2.6	429.5	0.59	316.4	0.83
0.075	2.6	208.6	0.75	198.7	0.98
0.100	2.6	51.4	1.20	169.6	2.32
0.125	2.6			218.3*	7.49*

* Slugging.

Table 4.17 Dispersion Coefficients.

12" Column. 5% and 10% W/V Yeast.

Distributor Porosity 2.

ϵ	v_{ls} cm/s	5% W/V Yeast		10% W/V Yeast	
		D_l cm^2/s	v_{gs} cm/s	D_l cm^2/s	v_{gs} cm/s
0	0.8	3.26	0		
0.025	0.8	4.40	0.22	22.08	0.28
0.050	0.8	8.95	0.83	20.99	0.85
0.075	0.8	10.46	1.27	14.84	1.35
0.100	0.8	10.38	1.92		
0.125	0.8	8.06	2.74		
0	2.0	9.20	0		
0.025	2.0	116.3	0.61	25.46	0.44
0.050	2.0	74.5	1.06		

Table 4.18 Dispersion Coefficients of repeated experiments.

6" Column. Porosity 1. Air/Water.

ϵ	v_{ls} cm/s	D_l cm^2/s	v_{gs}
0.05	1.0	3.72	1.38
0.20	1.0	17.1	4.86
0.10	2.6	46.1	1.60

12" Column. Porosity 3. Air/Water.

ϵ	v_{ls} cm/s	D_l cm^2/s	v_{gs}
0.10	0.8	4.08	2.64

6" Column. Porosity 2. Air/5% W/V Yeast.

ϵ	v_{ls} cm/s	D_l cm^2/s	v_{gs}
0.075	0.5	1.40	1.25

Table 4.19 Relationship between the two Mean Residence Times.

6" Column. Air/Water. (All Porosities)

ϵ	v_{ls} cm/s.	m.r.t. min.	$\Delta\mu$ min.	$\Delta\mu$/m.r.t.
0	0.5	6.60	4.46	0.68
0.025	0.5	6.44	4.57	0.71
0.050	0.5	6.26	1.46	0.23
0.075	0.5	6.10	2.67	0.44
0.100	0.5	5.94	1.23	0.21
0.200	0.5	5.26	1.21	0.23
0	1.0	3.30	2.36	0.72
0.05	1.0	3.13	1.10	0.35
0.10	1.0	2.97	1.18	0.40
0.20	1.0	2.63	0.76	0.29
0	2.6	1.27	1.88	1.48
0.025	2.6	1.24	1.29	1.04
0.050	2.6	1.21	1.01	0.83
0.075	2.6	1.17	1.76	1.50
0.100	2.6	1.14	0.65	0.57

Table 4.20 Relationship between the two Mean Residence Times.

12" Column. Air/Water. (All porosities)

ϵ	v_{ls} cm/s.	m.r.t. min.	$\Delta\mu$ min.	$\Delta\mu$/m.r.t.
0	0.8	2.71	2.36	0.87
0.025	0.8	2.64	0.58	0.22
0.050	0.8	2.57	0.81	0.32
0.075	0.8	2.51	0.29	0.12
0.100	0.8	2.44	0.54	0.22
0.140	0.8	2.33	0.28	0.12
0.150	0.8	2.30	0.54	0.23
0	1.0	2.17	1.46	0.67
0.05	1.0	2.06	0.46	0.22
0.10	1.0	1.94	0.66	0.34
0.15	1.0	1.85	0.74	0.40
0	2.0	1.09	0.86	0.79
0.025	2.0	1.06	1.11	1.05
0.050	2.0	1.03	0.45	0.44
0.075	2.0	1.00	0.34	0.34
0.100	2.0	0.97	0.34	0.35
0.135	2.0	0.94	0.95	1.01

Table 4.21 Relationship between the two Mean Residence Times.

6" Column. Air/5% W/V Yeast. (Porosity 2)

ϵ	v_{ls} cm/s.	m.r.t. min,	$\Delta \mu$ min.	$\Delta \mu$/m.r.t.
0	0.5	6.60	3.61	0.55
0.025	0.5	6.44	0.96	0.15
0.050	0.5	6.26	1.23	0.20
0.075	0.5	6.10	1.31	0.22
0.100	0.5	5.94	0.87	0.15
0	2.6	1.27	1.93	1.52
0.025	2,6	1.24	1.93	1.56
0.050	2.6	1.21	2.44	2.02
0.075	2.6	1.17	1.46	1.25
0.100	2.6	1.14	0.05	0.04

Table 4.22 Relationship between the two Mean Residence Times.

6" Column. Air/10% W/V Yeast. (Porosity 2)

ϵ	v_{ls} cm/s.	m.r.t. min.	$\Delta\mu$ min.	$\Delta\mu$/m.r.t.
0	0.5	6.60	4.58	0.69
0.025	0.5	6.44	1.89	0.29
0.050	0.5	6.26	1.79	0.29
0.075	0.5	6.10	0.97	0.16
0.100	0.5	5.94	0.57	0.09
0	2.6	1.27	2.63	2.07
0.025	2.6	1.24	1.35	1.09
0.050	2.6	1.21	1.57	1.30
0.075	2.6	1.17	0.97	0.83
0.100	2.6	1.14	1.00	0.88
0.125	2.6	1.11	0.99	0.89

Table 4.23 Relationship between the two Mean Residence Times.

12" Column. Air/5% W/V Yeast. (Porosity 2)

ϵ	v_{ls} cm/s.	m.r.t. min.	$\Delta\mu$ min.	$\Delta\mu$/m.r.t.
0	0.8	2.71	3.13	1.15
0.025	0.8	2.64	0.71	0.27
0.050	0.8	2.57	0.66	0.26
0.075	0.8	2.51	0.87	0.35
0.100	0.8	2.44	0.93	0.38
0.125	0.8	2.37	0.65	0.27
0	2.0	1.09	0.70	0.64
0.025	2.0	1.06	0.92	0.87
0.050	2.0	1.03	0.84	0.82

Table 2.24 Relationship between the two Mean Residence Times.

12" Column. Air/10% W/V Yeast. (Porosity 2)

ϵ	v_{ls} cm/s	m.r.t. min.	$\Delta\mu$ min.	$\Delta\mu$/m.r.t.
0.025	0.8	2.64	1.41	0.53
0.050	0.8	2.57	1.38	0.54
0.075	0.8	2.51	1.03	0.41
0.025	2.0	1.06	0.25	0.24

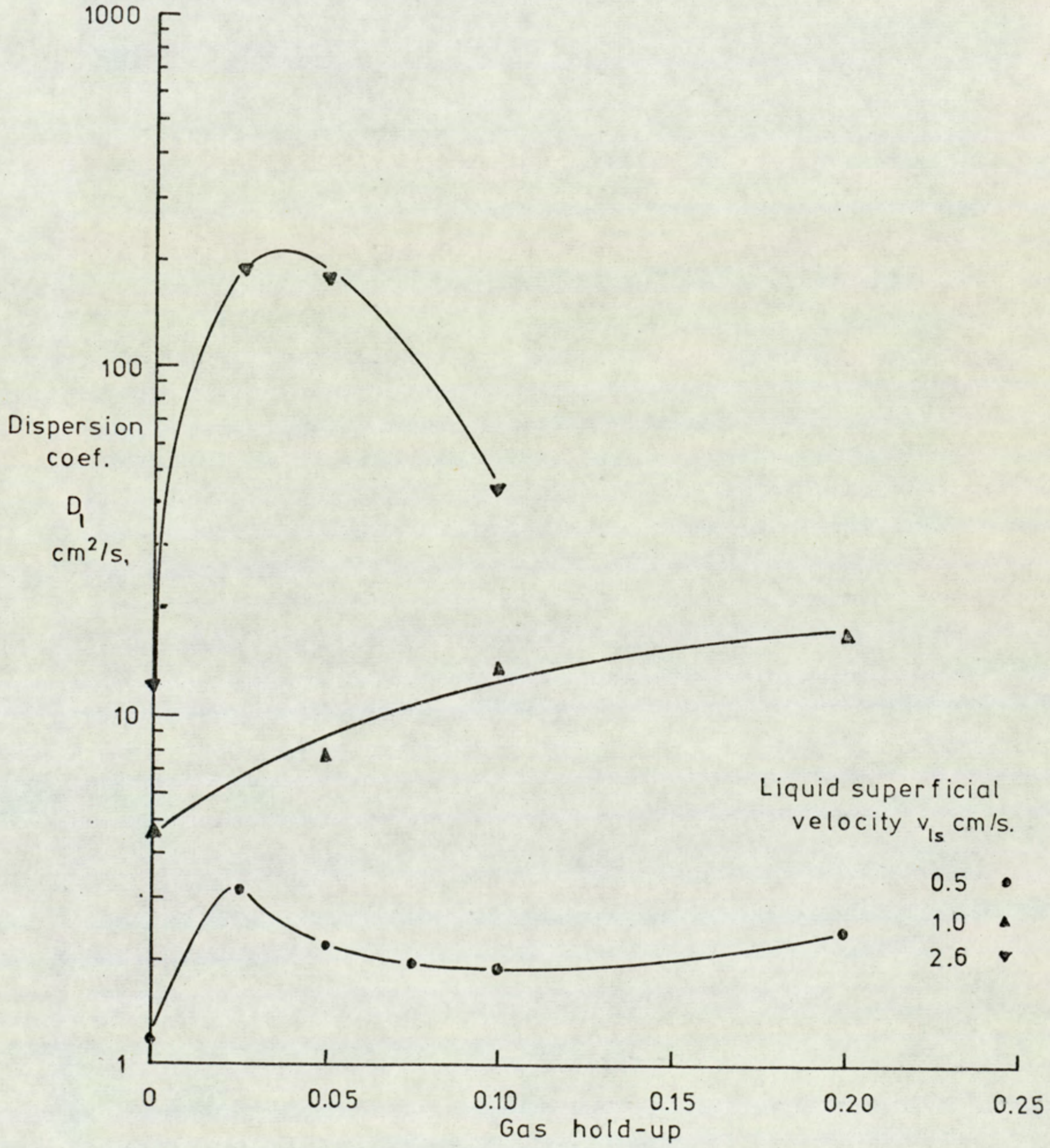

FIG 4.6 Dispersion coefficients, 6" column, air/water.

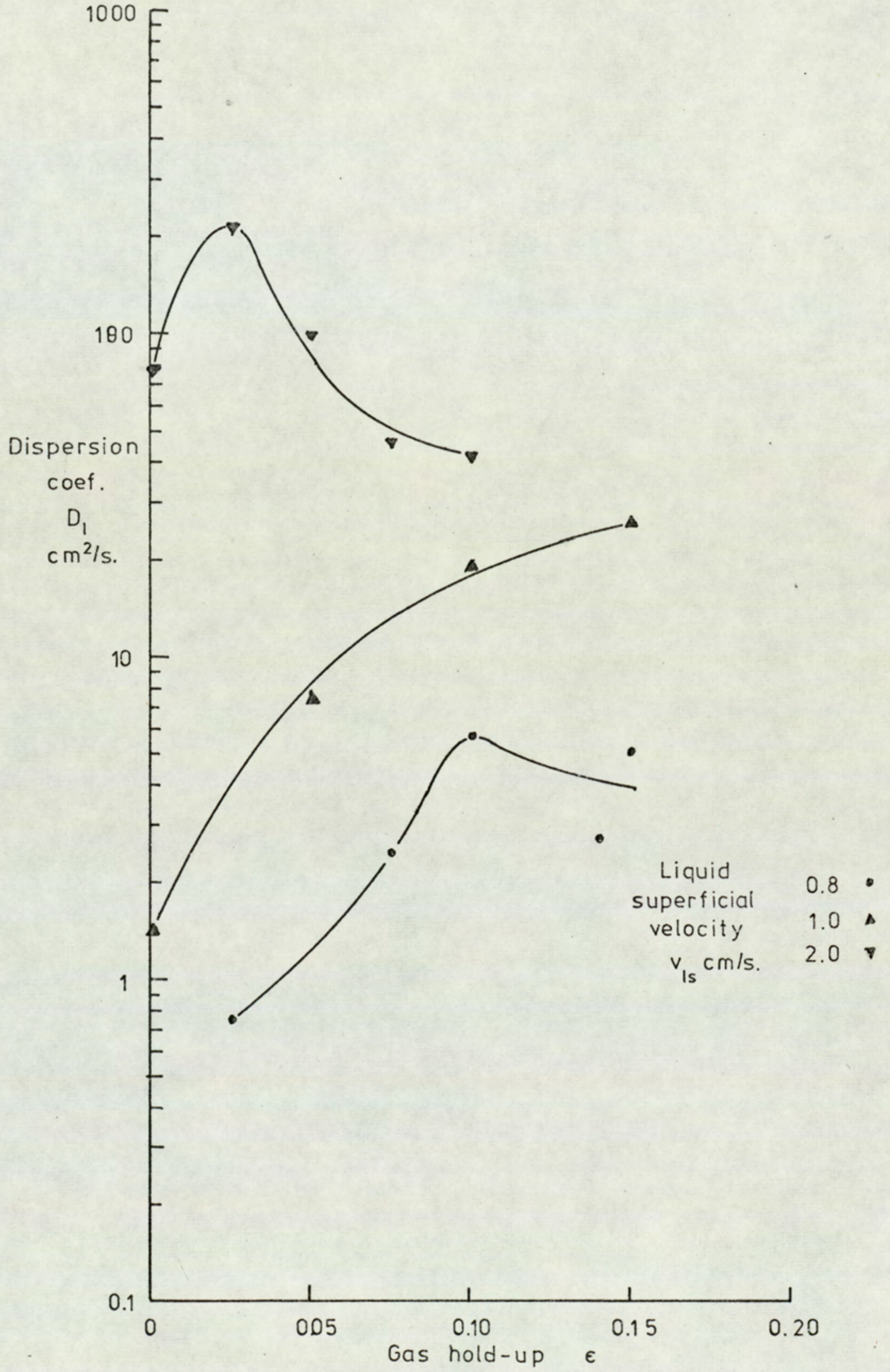

FIG 4.7 Dispersion coefficients, 12″ column, air/water.

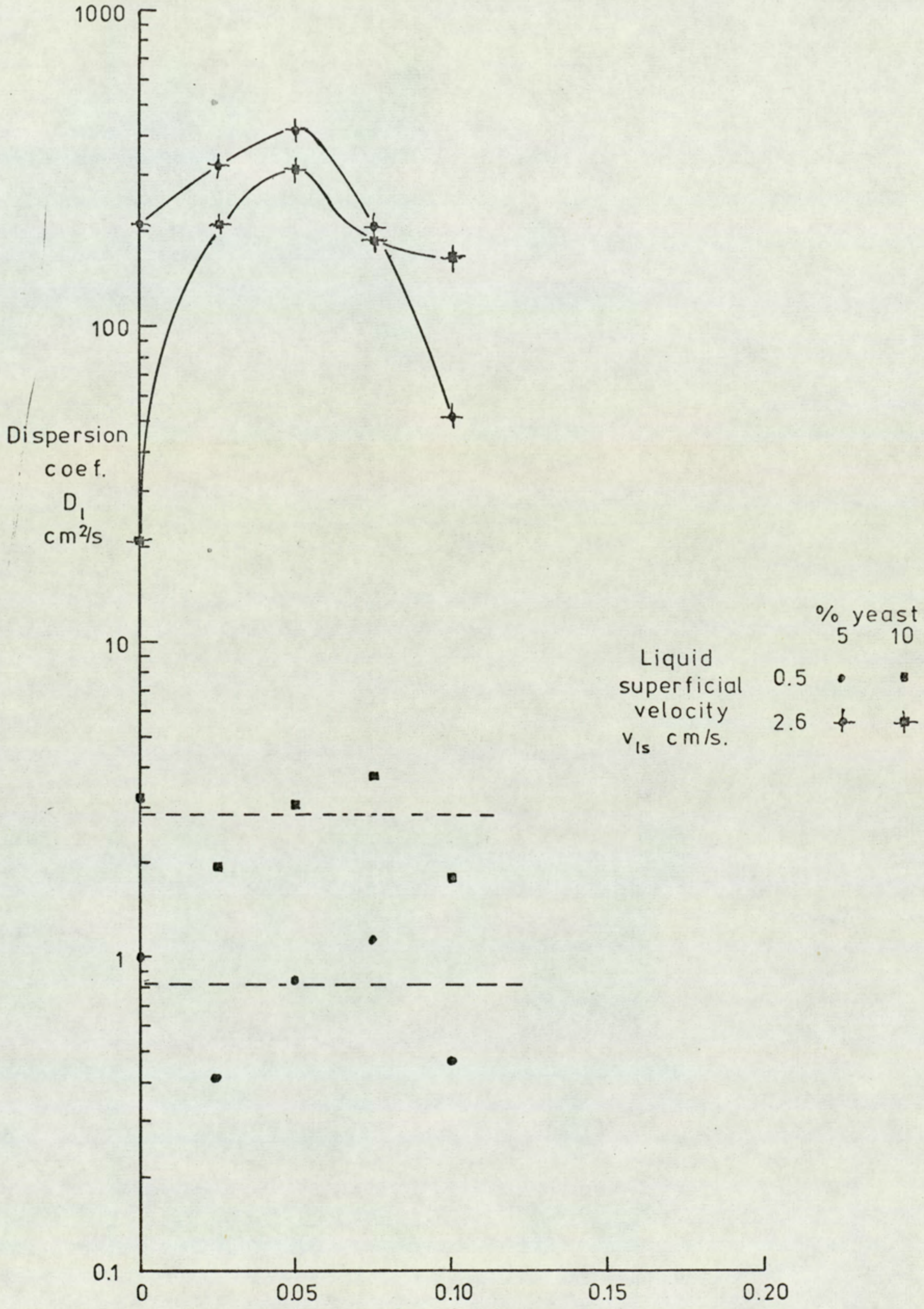

FIG 4.8 Dispersion coefficients, 6" column, air/5 and 10% yeast suspensions.

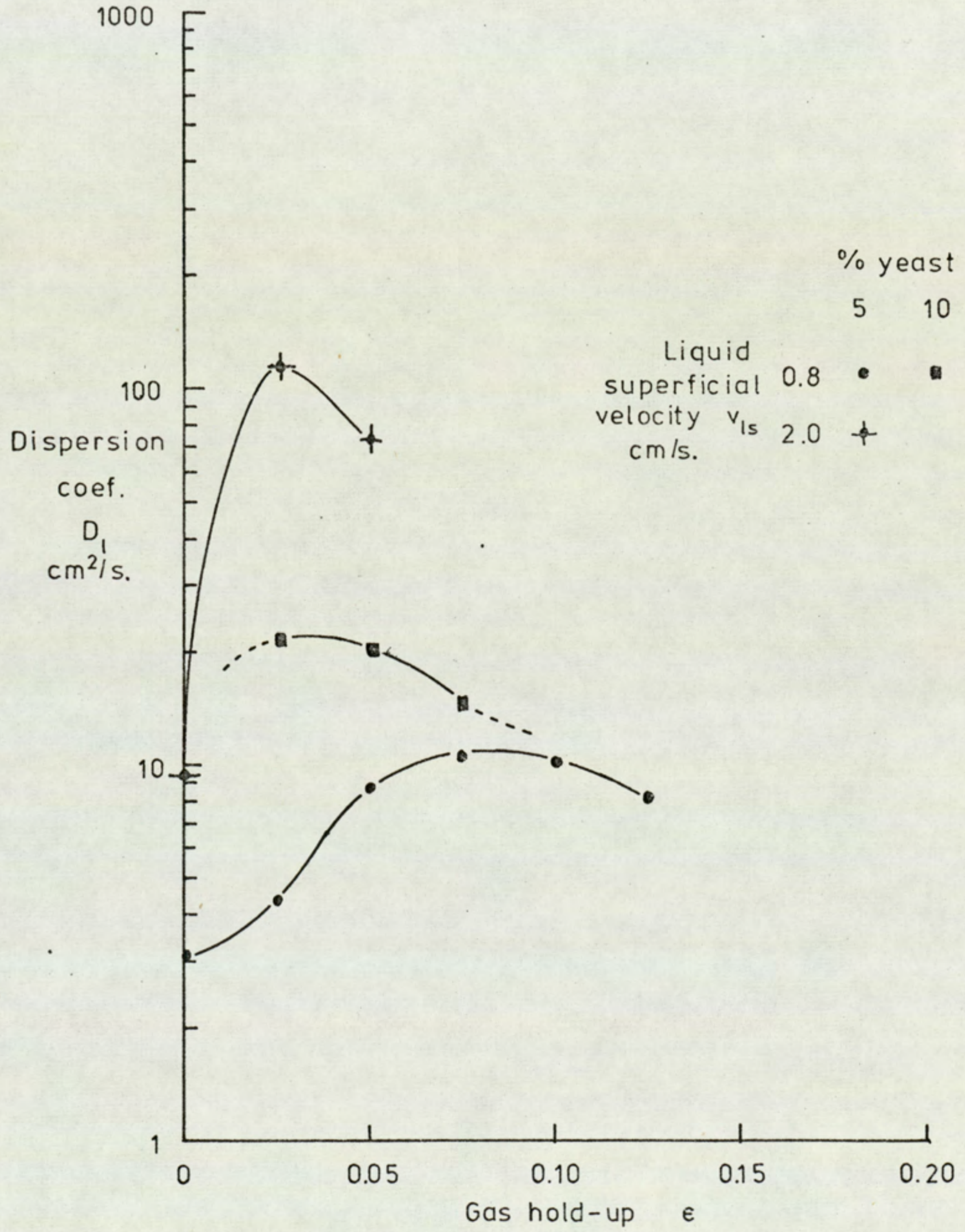

FIG 4.9 Dispersion coefficients, 12" column, air/5 and 10% yeast suspensions.

Tables 4.19 to 4.24 inclusive show the relationship between the mean residence times calculated a) as $\Delta\mu$ and b) by using the true liquid velocity. The last column represents the ratio of these two values. In Tables 4.19 and 4.20 the values listed under $\Delta\mu$ have been averaged for the various porosities used for the sake of convenience. In Tables 4.19 to 4.23 inclusive $\Delta\mu$ is the difference between the first moments measured at the sampling points and m.r.t. is the mean residence time calculated from the true liquid velocity and the distance between the sampling points.

4.4.5 CONCLUSIONS

The mixing in the liquid-phase, as determined assuming the dispersed plug-flow model to apply, can be divided into four sections, viz.

1. Effect of liquid superficial velocity.
2. Effect of gas superficial velocity (measured as gas hold-up)
3. Effect of liquid properties.

and 4. Analysis of the model used, based on the results obtained.

1. Effect of liquid superficial velocity.

This parameter has the most profound effect on the dispersion coefficient, as can be seen from the graphical results. Doubling the liquid velocity has the effect of increasing D_l by a factor of 10 to 100. The greatest increase, when operating with the 6" column occurs when the liquid-phase transition from laminar to turbulent-flow takes place, i.e. when the liquid superficial velocity increases from 1.0 to 2.0 cm/s. In the 12" column, however, this transition takes place when v_{1s} increases from 0.8 to 1.0 cm/s (in fact at $v_{1s} = 0.8$ cm/s the flow is within the transition region).

2. Effect of gas superficial velocity.

At high liquid flow-rates the dispersion coefficient increases rapidly from a fairly low value ($D_1 \simeq 10$ cm^2/s) when there is only a single-phase present. This rapid increase in D_1 tends to reach a maximum at a gas hold-up of approximately 0.5 and D_1 decreases with increasing gas hold-up. This transition occurs at a Reynolds Number of approximately 200 (based on the true gas velocity).

This suggests that there is a transition at this point which considerably alters the liquid flow pattern.

At lower liquid flow-rates the dispersion coefficient appears to increase slowly with increasing gas hold-up, although at the lowest flow-rate encountered, especially with the yeast solutions, it is difficult to determine any relationship between the values. In fact, in Fig. 4.8 the dashed-lines represent the mean value of the points.

3. Effect of liquid properties.

The order of magnitude of the dispersion coefficients is the same in each of the graphs (Figs. 4.6 to 4.9). The only conclusion that can be drawn from this is that the liquid physical properties have little or no effect on the values of D_1.

The repeat experiments that were carried out, the results of which are shown in Table 4.18, show very little variation from the other results; thus confirming that the basic method of measurement and analysis is sound.

4. Analysis of the data, using the dispersed plug-flow model.

As can be seen in Tables 4.19 to 4.24, the ratio of the measured and calculated mean residence times falls below 1.0 in all cases where the liquid superficial velocity is less than 2.0 cm/s.

This means that the dispersed plug-flow model used is not necessarily the best way of analysing the data at the lower flow-rates. The advantage of this method is that there is only one parameter, D_1, which is relatively simple to extract from the experimental data.

Even though this is not the best model, the results are comparative with one another and as the first stage in this investigation it is a good approximation.

Other models which should be applied to the system are either a series of stirred tanks, or a new model based on the following premise:

> dispersion in two directions, backward and forward, with the backward dispersion much greater than the forward.

The disadvantage in both these models would be that the complexity of handling them would increase greatly as the number of parameters increased.

APPENDIX A

The following tables refer to

Chapter 2

Bubble Sizes and Size Distributions

Table A.1 Distribution of Bubble Sizes.

Length of slug. mm.	Dia. d_b of equiv.sphere	No. of Bubbles of dia. d_b			
		Orifice 1	2	3	4
4	2.52				1 (5)
5	2.71				3 (15)
6	2.88				4 (20)
7	3.03				12 (60)
8	3.17				13 (65)
9	3.30				15 (75)
10	3.42				16 (80)
11	3.53				20 (100)
12	3.63				11 (55)
13	3.73				2 (10)
14	3.82				2 (10)
15	3.91			1 (2.9)	1 (5)
16	4.00			0 (0)	
17	4.08			3 (8.8)	
18	4.16			9 (26.4)	
19	4.23		1 (4)	34 (100)	
20	4.30		1 (4)	31 (91)	
21	4.38		1 (4)	14 (41.1)	
22	4.44		5 (20)	7 (20.5)	
23	4.51		7 (28)	0 (0)	
24	4.57		3 (12)	1 (2.9)	
25	4.64		8 (32)		
26	4.70		15 (60)		
27	4.76		25 (100)		
28	4.82		13 (52)		
29	4.87	1 (3.4)	11 (44)		
30	4.93	3 (10.3)	6 (24)		
31	4.98	13 (44.8)	2 (8)		
32	5.04	29 (100)	0 (0)		
33	5.09	22 (75.9)	1 (4)		
34	5.14	9 (31.0)	0 (0)		
35	5.19	12 (41.4)	1 (4)		
36	5.24	3 (10.3)			
37	5.29	1 (3.4)			
38	5.33	2 (6.9)			
39	5.38	3 (10.3)			
40	5.42	2 (6.9)			

"Normalised" distributions shown in brackets.

Table A.2 Calibration Data.

Liquid Phase / Bead dia. mm.	Water		0.1N KCl		5% Yeast		10% Yeast		15% Yeast		20% Yeast		25% Yeast		30% Yeast	
	l	$l^{\frac{1}{3}}$	l	$l^{\frac{1}{3}}$	l	$l^{\frac{1}{3}}$	l	$l^{\frac{1}{3}}$	l	$l^{\frac{1}{3}}$	l	$l^{\frac{1}{3}}$	l	$l^{\frac{1}{3}}$	l	$l^{\frac{1}{3}}$
3.000	6.43	1.86	5.27	1.74			2.85	1.42	4.57	1.66	3.72	1.55	3.87	1.57	3.76	1.56
3.175			6.13	1.83	4.48	1.65	3.40	1.50	4.74	1.68						
4.000	15.26	2.48	11.24	2.24	8.74	2.06					8.87	2.07	8.49	2.04	8.25	2.02
6.000	52.32	3.74	37.92	3.36	29.4	3.09	29.42	3.09	37.26	3.34	29.22	3.08	29.79	3.10	28.05	3.03

Table A.3 Bubble sizes determined by Resistance Measurement. (Air/Water).

Orifice dia. cm.	$\bar{I}_d$	$\bar{I}_d^{1/3}$	$\bar{d}_b$ cm
0.141	33.26	3.22	0.515
0.101	26.89	2.96	0.474
0.075	19.39	2.68	0.429
0.037	9.47	2.12	0.339

Table A.4 Bubble Diameter as a function of Bubble Frequency.

Orifice diameter = 0.253 cm.

Air / 0.1N KCl

Bubbles/sec.	Minimum Chamber Volume				Maximum Chamber Volume			
	0.26	0.78	2.0	5.0	0.29	0.63	2.8	5.3
l_d	No. of bubbles of size l_d				No. of bubbles of size l_d			
31	4				2			
32	4	6	1		5	2		
33	3	9	5		6	5		
34	3	3	9		2	6		
35	1	5	6	4	1	2	2	3
36	3	0	5	5	4	4	6	7
37	1	3	4	6	1	0	9	11
38	4	5	5	4	2	4	7	8
39	1	4	5	2	2	3	6	3
40	2	3	5	12	0	1	19	14
41	3	1	4	10	1		16	10
$\bar{l}_d$	35.41	35.46	36.53	38.65	34.57	35.36	39.00	38.48
$\bar{l}^{\frac{1}{3}}$	3.28	3.29	3.32	3.39	3.26	3.28	3.39	3.38
$\bar{d}_b$ mm	5.81	5.82	5.88	6.00	5.77	5.81	6.00	5.98

Table A.5 Bubble Diameter as a function of Bubble Frequency.

Orifice diameter = 0.201 cm.

Air / 0.1N KCl

	Minimum Chamber Volume				Maximum Chamber Volume			
Bubbles/ sec.	0.14	0.77	3.2	4.5	0.33	0.78	1.7	4.6
l_d	No. of bubbles of size l_d				No. of bubbles of size l_d			
21		1						
22	3	3			3	1	2	
23	6	7			3	2	4	
24	3	5	2		1	4	7	
25	4	2	8	3	6	3	9	4
26	4	4	7	4	7	4	7	5
27	4	2	10	4	3	4	8	5
28	1	1	9	6	5	6	7	5
29	0	2	9	6	1	3	5	5
30	0	2	6	5	1	2	5	5
31	1	1	4	4	1	2	3	3
32			3	2	2	1	2	1
33			2	2		1	2	0
34				3		0	1	1
35				2		1	1	2
36							1	2
37								1
$\bar{l}_d$	24.88	25.63	27.98	29.29	25.93	27.58	27.28	29.17
$\bar{l}_d^{\frac{1}{3}}$	2.92	2.95	3.03	3.08	2.96	3.02	3.01	3.08
$\bar{d}_b$ mm	5.17	5.22	5.36	5.45	5.24	5.35	5.33	5.45

Table A.6 Bubble Diameter as a function of Bubble Frequency.

Orifice diameter = 0.198 cm.

Air / 0.1N KCl

	Minimum Chamber Volume				Maximum Chamber Volume			
Bubbles/sec.	0.094	0.68	2.28	5.58	0.26	0.95	3.0	5.0
l_d	No. of bubbles of size l_d				No. of bubbles of size l_d			
17		1						
18		0						
19	1	0						
20	2	0						
21	4	2			2			
22	4	1			7	4		
23	4	1		1	6	4		
24	3	7		0	4	2		
25	3	5	4	2	3	4		
26	4	3	13	3	3	9	3	
27	0	3	5	4	0	2	4	
28	0	3	5	13	0	4	7	
29	1	1	6	7	1	3	6	
30	1	1	7	7	2	2	6	
31		2	5	4			5	
32		2	4	4			3	2
33			3	2			3	7
34			3	2			2	5
35			1	2			1	7
36				1			1	7
37				1				3
38				1				3
39								2
40								5
41								3
$\bar{l}_d$	23.44	25.78	28.91	30.61	23.78	25.76	29.87	36.09
$\bar{l}_d^{\frac{1}{3}}$	2.86	2.95	3.07	3.13	2.88	2.95	3.10	3.30
$\bar{d}_b$ mm	5.06	5.22	5.43	5.54	5.10	5.22	5.49	5.84

Table A.7 Bubble Diameter as a function of Bubble Frequency.

Orifice diameter = 0.147 cm.

Air / 0.1N KCl

	Minimum Chamber Volume					Maximum Chamber Volume			
Bubbles/sec.	0.17	0.5	0.77	2.1	4.8	0.35	1.2	3.1	4.9
l_d	No. of bubbles of size l_d					No.of bubbles of size l_d			
16	1					1			
17	5	1	2			0			
18	6	4	8	1	1	2			
19	5	4	9	5	7	5			
20	2	4	7	12	8	6			
21	3	5	7	9	12	6			
22	2	2	6	6	7	7	3		
23	2	0	3	5	6	5	3		
24	2	0	0	5	4	0	1	5	
25	1	0	1	4	2	1	3	8	
26		1		1	2		4	7	3
27				1	2		3	7	7
28				1	1		3	6	8
29					1		2	4	5
30							1	2	4
31							1	2	3
32								2	3
33								2	3
34								2	1
35								1	1
36									1
37									1
38									1
39									1
$\bar{l}_d$	19.65	20.00	20.07	21.80	21.96	20.51	24.66	27.70	30.07
$\bar{l}_d^{\frac{1}{3}}$	2.67	2.71	2.72	2.79	2.80	2.74	2.91	3.03	3.11
$\bar{d}_b$ mm	4.73	4.80	4.81	4.94	4.95	4.85	5.15	5.36	5.51

Table A.8 Bubble Diameter as a function of Bubble Frequency.

Orifice diameter = 0.117 cm.

Air / 0.1N KCl

	Minimum Chamber Volume			
Bubbles/ sec.	0.09	0.5	2.5	3.5
l_d	Number of bubbles of size l_d			
13	3	1		
14	6	5	2	4
15	4	5	11	9
16	5	6	14	14
17	4	3	15	11
18	1	5	13	6
19	1	4	10	5
20	1	1	3	4
21	1		1	1
22			1	1
23			2	1
24			1	
$\bar{l}_d$	15.72	14.70	17.34	17.0
$\bar{l}_d^{\frac{1}{3}}$	2.51	2.45	2.59	2.57
$\bar{d}_b$ mm	4.44	4.34	4.58	4.55

Table A.9 Bubble Diameter as a function of Bubble Frequency.

Orifice diameter = 0.101 cm.

Air / 0.1N KCl

	Minimum Chamber Volume			
Bubbles/sec.	0.1	0.5	1.85	2.42
l_d	Number of bubbles of size l_d			
5	5			
6	7			
7	8			
8	9		1	
9	6	1	0	
10	3	3	0	
11	2	11	8	8
12		13	15	16
13		4	15	11
14		3	5	5
15		2	3	1
16		2	2	1
17		1	1	1
18				0
19				0
20				1
$\bar{l}_d$	7.53	12.12	12.70	12.75
$\bar{l}_d^{\frac{1}{3}}$	1.96	2.30	2.33	2.34
d_b mm.	3.47	4.07	4.12	4.14

Table A.10 Bubble Diameter as a function of Bubble Frequency.

Orifice diameter = 0.094 cm.

Air / 0.1N KCl

Bubbles/sec. l_d	Minimum Chamber Volume				
	0.11	0.23	1.25	1.55	4.8
	Number of bubbles of size l_d				
5	1				
6	5				
7	11	17	8	3	
8	8	20	36	25	11
9	7	10	25	33	16
10	0	2	11	17	12
11	0	0	5	6	6
12	1	2	3	5	4
13		1	2	4	3
14			1		1
15			1		
$\bar{l}_d$	7.6	8.19	8.96	9.31	9.79
$\bar{l}_d^{\frac{1}{3}}$	1.97	2.02	2.08	2.10	2.14
$\bar{d}_b$ mm	3.49	3.58	3.68	3.72	3.79

Table A.11 Bubble Diameter as a function of Bubble Frequency.

Orifice diameter = 0.075

Air / 0.1N KCl

Bubbles/sec.	Minimum Chamber Volume				
	0.06	0.35	1.1	3.0	5.2
l_d	Number of bubbles of size l_d				
5	4				
6	8	12	7	1	11
7	6	16	34	15	10
8	3	1	19	32	12
9	2	1	7	13	8
10	1	1	4	6	9
11		0	2	6	5
12		0	1	3	3
13		1		2	1
14		0			
15		1			
$\bar{l}_d$	6.75	7.24	7.69	8.61	8.44
$\bar{l}_d^{\frac{1}{3}}$	1.89	1.93	1.97	2.05	2.04
$\bar{d}_b$ mm	3.35	3.42	3.49	3.63	3.61

Table A.12 Bubble Diameter as a function of Bubble Frequency.

Orifice diameter = 0.037 cm.

Air / 0.1N KCl

	Minimum Chamber Volume			
Bubbles/ sec.	0.12	1.18	2.4	5.4
l_d	Number of bubbles of size l_d			
4	19	7	19	17
5	9	25	32	28
6	7	13	5	10
7	4	4	3	8
8	2	2	1	3
9		1		1
$\bar{l}_d$	5.05	5.46	4.92	5.32
$\bar{l}_d^{\frac{1}{3}}$	1.72	1.76	1.70	1.79
$\bar{d}_b$ mm	3.04	3.12	3.01	3.17

Table A.13 Bubble Size Distribution.

Air / 5% W/V Yeast

	Minimum Chamber Volume				
Orifice No.	1	2	4	5	8
l_d	No. of bubbles of size l_d				
1					(100) 26
2				(13) 13	(54) 14
3			(6) 2	(100)100	
4			(6) 2	(33) 33	
5		(3) 1	(15) 5		
6			(33) 11		
7		(3) 1	(100) 33		
8		(3) 1	(75) 25		
9	(8) 2	(22) 8	(19) 3		
10	(12) 3	(89) 33			
11	(12) 3	(100) 37			
12	(12) 3	(24) 9			
13	(29) 7				
14	(100) 24				
15	(92) 22				
16	(63) 15				
17	(17) 4				
$\bar{d}_b$ mm	4.68	4.21	3.67	2.84	2.14

"Normalised" distribution in brackets.

Table A.14 Bubble Size Distribution.

Air / 10% W/V Yeast

Minimum Chamber Volume

Orifice No. / l_d	1	2	4	5	8
	Number of bubbles of size l_d				
0.5					(100) 29
1.0				(11) 4	(59) 17
1.5					(55) 16
2.0			(18) 6	(42) 16	(72) 21
2.5					(14) 4
3.0			(18) 6	(53) 20	
4.0	(3) 1		(100) 34	(100) 38	
5.0	(15) 5	(2) 1	(82) 28	(5) 2	
6.0	(24) 8	(3) 2			
7.0	(27) 9	(27) 17			
8.0	(30) 10	(100) 63			
9.0	(36) 12	(48) 30			
10.0	(100) 33	(2) 1			
11.0	(66) 22				
12.0	(9) 3				
$\bar{d}_b$ mm	4.16	4.04	3.22	2.96	2.14

"Normalised" distribution in brackets.

Table A.15 Bubble Size Distribution.

Air / 15% W/V Yeast

Minimum Chamber Volume

Orifice No. / l_d	1	2	4	5	7
	Number of bubbles of size l_d				
1					(6) 2
2			(8) 2	(31) 15	(100) 33
3			(27) 7	(100) 49	(58) 19
4	(4) 2		(50) 13	(15) 7	(6) 2
5	(4) 2		(50) 13		
6	(4) 2	(4) 2	(62) 16		
7	(4) 2	(15) 7	(100) 26		
8	(7) 4	(100) 49	(23) 6		
9	(53) 29	(33) 16			
10	(100) 55				
11	(42) 23				
$\bar{d}_b$ mm	3.82	3.62	3.21	2.56	2.40

"Normalised" distribution in brackets.

Table A.16 Bubble Size Distribution.

Air / 20% W/V Yeast

Minimum Chamber Volume

Orifice No. / l_d	1	2	4	5	7
	Number of bubbles of size l_d				
1				(7) 7	(55) 32
2				(100) 95	(100) 58
3			(10) 7	(50) 47	(10) 6
4			(100) 66		
5		(100) 45	(12) 8		
6	(52) 29	(84) 38	(2) 1		
7	(100) 56				
8	(4) 2				
$\bar{d}_b$ mm	3.65	3.42	3.16	2.54	2.33

"Normalised" distribution in brackets.

Table A.17 Bubble Size Distribution.

Air / 25% W/V Yeast

Minimum Chamber Volume

Orifice No.	1	2	4	5	7
l_d	Number of bubbles of size l_d				
0.5					(11) 6
1.0			(30) 15		(100) 55
1.5				(30) 27	(64) 35
2.0			(48) 24	(100) 89	(5) 3
2.5				(9) 8	(2) 1
3.0		(7) 3	(100) 50		
4.0	(12) 7	(100) 44	(10) 35		
5.0	(100) 61	(80) 35			
6.0	(2) 1	(11) 5			
$\bar{d}_b$ mm	3.30	3.20	2.74	2.41	2.06

"Normalised" distribution in brackets.

Table A.18 Bubble Size Distribution.

Air / 30% W/V Yeast

Minimum Chamber Volume

Orifice No.	1	2	4	5	7
l_d	Number of bubbles of size l_d				
2				3	5
3			23	8	37
4		4	28	45	11
5		4	21	8	
6		10	19	1	
7	13	26			
8	27	49			
9		14			
$\bar{d}_b$ mm	3.87	3.83	3.22	3.09	2.87

Table A.19 Bubble Size Distribution.

Air / 5% W/V Yeast

Maximum Chamber Volume

Orifice No.	1	2
l_d	Number of bubbles of size l_d	
10		14
11		41
12		44
13		19
14		1
15	1	
16	5	
17	18	
18	34	
19	25	
20	13	
21	3	
22	-	
23	1	
$\bar{d}_b$ mm	5.10	4.37

Table A.20 Bubble Size Distribution.

Air / 10% W/V Yeast

Maximum Chamber Volume

Orifice No.	1	2
l_d	Number of bubbles of size l_d	
8		40
9		69
10		27
11	22	
12	69	
13	32	
14	6	
$\bar{d}_b$ mm	4.58	4.14

Table A.21 Bubble Size Distribution.

Air / 15% W/V Yeast

Maximum Chamber Volume

Orifice No.	1	2
l_d	Number of bubbles of size l_d	
5		1
6		-
7		8
8		39
9		22
10	21	
11	48	
12	16	
$\bar{d}_b$ mm	4.00	3.64

Table A.22 Bubble Size Distribution.

Air / 20% W/V Yeast

Maximum Chamber Volume

Orifice No.	1	2	3
l_d	Number of bubbles of size l_d		
4			23
5		31	79
6	1	53	4
7	35		
8	39		
$\bar{d}_b$ mm	3.80	3.45	3.28

Table A.23 Bubble Size Distribution.

Air / 25% W/V Yeast

Maximum Chamber Volume

Orifice No. / l_d	1	2	4	5
	Number of bubbles of size l_d			
2		2		
3		6		
4		10	18	40
5		18	85	27
6	48	28	13	3
7	40	8		
8		4		
9		3		
$\bar{d}_b$ mm	3.61	3.42	3.32	3.20

Table A.24 Bubble Size Distribution.

Air / 30% W/V Yeast

Maximum Chamber Volume

Orifice No. / l_d	1	2	4
	Number of bubbles of size l_d		
7		18	31
8	35	49	28
9	10	32	2
$\bar{d}_b$ mm	3.99	3.97	3.85

Table A.25 Bubbling Frequencies (minimum air chamber volume)

% Yeast / d_o cm	5%	10%	15%	20%	25%	30%
	Bubbling Frequency bubbles/s					
0.253	1.35	1.60	1.80	1.36	1.04	0.91
0.201	1.21	1.77	1.11	1.24	1.32	1.60
0.147	1.52	1.21	1.26	1.19	1.85	1.36
0.117	2.43	1.21	1.06	2.26	1.85	0.96
0.094	-	-	0.93	1.32	1.51	1.28
0.075	1.64	1.22	-	-	-	-

Table A.26 Bubbling Frequencies (maximum air chamber volume)

% Yeast / d_o cm	5%	10%	15%	20%	25%	30%
	Bubbling Frequency bubbles/s					
0.253	0.75	2.20	1.27	1.15	1.31	0.87
0.201	0.79	2.03	1.13	1.29	1.21	1.19
0.147	-	-	-	1.56	2.15	0.93
0.117	-	-	-	-	1.85	-

Table A.27 Relationship between Mean Diameter and diameter at which Maximum Number of Bubbles occurred.

	Dia.at which Maximum No. of Bubbles occurs. mm.	Mean Dia. mm. Equation 2.3.
5% Yeast	4.66	4.68
	4.29	4.21
	3.69	3.67
	2.78	2.84
	1.93	2.14
10% Yeast	4.30	4.16
	4.00	4.04
	3.18	3.22
	3.18	2.96
	1.47	2.14
15% Yeast	3.87	3.82
	3.60	3.62
	3.44	3.21
	2.59	2.56
	2.27	2.40
20% Yeast	3.71	3.65
	3.32	3.42
	3.09	3.16
	2.45	2.54
	2.45	2.33
25% Yeast	3.32	3.30
	3.09	3.20
	2.80	2.74
	2.45	2.41
	1.94	2.06

Table A.28 Frequency of occurrence of Bubbles for all orifice sizes.

Air / 5% W/V Yeast.

(z_i)	$y(z_i)$	(z_i)	$y(z_i)$	(z_i)	$y(z_i)$	(z_i)	$y(z_i)$	(z_i)	$y(z_i)$
0.35	0								
0.28	17			0.43	0				
0.20	63	0.22	0	0.31	9	0.47	0	0.85	0
0.12	92	0.10	14	0.17	75	0.28	33	0.43	49
0.00	100	0	100	0	100	0	100	0	100
- 0.13	27	- 0.20	89	- 0.17	33	- 0.42	13	- 0.50	0
- 0.25	14	- 0.32	22	- 0.45	15	- 0.85	0		
- 0.35	12	- 0.46	41	- 0.64	6				
- 0.55	12	- 0.63	3	- 0.92	6				
- 0.63	8	- 0.80	3	- 1.54	0				
- 0.81	0	- 1.08	3						
		- 1.27	0						

Table A.29 Frequency of occurrence of Bubbles for all orifice sizes.

Air / 10% W/V Yeast.

(z_i)	$y(z_i)$	(z_i)	$y(z_i)$	(z_i)	$y(z_i)$
0.42	0				
0.30	9	0.26	0	0.47	0
0.20	66	0.14	36	0.19	82
0.00	100	0	100	0	100
- 0.12	48	- 0.17	27	- 0.28	18
- 0.26	30	- 0.34	3	- 0.70	18
- 0.43	27	- 0.62	3	- 0.13	0
- 0.60	24	- 0.81	2		
- 0.88	15	- 1.09	0		
- 1.05	0				

Table A.30 Frequency of occurrence of Bubbles for all orifice sizes.

Air / 15% W/V Yeast.

(z_i)	$y(z_i)$	(z_i)	$y(z_i)$	(z_i)	$y(z_i)$	(z_i)	$y(z_i)$	(z_i)	$y(z_i)$
								0.89	0
0.30	0	0.26	0	0.31	0	0.47	0	0.70	6
0.20	42	0.14	33	0.17	23	0.28	15	0.42	58
0	100	0	100	0	100	0	100	0	100
- 0.12	16	- 0.17	15	- 0.17	62	- 0.42	31	- 0.43	6
- 0.26	7	- 0.34	4	- 0.45	50	- 0.85	0	- 0.93	0
- 0.43	4	- 0.62	0	- 0.64	50				
- 0.60	4			- 0.92	27				
- 0.88	4			- 1.34	8				
- 1.07	4			- 1.77	0				
- 1.35	0								

Table A.31 Frequency of occurrence of Bubbles for all orifice sizes.

Air / 20% W/V Yeast.

(z_i)	$y(z_i)$	(z_i)	$y(z_i)$	(z_i)	$y(z_i)$	(z_i)	$y(z_i)$
				0.64	0		
0.31	0	0.45	0	0.47	2	0.70	0
0.17	4	0.28	87	0.19	12	0.42	50
0	100	0	100	0	100	0	100
- 0.17	52	- 0.19	0	- 0.28	10	- 0.43	8
- 0.45	0			- 0.70	0	- 0.93	0

Table A.32 Frequency of occurrence of Bubbles for all orifice sizes.

Air / 25% W/V Yeast.

(z_i)	$y(z_i)$	(z_i)	$y(z_i)$	(z_i)	$y(z_i)$	(z_i)	$y(z_i)$	(z_i)	$y(z_i)$
								0.85	0
		0.64	0					0.67	1
0.45	0	0.47	11	0.47	0	0.42	0	0.43	5
0.28	2	0.19	80	0.28	70	0.24	9	0.25	64
0	100	0	100	0	100	0	100	0	100
- 0.19	12	- 0.28	7	- 0.42	48	- 0.18	30	- 0.50	11
- 0.47	0	- 0.46	0	- 0.85	30	- 0.43	0	- 1.05	0
				- 1.35	0				

Table A.33 Calculated Bubble Size-Distribution.

Air / 5% W/V Yeast.

z_i	$y(z_i)$	$(1 + \frac{z_i}{l_1})$	$(1 - \frac{z_i}{l_2})$	$y_1\ (z_i)$
0.35	0	1.35	0.13	2.9
0.31	9	1.31	0.23	8.3
0.28	17	1.28	0.30	17.2
0.22	0	1.22	0.45	40.5
0.20	63	1.20	0.50	49.1
0.17	75	1.17	0.58	61.9
0.12	92	1.12	0.70	80.3
0.10	14	1.10	0.75	86.1
0	100			100
- 0.13	27	0.87	1.33	81.7
- 0.17	33	0.83	1.43	71.5
- 0.20	89	0.80	1.50	63.5
- 0.25	14	0.75	1.63	49.8
- 0.32	22	0.68	1.80	32.7
- 0.35	12	0.65	1.88	24.4
- 0.42	13	0.58	2.05	14.6
- 0.45	15	0.55	2.13	10.6
- 0.46	4	0.54	2.15	9.7
- 0.50	0	0.50	2.25	6.4
- 0.55	12	0.45	2.38	3.3
- 0.63	3	0.37	2.58	1.0
- 0.64	6	0.36	2.60	0.8
- 0.80	3	0.20	3.00	0.1
- 0.81	0	0.19	3.03	0
- 0.85	0	0.15	3.12	0
- 0.92	6	0.08	3.30	0

Table A.34 Calculated Bubble Size-Distribution.

Air / 10% W/V Yeast.

z_i	$y(z_i)$	$(1 + \frac{z_i}{l_1})$	$(1 - \frac{z_i}{l_2})$	$y_1 (z_i)$
0.40	0	1.37	0.15	0.8
0.35		1.32	0.26	7.1
0.30	9	1.28	0.36	23.7
0.25		1.23	0.47	49.8
0.20	66	1.18	0.58	77.2
0.19	82	1.17	0.60	83.4
0.14	36	1.16	0.61	92.5
0	100			100
- 0.12	48	0.89	1.26	57.2
- 0.17	27	0.85	1.36	37.4
- 0.21		0.81	1.45	25.8
- 0.26	30	0.76	1.55	15.3
- 0.28	18	0.74	1.60	12.2
- 0.34	3	0.69	1.72	5.6
- 0.43	27	0.61	1.91	1.4
- 0.60	24	0.45	2.28	
- 0.62	3	0.43	2.32	0.1
- 0.70	18	0.36	2.49	
- 0.81	2			
- 0.88	15			
- 1.09	0			

Table A.35 Calculated Bubble Size-Distribution.

Air / 15% W/V Yeast.

z_i	$y(z_i)$	$(1 + \frac{z_i}{l_1})$	$(1 - \frac{z_i}{l_2})$	$y_1\ (z_i)$
0.31	0	1.28	0.23	5.5
0.30	0	1.27	0.25	6.0
0.28	15	1.25	0.30	8.0
0.26	0	1.24	0.35	9.0
0.20	42	1.18	0.50	15.2
0.17	23	1.16	0.58	28.3
0.14	33	1.13	0.65	44.4
0	100			100
- 0.12	16	0.89	1.30	62.3
- 0.17	62	0.85	1.43	47.6
- 0.21		0.81	1.53	28.5
- 0.26	7	0.76	1.65	14.7
- 0.30		0.73	1.75	8.2
- 0.34	4	0.69	1.85	4.0
- 0.42	31	0.62	2.05	1.0
- 0.43	5	0.61	2.08	0.9
- 0.45	50	0.59	2.13	
- 0.50		0.55	2.25	
- 0.60	4	0.46	2.50	
- 0.64	50	0.42	2.60	
- 0.70		0.36	2.75	
- 0.85	0	0.23	3,13	
- 0.92	27	0.16	3.30	
- 1.07	4			

Table A.36 Calculated Bubble Size-Distribution.

Air / 20% W/V Yeast.

z_i	$y(z_i)$	$(1 + \frac{z_i}{l_1})$	$(1 - \frac{z_i}{l_2})$	$y_1 (z_i)$
0.36		1.33	0.10	0
0.31	0	1.31	0.25	
0.28	87	1.26	0.30	0.5
0.19	12	1.76	0.53	18.7
0.17	4	1.16	0.58	27.1
0.09		1.08	0.78	78.9
0	100			100
- 0.07		0.94	1.18	83.3
- 0.17	52	0.84	1.43	24.4
- 0.19	0	0.83	1.48	18.8
- 0.28	10	0.75	1.70	5.9
- 0.30		0.72	1.75	
- 0.35		0.67	1.88	0.7
- 0.43	8	0.60	2.08	
- 0.45	0	0.58	2.13	
- 0.70	0			
- 0.93	0			

Table A.37 Calculated Bubble Size-Distribution.

Air / 25% W/V Yeast.

z_i	$y(z_i)$	$(1 + \frac{z_i}{l_1})$	$(1 - \frac{z_i}{l_2})$	$y_1\ (z_i)$
0.28	2	1.26	0.3	0.0
0.25	64			
0.24	9			
0.19	80	1.18	0.52	7.6
0.09	0	1.08	0.78	64.2
0	100			100
- 0.10	0	0.91	1.25	56.2
- 0.18	30			17.0
- 0.19	12	0.83	1.48	15.3
- 0.24	0	0.77	1.60	5.3
- 0.28	7	0.75	1.70	2.9
- 0.35	0	0.66	1.88	0.3
- 0.42	48			
- 0.43	0	0.60	2.08	
- 0.50	11			
- 0.60	0	0.45	2.50	
- 0.85	30			
- 1.05	0			

APPENDIX B

The following tables refer to

Chapter 3

Bubble Swarm Systems

Table B 1 Derived Measurements.

Run No.	Air Flow Rate l/min S.T.P.	Air Hold-up ϵ	Liquid Flow Rate l/min	Liquid Hold-up $1 - \epsilon$	G_v/L_v	Air Superficial Velocity cm/s	Liquid Superficial Velocity cm/s
1	2.5	5.6	0.045	94.4	55.2	3.61	0.060
2	2.3	4.4	0.230	95.6	10.2	3.41	0.336
3	4.2	10.8	0.045	89.2	94.1	6.20	0.060
4	4.2	9.7	0.230	90.3	18.5	6.20	0.336
5	5.9	17.2	0.045	82.8	130.8	8.58	0.060
6	5.7	14.5	0.230	85.5	24.6	8.27	0.336
7	7.6	22.7	0.045	77.3	168.3	11.05	0.060
8	7.4	22.1	0.230	77.9	32.3	10.74	0.336
9	2.1	4.9	0.045	95.1	47.4	3.10	0.060
10	2.1	4.4	0.230	95.6	8.9	3.00	0.336
11	3.2	9.4	0.045	90.6	70.7	4.65	0.060
12	3.1	8.0	0.230	92.0	13.5	4.55	0.336
13	4.7	16.5	0.045	83.5	105.4	6.92	0.060
14	4.7	14.2	0.230	85.8	20.3	6.82	0.336
15	7.8	25.6	0.045	74.4	174.0	11.47	0.060
16	7.8	21.8	0.230	78.2	34.2	11.47	0.336
17	2.2	5.3	0.045	94.7	48.8	3.20	0.060
18	2.2	5.3	0.230	94.7	9.5	3.20	0.336
19	3.3	10.0	0.045	90.0	73.5	4.86	0.060
20	3.5	9.0	0.230	91.0	15.1	5.06	0.336
21	5.3	15.2	0.045	84.8	117.4	7.75	0.060
22	5.3	14.2	0.230	58.8	23.1	7.75	0.336
23	6.8	20.3	0.045	79.7	150.6	9.92	0.060
24	6.8	18.5	0.230	81.5	29.5	9.92	0.336
25	1.6	1.6	0.230	98.4	7.1	2.38	0.336
26	3.3	11.3	0.230	88.7	14.4	4.86	0.336
27	5.0	20.1	0.230	79.9	21.5	7.66	0.336
28	3.5	14.6	0.230	85.4	15.4	5.17	0.336

Table B.2 Bubble Size Distributions.

Size Range of Bubbles mm.	Mean Dia.	Run Numbers											
		5	6	7	8	9	10	11	12	13	14	15	16
0 - 1.33	0.67	91	38	43	57	1	1	0	2	2	4	34	44
1.33- 2.66	2.00	7	7	25	36	0	1	5	2	12	7	42	34
2.66- 4.00	3.33	15	8	15	16	14	5	8	7	14	17	49	23
4.00- 5.33	4.67	26	17	17	19	13	19	13	15	19	20	26	27
5.33- 6.66	6.00	11	7	12	14	17	25	35	26	48	24	19	18
6.66- 8.00	7.33	11	6	13	8	12	12	16	9	15	12	2	18
8.00- 9.33	8.67	4	20	11	12	10	10	14	6	8	4	3	6
9.33-10.66	1.00	3	4	2	3	2	9	9	5	5	4	0	2
> 10.66		3	6	2	3	0	9	2	7	3	3	0	1
TOTALS		171	113	140	168	69	91	102	79	126	95	175	173
Mean Bubble Dia.mm.		2.43	5.12	3.45	3.39	5.66	6.20	6.22	5.57	4.86	4.52	3.18	3.06

Continued...............

Table B.2 Bubble Size Distributions continued.

Size Range of Bubbles mm.	Mean Dia.	Run Numbers									
		17	18	19	20	21	22	23	24	25	26
0 - 1.33	0.67	990*	1440*	1114*	1008*	500*	500*	450*	792*	178	158
1.33- 2.66	2.00	990*	720*	537*	1008*	502*	500*	450*	400*	262	99
2.66- 4.00	3.33	16	5	13	3	7	8	16	23	85	42
4.00- 5.33	4.67	8	2	16	9	9	22	14	26	38	55
5.33- 6.66	6.00	4	3	3	7	11	14	4	18	17	19
6.66- 8.00	7.33	2	3	7	4	5	3	9	8	3	32
8.00- 9.33	8.67	1	3	3	1	3	2	5	2	2	2
9.33-10.66	1.00	0	0	3	1	2	3	1	0	2	1
10.66		0	2	2	1	1	1	0	4	6	0
TOTALS		2011	2178	1718	2042	1040	1053	949	1273	587	379
Mean Bubble Dia.mm.		1.40	1.17	1.23	1.39	1.50	1.55	1.54	1.34	2.16	2.28

* Approximated values only.

Table B.3 Pressure Drops across dry gas distributors for various porosities (6" Column).

Gas Volumetric Flow (standard conditions) l/min.	Gas Superficial Velocity. cm/s.	Pressure Drop cm. Hg.		
		Porosity 1	Porosity 2	Porosity 3
11.90	1.09	0.1	0.2	0.6
19.0	1.74		0.3	1.0
30.9	2.83	0.2	0.4	1.6
44.5	4.06		0.6	2.4
58.72	5.36	0.5	0.8	3.2
74.6	6.81		1.0	4.3
34.9	3.19	0.2	0.40	2.0
55.6	5.07	0.4	0.75	3.2
95.3	8.70	0.7	1.15	5.2
136.5	12.47	1.10	1.70	7.2
179.5	16.38	1.45	2.30	9.6
227.1	20.73	1.80	3.00	12.2

Table B.4 Pressure Drop across dry gas distributors for various porosities (12" Column).

Gas Volumetric Flow (standard conditions) l/min.	Gas Superficial Velocity. cm/s.	Pressure Drop cm. Hg.	
		Porosity 2	Porosity 3
12.2	0.28	0.10	0.15
19.5	0.45	0.10	
31.8	0.72	0.15	0.45
45.6	1.04	0.20	
60.3	1.44	0.30	0.85
76.6	1.75	0.40	
35.9	0.82	0.15	0.65
57.0	1.29	0.20	1.00
97.8	2.23	0.35	1.60
143.3	3.19	0.55	2.15
184.1	4.20	0.75	2.85
233.0	5.31	1.00	3.55

Table B.5 Bubble Swarm Velocities (6" Column)

(Air/Water)

v_{ls} cm/s	ϵ	Porosity 1		Porosity 2		Porosity 3	
		v_{gs} cm/s	v_{bs} cm/s	v_{gs} cm/s	v_{bs} cm/s	v_{gs} cm/s	v_{bs} cm/s
0	0.05	0.99	19.94	1.10	20.45	1.00	20.20
0	0.10	2.11	17.39	2.39	18.05	2.46	18.18
0	0.15	3.03	16.23	4.65	17.45	3.25	17.01
0	0.20	4.85	15.58	4.79	17.01	4.66	16.29
0.5	0.05	1.19	19.92	1.17	20.79	1.24	20.41
0.5	0.10	2.46	18.38	2.79	18.21	2.72	19.01
0.5	0.15	3.54	16.84	6.16	17.99	4.25	17.48
0.5	0.20	5.37	16.50	5.39	17.73	4.86	16.78
1.0	0.05	1.21	20.66	1.25	21.19	1.37	20.92
1.0	0.10	2.65	18.90	2.83	19.46	2.89	19.31
1.0	0.15	3.79	17.15	6.50	18.80	4.09	17.76
1.0	0.20	5.58	16.92				
2.6	0.05			1.76	21.79	1.59	22.88
2.6	0.10			3.00	20.00	3.50	20.88

Table B.5 A Average Bubble Swarm Velocities (for all porosities) for 6" Column. (Air/Water)

v_{ls} cm/s	ϵ	$\bar{v}_{gs}$ cm/s	$\bar{v}_{bs}$ cm/s	$(\bar{v}_{bs} - v_{ls})$ cm/s
0	0.05	1.03	20.2	20.2
0	0.10	2.66	17.87	17.87
0	0.15	3.64	16.90	16.90
0	0.20	4.77	16.29	16.29
0.5	0.05	1.20	20.37	19.87
0.5	0.10	2.66	18.53	18.03
0.5	0.15	4.65	17.44	16.94
0.5	0.20	5.21	17.00	16.50
1.0	0.05	1.28	20.92	19.92
1.0	0.10	2.79	19.22	18.22
1.0	0.15	3.17	17.90	16.90
1.0	0.20	5.58	16.92	15.42
2.6	0.05	1.66	22.34	19.74
2.6	0.10	3.25	20.44	17.84

Table B.6 Bubble Swarm Velocities (Porosity 2)
and relative Bubble Swarm Velocities. (12" Column)
(Air/Water)

v_{ls} cm/s	ϵ	v_{gs} cm/s	v_{bs} cm/s	$v_{bs} - v_{ls}$ cm/s
0	0.05	1.38	20.53	20.53
0	0.10	2.29	18.05	18.05
0	0.15	4.10	16.42	16.42
0.8	0.05	1.50	21.19	20.39
0.8	0.10	2.64	18.83	18.03
0.8	0.15	4.31	17.61	16.81
1.0	0.05	1.46	22.17	21.17
1.0	0.10	2.88	19.88	18.88
1.0	0.15	7.27*	18.66	17.66
2.0	0.05	2.02	23.20	21.20
2.0	0.10	2.97	20.96	18.96

These results were limited due to the amount of air available.

* Some slugging was occurring at this hold-up and stable bubbling was difficult to maintain.

Table B.7 Gas Superficial Velocities and Hold-ups. 6" Column.

(Porosity 1) (Air/Water)

Hold-up / Liquid Superficial Velocity cm/s	0.025	0.05	0.075	0.10	0.15	0.20
	Gas Superficial Velocity cm/s					
0		0.99		2.11	3.03	4.85
0		1.02				4.65
0.5	0.837	1.19		2.46	3.53	5.37
0.5	0.68	1.09	1.86	2.36		4.64
1.0		1.21		2.65	3.79	5.58
1.0		1.38		2.51		4.86
2.6	1.06	1.18	1.89	2.90		
2.6		1.60				

Table B.8 Gas Superficial Velocities and Hold-ups. 6" Column.
(Porosity 2) (Air/Water)

Hold-up	0.05	0.10	0.15	0.20
Liquid Superficial Velocity cm/s	Gas Superficial Velocity cm/s			
0	1.10	2.39	4.65	4.79
0	1.27	2.10		4.78
0.5	1.17	2.79	6.16	5.39
0.5	1.49	2.52		4.81
1.0	1.25	2.83	6.50	5.58
1.0	1.39	2.65		5.00
2.6	1.76	3.00		
2.6	1.54	3.05		

Table B.9 Gas Superficial Velocities and Hold-ups. 6" Column.

(Porosity 3) (Air/Water)

Hold-up / Liquid Superficial Velocity cm/s	0.05	0.10	0.15	0.20
	Gas Superficial Velocity cm/s			
0	1.00	2.46	3.25	4.66
0	1.69			5.29
0.5	1.24	2.72	2.72	4.86
0.5	1.84	3.77		5.86
1.0	1.37	2.89	4.09	
1.0	2.06	3.62		5.43
2.6	1.59	3.50		
2.6	1.84	3.05		

Table B.10 Mean Values of Gas Superficial Velocities as a function of Liquid Velocity and Distributor Porosity. 6" Column. (Air/Water).

Liquid Superficial Velocity cm/s.	Hold-up	0.025	0.05	0.075	0.10	0.15	0.20
	Porosity	Gas Superficial Velocity cm/s Mean Values					
0	1		1.01		2.11	3.03	4.75
	2		1.19		2.25	4.65*	5.10
	3		1.34		2.46	3.25	4.98
0.5	1	0.76	1.14	1.86	2.41	3.53	5.01
	2		1.33		2.66	6.16*	5.01
	3		1.54		3.25	2.72	5.36
1.0	1		1.30		2.58	3.79	5.22
	2		1.32		2.74	6.50*	5.29
	3		1.72		3.26	4.09	5.43
2.6	1	1.06	1.39	1.89	2.90		
	2		1.65		3.03		
	3		1.72		3.28		

Mean values calculated from Tables B.7, B.8, and B.9.

* Slugging observed

Table B.11 Mean Values of Gas Superficial Velocity and Calculated Values of relative Superficial Velocity irrespective of Porosity. (Air/Water). 6" Column.

v_{ls} cm/s	ϵ	v_{gs} cm/s	v_{Rs} cm/s
0	0.05	1.18	1.18
0	0.10	2.27	2.27
0	0.15	3.64	3.64
0	0.20	4.94	4.94
0.5	0.025	0.76	0.26
0.5	0.050	1.34	0.84
0.5	0.075	1.86	1.36
0.5	0.100	2.77	2.27
0.5	0.150	4.14	3.64
0.5	0.200	5.13	4.63
1.0	0.05	1.45	0.45
1.0	0.10	2.86	1.86
1.0	0.15	4.79	3.79
1.0	0.20	5.31	4.31
2.6	0.025	1.06	- 1.54
2.6	0.050	1.59	- 1.01
2.6	0.075	1.89	- 0.71
2.6	0.100	3.07	+ 0.47

Table B.12 Values of relative Superficial Velocity calculated irrespective of Distributor Porosity. 6" Column. (Air/Water).

ϵ	v_{Rs} cm/s
0.025	- 1.28
0.050	0.36
0.075	0.31
0.100	1.72
0.150	2.90
0.200	4.63

Table B.13 Calculated Pressure Drops. 6" Column. (Air/Water).

ϵ	Porosity 1			Porosity 2			Porosity 3		
	v_{gs} cm/s	ΔP_1 cm Hg	ΔP_2 cm Hg	v_{gs} cm/s	ΔP_1 cm Hg	ΔP_2 cm Hg	v_{gs} cm/s	ΔP_1 cm Hg	ΔP_2 cm Hg
0.025	-			0.86	3.90	3.75	-		
0.05	1.21	2.48	2.38	1.37	4.17	3.87	1.58	7.83	6.83
0.10	2.50	3.05	2.85	2.67	4.45	4.05	3.14	8.60	6.75
0.15	4.65	4.13	3.73						
0.20	4.99	5.06	4.61	5.06	6.17	5.62	5.22	10.80	7.70

$$\Delta P_1 = \Delta P_{TOTAL} - \Delta P_H$$

$$\Delta P_2 = \Delta P_{TOTAL} - (\Delta P_H + \Delta P_D)$$

Table B.14 Gas Superficial Velocity and Hold-up for 12" Column, Porosity 2. (Air/Water).

Hold-up / Liquid Superficial Velocity cm/s	0.025	0.05	0.075	0.10	0.15
	Gas Superficial Velocity cm/s				
0		1.38		2.29	4.10
0.8		1.50		2.69	4.31
	0.62	0.95	1.59	2.71	5.24 (14%)
1.0		1.46		2.88	7.27*
2.0	0.94	2.02		2.97	7.39* (14%)
	0.78	1.69	2.46	3.78	3.93 (12.5%)

* Some slugging was in evidence.

Table B.15 Gas Superficial Velocity and Hold-up for 12" Column, Porosity 3. (Air/Water).

Hold-up / Liquid Superficial Velocity cm/s	0.05	0.10	0.15	0.175
	Gas Superficial Velocity cm/s			
0	0.93			5.54
0.8	1.31	2.64	6.88	
1.0	1.56	3.04	7.38	
2.0	1.53			

Table B.16 Mean Values of v_{gs} and ϵ for Porosities P_2 and P_3.
12" Column. (Air/Water).

v_{ls} cm/s	Hold-up / Porosity	0.025	0.050	0.075	0.100	0.120 - 0.175*
		Gas Superficial Velocities cm/s				
0	2		1.38		2.29	4.10 (0.15)
	3		0.93			5.54 (0.175)
0.8	2	0.62	1.23	1.59	2.68	4.31 (0.15) 5.24 (0.14)
	3		1.31		2.64	6.88 (0.15)
1.0	2		1.46		2.88	7.27 (0.15)
	3		1.56		3.04	7.38 (0.15)
2.0	2	0.86	1.86	2.46	5.38	7.39 (0.14) 3.93(0.125)

* Values in brackets represent the Gas Hold-up.

Table B.17 Mean Values of v_{gs} irrespective of porosity.
12" Column. (Air/Water).

Hold-up / v_{ls} cm/s	0.025	0.050	0.075	0.100	0.120 - 0.175*
	Gas Superficial Velocities cm/s				
0		1.16		2.29	4.10 (0.15) 5.54(0.175)
0.8	0.62	1.26	1.59	2.66	5.24 (0.14) 5.60(0.15)
1.0		1.51		2.96	7.33 (0.15)
2.0	0.86	1.70	2.46	3.38	7.39 (0.14) 3.93(0.125)

* Values in brackets represent the Gas Hold-up.

Table B.18 Values of v_{Rs} for Porosity 2 and 3 and Mean Values for both porosities. 12" Column. (Air/Water).

ϵ	Porosity 2 v_{Rs} cm/s	Porosity 3 v_{Rs} cm/s	Mean cm/s
0.025	- 0.82		- 0.82
0.050	0.40	0.38	0.39
0.075	0.63		0.63
0.100	1.78	2.44	2.11
0.125	1.93		1.93
0.140	4.91		4.91
0.150	4.63	6.23	5.43
0.175		5.54	5.54

Table B.19 Calculated Pressure Drops. 12" Column. (Air/Water).

ϵ	Porosity 2			Porosity 3		
	v_{gs} cm/s	ΔP_1 cm Hg	ΔP_2 cm Hg	v_{gs} cm/s	ΔP_1 cm Hg	ΔP_2 cm Hg
0.025	0.74	1.20	1.07			
0.050	1.47	4.40	4.13	1.33	5.90	5.00
0.075	2.03	5.10	4.70			
0.100	2.93	6.50	5.95	2.84	4.30	2.40
0.125	3.93	9.80	9.10			

$\Delta P_1 = \Delta P_{TOTAL} - \Delta P_H$

$\Delta P_2 = \Delta P_{TOTAL} - (\Delta P_H + \Delta P_D)$

Table B.20 Gas Hold-up and Superficial Velocity for 6" Column, continuing 5% and 10% Yeast Suspension.

Liquid Superficial Velocity cm/s	Hold-up / % Yeast Dry Weight	0.025	0.05	0.075	0.10	0.10
		Gas Superficial Velocity cm/s				
0.5	5	0.59	0.81	1.25	1.71	
	10	0.73	0.85	0.97	1.10	
2.6	5	0.46	0.59	0.75	1.20	
	10	0.66	0.82	0.98	2.31*	7.49 (0.125)*

* Evidence of slugging at these rates.

Table B.21 Gas Hold-up and Superficial Velocity for 12" Column, continuing 5% and 10% Yeast Suspension.

Liquid Superficial Velocity cm/s	Hold-up / % Yeast Dry Weight	0.025	0.05	0.075	0.10	>0.10
		Gas Superficial Velocity cm/s				
0.8	5	0.22	0.83	1.27	1.92	2.74(0.125)
	10	0.28	0.85	1.35		
2.0	5	0.61	1.06			
	10	0.44				

Table B.22 Relative Superficial Velocities. 6" Column.

5% and 10% Yeast Suspensions.

ϵ	Relative Superficial Velocities cm/s	
	5% Yeast	10% Yeast
0.025	- 1.03	- 0.85
0.050	- 0.95	- 0.72
0.075	- 0.55	- 0.58
0.100	- 0.09	+ 0.16

Table B.23 Relative Superficial Velocities. 12" Column.

5% and 10% Yeast Suspensions.

ϵ	Relative Superficial Velocities cm/s	
	5% Yeast	10% Yeast
0.025	- 0.98	- 0.82
0.050	- 0.31	0.05
0.075	0.77	0.55
0.100	1.42	
0.125	2.42	

Table B.24 Calculated Pressure Drop for 5% and 10% Yeast Suspension in both 6" and 12" Columns.

ϵ		6" Column		12" Column	
		5% Yeast	10% Yeast	5% Yeast	10% Yeast
0.025	v_{gs}	0.53	0.69	0.42	0.36
	ΔP_1	3.45	2.05	2.15	1.10
	ΔP_2	3.39	1.98	2.09	1.05
0.050	v_{gs}	0.70	0.83	0.95	0.85
	ΔP_1	4.00	2.45	2.95	2.30
	ΔP_2	3.93	2.33	2.83	2.19
0.075	v_{gs}	1.00	0.97	1.27	1.35
	ΔP_1	5.05	3.35	3.60	2.50
	ΔP_2	4.95	3.25	3.44	2.33
0.100	v_{gs}	1.25	1.70	1.92	
	ΔP_1	5.10	4.60	4.30	
	ΔP_2	4.98	4.44	4.06	
0.125	v_{gs}			2.74	
	ΔP_1			5.00	
	ΔP_2			4.66	

$\Delta P_1 = \Delta P_{TOTAL} - \Delta P_H$ cm Hg
$\Delta P_2 = \Delta P_{TOTAL} - (\Delta P_H + \Delta P_D)$ cm Hg
v_{gs} cm/s

APPENDIX C

The following tables and computer programme refer to

Chapter 4

Liquid - Phase Mixing in Two - Phase Columns

Algol Computer Programme used to determine the First Four Moments of a Distribution.

```
100    'BEGIN'
200    'INTEGER'  I, K, N, M;
300    'REAL' Z, U1, V2, V3  V4, A, B, SUM C, SUM 1, SUM 2, SUM 3, SUM 4;
400    K: = 0;  I: = READ;  L2:  K:  =  K + 1;
500    COPYTEXT   ( ' ( ' STOP ' ) ' );
600    M: = READ;
700    'BEGIN'
800    'REAL'  'ARRAY'   T,   C [1 : M] ,  U [1 : 4] ;
900    'FOR'  N: = 1 'STEP'  1 'UNTIL'  M  'DO'
1000   'BEGIN'
1100   T  [N]  :  =  READ;
1200   C  [N]  :  =  READ;
1300   SUM C: = SUM 1   : = SUM 2   : = SUM 3   : = SUM 4   : = 0.0;
1400   'END' ;
1500   'FOR'  N:  = 1 'STEP'  1  'UNTIL'  M  'DO'
1600   SUM C :  =  SUM C  +  C [N]  ;
1700   Z  :  =  SUM  C ;
1800   'FOR'  N :  =  1  'STEP'  1  'UNTIL'  M  'DO'
1900   'BEGIN'
2000   SUM  1:  =  SUM 1  +  T [N] x  C [N]  ;
2100   SUM  2:  =  SUM 2  +  T [N] ↑ 2  x  C [N]  ;
2200   SUM  3:  =  SUM 3  +  T [N] ↑ 3  x  C [N]  ;
2300   SUM  4:  =  SUM  4 +  T [N] ↑ 4  x  C  N   ;
2400   'END'
2500   U 1:  =  U [1]  :  =  SUM 1 / Z ;
2600   V 2:  =  SUM 2 / Z ;
2700   V 3:  =  SUM 3 / Z ;
```

```
2800    V 4: = SUM 4 / Z;
2900    U [2] : = V2 - U1↑2;
3000    U [3] : = V3 - 3 x V2 x U1 + 2 x U1↑3;
3100    U [4] : = V4 - 4 x V3 x U1 + 6 x V2 x U1 ↑ 2 - 3 x U1 ↑ 4;
3200    A : = U [3] / U [2] ↑1.5;
3300    B : = U [4] / U [2] ↑2;
3400    'FOR' N : + 1 'STEP' 1 'UNTIL' 4 'DO'
3500    'BEGIN'
3600    PRINT (U [N] , 5, 5); NEWLINE (1) ;
3700    'END' ;
3800    PRINT (A, 5, 5); NEWLINE (1); PRINT (B, 5, 5);
3900    'IF' K 'LT' I 'THEN' 'GOTO' L2;
4000    'END';
4100    'END';
```

The following definitions were used in the above programme.

K = No. of sets of data.

M = No. of readings per set of data.

A = α } Distribution shape characteristics.
B = β }

T = t time in min.

U_1 U_2 U_3 U_4 = Moments of the distribution.

V_2 V_3 V_4 = as defined by equations 4.4, 4.5 and 4.6.

In the following tables the tests are given experimental numbers of the following form:-

A / B / C / D / E

where A = Column Diameter
B = Liquid Superficial Velocity
C = Gas Hold-up Fraction
D = Porosity of the Distributor
E = First and second Downstream Measurement Position.

This has been done in order to facilitate the extraction of relevant data.

Table C.1 Distribution Moments.

6" Column. Porosity 1. Liquid-phase Water.

Experimental No.	U_1	U_2	U_3	U_4
6/0.5/0.025/1/1	2.85	7.20	11.10	89.08
6/0.5/0.025/1/2	7.42	12.92	- 28.93	256.19
6/0.5/0.050/1/1	3.67	4.00	- 0.49	23.22
6/0.5/0.050/1/2	4.73	5.27	- 5.47	42.44
6/0.5/0.075/1/1	4.05	10.32	4.55	138.77
6/0.5/0.075/1/2	6.72	11.69	- 19.02	199.06
6/0.5/0.10/1/1	2.88	3.29	- 0.21	16.43
6/0.5/0.10/1/2	4.79	5.37	- 5.91	44.49
6/0.5/0.20/1/1	3.27	3.95	- 1.37	23.10
6/0.5/0.20/1/2	4.45	5.39	- 5.49	43.82
6/1.0/0.05/1/1	1.66	1.31	0.26	2.98
6/1.0/0.05/1/2	2.54	1.65	0.13	4.86
6/1.0/0.10/1/1	2.06	1.98	0.43	6.75
6/1.0/0.10/1/2	3.43	3.07	- 0.64	14.77
6/1.0/0.20/1/1	2.66	1.98	- 1.48	6.90
6/1.0/0.20/1/2	3.15	2.95	- 0.58	13.70
6/2.6/0.025/1/1	1.49	1.80	1.32	6.13
6/2.6/0.025/1/2	2.78	2.91	1.15	14.96
6/2.6/0.05/1/1	0.84	0.31	0.02	0.17
6/2.6/0.05/1/2	1.57	0.59	0.02	0.64
6/2.6/0.075/1/1	1.54	1.43	0.61	3.59
6/2.6/0.075/1/2	3.30	3.70	0.59	22.56
6/2.6/0.10/1/1	0.73	0.25	0.02	0.11
6/2.6/0.10/1/2	1.38	0.49	0.02	0.45

Table C.2 Distribution Moments.

6" Column. Porosity 2. Liquid-phase Water.

Experimental No.	U_1	U_2	U_3	U_4
6/0.5/0.05/2/1	1.80	1.48	0.30	3.90
6/0.5/0.05/2/2	3.07	2.72	- 0.46	12.03
6/0.5/0.10/2/1	1.65	1.12	0.12	2.22
6/0.5/0.10/2/2	2.62	1.83	0.03	5.90
6/0.5/0.20/2/1	1.96	1.58	0.20	4.48
6/0.5/0.20/2/2	3.66	3.95	- 1.51	23.15
6/1.0/0.05/2/1	3.83	5.87	- 1.61	46.99
6/1.0/0.05/2/2	4.78	6.26	- 3.61	58.15
6/1.0/0.10/2/1	2.57	2.61	0.31	11.99
6/1.0/0.10/2/2	3.89	4.46	- 0.57	31.54
6/1.0/0.20/2/1	2.07	1.73	0.19	5.38
6/1.0/0.20/2/2	3.38	3.46	- 0.78	18.21
6/2.6/0.05/2/1	1.64	1.13	0.13	2.25
6/2.6/0.05/2/2	2.93	2.28	- 0.00	8.74

Table C.3 Distribution Moments.

6" Column. Porosity 3. Liquid-phase Water.

Experimental No.	U_1	U_2	U_3	U_4
6/0.5/0/3/1	1.43	1.82	2.87	10.47
6/0.5/0/3/2	5.89	2.85	0.55	15.79
6/0.5/0.05/3/1	1.78	1.39	0.25	3.42
6/0.5/0.05/3/2	3.84	4.19	0.41	31.96
6/0.5/0.10/3/1	2.66	2.99	- 0.09	13.79
6/0.5/0.10/3/2	3.66	3.87	- 1.68	22.39
6/0.5/0.20/3/1	1.96	1.64	0.24	4.68
6/0.5/0.20/3/2	2.72	2.38	- 0.08	9.35
6/1.0/0/3/1	0.68	0.22	0.05	0.10
6/1.0/0/3/2	3.04	0.74	0.09	1.04
6/1.0/0.05/3/1	1.13	0.66	0.13	0.76
6/1.0/0.05/3/2	2.60	1.87	0.08	6.15
6/1.0/0.10/3/1	1.77	1.40	0.26	3.49
6/1.0/0.10/3/2	2.54	1.82	0.29	6.18
6/1.0/0.20/3/1	2.28	2.16	0.22	7.95
6/1.0/0.20/3/2	2.78	3.34	- 0.02	9.12
6/2.6/0/3/1	0.60	0.34	0.20	0.31
6/2.6/0/3/2	2.48	0.43	0.10	0.39
6/2.6/0.05/3/1	1.28	0.81	0.16	1.15
6/2.6/0.05/3/2	2.49	1.59	0.13	4.52
6/2.6/0.10/3/1	0.93	0.42	0.06	0.32
6/2.6/0.10/3/2	1.67	0.59	0.03	0.64

Table C.4 Distribution Moments.

12" Column. Porosity 2. Liquid-phase Water.

Experimental No.	U_1	U_2	U_3	U_4
12/0.8/0.025/2/1	3.27	4.07	0.08	26.99
12/0.8/0.025/2/2	3.85	4.17	- 0.91	28.09
12/0.8/0.050/2/1	3.43	4.39	- 0.31	30.82
12/0.8/0.050/2/2	3.87	4.59	- 0.99	33.27
12/0.8/0.075/2/1	3.53	4.44	- 0.59	31.47
12/0.8/0.075/2/2	3.82	4.72	- 1.13	34.89
12/0.8/0.100/2/1	3.37	4.15	- 0.29	28.06
12/0.8/0.100/2/2	3.78	4.61	- 1.08	33.55
12/0.8/0.140/2/1	3.38	4.14	- 0.31	27.81
12/0.8/0.140/2/2	3.66	4.38	- 0.78	30.75
12/2.0/0.025/2/1	2.37	2.11	0.18	7.96
12/2.0/0.025/2/2	3.48	3.95	- 0.38	25.64
12/2.0/0.050/2/1	2.27	2.07	0.27	7.64
12/2.0/0.050/2/2	2.78	2.59	0.21	11.92
12/2.0/0.075/2/1	2.93	3.26	0.21	18.12
12/2.0/0.075/2/2	3.27	3.59	- 0.07	21.55
12/2.0/0.100/2/1	2.11	1.73	0.16	5.33
12/2.0/0.100/2/2	2.45	2.01	0.12	7.22
12/2.0/0.135/2/1	2.75	2.84	0.21	14.17
12/2.0/0.135/2/2	3.70	4.76	- 1.08	32.29

Table C.5 Distribution Moments.

12" Column. Porosity 3. Liquid-phase Water.

Experimental No.	U_1	U_2	U_3	U_4
12/0.8/0/3/1	2.88	2.50	0.63	11.44
12/0.8/0/3/2	5.24	3.93	- 0.34	25.63
12/0.8/0.05/3/1	3.75	5.33	- 0.80	43.02
12/0.8/0.05/3/2	4.92	7.01	- 5.74	73.29
12/0.8/0.10/3/1	3.51	4.81	- 0.33	36.26
12/0.8/0.10/3/2	4.17	5.60	- 2.23	47.52
12/0.8/0.15/3/1	2.92	3.31	0.49	18.73
12/0.8/0.15/3/2	3.44	3.75	- 0.01	23.33
12/1.0/0/3/1	2.03	1.19	0.24	2.57
12/1.0/0/3/2	3.49	1.29	0.13	3.06
12/1.0/0.05/3/1	2.89	3.27	0.32	18.36
12/1.0/0.05/3/2	3.35	3.74	- 0.07	23.32
12/1.0/0.10/3/1	3.46	4.52	- 0.36	32.57
12/1.0/0.10/3/2	4.12	5.52	- 2.07	46.08
12/1.0/0.15/3/1	3.05	3.54	0.19	21.20
12/1.0/0.15/3/2	3.79	4.74	- 0.96	35.12
12/2.0/0/3/1	0.86	0.24	0.04	0.11
12/2.0/0/3/2	1.72	0.53	0.04	0.52
12/2.0/0.05/3/1	2.78	3.26	0.44	18.26
12/2.0/0.05/3/2	3.17	3.37	0.05	19.30

Table C.6 Distribution Moments.

6" Column. Porosity 2. Liquid-phase 5% W/V Yeast.

Experimental No.	U_1	U_2	U_3	U_4
6/0.5/0/2/1	2.41	2.96	1.90	15.72
6/0.5/0/2/2	6.02	3.89	- 0.44	25.31
6/0.5/0.025/2/1	2.49	2.64	0.59	12.27
6/0.5/0.025/2/2	3.45	2.98	0.12	15.65
6/0.5/0.050/2/1	1.92	1.95	0.66	6.70
6/0.5/0.050/2/2	3.15	2.58	0.17	12.09
6/0.5/0.075/2/1	1.78	1.74	0.55	5.28
6/0.5/0.075/2/2	3.09	2.52	0.22	11.52
6/0.5/0.100/2/1	2.18	2.31	0.56	9.29
6/0.5/0.100/2/2	3.05	2.62	0.18	12.33
6/2.6/0/2/1	0.92	0.44	0.12	0.36
6/2.6/0/2/2	2.85	1.81	0.24	6.37
6/2.6/0.025/2/1	1.48	1.12	0.27	2.18
6/2.6/0.025/2/2	3.41	2.99	0.28	15.77
6/2.6/0.050/2/1	0.64	0.25	0.05	0.12
6/2.6/0.050/2/2	3.08	2.57	0.27	11.81
6/2.6/0.075/2/1	1.04	0.57	0.11	0.56
6/2.6/0.075/2/2	2.50	1.59	0.12	4.57
6/2.6/0.100/2/1	1.83	0.65	- 0.02	0.87
6/2.6/0.100/2/2	1.88	0.88	0.03	1.42

Table C.7 Distribution Moments.

6" Column. Porosity 2. Liquid-phase 10% W/V Yeast.

Experimental No.	U_1	U_2	U_3	U_4
6/0.5/0/2/1	2.63	3.19	2.22	18.45
6/0.5/0/2/2	7.21	6.16	- 4.32	57.97
6/0.5/0.025/2/1	3.36	5.41	1.29	44.43
6/0.5/0.025/2/2	5.19	6.98	- 5.73	72.61
6/0.5/0.050/2/1	3.48	4.94	- 0.29	37.60
6/0.5/0.050/2/2	5.27	7.30	- 7.79	81.13
6/0.5/0.075/2/1	2.84	3.21	0.30	17.10
6/0.5/0.075/2/2	3.71	5.79	- 0.03	17.67
6/0.5/0.100/2/1	2.66	2.98	0.42	13.14
6/0.5/0.100/2/2	2.23	4.13	0.03	15.28
6/2.6/0/2/1	1.43	0.86	0.16	1.31
6/2.6/0/2/2	4.06	0.99	0.08	1.79
6/2.6/0.025/2/1	2.05	1.76	0.29	5.43
6/2.6/0.025/2/2	3.40	3.08	0.08	16.62
6/2.6/0.050/2/1	1.43	0.82	0.07	1.20
6/2.6/0.050/2/2	3.00	2.53	0.16	1.58
6/2.6/0.075/2/1	1.60	0.97	0.06	1.69
6/2.6/0.075/2/2	2.57	1.95	0.10	6.92
6/2.6/0.100/2/1	1.76	1.36	0.17	3.24
6/2.6/0.100/2/2	2.76	2.13	0.12	8.23
6/2.6/0.125/2/1	1.86	1.38	0.12	3.37
6/2.6/0.125/2/2	2.75	2.29	0.17	9.50

Table C.8 Distribution Moments.

12" Column. Porosity 2. Liquid-phase 5% W/V Yeast.

Experimental No.	U_1	U_2	U_3	U_4
12/0.8/0/2/1	5.11	5.69	- 2.26	48.64
12/0.8/0/2/2	8.24	6.15	- 4.09	57.38
12/0.8/0.025/2/1	3.71	4.55	- 0.93	32.84
12/0.8/0.025/2/2	4.42	5.12	- 2.52	40.85
12/0.8/0.050/2/1	3.24	3.48	- 0.16	20.63
12/0.8/0.050/2/2	3.90	4.56	- 1.18	33.66
12/0.8/0.075/2/1	1.95	1.41	0.07	3.58
12/0.8/0.075/2/2	2.82	2.58	0.09	11.91
12/0.8/0.100/2/1	1.56	0.91	0.04	1.48
12/0.8/0.100/2/2	2.49	1.98	0.10	7.07
12/0.8/0.125/2/1	1.81	1.20	0.06	2.58
12/0.8/0.125/2/2	2.46	1.96	0.12	6.96
12/2.0/0/2/1	1.28	0.43	0.02	0.33
12/2.0/0/2/2	1.98	0.51	0.02	0.47
12/2.0/0.025/2/1	1.40	0.76	0.04	1.04
12/2.0/0.025/2/2	2.32	1.74	0.09	5.49
12/2.0/0.050/2/1	1.23	0.67	0.13	0.86
12/2.0/0.050/2/2	2.07	1.26	0.05	2.85

Table C.9 Distribution Moments.

12" Column. Porosity 2. Liquid-phase 10% W/V Yeast.

Experimental No.	U_1	U_2	U_3	U_4
12/0.8/0.025/2/1	3.77	4.58	- 1.20	32.94
12/0.8/0.025/2/2	5.18	7.46	- 7.85	84.18
12/0.8/0.050/2/1	3.15	3.37	- 0.12	19.62
12/0.8/0.050/2/2	4.53	5.90	- 3.38	53.07
12/0.8/0.075/2/1	2.26	1.67	0.09	5.02
12/0.8/0.075/2/2	3.29	3.33	- 0.04	18.99
12/2.0/0.025/2/1	2.21	1.61	0.08	4.67
12/2.0/0.025/2/2	2.46	1.83	0.10	6.02

Table C.10 Distribution Moments for Repeat Experiments.

Experimental No.	U_1	U_2	U_3	U_4
6" Column (Porosity 1. Air/Water)				
6/1.0/0.05/1/1	1.59	1.28	0.21	2.97
6/1.0/0.05/1/2	2.49	1.63	0.12	4.83
6/1.0/0.20/1/1	2.65	2.01	- 1.46	7.20
6/1.0/0.20/1/2	3.17	2.97	- 0.41	13.42
6/2.6/0.10/1/1	1.02	0.51	0.06	0.22
6/2.6/0.10/1/2	1.75	0.72	0.03	0.79
12" Column (Porosity 3. Air/Water)				
12/0.8/0.15/3/1	2.64	3.09	0.05	19.95
12/0.8/0.15/3/2	3.12	3.51	- 0.09	25.54
6" Column (Porosity 2. Air 5% W/V Yeast)				
6/0.5/0.075/2/1	2.21	2.19	0.71	7.19
6/0.5/0.075/2/2	3.62	2.99	0.33	13.41

NOMENCLATURE

A	area	cm^2
A_o	orifice cross-section area	"
A_c	column cross-section area	"
B	constant	
c	velocity of sound	cm/s
C	concentration	gm/cc
C_p	specific heat	cal/gm °C
d	diameter	cm
d_b	bubble diameter	"
$\bar{d}_b$	mean bubble diameter defined by eqn. 2.3	"
d_c	column diameter	"
d_o	orifice diameter	"
D	dispersion coefficient	cm^2/s
D_B	bubble dispersion coefficient	"
D_l	longitudinal dispersion coefficient	"
D_M	Molecular dispersion coefficient	"
D_r	radial dispersion coefficient	"
f	bubble generation rate	sec^{-1}
F	resistive force defined by eqn. 1.22	
F_r	Froude number	
g	gravity	cm/s^2

G_c	conversion factor	
G_m	gas flow rate (mass)	gm/s
G_v	gas flow rate (volumetric)	l/s
G'_v	gas flow rate (volumetric)	l/min
h	manometric height	cm Hg
H	height	cm
k	constant	
k_ϵ	constant	
K	constant	
K^1	constant	
l	length	cm
l_d	deflection length	
l_h	bubble bed height (eqn. 1.89 & 190)	cm
l_m	length of measuring section	"
l_t	tracer height (eqn. 1.89 & 190)	"
L_m	liquid flow rate (mass)	gm/s
L_v	liquid flow rate (volumetric)	l/s
m.r.t.	mean residence time	min
n	frequency of occurrence	
N	normality	eq. /l
N_c	capacitance number	

N_{τ}	surface tension number	
P	porosity	μ
ΔP	pressure drop	cm Hg
Pe_d	Peclet number (based on column diameter)	
Pe_l	Peclet number (based on column length)	
Pr	Prandtl number	
q_1 q_2	integers (eqn. 2.29)	
r_c	reaction term (eqn. 4.2)	
R	resistance	ohms
R_1^1	resistance defined by equation 2.2	"
Re_b	Reynolds number (bubble)	
Re_o	Reynolds number (orifice)	
S	source term (eqn. 4.2)	
t	time	min
t_r	reduced time	
U_{1-4}	moments of distribution curve	
v	velocity	cm/s
v_{bs}	bubble swarm velocity	"
v_c	rise velocity of a single bubble in a narrow tube	"
v_{gs}	gas superficial velocity	"

v_{gt}	gas true velocity	cm/s
v_{ls}	liquid superficial velocity	"
v_{lt}	liquid true velocity	"
v^*	gas velocity through orifice	"
v_{Rs}	relative superficial velocity	"
v_{Rt}	relative true velocity	"
v_s	slip velocity	"
v_∞	rise velocity of single bubbles in an infinite media	"
V	volume	cm^3
V_{1-4}	defined by equations 4.3 to 4.6	
V_b	bubble volume	cm^3
V_{BD}	potential difference (Fig. 2.1 and eqn. 2.2)	mV
V_c	volume of gas chamber beneath orifice	cm^3
w	constant	
X	Lockhart-Martinelli parameter (eqn. 1.59 & 1.60)	
$y(z_i)$	frequency (eqn. 2.29)	
(z_i)	displacement (eqn. 2.29)	

GREEK LETTERS

α β	shape function of a distribution curve	
δ	delta function input	
Δ	difference	
ϵ	gas hold-up	
η	thermal conductivity	cal cm/cm^2 s ^{o}C
θ	angle	
κ	constant defined by velocity distribution (eqn. 1.94)	
λ	coefficient of friction	
μ_g	gas viscosity	poise
μ_l	liquid viscosity	"
ν	kinematic viscosity	cm^2/s
π	3.142	
ρ_g	gas density	gm/cm^3
ρ_l	liquid density	"
σ^2	variance	
σ^2	reduced variance	
τ	surface tension	
ϕ	Lockhart-Martinelli parameter(eqn. 1.59 & 160)	

χ	specific conductance	$\mathrm{ohm}^{-1}\ \mathrm{cm}^{-1}$
ψ	Hughmark-Pressburg parameter (eqn. 1.61)	

SUBSCRIPTS

D	dry
F	friction
H	hydrostatic
i	species
TOT	total

DIMENSIONLESS GROUPS

$$Fr = \frac{v_{gs}^2}{\epsilon^2 g d_o}$$

$$N_c = \frac{g(\rho_l - \rho_g) V_c}{A_o \rho_g c}$$

$$N_\tau = \frac{G_c \tau \rho_l d_o}{\mu_l^2}$$

$$Pe_d = \frac{v d_c}{D}$$

$$Pe_l = \frac{v l}{D}$$

$$Pr = \frac{\mu C_p}{\eta}$$

$$Re_b = \frac{2 \rho_l d_b^4 f}{3 \mu_l d_o^2}$$

$$Re_o = \frac{4 \rho_l G_v}{\pi \mu_l d_o}$$

BIBLIOGRAPHY

1. Valentin F.H.H. Adsorption in Gas Liquid Dispersions Spon (1967)
2. Hughes R.R. Handloss A.M. Evans H.D. Maycock R.L. Chem. Eng. Prog. 51 557 (1955)
3. Kupferberg A. Jameson G.J. T.I.C.E. 47 241 (1969)
4. Datta R.L. Napier D.H. Hewitt D.M. T.I.C.E. 28 14 (1950)
5. Davidson L. Amick E.H. A.I.Ch.E.J. 2 337 (1956)
6. Wraith A.E. Chem. Eng. Sci. 26 1659 (1971)
7. Davidson J.F. Schüler B.O.G. T.I.C.E. 38 144 (1960)
8. Davidson J.F. Harrison D. Fluidised Particles C.U.P. (1963)
9. Walters J.K. Davidson J.F. J.Fluid Mech. 17 321 (1962)
10. Maier C.G. U.S. Bureau of Mines Bulletin 260 (1927)
11. Sprague R.O. M.S. Thesis, Columbia University, New York (1948)
12. Hagerty P.F. M.S. Thesis, Massachusetts Institute of Technology (1947)
13. Eversole W.G. Wagner G.M. Stackhouse E. Ind. Eng. Chem. 33 1451 (1941)
14. Van Krevelen D.W. Hoftijzer P.J. Chem. Eng. Prog. 46 29 (1950)
15. Leibson I. Holcombe G. Cacoso A.G. Jacmic J.J. A.I.Ch.E.J. 2 296 (1950)
16. Quigley C.J. Johnson A.I. Harris B.L. Chem. Eng. Prog. Symposium Series 51 (16) 31 (1955)
17. Calderbank P.H. Brit. Chem. Eng. 1 206 (1956)
18. Bashforth F. Adams H. Capillary Action, Cambridge (1883)
19. Poultanen A.A. Johnson A.I. Can. J. Chem. Eng. 38 93 (1960)
20. Houghton G. McLean A.M. Ritchie P.D. Chem Eng. Sci. 7 40 (1957)
21. Davies R.M. Taylor G.I. Proc. Roy. Soc. A200 375 (1950)

22. Davidson J.F. Schüler B.O.G. T.I.C.E. 38 335 (1960)

23. Pattle R.E. T.I.C.E. 28 32 (1958)

24. Hayes W.B. Hardy B.W. Holland C.D. A.I.Ch.E.J. 5 319 (1954)

25. Prince R.G.H. Chan B.K.C. T.I.C.E. 43 49 (1965)

26. Lockhart R.W. Martinelli R.C. Chem. Eng. Prog. 45 39 (1949)

27. Haberman W.L. Morton R.K. Report No. 802 NS 715-102 (1953)
also Trans. Am. Soc. Civil Eng$^{rs.}$ 121 227 (1956)

28. Peebles F.N. Garber H.J. Chem. Eng. Prog. 49 88 (1953)

29. Angelino H. Charzat C. Williams R. Chem. Eng. Sci. 19 289 (1964)

30. Stokes G.G. Mathematical and Physical Papers Vol. 1 C.U.P. (1880)

31. Coppock P.D. Meiklejohn G.T. T.I.C.E. 29 75 (1951)

32. Garner F.H. Hammerton D. Chem. Eng. Sci. 3 1 (1954)

33. Hadamard J. Compt. Rend. 152 1735 (1911)

34. Lamb H. Hydrodynamics C.U.P. (1932)

35. Uno S. Kintner R.C. A.I.Ch.E.J. 2 3 (1956)

36. Sideman S. Hortescu O. Fulton J.W. Ind. Eng. Chem. 58 (7) 32 (1966)

37. Calderbank P.H. T.I.C.E. 45 209 (1967)

38. Helsby F.W. Ph.D. Thesis, University of London (1958)

39. Freedman W. Davidson J.F. T.I.C.E. 47 251 (1969)

40. Mashelkar R.A. Brit. Chem. Eng. 15 (10) 1297 (1970)

41. Ostergaard K. Michelson M.L. Can J. Chem. Eng. 47 (2) 107 (1967)

42. Scott D.S. Adv. Chem. Eng. 4 200 (1964)

43. Griffith P. Wallis G.B. Am. Soc. Mech. Eng. J. Heat Trans. 83 307 (1961)

44. Govier G.W. Radford B.A. Dunn J.S.C. Can J. Chem. Eng. 35 58 (1957)

45. Brown R.A.S. Govier G.W. Sullivan G.A. Can J. Chem. Eng. 32 62 (1954)

46. Nicklin D.J. Wilkes J.O. Davidson J.F. T.I.C.E. 40 61 (1962)

47. Wallis G.B. Ph.D. Thesis, University of Cambridge (1961)

48. Fair J.R. Chem. Eng. 74 (14) 67 (1967)

49. Pasveer A. Sewage Industrial Wastes 27 1130 (1955)

50. Eckenfelder W.W. Barnhart E.L. A.I.Ch.E.J. 7 631 (1961)

51. Shulman H.L. Molstad M.C. Ind. Eng. Chem. 42 1058 (1950)

52. Fair J.R. Lambright A.J. Andersen J.W. Ind. Eng. Chem. Proc. Des. & Dev. 1 33 (1962)

53. Yoshida F. Akita K. A.I.Ch.E,J. 11 9 (1965)

54. Braulick W.J. Fair J.R. Lerner B.J. A.I.Ch.E.J. 11 73 (1965)

55. Koide K. Kato S. Tanaka Y. Kubota H. Chem.Eng.(Japan) 1 (1) 51 (1968)

56. Petrick M. Transactions, Argonne National Lab. No. 6581 (1962)

57. Bridge A.G. Lapidus L. Elgin J.C. A.I.Ch.E.J. 10 819 (1964)

58. Vermeulen T. Williams G.H. Langlois G.E. Chem.Eng.Prog. 51 (2) 85 (1955)

59. Calderbank P.H. T.I.C.E. 36 443 (1958)

60. Calderbank P.H. T.I.C.E. 37 173 (1959)

61. Harmarthy T.Z. A.I.Ch.E.J. 6 281 (1960)

62. West F.B. Gilbert W.D. Shimizu T. Ind. Eng. Chem. 44 2470 (1952)

63. Nicklin D.J. Chem. Eng. Sci. 17 693 (1962)

64. Wallis G.B. Int. Dev. Heat. Trans. Proc. Am. Soc. Mech. Eng. Heat Trans Conference p.319 1961/2

65. Vershoor H. T.I.C.E. 28 52 (1950)

66. Novosad Z. Czech. Chem. Comm (1954)

67. Kölbel H. Siemes W. Dechema Monograph 29 334 (1957)

68. Towell G.D. Strand C.P. Ackerman C.H. A.I.Ch.E. - Inst.Chem.Eng. Joint Meeting Series No.10 97 (1965)

69. Mendelson H.D. A.I.Ch.E.J. 13 250 (1967)

70. Maneri C.C. Mendelson H.D. A.I.Ch.E.J. 14 295 (1968)

71. Happel J. Ast P.A. Chem.Eng.Sci. 11 286 (1960)

72. Marrucci G. Ind. Eng. Chem. Fundamentals 4 224 (1964)

73. Dumitrescu D.T.Z. Angew Math. U. Mech. 23 139 (1943)

74. Van Krevelen D.W. Chem. Ing. Tech. 30 (9) 553 (1958)

75. Turner J.C.R. Chem. Emg. Sci. 21 (11) 971 (1966)

76. Hughmark G.A. Pressburg B.S. A.I.Ch.E.J. 7 (4) 677 (1961)

77. Chisholm D. Laird A.D.K. Trans. Am. Soc. Mech. Eng. 80 276 (1958)

78. Bankhoff S.G. J.Heat Trans. 82 265 (1960)

79. Hughmark G.A. Chem. Eng. Prog. 58 (4) 64 (1962)

80. Gomezplata A. Nichols C.R. Chem. Eng. 74 (4) 182 (1967)

81. Hughmark G.A. Ind. Eng. Chem. Proc. Des. & Dev. 6 (2) 218 (1967)

82. Calderbank P.H. Rennie J. T.I.C.E. 40 3 (1962)

83. Reith T. Renken S. Israel B.A. Chem. Eng. Sci. 23 (6) 619 (1968)

84. Argo W.B. Cova D.R. Ind. Eng. Chem. Proc. Des. & Dev. 4 (4) 352 (1965)

85. Ellis J.E. Jones E.L. Two-phase Flow Symposium, Exeter, 2 B102 (June 1965)

86. Bischoff K.B. Phillips J.B. Ind. Eng. Chem. Proc. Des. & Dev. 5 416 (1966)

87. Bartholomew W.H. Karow E.O. Sfat M.R. Wilhelm R.M. Ind. Eng. Chem. 42 1801 (1950)

88. Dukler A.E. Wicks M. Cleveland R.G. A.I.Ch.E.J. 10 (1) 38 (1964)

89. Bhatia V.K. A.I.Ch.E.J. 15 (3) 466 (1969)

90. Othmers D.M. Rase H.F. Ind. Eng. Chem. Fundamentals 3 106 (1964)

91. Gilliland E.R. Mason E.A. Ind. Eng. Chem. 41 (1) 1191 (1949)

92. Dal'man V.V. Zhilyaeva T.A. Khim i Tekh. Topliv i Masel 10 (12) 36 (1965)

93. Taylor G.I. Proc. Roy. Soc. A219 186 (1953)

94. Ohki Y. Inoue H. Chem. Eng. Sci. 25 (1) 1 (1970)

95. Aris R. Proc. Roy. Soc. A235 67 (1956)

96. Yoshitome H. Ph.D. Thesis, Tokyo University (1967)

97. Kato Y. Dr. Eng. Thesis, Tokyo University (1961)

98. Aoyama Y. Ogushi K. Koide K. Kubota H. J.Chem.Eng.(Japan) 1 158 (1968)

99. Tadaki T. Maeda S. Chem. Eng. Japan 28 (4) 270 (1964)

100. Siemes W. Borchers E. Chem. Eng. Sci. 12 77 (1960)

101. Levenspiel O. Ind. Eng. Chem. 50 (3) 343 (1958)

102. Levenspiel O. Chemical Reaction Engineering Wiley New York (1962)

103. Bischoff K.B. Ind. Eng. Chem 58 (11) 18 (1966)

104. Horn F.J.M. Parish T.D. Chem.Eng.Sci. 22 (12) 1549 (1967)

105. Levenspiel O. Bischoff K.B. Adv. Chem. Eng. 4 98 (1963)

106. Levenspiel O. Smith W.K. Chem. Eng. Sci. 6 227 (1957)

107. Langlois G.E. Gulberry J.E. Vermeulen T.E. Rev. Sci. Inst. 25 360 (1954)

108. Mie P. Ann. Phys. Lpz. 33 1275 (1910)

109. Brown D.E. Craddock J. I.C.E. Symposium on Mixing, Leeds (Sept. 1968)

110. Kilkarni M.Sc. Thesis, University of Aston in Birmingham (1968)

111. Mitropolskij A.Ch. Technika Statisticeskich Vycislernig Moscow (1961)

112. Van der Laan E. Th. Chem. Eng. Sci. 7 187 (1958)

113. Wehner J.F. Wilhelm R.H. Chem. Eng. Sci. 6 89 (1956)

114. Aris R. Chem. Eng. Sci. 9 266 (1959)

115. Bischoff K.B. Chem. Eng. Sci. 12 69 (1960)

116. Levenspiel O. Bischoff K.B. Chem. Eng. Sci. 17 245 (1962)

117. Collier J.G. Hewitt G.F. Brit.Chem.Eng. 11 (12) 1526 (1966)

118. Cooper K.D. Hewitt G.F. Pinchin B. A.E.R.E. R4301 (1963)

119. Kintner R.C. Morton T.J. Graumann R.E. Amberker S. Can.J.Chem.Eng. 36 (6) 235 (1961)